Université Paris V – René Descartes

Ecole doctorale Bio-Sorbonne Paris Cité

Biologie Cellulaire et Moléculaire, Physiologie, Physiopathologie

INSERM U970, Centre de recherche cardiovasculaire Parisien - HEGP

Rôle de l'autophagie dans les cellules endothéliales du foie dans le développement de la stéatohépatite non alcoolique

Role of autophagy in liver sinusoidal endothelial cells in nonalcoholic steatohepatitis

Par Adel Hammoutene

Thèse de physiologie et physiopathologie en vue de l'obtention du titre de

DOCTEUR DE L'UNIVERSITE PARIS DESCARTES

Dirigée par Pr. Pierre-Emmanuel Rautou

Présentée et soutenue publiquement le 17 Décembre 2018

Devant un jury composé de :

Pr. Isabelle Colle	*Rapporteur*
Pr. Chantal Housset	*Rapporteur*
Dr. Chantal Desdouets	*Examinateur*
Dr. Richar Moreau	*Examinateur*
Pr. Vlad Ratziu.	*Examinateur*
Pr. Pierre-Emmanuel Rautou	*Directeur de thèse*

A mes parents,

A mes frères,

REMERCIEMENTS

Tout d'abords, je tiens à remercier vivement les membres du jury d'avoir accepté d'évaluer mon travail de thèse.

- *Le Pr Chantal Housset ainsi que le Pr Isabelle Colle, qui ont pris le temps d'examiner avec attention mon travail en tant que rapporteurs.*
- *Le Dr Chantal Desdouets, le Dr Richard Moreau ainsi que le Pr Vlad Ratziu qui ont pris le temps d'évaluer mon travail en tant qu'examinateurs.*
- *Le Pr Pierre-Emmanuel Rautou qui a dirigé cette thèse.*

Je suis très honoré par votre présence dans ce jury.

Ensuite, je tiens à exprimer toute ma gratitude à tous ceux qui m'ont accompagné durant plusieurs années :

Au Pr Pierre-Emmanuel Rautou : tout d'abords, merci d'avoir dirigé cette thèse. Merci de m'avoir donné ma chance et d'avoir eu confiance en moi. Ensuite, merci pour ton énergie débordante (pour ne pas dire épuisante) et ton optimisme sans limite qui poussent les gens qui te côtoient à donner le meilleur d'eux-mêmes. C'est une chance pour ceux qui savent la saisir. Je retiendrais deux phrases clés que l'on a souvent entendues en réunion et qui illustrent bien ces propos : « 100% des gagnants auront tenté leur chance » et « on n'est pas à l'abri d'un coup de chance ». Merci pour ton humour et ta bonne humeur. C'était sincèrement un réel plaisir et un honneur de travailler avec toi. J'ai énormément appris à tes côtés pendant ces quelques années et je t'en suis très reconnaissant. Enfin, quelques mots pour te remercier pour tous les précieux conseils que tu m'as donnés pour des questions existentielles que j'ai pu me poser pendant ma thèse, pour les coups de « pub » qui m'aident dans la recherche de post-doc, pour ton soutien, pour ta disponibilité et pour tes qualités humaines exceptionnelles.

Au Dr Chantal Boulanger, je vous remercie de m'avoir accueilli dans votre équipe il y a de cela maintenant cinq ans. C'est ici que j'ai fait mes premiers pas en recherche. Merci pour votre disponibilité, pour toutes les discussions scientifiques que nous avons partagées ainsi que pour tous vos conseils avisés. J'ai également beaucoup appris à vos côtés.

Au Dr Alain Tedgui, merci de m'avoir accueilli dans ce magnifique centre de recherche qu'est le PARCC. On se sent vraiment bien dans ce laboratoire au sein duquel il fait bon travailler. Merci de votre gentillesse et de votre bonne humeur. Au nom de tous les étudiants du PARCC, merci de nous permettre de travailler dans de si bonnes conditions.

A Mr Philippe Coudol (Dj Fifi), il est difficile de parler de bonne ambiance au PARCC sans penser à toi ! Un grand merci à toi aussi pour ton immense contribution au bon fonctionnement du PARCC et à la bonne ambiance qui règne. Je suis vraiment ravi de t'avoir rencontré. Merci pour tes qualités humaines hors norme.

Je remercie chaleureusement tous les membres de l'équipe 1 pour votre bonne humeur, votre aide et tous les moments formidables passés avec vous. Les quelques lignes qui vont suivre ne seront certainement pas suffisantes pour vous remercier de tout ce que vous m'avez apporté durant ces années.

- *A Xavier, merci pour tout ce que tu m'as appris en bio-mol et pour tes conseils, surtout merci pour tes blagues parfois un peu « borderline » qui sont largement à la hauteur de celles des gastroentérologues. Je souligne que tu es un homme nouveau depuis qu'Abel est là, il était à une lettre de s'appeler Adel. Bien essayé !*
- *A Marion, la reine du FACS. Merci pour tous les dosages de microvésicules et pour tes nombreux coups de main et conseils en cytométrie entre autres. Marion c'est aussi la meilleure des meilleures pâtissières. Merci de nous avoir régalés avec tes gourmandises.*
- *A Cécile, j'espérais réussir à te convaincre de m'éliminer des plannings de nettoyage du L2 en étant ton voisin de bureau, c'est le plus gros échec de ma thèse. Plus sérieusement, merci pour ton soutien et la gestion parfaite de la culture cell.*
- *A Michael, fais attention à toi le tempérament de ton chef déteint sur toi. Merci pour les petits coins de PSM que tu m'as gracieusement laissés et pour tes blagues qui, comme je le disais, ressemblent parfois à celle de ton chef.*

- *Merci aux nouveaux débarqués de l'équipe : Shruti, Stephane, Fariza, Louise, Pierre-Michaël, pour votre bonne humeur. Vous avez désormais cette humble mission de maintenir cette réputation de l'équipe 1 comme meilleure équipe du labo (ce n'est pas pour rien que c'est la première équipe du PARCC). Un merci « particulier » à Pierre-Michaël pour les discussions de fin de parcours, pour tes précieux conseils sur l'après thèse (tu m'as aidé à y voir plus clair sur cette dernière ligne droite), pour ta bonne humeur et pour ta motivation sans faille à faire la fête avec nous. Tu as réussi avec brio ton intégration au groupe de personnes un peu disjonctées. Bravo ! Je crois que le flambeau te revient désormais pour perpétuer les traditions (festives) du PARCC.*
- *Aux anciens de l'équipe qui m'ont lâchement abandonné. Merci à Johanne et à Marouane pour votre aide, conseils, discussions diverses et variées, aux instants musicaux et à tous les bons moments passés avec vous. A Jean-Marie, le porté disparu, merci pour ta bonne humeur et ta gentillesse contagieuse. Anne-Clémence, tu es la première avec qui j'ai travaillé au PARCC. C'est toi qui m'as initié aux manips ! Merci pour tout ce que tu m'as appris.*
- *Dans le registre des anciens, je gardais le meilleur pour la fin. Un ENORME merci à toi Juliette, tu m'as été d'une aide titanesque pendant cette thèse que tu as quasiment suivi de A à Z. Merci pour tout le travail que tu as fourni pour ce projet, pour ton aide et pour ton soutien indéfectibles. Merci pour tous tes conseils lors de discussions professionnelles ET personnelles que nous avons eues et que nous avons encore d'ailleurs. Merci pour tous les bons moments passés ensemble au labo ET en dehors du labo. Je suis vraiment ravi de t'avoir comme amie.*
- *A l'équipe OBB : merci Olivier, Dominique, Sihem, Anis, Marie pour vos conseils et discussions lors des réunions d'équipe.*
- *Enfin, merci à tous les stagiaires qui sont passés dans l'équipe : Hortense, Kyle, Rémi, Mendel, Fatou, Marie-Belle, Eléonore, Samir, Alice. Jules (Crusty), tu m'as vraiment beaucoup aidé pendant ton M2 et je t'en remercie. Je suis content de savoir que tu voles de tes propres ailes maintenant. Merci pour ta Zen-attitude. Tu t'es également parfaitement intégré à l'esprit de l'équipe et du PARCC. Autrement dit, tu sais faire la fête comme on aime la faire. J'en garde d'excellents souvenirs. Mélanie, la phrase qui te caractérise le mieux : petite par la taille, grande par le gout (restos gastronomiques, hôtel de luxe au ski, madame ne boit que du vin ou du champagne, et j'en passe… une vraie bobo). Comme me l'a souvent dit PE, je cite : « ce n'est pas la taille qui compte*

Adel ». Cette phrase a pris tout son sens avec toi car derrière cette petite dame d'apparence innocente se cache une grande dame au caractère bien trempé, mais c'est pour ça qu'on t'apprécie. Ceci dit, tu m'as bien fait rire cette dernière année.

Merci aux habitants du 2^{ème} étage, chercheurs et ingénieurs, vous êtes géniaux. A José, le MacGyver du labo, le pilier du 2^{ème}, ou plutôt du PARCC devrais-je dire. Les gens du 2^{ème} ne sont pas les seuls à recourir à ton savoir. Soraya, Stéphane, Bruno, Ludivine, Mouna, Mélanie, Jean-Sé, Hafid, Pierre-Louis. Je tiens à vous remercier pour les discussions scientifiques que nous avons pu avoir. Je remercie particulièrement certains d'entre vous (je ne citerai pas de noms, ils se reconnaîtront) pour vos participations remarquables (ou remarquées) aux soirées du PARCC, retraites etc…

A mes amis du 2^{ème}, thésard, ex-thésards, ingénieurs, stagiaires ou ex-stagiaires : Jennifer (et oui, tu as habité au 2^{ème} à une époque), Andréas (Girax), Lynda (Z), Yacine (Patate), Blaise (Robin des bois), Juliette (Juju, encore toi !), Hélène, Marie (la rousse), Nadajoe, Yujiao, Marouane (Makhlouf), Sihem, Min, Johanne (Jojo), Ivana (Zlatan), Pierre-Michaël (Dr Coly, encore toi !), Paul (Polo), Michmich, Josito, et bien d'autres (la liste est bien top longue)… C'était vraiment un grand plaisir de travailler à vos côtés. Merci pour tous les moments passés avec vous, les déjeuners, les cafés, les vendredis au terminus Balard, les soirées, les retraites… Je garde un paquet de très bons souvenirs avec chacun d'entre vous.
Blaise et Girax, assurément les rois de la fête ! Vous déchirez les gars !
Yacine, merci pour tous les instants sportifs !
Lynda, merci pour ta bonne humeur, pour les soirées et pour les séances de run à l'aquaboulevard avec Girax, Jenn, Yacine, Juliette.

Merci aux habitants des autres étages (oui, il n'y a pas que le 2^{ème} au PARCC) que l'on croise dans les couloirs, à la machine à café, à la cantine : Bamba, Ludovic, Judith, Rami, Thomas, Fabio, Chahra, Habib et bien d'autres…

J'aimerais exprimer ma très grande gratitude aux personnes de la plateforme administrative et de l'ERI. Merci de mener la barque comme vous le faites. A ceux qui sont partis et à ceux qui sont là : Cyrille, Murielle, Catherine, Martine, Bruno, Philippe, Elizabeth, Nicolas, merci pour votre gentillesse et votre bonne humeur. Véronique, maman poule, merci de gérer tes *petits poussins comme tu le fais, tu es formidable. Annette, Nenette, merci pour ta joie de vivre vraiment permanente, tu es impressionnante ! Stéphanie, merci pour ta bonne humeur dès 7h du matin, merci pour tous ces autoclaves faits en urgence ou encore les commandes magasins aussi livrées en urgence. Vive le PSG ! Camille, d'abord merci pour les compensations au LSR, mais surtout merci pour les discussions sportives. Merci aux zootechniciens, Gwendoline, Corina, Guillaume, Pauline, Stacy, Emma, Noémie, Françoise. Merci à vous tous. Vous faites un travail vraiment extraordinaire et c'est aussi en grande partie grâce à vous qu'on travaille dans de si bonnes conditions.*

J'exprime tout ma gratitude également à ceux avec qui j'ai pu collaborer et qui m'ont aidé dans la réalisation de ce travail de thèse. Le Pr Valérie Paradis, Nathalie Colnot, Samira Louirem, Le Dr Sophie Lotersztajn, Le Dr Patrice Codogno et son équipe.

A mes proches,

Jennifer, tu as participé à cette thèse certainement bien plus que ce que tu ne le crois. D'abord par ce que tu as habité au 2ème à une époque, puis parce que tu as squatté à toutes les soirées du PARCC. Troisièmement, parce que tu as partagé (pour ne pas dire volé) certains de mes amis (exemples : Juliette, Z…) etc… Merci pour tous les moments qu'on a partagés. Merci pour ton soutien sans faille, merci de m'avoir supporté ces 3 ans et particulièrement cette dernière année. Tu as du mérite, une médaille devrait t'être décernée.

A ma famille,
Mes parents, vous êtes des exemples pour moi et une profonde source d'inspiration et de motivation. Je ne vous remercierai jamais assez pour tout le bonheur, l'affection, le soutien et les encouragements que vous m'avez donnés... Je vous dédie cette thèse en guise de remerciement pour tout ce que vous faites pour nous trois.
Mehdi et Salim, mes frères, mes piliers, vous aussi je ne vous remercierai jamais assez pour votre indéfectible soutien, votre affection, vos encouragements et pour les moments exceptionnels que je passe avec vous quand je rentre à la maison. Je suis heureux de vous avoir dans mon entourage. Merci pour tout.

TABLE OF CONTENTS

I- LIST OF ABBREVIATIONS......9

II- SUMMARY......12

III- INTRODUCTION......14

A. Nonalcoholic steatohepatitis......14

1. Definition......14
2. Epidemiology......16
3. Risk factors......17
    - a- Metabolic risk factors......17
    - b- Genetic risk factors......18
    - c- Other risk factors......20
4. Diagnosis......20
5. Pathogenesis......23
    - a- Mechanisms of liver steatosis......23
    - b- Lipotoxicity and oxidative stress......25
    - c- Mechanisms of liver inflammation......28
    - d- Mechanisms of liver fibrosis......33
6. Treatments......35
    - a. Non-pharmacological approaches......35
    - b. Pharmacological approaches......36
    - c. Future therapeutic drugs......38

B. Role of liver sinusoidal endothelial cells in nonalcoholic fatty liver disease......39

1. Liver sinusoidal endothelial cells (LSECs)......39
2. Role of LSECs in simple steatosis......41
3. Role of LSECs in nonalcoholic steatohepatitis (NASH)......48
4. Role of LSECs in NASH-related fibrosis......55
5. Role of LSECs in cirrhosis in NAFLD setting......60
6. Role of LSECs in hepatocellular carcinoma in NAFLD setting......62

C. Autophagy......65

1. Definition......65
2. Types of autophagy......67
    - a. Chaperone-mediated autophagy......67
    - b. Microautophagy......68
    - c. Macroautophagy......69
3. Molecular machinery of macroautophagy......70
    - a- Initiation/Nucleation......70
    - b- Elongation and closure......71
    - c- Maturation/Fusion......73
4. Signaling pathways and macroautophgy regulation......76
    - a. mTOR......76
    - b. Class I PI3K......77
    - c. AMPK......77

    d. FOXO 78
    e. p53 79
    f. E2F1 and NFκB 80

D. Autophagy in the liver........ 81

1. Autophagy in liver metabolism and homeostasis 81

2. Autophagy in nonalcoholic steatohepatitis 86
    a- Autophagy in hepatocytes 88
    b- Autophagy in macrophages 89
    c- Autophagy in hepatic stellate cells 90

IV- THESIS WORK........ 93

A- Background, hypothesis and aims........ 93

B- Role of autophagy in LSECs in NASH........ 95

Article: A defect in autophagy in liver sinusoidal endothelial cells occurs in nonalcoholic steatohepatitis and promotes liver inflammation and fibrosis........ 95

V- DISCUSSION AND PROSPECTS........ 144

VI- REFERENCES........ 152

VII- APPENDIX........ 179

A. Co-authorship publications........ 179

1. Autophagy is required for endothelial cell alignment and atheroprotection under physiological blood flow........ 179

2. Endothelial autophagic flux hampers atherosclerotic lesion development........ 216

3. Endothelial JAK2^{V617F} does not enhance liver lesions in mice with Budd-Chiari syndrome 220

4. Primary cilia sensitize endothelial cells to BMP and prevent excessive vascular regression........ 223

5. Paradoxical suppression of atherosclerosis in the absence of microRNA-146a........ 239

B. Curriculum vitae........ 254

I- LIST OF ABBREVIATIONS

α-SMA: Alpha smooth muscle actin
AAV: Adeno-associated viruses
ACC: Acetyl-CoA carboxylase
AKT: Protein kinase B
ALT: Alanine aminotransferase
AMBRA1: Activating molecule in BECN1- regulated autophagy protein 1
AMP: Adenosine monophosphate
AMPK: AMP-activated protein kinase
AST: Alanine aminotransferase
ATG: Autophagy related gene
ATP: Adenosine triphosphate
BCL2: B-cell lymphoma 2
BMI: Body mass index
BNIP3: BCL2/adenovirus E1B 19 kDa protein-interacting protein 3
cDNA: Complementary deoxyribonucleic acid
cGMP: Cyclic guanosine monophosphate
CCR: C–C motif chemokine receptor
CK-18: Cytokeratin 18
CMA: Chaperone-mediated autophagy
CT: Cycle threshold
CTGF: Connective tissue growth factor
CYP2E1: Cytochrome P450 2E1
DAMPs: Damaged-associated molecular patterns
DDR: Discoidin domaincontaining peptidyl
DMEM: Dulbecco's modified Eagle medium
DPP4: Dipeptidyl peptidase 4
DRAM: DNA damage-regulated autophagy modulator protein
E2F1: E2F transcription factor 1
ECGS: Endothelial Cell Growth Supplement
EDTA: Ethylenediaminetetraacetic acid
EF1α: Elongation factor 1 alpha
eNOS: Endothelial nitric oxide synthase
ERK: Extracellular signal-regulated kinase
ESCRT: Endosomal sorting complexes required for transport
FABP4: Fatty acid binding protein 4
FFA: Free fatty acid
FIP200: RB1-inducible coiled-coil protein 1
FOXO: Forkhead box O
FXR: Farnesoid X receptor
GAPDH: Glycéraldéhyde-3-phosphate dehydrogenase
GFAP: Glial fibrillary acidic protein
GLP-1: Glucagon-like peptide 1
GTP: Guanosine triphosphate
H2O2: Hydrogen peroxide
HCC: Hepatocellular carcinoma
HE: Hematoxylin and Eosin
HCL: Hydrochloride
HDL: High density lipoprotein
HIF: Hypoxia inducible factors
HPRT: Hypoxanthine-guanine phosphoribosyltransferase
HSCs: Hepatic stellate cells
HSC70: Heat shock cognate 70 kDa
HSP90: Heat shock protein 90
ICAM-1: Intercellular adhesion molecule 1
IGF1: Insulin growth factor 1
IL: Interleukin
iNOS: Inducible nitric oxide synthase
IPTG: Isopropyl β-D-1-thiogalactopyranoside
IQR: Interquartile range
IRE1 α: Inositol-requiring enzyme 1
IκB: Inhibitor of KB
JNK: C jun *N*-terminal kinase
KLF: Krüppel-like factor
LAMP-2: Lysosome-associated membrane glycoprotein 2
LC3: Microtubule-associated proteins 1A/1B light chain 3

LDL: Low density lipoprotein
LKB1: Liver kinase B1
LPS: Lipopolysaccharide
LSECs: Liver sinusoidal endothelial cells
MAPK: Mitogen activated protein kinase
MCP-1: Monocyte Chemoattractant Protein 1
MOI: Multiplicity of infection
mTOR: Mammalian target of rapamycin
mTORC: Mammalian target of rapamycin complex
NaCl: Sodium chloride
NADPH: Nicotinamide adenine dinucleotide phosphate
NAFL: Nonalcoholic fatty liver
NAFLD: Nonalcoholic fatty liver disease
NAS: NAFLD activity score
NASH: Nonalcoholic steatohepatitis
NF-κB: Nuclear factor-kappa B
NK: Natural killer cells
NKT: Natural killer T cells
NO: Nitric oxide
ox-LDL: Oxidized low-density lipoprotein
PAMPs: Pathogen-associated molecular protein
PBS: Phosphate buffered saline
PCR: Polymerase chain reaction
PDGF: Platelet derived growth factor
PDGFR: Platelet derived growth factor receptor
PFP: Plasma free platelets
PI3K: Phosphatidylinositol-4,5-bisphosphate 3-kinase
PI3P: Phosphatidylinositol-3-phosphate
PINK1: PTEN Induced Putative Kinase 1
PKB: Protein kinase B
PLVAP: Plasmalemma vesicle-associated protein
PNPLA3: Patatin-like phospholipase domain-containing protein 3
PPIA: Peptidylprolyl isomerase A
Rab7: Ras-related protein Rab-7
RANTES: Regulated on Activation, Normal T Cell Expressed and Secreted
Rheb: Ras homolog enriched in brain
RIPA: Radioimmunoprecipitation assay
ROS: Reactive oxygen species
SAF: Steatosis Activity Fibrosis
SEM: Standard error of the mean
SH3GLB1/Bif-1: SH3 Domain Containing GRB2 Like, Endophilin B1
shRNA: short hairpin ribonucleic acid
SMAD 3: Mothers against decapentaplegic homolog 3
SNAP-29: Synaptosomal-associated protein 29
SNARE: Soluble N-ethylmaleimide-sensitive-factor Attachment protein REceptor
SQSTM1: Sequestosome 1
STAT3: Signal transducer and activator of transcription 3
STX17: Syntaxin 17
TECPR1: Tectonin beta-Propeller Repeat Containing protein 1
TFEB: Transcription factor EB
TGF-β: Transforming growth factor beta
TGF-βR: Transforming growth factor beta receptor
TGR5: G protein-coupled bile acid receptor 1
TLRs: Toll-Like receptors
TSC1/2: Tuberous sclerosis complex 1/2
TSECs: Transformed liver sinusoidal endothelial cells
ULK1/2: unc-51 like autophagy activating kinase 1
UPR: Unfolded protein response
UVRAG: UV radiation resistance-associated gene protein
VAMP8: Vesicle-associated membrane protein 8
VAP-1: Vascular adhesion protein 1

VCAM-1: Vascular cell adhesion protein 1
VEGF: Vascular endothelial growth factor
VEGFR: Vascular endothelial growth factor receptor
VLDL: Very low-density lipoprotein
VPS15: Phosphoinositide 3-kinase regulatory subunit 4
VPS34: Phosphatidylinositol 3-kinase catalytic subunit type 3
XBP1: X-box binding protein 1
YAP1: Yes-associated protein 1

II- SUMMARY

Nonalcoholic steatohepatitis (NASH) is defined as the excessive lipid accumulation in the liver, hepatocellular injury and inflammation with or without fibrosis. NASH has the potential for cirrhosis and hepatocellular carcinoma. Recent studies suggested that endothelial alterations precede inflammation and fibrosis in NASH. Autophagy is a cellular process by which the dysfunctional cytoplasmic material joins lysosomes for degradation. The role of autophagy in hepatocytes, in macrophages and in hepatic stellate cells has been studied but nothing was known about the role of autophagy in liver sinusoidal endothelial cells (LSECs) in NASH. The aim of my thesis work was to investigate the role of autophagy in LSECs in NASH and liver fibrosis.

I demonstrated using human liver biopsies that autophagy in LSECs is defective in patients with NASH. *In vitro*, the combination of the inflammatory mediators TNFα and IL6 decreased autophagy level in LSECs as a result of AMPKα pathway inhibition. LSECs deficient in autophagy overexpressed *Mcp1*, *Rantes* and VCAM-1 suggesting endothelial inflammation. Deficiency in autophagy in LSECs induced the expression of endothelial-to-mesenchymal transition markers (*α-SMA*, *Tgf-β1* and *Collagen1a2*). Endothelial autophagy deficiency also promoted apoptosis of LSECs. *In vivo*, mice deficient in endothelial ATG5 fed a high fat diet had a more frequent nodular liver surface, a higher liver inflammation (increased liver expression of *Mcp-1*, *Rantes* and VCAM1) and more liver fibrosis (increased liver expression of α-SMA, *Tgfβ1* and *Collagen1α2* and more collagen deposition). Mice deficient in ATG5 in endothelial cells treated with carbon tetrachloride had more liver fibrosis (increased liver gene expression of *α-SMA*, *Tgf-β1* and *Collagen 1α2* and more collagen deposition).

In conclusion, autophagy is defective in LSECs of patients with NASH. This defect can be attributed to inflammatory mediators present in the portal venous blood of patients with NASH. Deficiency in autophagy in LSECs induces endothelial alterations (inflammation, endothelial-to-mesenchymal transition and apoptosis) and strongly contributes to liver inflammation and fibrosis at early and advanced stages of chronic liver disease. Deficiency in endothelial autophagy might in part explain how patients with steatosis progress to NASH. This observation of a protective role of endothelial autophagy completes the picture of the role of autophagy in chronic liver diseases. Targeting endothelial autophagy could be an attractive strategy to treat NASH.

III- INTRODUCTION

A. Nonalcoholic steatohepatitis

1. Definition

The metabolic syndrome is defined as the combination of cardiovascular risk factors including hyperglycemia, dyslipidemia (increased levels of low-density lipoprotein (LDL) and decreased levels of high-density lipoprotein (HDL)), hypertension and obesity (central obesity with an increased waist circumference) [1]. This syndrome is a major public health issue since the number of affected individuals is constantly increasing due to sedentary lifestyles and the high prevalence of obesity. Nonalcoholic fatty liver disease (NAFLD) is the hepatic manifestation of the metabolic syndrome and encompasses a spectrum of conditions including simple steatosis (nonalcoholic fatty liver, NAFL) and nonalcoholic steatohepatitis (NASH).

The first observations of NAFLD were made in the 1950s when Zelman observed the presence of steatosis in obese patients [2]. Similar observations were made few years later in obese patients [3–5], diabetics [6–8] and in patients undergoing enteric surgery for morbid obesity [9,10]. Historically, the acronym NASH for "nonalcoholic steatohepatitis" was used for the first time in 1980 by Ludwig and coworkers that described a disease reproducing the histological lesions of alcoholic hepatitis which can progress to cirrhosis and associated it with obesity and type 2 diabetes [11]. NAFLD affects people who have no or low alcohol consumption (less or equal to 20 g / day for women or 30 g / day for men) [12,13]. Nonalcoholic fatty liver (NAFL) is defined as the excessive accumulation of triglyceride in the liver (steatosis) without hepatocellular injury, inflammation or fibrosis. NASH is characterized by steatosis combined with lobular inflammation and hepatocytes injury with or without fibrosis [14] (Figure 1). It is agreed that patients with NAFL have slow or no histological progression while patients with NASH have potential for cirrhosis and its complications such as ascites, variceal bleeding and hepatocellular carcinoma and may require liver transplantation [13,15]. Importantly, patients with NASH also develop hepatocellular carcinoma (HCC) in the absence of cirrhosis [16–18]. NASH is currently a leading cause of liver disease among adults awaiting liver transplantation in Europe and in the United States and is projected to become the most common indication for liver transplantation in the next decade [18,19]. NASH also increases the risks of non-liver-related outcomes compared to those of patients with NAFL alone. Non-hepatic outcomes related to NASH are primarily cardiovascular disease and malignancy [20,21]. NASH is also an emerging risk factor for type 2 diabetes and end-stage kidney disease [22,23]. Despite its prevalence and severity, there is no approved therapy for NASH and available treatments only aim to control associated conditions [17]. Therefore, understanding the mechanisms of NASH, and in particular how simple steatosis progresses to NASH and then to cirrhosis or cancer only in certain individuals, is of utmost importance [24].

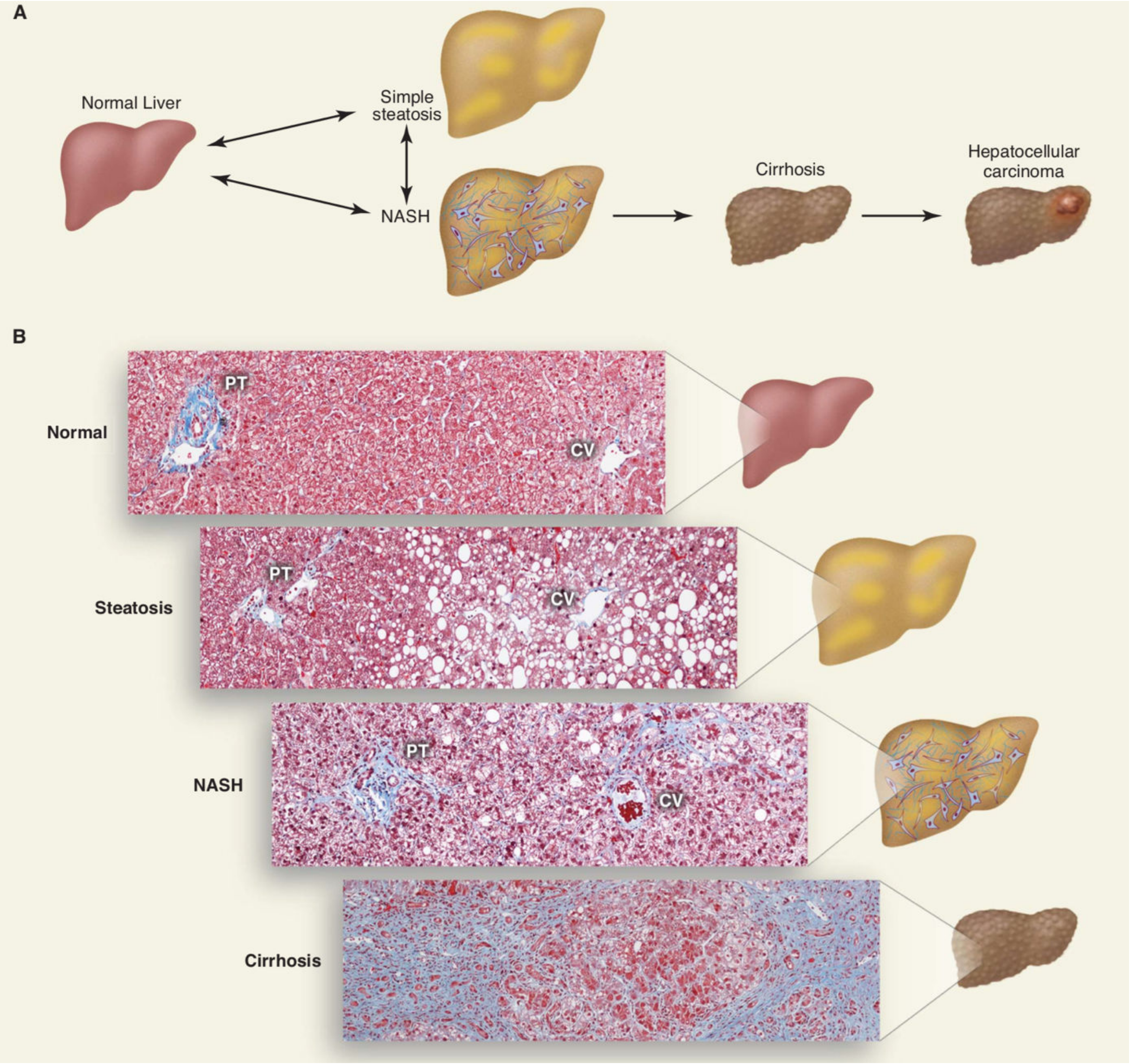
A
Normal Liver
Simple steatosis
NASH
Cirrhosis
Hepatocellular carcinoma
B
Normal
PT
CV
Steatosis
PT
CV
NASH
PT
CV
Cirrhosis

Figure 1: The pathological spectrum of NAFLD (From Cohen JC et al., *Science*, 2011) [25]. A: Schematic progression of NAFLD, cirrhosis and hepatocellular carcinoma. B: Histological progression of NAFLD and cirrhosis.

2. Epidemiology

Nonalcoholic fatty liver disease is an expanding health problem with an estimated global prevalence of 25% [26]. The prevalence of NAFLD can vary depending on the studied population and the definition used. In the United States, the number of NAFLD cases is projected to expand from 83 million in 2015, corresponding to about 25% of the population, to 100 million in 2030, corresponding to more than 33% of the population [27].

The estimated prevalence of NASH is 5% in the general population [13,15,28]. Most patients with NASH are asymptomatic without clinically relevant outcomes for decades but about 20% of NASH patients rapidly progress to advanced fibrosis and cirrhosis [29,30]. NASH is an increasingly relevant public health issue owing to its close association with the worldwide epidemics of diabetes and obesity and to population aging [17,27]. A recent modeling approach estimated that NASH cases in the United States will increase from 16 million in 2015 to 27 million in 2030, corresponding to 8% of the general population. In the NAFLD population, NASH will progress from 20% to 27% during this interval time [27]. Prevalence in the European Union follows similar trends [31]. Whereas NAFLD and NASH are typically accompanied by central obesity in Europe and the United States, there is a sizable percentage in Asia of patients with normal body mass index (BMI) who develop a "lean NASH" [32]. As mentioned above, a large percentage (between 35–50%) of hepatocellular cancers that arise in NASH setting occurs before cirrhosis when compared to incidence in other liver diseases [16–18,33]. NASH is thus a major public health issue due to its rising prevalence thus representing a growing economic burden [31].

3. Risk factors

a- Metabolic risk factors

Both increased age and metabolic comorbidities increase the occurrence and severity of NASH [14]. The metabolic syndrome is the strongest risk factor for NAFLD and NASH. As mentioned above, the metabolic syndrome is defined as a combination of cardiovascular risk factors that includes central obesity, hyperglycemia, dyslipidemia and arterial hypertension [1]. Among these risk factors, type 2 diabetes has the clearest biologic link to NAFLD progression. Up to 75% of patients with type 2 diabetes have NAFLD. Moreover, among patients with type 2 diabetes and NAFLD, the prevalence of NASH and advanced fibrosis is also increased compared to the prevalence in patients with NAFLD alone (without diabetes) [14]. Insulin resistance is a major feature in the pathogenesis of NAFLD [34]. Improving insulin resistance improves NASH but is not sufficient to attenuate the progression of the disease [14]. Furthermore, individuals with NAFLD are at higher risk to develop diabetes mellitus [35].

Systemic arterial hypertension is also closely linked to NAFLD and NASH. 50% of the patients with arterial hypertension have NAFLD [36] and hypertension is strongly associated with fibrosis. Hypertensive patients with NAFLD have a higher risk to fibrosis progression than patients without hypertension [30,37]. Moreover, the antagonism of the renin–angiotensin system, which contributes to hypertension, may improve liver fibrosis and NASH [38,39].

b- Genetic risk factors

Genetic risk factors that increase the risk of developing NASH have been identified [40]. The best characterized and the most strongly associated with NASH is the mutation in the *PNPLA3* gene that consists on a single nucleotide polymorphism in this gene which regulates lipolysis in hepatocytes [41,42]. PNPLA3 protein (Patatin-like phospholipase domain-containing protein 3) is a triacylglycerol lipase involved in triglycerides lipolysis through the mobilization of lipids from lipid droplets to direct them to the proteasome. PNPLA3-I148M variant consists on the substitution of a cytosine by a guanine that changes codon 148 from isoleucine to methionine [43]. PNPLA3-I148M variant is resistant to proteasomal degradation and escape from proteosomal degradation and accumulates in lipid droplets leading to disruptions in lipid lipolysis [44]. Interestingly, the risk of NASH in patients with this variant form is amplified when it coexists with adiposity, illustrating the additive effects of genetic and environmental drivers in this disease [45].

A genome-wide association study recently described in four independent cohorts of patients a splice variant in *HSD17B13* gene (HSD17B13 rs72613567:TA variant). This gene encodes the hepatic lipid droplet protein 17β-hydroxysteroid dehydrogenase type 13 which has an enzymatic activity on several bioactive lipid species involved in lipid-mediated inflammation. The mutation leads to a truncated and nonfunctional protein which is associated with a reduction of serum amino-transferase levels (AST and ALT), suggestive of a reduced liver injury and inflammation in patients with fatty liver, and a reduced risk for NASH and cirrhosis [46]. This suggests that the non-muted *HSD17B13* generates a product (still not identified) which promotes hepatocellular injury. Moreover, The HSD17B13 rs72613567:TA variant also reduces the risk of liver injury in individuals genetically predisposed to NAFLD by the PNPLA3-I148M variant. Interestingly, the HSD17B13 rs72613567:TA variant is associated with a decrease of *PNPLA3* mRNA expression [46]. Altogether, these data support a role for HSD17B13 in the progression from steatosis to NASH, fibrosis and cirrhosis.

Another variant in *TM6SF2* gene (a gene of unknown function) which encodes transmembrane 6 superfamily member 2 (TM6SF2) protein is also associated with NASH [43,47,48]. The Glu167LysTM6SF2 variant consists on a substitution of an adenine by a guanine in coding nucleotide 499 that substitutes a glutamate by a lysine at residue 167 of the protein. When transfected to hepatocytes in vitro, the Glu167LysTM6SF2 variant leads to 50% less protein production than wild-type TM6SF2 [43]. Glu167LysTM6SF2 variant is associated with higher ALT levels in humans and shRNA knockdown of *Tm6sf2* increases liver triglyceride content in mice [43]. Furthermore, TM6SF2 mutation has been associated with the severity of the disease [48]. In two histologically characterized cohorts encompassing steatosis, NASH, fibrosis and cirrhosis, TM6SF2 mutation has been associated with advanced liver fibrosis and cirrhosis, independently of confounding factors such as age, BMI or type 2 diabetes mellitus [47].

c- Other risk factors

Other risk factors are the age, the gender and the ethnicity [49]. The prevalence of NAFLD increases with age, and is higher among peoples between 40 and 65 years [50] but older individuals have significantly more metabolic risk factors. Studies have reported that the prevalence of NAFLD is higher in men than in women. Women of reproductive age are protected from NAFLD but the gender difference disappears after menopause suggesting a protective role of estrogens in the pathogenesis of the disease [49,51]. Finally, the prevalence of NAFLD varies with ethnicity since studies have found a higher prevalence in subjects from Hispanic origin in the United States while those from African origin appear to be protected from NAFLD despite the high rates of obesity and diabetes in this population [52]. This inter-ethnic heterogeneity cannot be attributed only to socio-economic, cultural or lifestyle differences and highlight the role of genetic factors.

4. Diagnosis

The diagnosis of NAFLD requires the exclusion of other causes of liver disease, such as excessive alcohol consumption, chronic hepatotoxic treatment or hepatitis (viral, autoimmune, drug), lipodystrophy, hemochromatosis or Wilson's disease and nutrition disorders (malnutrition, parenteral nutrition, rapid weight loss) [53,54].

Most patients with NASH are asymptomatic without clinically relevant outcomes for decades. A diagnosis of NASH can be considered when aminotransferases levels are elevated or when hepatic fat is detected with abdominal imaging.

The increase in transaminases levels is observed in approximately 50% of the patients with simple steatosis [54,55] and in 80% of the patients with NASH [56]. Nevertheless, a significant proportion of subjects can have normal transaminases [57]. It has been proposed that an AST/ALT ratio greater than 1.0 is suggestive of advanced fibrosis [58].

Steatosis can be identified noninvasively with imaging technics such as magnetic resonance imaging, ultrasound or computed tomography. Among these modalities, magnetic resonance imaging is the most sensitive since it can detect as little as 5% steatosis, but is at higher cost than other imaging tests. Ultrasound and computed tomography can detect steatosis when it is higher or equal to 20% of the liver mass.

The diagnosis of NASH, characterized by steatosis, hepatocellular injury, inflammation and eventual varying degrees of fibrosis, requires an invasive liver biopsy which can be used to histological analyses. Liver biopsy is actually the only way to firmly diagnose steatohepatitis. There are no approved noninvasive methods for the diagnosis of NASH but many biochemical markers have been proposed to estimate the presence of NASH such as liver enzymes (AST and ALT), markers of hepatocytes apoptosis (CK-18), cytokines and adipokines (TNFα, IL-6, adiponectin, adipocyte fatty acid binding proteins), serum prolidase enzyme activity, soluble receptor for advanced glycation end products and oxidative stress markers [54]. Promising serum biomarkers and imaging techniques are undergoing evaluation in clinical trials and may ultimately obviate the need of liver biopsy to establish a diagnosis of NASH [14].

Many histological scoring systems have been successively developed for the analysis of liver biopsies and for the classification of patients with NAFLD and NASH. Among these scoring systems, the NAS score (NAFLD activity score) has been proposed by the Nonalcoholic Steatohepatitis Clinical Research Network and consists on the summation of semiquantitative evaluation of steatosis, ballooning and lobular inflammation [59]. NAS score ranges from 0 to 8. A score below 3 excludes a diagnosis of NASH while a score higher than 4 confirms the presence of NASH. However, this score does not perfectly match with the diagnosis of NASH. Although extreme values are closely linked to the absence (NAS < 3) or the presence (NAS > 4) of NASH, a gray zone exists with intermediate values (2 < NAS < 5) [60].

Recently, the SAF score (Steatosis Activity Fibrosis) has been proposed to simplify the classification of liver lesions in patients with NAFLD [60]. The SAF score evaluates semi-quantitatively and separately steatosis, inflammatory activity (ballooning and lobular inflammation) and fibrosis [60]. In this system, steatosis score (S) assesses the quantities of large or medium-sized lipid droplets, from 0 to 3 (S0: <5%, no steatosis; S1: 5%-33%, mild steatosis; S2: 34%-66%, moderate steatosis; S3: >67%, marked steatosis). Activity grade (A, scored from 0 to 4) is defined as the addition of hepatocyte ballooning (0-2) and lobular inflammation (0-2). Fibrosis is assessed using the score described by NASH-CRN as follows: stage 0 (F0, no fibrosis); stage 1 (F1: 1a or 1b zone 3 perisinusoidal fibrosis or 1c portal fibrosis), stage 2 (F2: perisinusoidal and peri-portal fibrosis without bridging), stage 3 (F3: bridging fibrosis) and stage 4 (F4: cirrhosis) [59]. SAF score is a simple scoring system that dissociates grade of steatosis, activity and fibrosis stages. This scoring system seems more relevant than simply dichotomizing patients according to the absence or the presence of NASH since it can identify special subgroups of patients difficult to classify, such as those with steatosis and perisinusoidal fibrosis, without cell injuries or inflammation ($S_{\geq 1}A_0F_1$) or patients with inflammation and cell injuries without steatosis ($S_0A_{\geq 2}F_{any}$) [60]. The SAF score is therefore better than other scoring systems.

5. Pathogenesis

The pathogenesis of NASH and particularly how patients with simple steatosis progress to NASH and then to cirrhosis or cancer only in certain individuals is still incompletely understood [61–63]. A two-hit theory was proposed several years ago to explain the pathogenesis of NASH [64]. In this theory, the first hit constituted by steatosis, requires a second hit from other factors such as inflammation to initiates NASH development. This view is now outdated since it is not certain whether NASH is always preceded by steatosis, the pathogenic drivers are not identical among patients, the clinical manifestations are highly heterogeneous between patients and many molecular pathways contributing to NASH have been identified [14]. The pathogenesis of NASH is now considered as a "multi-hit" or multifactorial process [14].

a- Mechanisms of liver steatosis

Initially, steatosis occurs when the import or synthesis of lipids exceeds their export or their degradation. Normally, the liver eliminates excess lipids by β-oxidation or by exporting them as VLDL (very low-density lipoprotein). In conditions of chronic energy surplus, these adaptations are not sufficient to reduce fat accumulation in the liver and are switched towards triglycerides synthesis which are stored in lipid droplets [62]. The disposal of fatty acids in lipid droplets is an adaptive process to a supply of fatty acids that exceeds the capacity to metabolize them [65].

Free fatty acids (FFA) play a major role in the pathogenesis of NASH. The main sources of fatty acids in the liver are plasma FFA arriving from dietary fatty acids and from the adipose tissue. Metabolic and inflammatory events in the adipose tissue can drive the pathogenesis of NASH since FFA, adipokines and adipocytokines can reach the liver through the portal blood flow [14,66]. The second major source of free fatty acids in the liver is the hepatic *de novo* lipogenesis from glucose and fructose [14,62,67]. The third source of FFA is the breakdown of lipid droplets. PNPLA3 is involved in this lipolytic step, and, as stated above, the PNPLA3-I148M variant is strongly associated with the progression of NASH since it is associated with lipolysis abnormalities (see paragraph III-A-3: risk factors) [14,41,42] (Figure 2).

Chronic exposure of the liver to fatty acids stimulates in turn the synthesis of triglycerides in hepatocytes [67]. Insulin resistance and hyperinsulinemia in individuals with metabolic syndrome (typically in obese and diabetic individuals), favor both lipid uptake and synthesis leading to a progressive accumulation of lipids in the liver. The ability of the liver to regulate fat metabolism becomes exceeded in this setting leading to the accumulation of toxic lipid species (lipotoxicity) that initiates NASH progression [68,69] (Figure 2). In turn, hepatic fat accumulation exacerbates insulin resistance and hyperinsulinemia [70] which exacerbates fat accumulation in the liver [71] and promotes inflammatory [72], fibrogenic [73] and mitogenic responses that can be carcinogenic [71] (Figure 2).

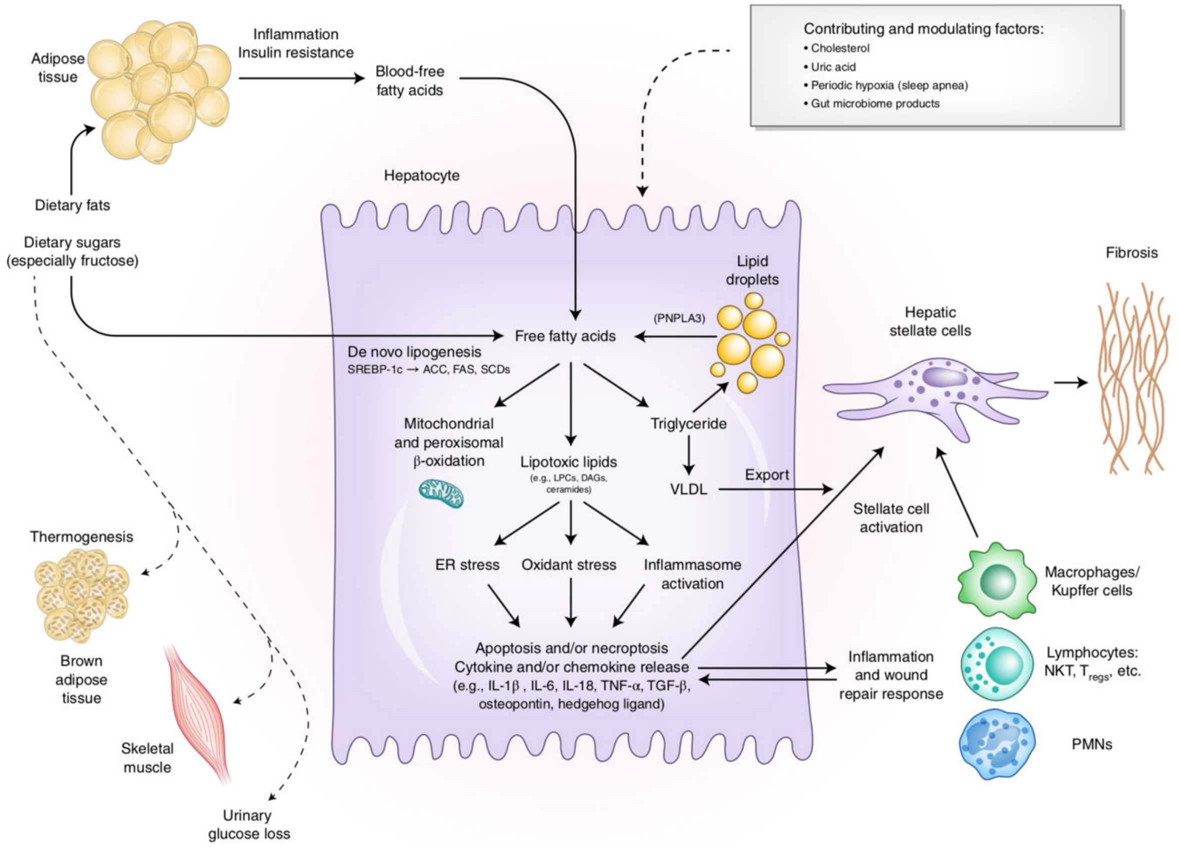
Adipose tissue
Inflammation
Insulin resistance
Blood-free fatty acids
Contributing and modulating factors:
• Cholesterol
• Uric acid
• Periodic hypoxia (sleep apnea)
• Gut microbiome products
Hepatocyte
Dietary fats
Dietary sugars (especially fructose)
Lipid droplets
(PNPLA3)
Free fatty acids
De novo lipogenesis
SREBP-1c → ACC, FAS, SCDs
Mitochondrial and peroxisomal β-oxidation
Lipotoxic lipids
(e.g., LPCs, DAGs, ceramides)
Triglyceride
VLDL
Export
ER stress
Oxidant stress
Inflammasome activation
Apoptosis and/or necroptosis
Cytokine and/or chemokine release
(e.g., IL-1β , IL-6, IL-18, TNF-α, TGF-β, osteopontin, hedgehog ligand)
Thermogenesis
Brown adipose tissue
Skeletal muscle
Urinary glucose loss
Fibrosis
Hepatic stellate cells
Stellate cell activation
Inflammation and wound repair response
Macrophages/ Kupffer cells
Lymphocytes: NKT, T_regs, etc.
PMNs

Figure 2: Lipotoxicity and liver injury in the pathogenesis of NASH (From Friedman SL et al., *Nature Medicine*, 2018) [14]

b- Lipotoxicity and oxidative stress

At least three major events are involved in the progression of fatty liver to NASH, including lipotoxicity, oxidative stress associated with the overproduction of reactive oxygen species (ROS), and increased release of pro-inflammatory and pro-fibrogenic mediators [74,75].

Lipotoxicity is defined as the dysregulation of the lipid environment or intracellular lipid content/composition that leads to the accumulation of toxic lipids which in turn induces organelle dysfunction, cellular injury and cell death [76]. Lipotoxicity is intimately linked to liver inflammation which is a main feature distinguishing NASH from NAFL. In NASH, lipotoxicity is in part related to visceral adipose tissue and its secretory products. Abnormal visceral adipose tissue function, primarily due to obesity, amplifies the release of adipocytokines from fatty tissue, which can lead to systemic effects, such as low-grade systemic inflammation and an altered metabolic state with insulin resistance. The increased lipid content in visceral adipose tissue enhances FFA delivery from the adipocytes into the liver, impairing the hepatic lipid content and promoting hepatic insulin resistance and hepatocyte apoptosis [77–79].

Lipotoxicity can result in oxidative stress through diverse mechanisms. Mitochondrial and peroxisomal fatty acid oxidation generate ROS thus favoring the vulnerability of hepatocytes to other factors [74,80]. Damaged mitochondria fail to metabolize fatty acids efficiently which accumulate in these organelles [81]. Accumulation of fatty acids within mitochondria makes them more vulnerable to other factors, such as TNFα, that promotes mitochondrial damages and the release of mitochondrial apoptotic factors [82]. Damaged mitochondria also fail to produce ATP thus promoting cellular necrosis [83].

Changes in cell signaling are also induced and associated with lipotoxicity. Indeed, fatty acids interact with innate immune receptors such as TLRs (Toll-like receptors) and transcription factors thus inducing changes in signaling pathways that regulate metabolism and inflammation [84–86]. This disrupts hepatocyte metabolic homeostasis and potentiate liver cell injury and death [68,87] which is a key feature of NASH that distinguishes it from NAFL [88]. Lipotoxicity also induces endoplasmic reticulum stress [89] and impairs autophagy in hepatocytes (lipophagy specifically which is the ability to regulate lipid content via autophagy) [87,90].

NAFLD also includes alterations in carbohydrate metabolism which contribute to the pathogenesis of NASH through glucotoxicity [76]. Excess carbohydrates activate lipogenic pathways that stimulates *de novo* lipogenesis thus contributing to steatosis [91].

Lipotoxicity also acts on hepatic non-parenchymal cells including Kupffer cells, hepatic stellate cells, cholangiocytes and liver sinusoidal endothelial cells (LSECs) [76,92]. FFA activate macrophages after binding to TLRs (TLR2 and TLR4) thus inhibiting insulin-like growth factor binding protein-3 which acts as an anti-inflammatory feedback [93]. Interestingly, Kupffer cell depletion inhibits steatosis [94] suggesting that liver inflammation should be considered as a consequence and a causative trigger for steatosis [94,95]. In hepatic stellate cells, lipotoxicity sensitizes them to TGF-β, a potent fibrogenic factors, *via* increased TLR4 signaling [96]. In cholangiocytes, lipotoxicity induces apoptosis via pathways involving FOXO3 and PUMA [97]. LSECs are main targets of lipotoxicity since they are among the first liver cells in contact with products derived from the visceral adipose tissue including fatty acids, adipokines and adipocytokines. The lipotoxic response of LSECs will be discussed later (see paragraph III-B-2: role of liver LSECs in NASH).

Lysosomal pathways are also affected in NAFLD. Excess FFA exposure induces the release of cathepsin B from the lysosomal membrane to cytosol which is involved in mitochondrial dysfunction and apoptosis [98]. Lysosomal function can also generate ER stress thus promoting apoptosis [99].

Oxidative stress results from elevated ROS levels during NAFLD and NASH. Higher ROS levels could be explained by different mechanisms related to organelles dysfunction. Interestingly, liver mitochondria of patients with NAFLD display abnormalities [74]. First, mitochondrial and peroxisomal fatty acids β-oxidation generate ROS that may be toxic by themselves or indirectly by depleting cellular antioxidant reserves. Indeed, enhancement of the mitochondrial fatty acid β-oxidation induces ROS overproduction if it is not accompanied with an up-regulation of the activity of the mitochondrial respiratory chain. Peroxisomal fatty acids oxidation is enhanced in NAFLD and constitutes the first enzymatic step that produces H2O2 [74]. Secondly, CYP2E1, which is an enzyme located in mitochondria and endoplasmic reticulum that produces ROS and affects mitochondrial function, is induced in NAFLD [100]. Thirdly, the reduction of ROS detoxification favors oxidative stress. Fourth, decreased expression and/or activity of antioxidant enzymes such as superoxide dismutase can occur at the mitochondrial level thus promoting oxidative stress [74]. Fifthly, high glucose levels promote ROS production in hepatocytes [101]. Finally, another source of ROS may be attributed to the higher hepatic expression of the inducible nitric oxide synthase (iNOS) during NAFLD as a consequence of TNFα overproduction by activated cells. Nitric oxide can react with superoxide anions to generate reactive nitrogen species, that perpetuate oxidative stress and impairs mitochondrial function [74].

c- Mechanisms of liver inflammation

Liver injury result in wound-healing responses to replace dying hepatocytes [102]. Among these processes, inflammation, which includes the activation of resident immune cells (Kupffer cells) and the recruitment of bone marrow-derived inflammatory cells from the bloodstream, fibrogenesis (matrix remodeling), angiogenesis, and the mobilization of liver progenitor cells [103] (Figure 3).

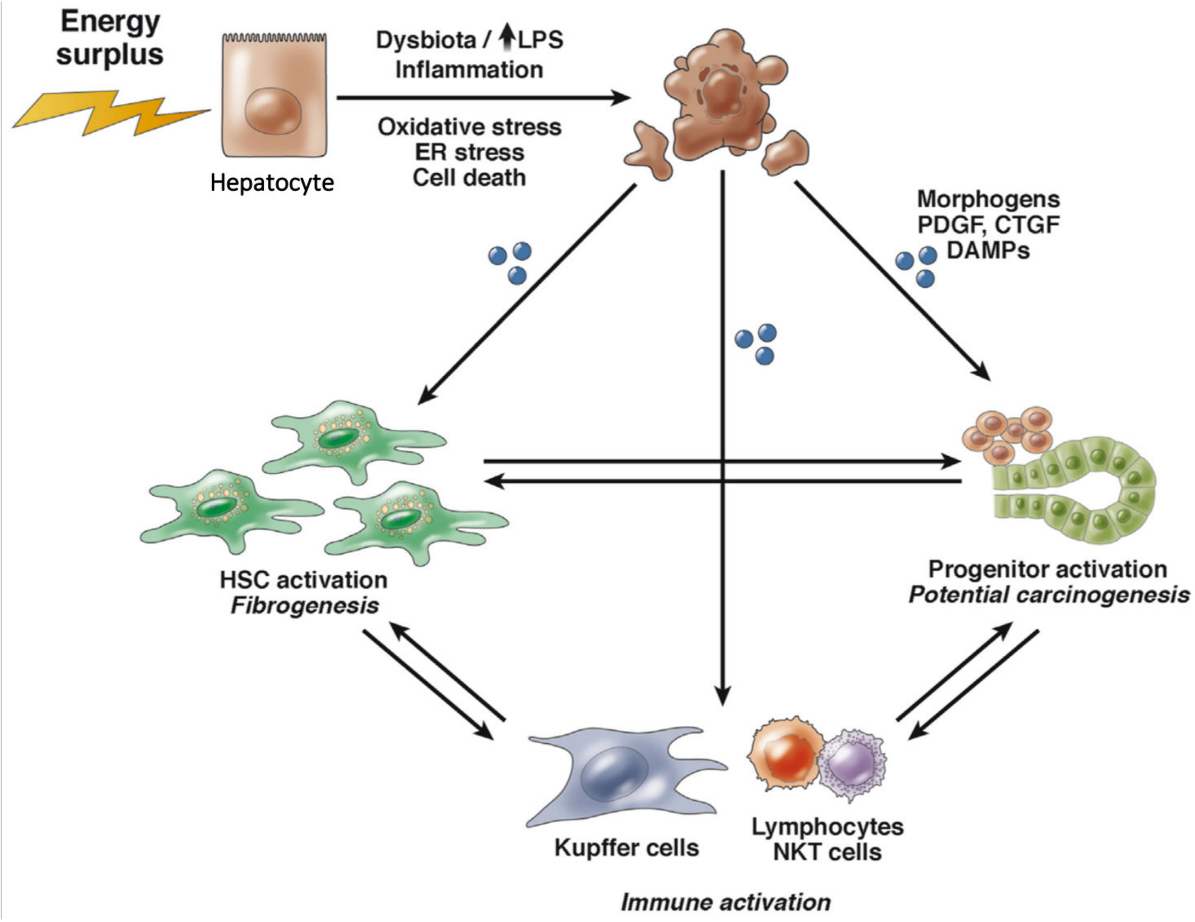
Energy surplus
Hepatocyte
Dysbiota / ↑LPS
Inflammation
Oxidative stress
ER stress
Cell death
Morphogens
PDGF, CTGF
DAMPs
HSC activation
Fibrogenesis
Progenitor activation
Potential carcinogenesis
Kupffer cells
Lymphocytes
NKT cells
Immune activation

Figure 3: Lipotoxicity and NASH pathogenesis (Adapted from Machado and Diehl, *Gastroenterology*, 2016) [62]

Liver inflammation can result at least from three major components including the metabolic/inflammatory events occurring in the adipose tissue, the hepatic inflammatory response to lipotoxicity, and the gut microbiota derived products.

First, metabolic and inflammatory events in the adipose tissue contribute to liver inflammation through FFA and adipocytokines, such as TNFα and IL-6, which reach the liver *via* the portal venous blood, and activate inflammatory cells in the liver [104].

Second, lipotoxicity-induced hepatocellular injury directly results in inflammasome activation in the liver [105]. Inflammasome is a multiprotein complex that responds to DAMPs (damaged-associated molecular patterns) including fatty acids, and PAMPs (pathogen-associated molecular protein) including products derived from the gut microbiota [14,106]. Inflammasome activation in the liver links the initial metabolic stress and subsequent inflammatory responses and fibrogenesis in NASH [106]. Hepatic inflammasome activation leads to inflammatory cytokines production, such as IL-1β, TNFα and IL-6, and promotes apoptosis through caspase-1 activation [14].

Injured hepatocytes in stressful conditions (oxidative stress, endoplasmic reticulum stress and apoptosis) release signaling molecules to neighboring cells (Figure 3). These signaling molecules include cytokines, DAMPs, microRNAs and Hedghog molecules [62,107]. Hedgehog signaling is a key pathway involved in NASH. While hepatocytes in healthy livers do not express detectable levels of sonic hedgehog, stressed hepatocytes rapidly up-regulate sonic hedgehog mRNA and protein [108]. Hedgehog molecules can be released directly in the extracellular environment or incorporated and released into extracellular vesicles such as exosomes [109] that signal to other hepatocytes, Kupffer cells, hepatic stellate cells, and LSECs [110–114] (Figure 4). For example, hedgehog signaling induces expression of TGF-β by hepatic stellate cells [62] and stimulates LSECs to produce vascular endothelial growth factor (VEGF) which promotes angiogenesis [114]. These hepatic non-parenchymal cells have been shown to be both Hedgehog-producing and Hedgehog sensitive cells depending on their activation state, and to participate to liver inflammation and fibrosis [109,114–116].

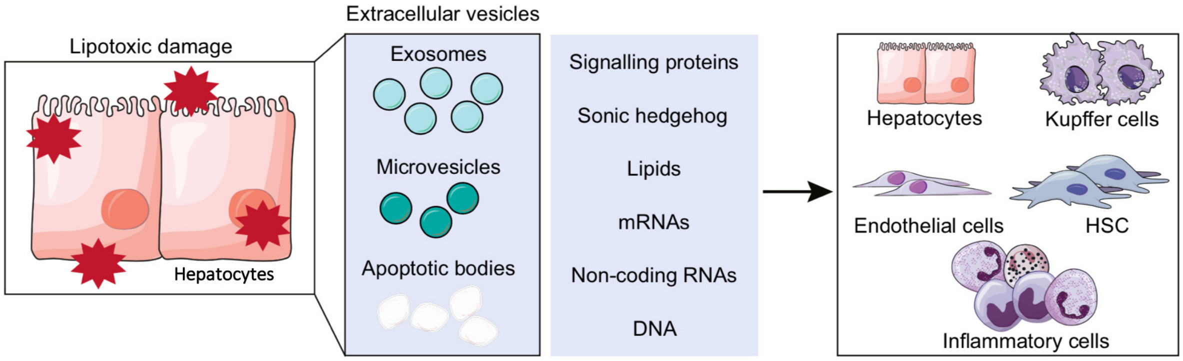
Lipotoxic damage
Hepatocytes
Extracellular vesicles
Exosomes
Microvesicles
Apoptotic bodies
Signalling proteins
Sonic hedgehog
Lipids
mRNAs
Non-coding RNAs
DNA
Hepatocytes
Kupffer cells
Endothelial cells
HSC
Inflammatory cells

Figure 4: Intercellular communications in the pathogenesis of NASH (Adapted from Marra F et al., *Journal of Hepatology*, 2017) [76]

Finally, recent evidences point toward another tissue, the gastrointestinal tract, as a source for liver inflammation [76] (Figure 5). Gut microbiota is defined as the complex of microorganisms harbored by each individual in the gut [76] that contribute to digestion, vitamin synthesis, resistance of the intestine to pathogens infection, regulation of intestinal homeostasis and metabolic functions [117]. Normal gut microbiota confers several physiologic benefits to the host but its composition can be influenced by several factors such as ageing, diet and antibiotic use leading to dysbiosis [118] which is an additional risk factor for NAFLD and NASH. Diet-induced dysbiosis has been demonstrated in humans and rodents and decreased microbial diversity and complexity correlates with obesity and NAFLD [117,119]. However, studies failed to define a clear microbial signature and to correlate it with NASH stages and disease progression [76].

Apart from altered gut microbiota during obesity, studies have shown intestinal barrier alterations and increased intestinal permeability during NASH, leading to bacterial translocation and increased levels of bacterial products such as lipopolysaccharide (LPS) and unmethylated CpG DNA [120]. These gut-derived bacterial products as well as bacterial translocation into the portal circulation is a major mechanism linking gut dysbiosis with NASH since it can activate the immune system in the liver via pro-inflammatory signaling pathways after binding to TLRs [121–123]. Intracellular signaling mediated by TLRs activation induces the secretion of inflammatory cytokines involved in liver injury and inflammation [124]. In addition to LPS, gut microbiota can expose the liver to endogenous ethanol. Indeed, ethanol-producing bacteria in the gut and blood ethanol concentrations are increased in patients with NASH when compared to healthy controls and to patients with NAFL. This suggests a role of alcohol-producing microbiota in NASH pathogenesis [125].

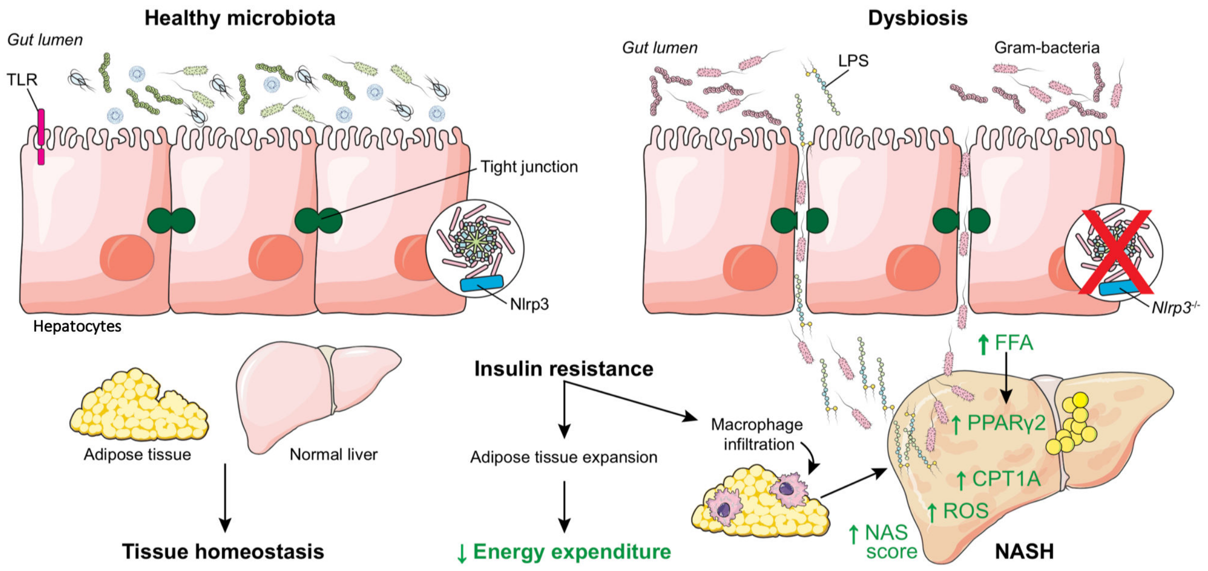
Healthy microbiota
Gut lumen
TLR
Tight junction
Nlrp3
Hepatocytes
Adipose tissue
Normal liver
Tissue homeostasis
Insulin resistance
Adipose tissue expansion
↓ Energy expenditure
Dysbiosis
Gut lumen
LPS
Gram-bacteria
Nlrp3-/-
↑ FFA
↑ PPARγ2
↑ CPT1A
↑ ROS
↑ NAS score
Macrophage infiltration
NASH

Figure 5: Role of the gut microbiota in the pathogenesis of NASH (Adapted from Marra F et al., *Journal of Hepatology*, 2017) [76]

d- Mechanisms of liver fibrosis

Liver fibrosis is defined as the excessive deposition of extracellular matrix in the liver parenchyma as a result of a long-standing wound healing process caused by hepatocellular injury and inflammation. Sustained hepatic inflammation resulting from liver injury is a major driving force for fibrosis progression. Distinct subsets of innate (macrophages, dendritic cells), adaptive (B cells and T cells) and innate lymphoid cells regulate the fibrogenic process [126]. However, excessive wound-healing responses can be harmful by inducing the progressive replacement of liver parenchyma by scar tissue (cirrhosis) and/or promoting liver cancer carcinogenesis (hepatocellular carcinoma) [62]. Fibrosis is the major cause of liver-related death in patients with NAFLD [14].

Liver fibrosis is mediated by the activation of resident hepatic stellate cells. HSCs, originally described by von Kupffer in 1876, are localized in the space of Disse, interposed between liver sinusoidal endothelial cells (LSECs) and hepatocytes, and represent about 10% of all resident liver cells. In physiological conditions, hepatic stellate cells maintain a quiescent non-proliferative phenotype and store retinoids such as vitamin A. In pathological conditions, hepatic stellate cells switch their phenotype to an activated myofibroblastic state. Activated hepatic stellate cells express smooth muscle α-actin (α-SMA), exhibits high proliferative activity, are motile and contractile, and produce proinflammatory and profibrogenic mediators, extracellular matrix proteins and inhibitors of matrix degradation enzymes [62,127]. Interestingly, a recent study showed that PNPLA3-I148M variant expression in hepatic stellate cells can modulate the fibrogenic process by acting directly on hepatic stellate cells activation. PNPLA3-I148M is expressed in hepatic stellate cells during the early phases of their activation and remains elevated in fully activated hepatic stellate cells. This variant potentiates the profibrogenic features of hepatic stellate cells, providing a molecular mechanism for the higher risk of progression and severity of liver diseases conferred to patients carrying this mutation [42]. Several fibrogenic and proliferative cytokines regulating hepatic stellate cells activation have been identified such as transforming growth factor-β (TGF-β), platelet derived growth factor (PDGF), vascular endothelial growth factor (VEGF) and connective tissue growth factor (CTGF) [127]. The extracellular stimuli of hepatic stellate cells activation are derived from a number of cell types in the liver including hepatocytes, liver sinusoidal endothelial cells (LSECs), macrophages, natural killers (NK) and NKT cells, B cells and platelets [127].

TGF-β is considered as the most potent fibrogenic cytokine and is released by several cell populations in the liver in a latent form [128]. TGF-β binds to TGF-β type 1 receptor in hepatic stellate cells. Its binding induces TGF-βR1 phosphorylation which induces the phosphorylation of downstream SMAD3. Activation of SMAD3 during hepatic stellate cells activation promotes transcription of collagen [129]. TGF-β also activates mitogen-activated protein kinase (MAPK) signaling pathways, including extracellular signal regulated kinase (ERK), p38 and c-jun *N*-terminal kinase (JNK), to promote hepatic stellate cells activation. PDGF drives hepatic stellate cells proliferation and migration after its binding to PDGFR-β. VEGF induces the proliferation of hepatic stellate cells [127]. CTGF is a potent fibrogenic cytokine expressed at low level in normal liver but it is highly upregulated in fibrotic liver. CTGF contributes to proliferation, migration, adhesion and survival of hepatic stellate cells as well as to extracellular matrix production [130].

Other pathways regulating hepatic stellate cells activation include Hedgehog signaling pathway and the interaction with extracellular matrix [127]. Hepatic stellate cells express two types of collagen receptors, integrins and discoidin domaincontaining receptors

(DDRs). Each type receives signals from extracellular matrix components to regulate cell adhesion, differentiation, proliferation and migration [131,132]. Integrins can control the release and activation of TGF-β. Integrin-β1 also regulates the profibrogenic phenotype of activated hepatic stellate cells through the serine/threonine protein kinase PAK1 and yes-associated protein 1 (YAP1) [133]. DDRs are tyrosine kinases receptor that signal in response to triple helical collagen [127].

6. Treatments

As mentioned above, there is no approved therapy for NASH despite its prevalence and severity. Available treatments only aim to control metabolic disorders associated with NASH. The correction of metabolic syndrome factors, including overweight, hyperlipidemia, hypertension and type 2 diabetes, should be approached as a multidisciplinary process that involves several medical specialists (endocrinologists, nutritionists and cardiologists). Two complementary therapeutic approaches may be considered for the management of NASH. The first one is a non-pharmacological approach based on lifestyle changes and the second one requires the use of medication.

a. Non-pharmacological approaches

- Diet and exercise

Non-pharmacological approaches are based on lifestyles changes. It is now admitted that a weight loss of 5 to 7% from the initial body weight has a significant effect on steatosis and the severity of NASH [134]. A randomized study showed an improvement in NAS scores when weight loss was greater than 7% [135]. Insulin resistance is also improved by physical activity. A study has shown that 6 months of moderate exercise without weight loss improves insulin resistance in the adipose tissue and the liver [136]. However, this first therapeutic line combining diet and physical exercise programs, remains very heterogeneous and its efficiency has yet to be determined in the long term, given the low compliance of patients with this approach [134].

- Bariatric surgery

Bariatric surgery is the most powerful and effective treatment for achieving significant and sustained weight loss in morbidly obese patients [137]. Recent studies point to its high therapeutic potential in NASH [138]. The Swedish Obese Subjects study showed an improvement of aminotransferases levels that persists up after 10 years following the bariatric surgery [139]. Prospective studies have reported histological improvement of NASH without fibrosis worsening in large cohorts of patients [138,140–142]. In the last study, resolution of NASH occurred in 85% of patients subjected to the surgery [138].

b. Pharmacological approaches

- Insulin-sensitizers

The use of low-hepatotoxic drugs is needed when non-pharmacological approach fails to correct metabolic factors. For example, Metformin is a biguanide that decreases intrahepatic glucose production and increases its peripheral combustion. A controlled study conducted on a low number of patients over 6 months showed an improvement in glucose and lipid parameters but it did not improve aminotransferases or liver histology [143]. Glitazones improve insulin-resistance in adipocytes, induce adiponectin which exhibits anti-steatogenic effects [144]. Controlled studies using pioglitazone showed a decrease in steatosis, ALT levels and necro-inflammatory lesions without effect on fibrosis [145,146]. However, their tolerance profile is unsatisfactory [144].

- New anti-diabetics

Glucagon-like peptide 1 (GLP1) is an incretin released by the small intestine that decreases hepatic glucose production, induces satiety by delaying gastric emptying, and has cardioprotective effects. GLP1 analogues have been tested in NASH. Armstrong and colleagues have recently shown in a randomized, double-blind study in 52 patients that liraglutide improves body weight, gamma GT and histological features of NASH and improves key metabolic risk factors such as body weight and BMI, glucose level and HDL cholesterol. However, this drug had significant digestive side effects such as anorexia, diarrhea and nausea [147].

GLP-1 has a very short half-life (less than 2 minutes) due to its degradation by dipeptidyl peptidase 4 (DPP4). DPP4 inhibitors, such as exenatide [148] and sitagliptin [149] are attractive tools for the treatments of NASH [150].

- Hepatoprotective agents

Chronic oxidative stress in the liver is one of the main mechanisms involved in the progression from NAFL to NASH *via* the production of ROS. Vitamin E reduces oxidative stress and has been shown to significantly improve steatosis, ballooning and liver inflammation [145].

- Probiotics and prebiotics

Recent evidences point toward altered gut microbiota in the pathogenesis of NASH [76]. The use of probiotics (live micro-organisms that have positive effects on health when administered) or prebiotics (food substances that induce the growth of certain probiotic bacteria) to treat dysbiosis is thus an attractive therapeutic strategy in NASH. A recent meta-analysis has shown that the use of probiotics such as Lactobacillus, Bifidobacterium, Streptococcus and VSL#3 reduces the intestinal permeability and endotoxemia [151]. These probiotics also reduce aminotransferases levels, insulin resistance and blood cholesterol in patients with NAFLD [152,153].

c. Future therapeutic drugs

- Farnesoid X Receptor (FXR) Agonists

Bile acids synthesis requires nuclear hormone receptors such as FXR and TGR5 that have a role in carbohydrates and lipids metabolism. FXR activation improves insulin resistance, fatty acid oxidation and decreases hepatic inflammation [154]. A large study in 229 patients receiving the FXR selective agonist, obeticholic acid, for 72 weeks showed an improvement in histological features of NASH [155]. However, side effects have been reported such as severe pruritus observed in 17% of the patients in this study and increased LDL cholesterol levels [155]. Phase I studies with other FXR agonists, such as Px-102, are ongoing [156].

- Peroxisome proliferator-activated receptor (PPAR) alpha and delta agonists

The different isoforms of the PPARs nuclear receptors regulate the expression of genes involved in glucose and lipid homeostasis: PPAR-α is involved in fatty acids oxidation, PPAR-γ is involved in the storage of triglycerides and inflammatory signaling and PPAR-δ is involved in lipid homeostasis [157]. PPAR-δ activation induces hepatoprotective effects by improving hepatic metabolism, inflammation and fibrosis [157,158]. Elafibranor, a PPAR-α and -δ agonist, has been shown to induce resolution of NASH in patients with a NAS score ≥ 4, without fibrosis worsening [159]. The PPAR-α component increases fatty acid oxidation, whereas the PPAR-δ component has anti-inflammatory effects. The good tolerance of this molecule associated with the improvement of cardiovascular risk factors (insulin resistance, triglycerides, cholestérol) allowed a phase III study for this molecule. Other PPAR agonist molecules showing efficacy in mice are emerging [156].

- Immune targets

Cytokines and inflammatory cells are involved in the pathogenesis of NASH. The C–C motif chemokine receptor 2 (CCR2)–CCR5 chemokine axis amplifies the innate immune response in the liver and links inflammation and fibrosis since it is involved in hepatic stellate cells activation. Inhibition of the CCR2–CCR5 axis with Cenicriviroc (AURORA) reduces short-term fibrosis progression as assessed in a clinical trial of NASH. However, after 2 years of administration, the mean fibrosis stage was not significantly different from that of patients on placebo [160]. This molecule is also being evaluated in a phase 3 trial.

B. Role of liver sinusoidal endothelial cells in nonalcoholic fatty liver disease

1. Liver sinusoidal endothelial cells (LSECs)

Liver sinusoids are a highly differentiated vascular bed lined by specialized endothelial cells that have key physiological roles in endocytosis, immune function, and the rapid transfer of substrates between blood and hepatocytes. Liver sinusoidal endothelial cells are the most abundant non-parenchymal cells in the liver LSECs are perforated with numerous transcellular pores, called fenestrae, and are not associated with basement membrane [161,162]. Fenestrae are clustered in groups and have been termed sieve plates. Fenestration patterns vary across the liver lobule, with larger but fewer fenestrae per sieve plate in the periportal region and smaller but more numerous fenestrae per sieve plate in the centrilobular region [163]. Porosity, the amount of LSECs surface occupied by fenestrae, is twice higher in the centrilobular region than in the periportal region [163]. LSECs regulate the transport of macromolecules between the blood and liver parenchyma including lipids and lipoproteins through *fenestrae*.

LSECs are at the interface between the blood derived from the visceral adipose tissue and the gut on the one side, and hepatic stellate cells and hepatocytes on the other side. LSECs closely communicate with these cells. This intercellular communication is important for both LSECs and neighboring cells homeostasis [162]. For example, VEGF derived from adjacent hepatocytes and hepatic stellate cells is crucial for the maintenance of fenestrae and nitric oxide secreted by LSECs maintains hepatic stellate cells quiescence [163].

LSECs display high endocytic capacity and play a prominent role in the regulation of whole liver homeostasis [164]. Accordingly, in the liver, not only Kupffer cells but also LSECs are involved in waste clearance and these cells seem to complement each other. LSECs represent the professional pinocyting cells, clearing the blood from soluble macromolecules and small particles, while macrophages eliminate larger, insoluble particles by phagocytosis [165].

LSECs undergo significant structural changes with aging that have been termed pseudocapillarization and observed in humans, nonhuman primates, rats, and old aged mice [166,167]. Pseudocapillarization includes a marked reduction in fenestrae, an increase in endothelial thickness and altered expression of endothelial and extracellular matrix proteins among which von Willebrand factor and collagen [166,167]. The structure and function of LSECs are closely linked as defenestration is the first phenotypic marker of LSECs dysfunction [168].

Current view of the pathogenesis of NASH centers on the response of hepatocytes to insulin resistance and lipotoxicity, immune system and hepatic stellate cell activation being regarded as secondary events [14]. The vascular endothelium, representing the interface between the blood and the other tissues of the body, is not only a physical barrier but is implicated in different physiological roles, such as hemostasis, metabolites transportation, inflammation, thrombosis, angiogenesis and vascular tone [169]. The following sections will specifically focus on the role of LSECs in the pathophysiology of NAFLD and its progression to NASH, cirrhosis and hepatocellular carcinoma.

2. Role of LSECs in simple steatosis

- *Role of LSECs in lipid transfer in normal conditions*

Dietary lipids present in the circulation have to be transported through the vascular endothelium to be metabolized by tissues. In physiological conditions, LSECs are major regulators of the bidirectional lipid exchange between the blood and the liver parenchyma in two manners. LSECs *fenestrae* allow for efficient transfer of lipoproteins, small chylomicron remnants and other macromolecules, from the sinusoidal blood to the space of Disse, where they are taken up by hepatocytes [170–172]. Old studies using radiolabeled lipoproteins showed that small chylomicron remnants cross over the liver sieve while larger lipoproteins remains in the lumen of the sinusoid [173]. This primary role of endothelial cells in lipid transfer is also illustrated by the observation that mice deficient in VEGF-B, a key regulator of endothelial cell functions, show less accumulation of labeled oleic acid in the liver and in other organs (heart and muscles) than wild type mice, resulting in obesity since lipids that do not pass the endothelium accumulates in the adipose tissue [174]. Although this study was not focused on the liver and liver endothelial cells, it nicely illustrates the crucial role of LSECs in the uptake of fatty acids in physiology. Indeed, previous studies showed that LSECs lose their *fenestrae* when VEGF pathway is disrupted [168,172,175] thus impairing the uptake of fluorescently labelled chylomicron remnants [172]. LSECs also regulate lipid transfer through their high endocytosis capacity as attested by their high ability to rapidly uptake oxidized or acetylated low density lipoproteins [162,176,177].

- *LSECs capillarization occurs early in NAFLD and promotes steatosis*

LSECs undergo morphological and functional changes during liver steatosis. One of the most remarkable phenotypic changes is the loss of *fenestrae*, also called defenestration or sinusoidal capillarization, associated with the formation of a basement membrane on the abluminal surface of LSECs. Several independent groups reported that sinusoidal capillarization appears very early in NAFLD. Indeed, short-term exposure to a high-fat diet (3 weeks) impairs the morphology of *fenestrae* in rats [178]. Miyao and colleagues also demonstrated that defenestration begins after 1 week of choline-deficient, L-amino acid-defined diet in mice [179]. Cogger and coworkers demonstrated in mice challenged with several diets varying in content of macronutrients and energy that LSECs porosity and *fenestrae* frequency are inversely correlated with dietary fat intake while *fenestrae* diameter is inversely correlated with protein or carbohydrate intake [180]. In this study, the authors also demonstrated a negative correlation between LSECs *fenestrae* (frequency, porosity and diameter) and circulating free fatty acids (FFA) levels [180]. The triggers of sinusoidal capillarization are not fully identified, but we can speculate that excessive dietary macronutrients, including lipids and carbohydrates, could be responsible for this [180]. This view is supported by *in vitro* studies suggesting that defenestration occurs following excessive lipids exposition. For instance, exposure of human primary LSECs with oxidized LDL (ox-LDL) reduces the diameter and the porosity of the *fenestrae* [181]. Another *in vitro* study showed that addition of FFA in the culture medium (a mixture of saturated and unsaturated FFA) maintained *fenestrae* in rat primary LSECs until 5 days, while LSECs cultivated in FFA free medium lose their *fenestrae* [182]. Nevertheless, FFA alone does not maintain *fenestrae* at normal levels. Only about 5% of all FFA-treated cells expressed *fenestrae* in sieve plates and many of them presented large transcytotic pores (>1μm diameter while *fenestrae* measure about 150ηm in diameter [161]). Primary LSECs are difficult to maintain in a differentiated state in culture for scientific studies [161,162] and it seems difficult to extrapolate these *in vitro* results to the *in vivo* observations since FFA acids concentrations and composition depends on the metabolic state [183] and other factors, in addition to lipids, could be involved in NAFLD setting. Recent evidences point toward the gut microbiota in the pathogenesis of NAFLD. Cogger and colleagues showed that LSECs *fenestrae* were inversely correlated with the abundance of *Bacteroidetes* in the gut and positively correlated with the abundance of *Firmicutes* [180]. Moreover, it has been shown that a single injection of endotoxin in rats induces a decrease in both diameter and number of fenestrae [184] suggesting that gut microbiota-derived products may contribute to LSECs capillarization.

In turn, capillarization impacts on liver steatosis (Figure 1). Plasmalemma vesicle-associated protein (PLVAP) is an endothelial-specific integral membrane glycoprotein required for the formation of endothelial *fenestrae* [185]. PLVAP deficient mice exhibit a pronounced reduction in the number of LSECs *fenestrae,* associated with a decrease in the sinusoidal permeability [185]. Herrnberger and collaborators demonstrated that the lack of sinusoidal *fenestrae* causes pronounced microvesicular steatosis in 10 days old breastfeeding mice. In three weeks old *Plvap*$^{-/-}$ mice, livers spontaneously develop extensive multivesicular steatosis [185]. These mice also had hyperlipoproteinemia, and hypertriglyceridemia. A first hypothesis explaining this consequence of capillarization on steatosis could be the fact that reduced LSECs permeability impairs the passage of hepatocytes-derived very low-density lipoprotein toward the sinusoidal lumen thus inducing cholesterol retention in the liver. However, these lipoproteins may escape from the liver through the lymphatic system [186]. An alternative explanation could be that LSECs capillarization might impair lipid metabolism in hepatocytes since very low-density lipoprotein synthesis in the liver require triglycerides which in part derive from chylomicron remnants derived from the blood. The impairment of the passage of chylomicron remnants from sinusoidal blood to hepatocytes [172,185] might in turn stimulate hepatic *de novo* lipogenesis as a compensatory mechanism thus inducing steatosis. Moreover, chylomicron remnants and their dietary cholesterol will no longer pass the sieve to inhibit HMGCoA reductase and the synthesis of cholesterol in hepatocytes [187].

Taken together, these data suggest that features of metabolic syndrome are associated with LSECs capillarization which promotes steatosis (Figure 6).

- *LSECs dysfunction occurs early in NAFLD and promotes steatosis*

Liver steatosis is associated with an increased portal pressure and intrahepatic vascular resistance [188,189]. In patients, hepatic venous pressure gradient correlates with the degree of steatosis [188]. Using Doppler flowmetry, Seifalian and colleagues observed an impaired sinusoidal perfusion in fatty livers compared with healthy human liver grafts [190]. Similar results were obtained in rabbits and rats with diet-induced steatosis with an inverse correlation between hepatic parenchymal microcirculation and the severity of steatosis [191,192]. This increased intrahepatic vascular resistance has a mechanical and a dynamic component. The mechanical part is due to the compression of the sinusoidal lumen by enlarged fat-laden hepatocytes [188,193–195]. The dynamic part is due to a liver endothelial dysfunction. In general, endothelial dysfunction is a pathological condition defined as the inability of blood vessels to dilate in response to increased blood flow. The loss of nitric oxide bioavailability due to eNOS inhibition generally indicates an endothelial dysfunction [196].

Several lines of evidence show that LSECs dysfunction occurs in fatty livers and is involved in the increase of intrahepatic vascular resistance during steatosis. Steatosis induced by 1-month administration of rich saturated fatty acids diet to rats is associated with blunted activation of eNOS indicating an impaired capacity of LSECs to release nitric oxide under these conditions [197]. In these rats, portal perfusion pressure in the liver is higher, and the vasodilatory response to acetylcholine is reduced. These changes were observed in the absence of inflammation and fibrosis suggesting that endothelial dysfunction is an early feature associated with steatosis in NAFLD [197,198]. Likewise, eNOS activation and liver nitric oxide content have also been shown to be reduced after 4 weeks of high-fat feeding in mice [199].

Several mechanisms could account for this endothelial dysfunction in the liver. First, LSECs dysfunction can be induced by the overabundance of lipids during steatosis. *In vitro* experiments showed that ox-LDL stimulation of human primary LSECs downregulates eNOS expression through the ox-LDL receptor LOX1 [181]. In addition, exposure of primary LSECs to palmitic acid also attenuates nitric oxide bioavailability through peroxynitrite production by NOX1 (a nitric oxide consuming enzyme highly expressed in LSCEs of high-fat diet-fed mice) [200]. Second, insulin resistance is a key factor for LSECs dysfunction in NAFLD. In endothelial cells, insulin increases nitric oxide production *via* the upregulation of eNOS and the activation of phosphatidylinositol-4,5-bisphosphate 3-kinase and protein kinase B/Akt which activates eNOS *via* phosphorylation [201]. Interestingly, insulin resistance and LSECs dysfunction occur in rodent models of NAFLD [197,202]. As reviewed elsewhere [203], insulin resistance can be detected early in the course of the disease and contribute to its progression. Steatosis in rats induces insulin resistance in the liver sinusoidal endothelium with an impairment of insulin dependent vasodilation. This effect is due, on the one hand, to the downregulation of eNOS activity [197], and to the upregulation of iNOS, the inducible form of nitric oxide synthase which can cause endothelial dysfunction through increased nitro oxidative stress in the other hand [203–205]. Interestingly, therapies augmenting nitric oxide availability in the liver improve hepatic microcirculation. The V-PYRRO/NO, a diazeniumdiolate ion metabolized in the liver that spontaneously decomposes to nitric oxide with a very short half-life at physiological pH and triggering cyclic guanosine 3',5'-monophosphate (cGMP) synthesis is a stable, hepatoselective nitric oxide-releasing prodrug that lacks systemic vasodilation effects [206]. Kus and colleagues recently showed that three weeks treatment with the V-PYRRO/NO improves hepatic microcirculation in mice with high-fat diet-induced steatosis [207]. Therefore, LSECs dysfunction is a major event occurring in steatosis that compromises intrahepatic vascular resistance.

In turn, LSECs dysfunction impacts steatosis since nitric oxide is involved in the regulation of lipid metabolism in the liver (Figure 1). Nitric oxide deficiency in eNOS deficient mice result in massive fat droplets deposition and increased triglycerides content in the liver [199,208] suggesting that LSECs dysfunction worsens steatosis. Indeed, nitric oxide contributes to the regulation of hepatic lipid content by limiting citrate synthesis in mitochondria [209]. *In vitro*, nitric oxide attenuates the synthesis of fatty acids in isolated cultured rat hepatocytes by nitrosylation of acetyl-CoA [210] and AMP-activated protein kinase activation [211–213] that inhibits glycerol-3-phosphate acyltransferase and concomitantly triacylglycerol synthesis [214,215]. Interestingly, therapies augmenting nitric oxide availability in the liver improve steatosis [199,216]. The V-PYRRO/NO or the improvement of nitric oxide/cGMP signaling with the phosphodiesterase-5 inhibitor sildenafil protect against liver steatosis in high-fat diet-fed mice, mimicking metformin treatment. This anti-steatotic mechanism involves Akt activation and acetyl-CoA carboxylase phosphorylation to inhibits *de novo* fatty acid synthesis [216,217]. Moreover, simvastatin treatment also improves high-fat diet-induced steatosis in rats through increased eNOS expression in the liver [218].

To summarize, steatosis is associated with LSECs dysfunction which in turn worsens steatosis (Figure 6).

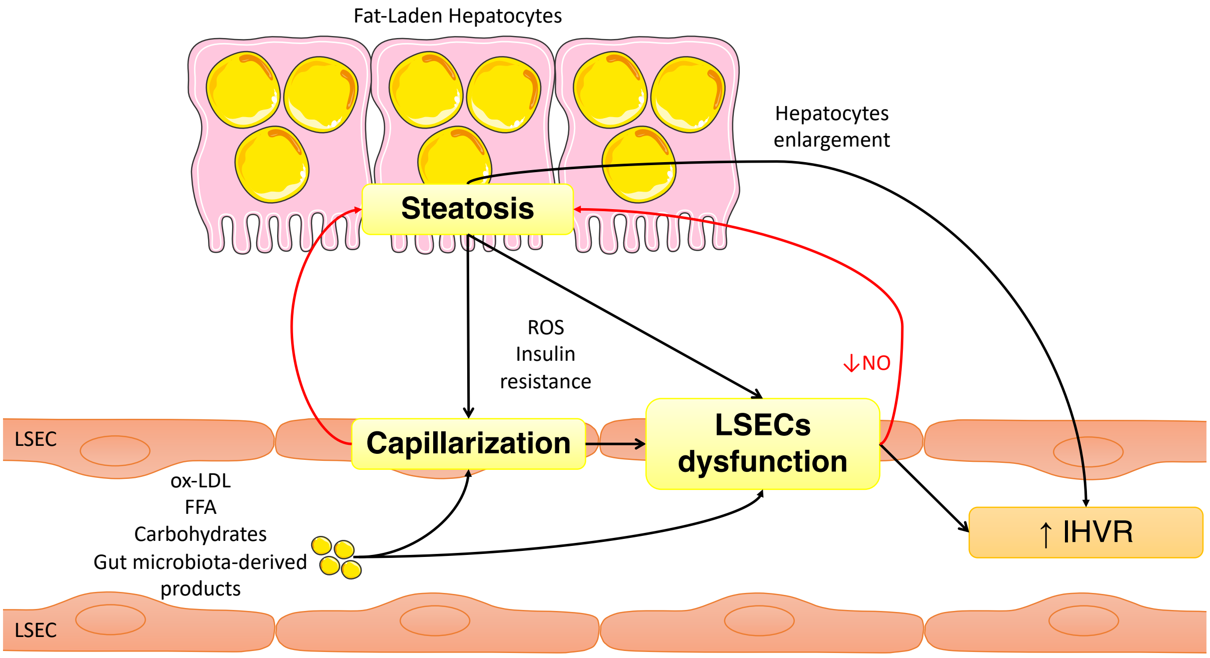
Fat-Laden Hepatocytes
Hepatocytes enlargement
Steatosis
ROS
Insulin resistance
↓NO
LSEC
Capillarization
LSECs dysfunction
ox-LDL
FFA
Carbohydrates
Gut microbiota-derived products
↑ IHVR
LSEC

Figure 6: Role of LSECs in simple steatosis

- *Angiogenesis and steatosis*

Angiogenesis is defined as the formation of new vessels from preexistent vessels and is a key event in the progression of NAFLD [219–223]. Vascular endothelial growth factor (VEGF) is the master pro-angiogenic regulator of this process supported by hypoxia inducible factors (HIF) activation in hypoxic areas [222]. Serum VEGF levels are higher in patients with biopsy-proven steatosis than in healthy individual [220,221,223]. In animal models, liver expression of VEGF levels and CD105, an endothelial cell marker, increase after 3 days of methionine and choline deficient diet in obese and diabetic *db/db* transgenic mice and after 1 week of this diet in C57BL6/J mice, before NASH apparition, suggesting angiogenesis initiation [221]. However, three independent studies reported that new vessels develops in the liver of patients with NASH but not in simple fatty and healthy livers [224–226]. This suggests that the molecular events associated with the up-regulation of angiogenic factors start early in the course of NAFLD while angiogenesis appears later as will be detailed afterward in this review. Nevertheless, anti-angiogenic treatment can prevent steatosis in murine models of NASH. Coulon and colleagues demonstrated that anti-VEGFR2 treatment in C57BL/6 mice on methionine and choline deficient diet reduces angiogenesis, improves the disrupted vasculature and decreases steatosis both in a preventive and therapeutic setting. This is supported by *in vitro* observations showing that anti-VEGFR2 treatment decreases lipid accumulation in fat laden primary hepatocytes [221].

3. Role of LSECs in nonalcoholic steatohepatitis (NASH)

NASH is a lipotoxic condition in which hepatocytes and non-parenchymal cells generate reactive oxygen species (ROS) and initiate robust inflammatory response that accentuates liver injury [14,104].

- *LSECs in liver injury in NAFLD*

Despite the chronic exposure of LSECs to lipid excess during steatosis, little is known about their contribution in liver injury. In addition to hepatocytes which are a major source of ROS in lipotoxic environment [14,104], some evidences suggest that LSECs lipotoxic response also involves ROS generation which have been postulated to play a key role in the progression of NAFLD [200,227]. Indeed, an old study detected the presence of ROS in hepatocytes and in sinusoidal cells as well in NASH [228]. Second, a recent study suggested that ROS generated by LSECs contributes to liver injury as demonstrated by the attenuation of serum ALT level and hepatic cleaved Caspase-3 expression induced by high-fat diet in NOX1 deficient mice. Of note, NOX-1 has been shown to be highly expressed in LSECs in NAFLD [200]. This result is supported by *in vitro* observations showing that exposure of murine LSECs to palmitic acid, thus mimicking NAFLD setting, reduces nitric oxide bioavailability through the upregulation of NOX1 and peroxynitrite production [200]. In addition, stimulation of human primary LSECs with ox-LDL increases ROS generation after binding to LOX1 [181]. Therefore, ROS derived from LSECs in NASH conditions contribute to hepatocyte injury.

- *LSECs alterations promote liver inflammation*

As detailed above, LSECs alterations arise very quickly in NAFLD and precedes liver inflammation [179,197]. Capillarization appears during the simple steatosis phase and precedes Kupffer cells activation [179]. In the same line, LSECs dysfunction also occurs before inflammation [189,197,199]. Hepatic nitric oxide content falls prior to NF-kB activation and TNFα, IL6 and ICAM-1 up-regulation in the liver [199]. eNOS deficient mice exhibit an accelerated hepatic inflammatory response attested by NF-kB activation, TNFα and IL6 overexpression [199]. Interestingly, improving nitric oxide/cGMP signaling with the phosphodiesterase-5 inhibitor sildenafil prevents liver inflammation in high-fat diet-fed mice [199]. Simvastatin treatment also improves high-fat diet-induced liver injury and inflammation in rats by inducing eNOS expression [218]. These results suggest that capillarization as well as LSECs dysfunction are permissive for liver inflammation establishment.

Several factors are involved in LSECs activation during NASH. Indeed, as a result of liver injury, hepatocytes and inflammatory cells release inflammatory mediators that can activate LSECs. Other triggers of LSECs activation are the products derived from the visceral adipose tissue such as ox-LDL, FFA and adipocytokines including TNFα, IL6, leptin and fatty acid binding protein 4 (FABP4). *In vitro* studies showed that ox-LDL and FFA (palmitate) stimulation of LSECs induces NFkB and toll-like receptor-4 (TLR-4) activation respectively [181,200,229] suggesting that lipid overabundance as seen in NAFLD induces LSECs activation. Gut microbiota has also an emerging role in NASH as a source for liver inflammation [14,104]. Studies showed increased intestinal permeability during NASH, which could lead to elevated levels of plasma lipopolysaccharide (LPS) [230] that has been shown to activate primary LSECs after binding to TLR-4 *in vitro* [231].

Activated LSECs acquire pro-inflammatory phenotype during NASH (Figure 2). LSECs progressively overexpress adhesion molecules at their surface such as ICAM-1, VCAM-1 and VAP-1. In obese mice, LSECs show increased expression of ICAM-1 and VCAM-1 and the hepatic expression of cell adhesion molecules is increased in dietary-induced steatohepatitis mouse models [226,232–235]. LSECs also produce a number of pro-inflammatory mediators in NASH including TNFα, IL-6, IL-1 and MCP1 [226,231,236].

Activated LSECs acquire pro-inflammatory function during NASH and contribute to liver inflammation (Figure 7). First, dysfunctional LSECs fail to maintain Kupffer cells quiescence [199]. Second, the release of inflammatory mediators by LSECs contributes to the inflammatory response by activating neighboring Kupffer cells on the one hand, and by recruiting leukocytes (lymphocytes, monocytes, NK cells, NKT cells) from the blood on the other hand, leading to the transendothelial migration of leucocytes into the parenchyma that orchestrates the liver immune response with resident Kupffer cells [237–239]. The detailed mechanisms of the interactions between leucocytes and LSECs have been previously reviewed [240,241]. Briefly, LSECs express ICAM-1 and VAP-1 and increasingly produce VCAM-1 allowing leukocytes transendothelial migration (Figure 7). For example, VAP-1 play a key role in lymphocyte recruitment to the liver [234,242]. VAP-1 is a 170kDa homodimeric glycoprotein constitutively expressed on hepatic sinusoids. Weston and colleagues demonstrated in a cohort of 74 patients with histologically confirmed NASH that serum sVAP-1 was significantly increased as well as well as VAP-1 expression in the liver tissue [234]. VAP-1 has been described as an important chemoattractant for lymphocytes in both soluble (sVAP-1) and receptor forms in three different animal models of steatohepatitis [234]. *In vivo* and *in vitro* studies showed reduced leukocytes adhesion to hepatic sinusoids when ICAM-1, VCAM-1 and VAP-1 are blocked or unfunctional [234,243].

To summarize, LSECs appear to try to compensate liver inflammation in the first line early in NAFLD but this anti-inflammatory function is rapidly exceeded and switched towards pro-inflammatory function. Lipotoxicity, dut microbiota-derived products and inflammation induce LSECs inflammatory phenotype that contributes to liver inflammation by releasing pro-inflammatory mediators on the one hand, and by overexpressing adhesion molecules in the other hand, that concomitantly recruits immune cells which exacerbates liver inflammation and injury (Figure 7).

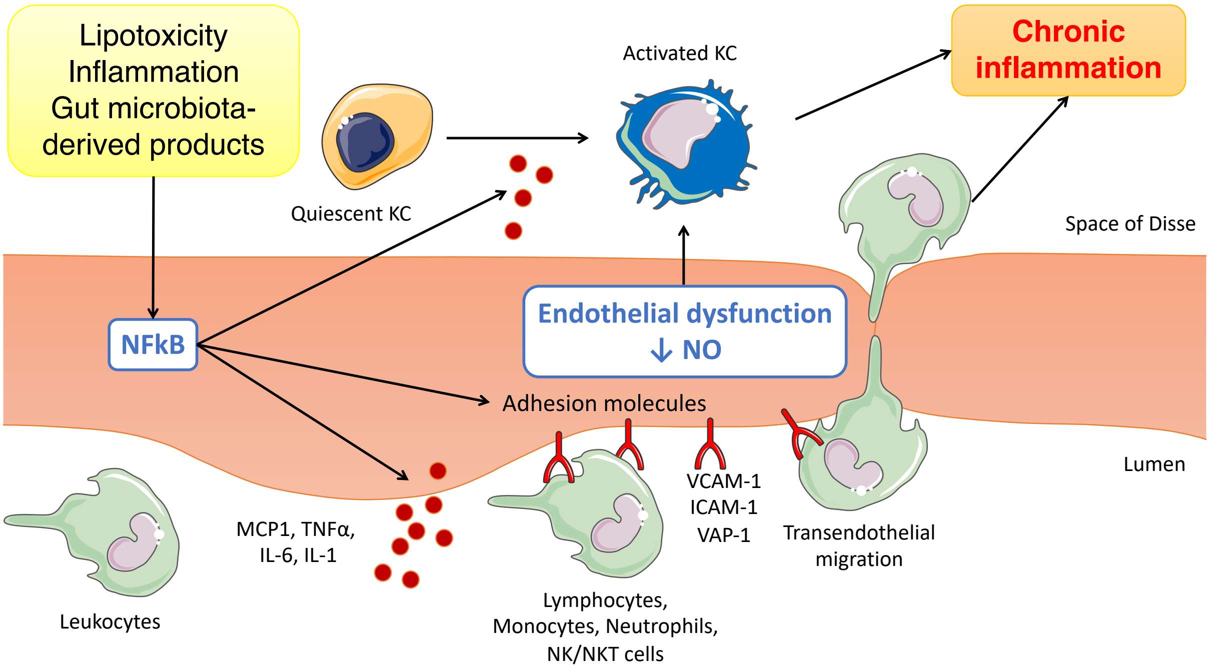
Lipotoxicity
Inflammation
Gut microbiota-derived products
Quiescent KC
Activated KC
Chronic inflammation
Space of Disse
NFkB
Endothelial dysfunction
↓ NO
Adhesion molecules
Lumen
VCAM-1
ICAM-1
VAP-1
Transendothelial migration
MCP1, TNFα, IL-6, IL-1
Leukocytes
Lymphocytes, Monocytes, Neutrophils, NK/NKT cells

Figure 7: Role of LSECs in liver inflammation in NASH

- *Angiogenesis and liver inflammation in NASH*

Pathologic angiogenesis increases with NASH progression [219,226,244,245] (Figure 8). Serum VEGF and sVEGFR1 levels increase in patients with biopsy-proven NASH [220,246] and several studies reported new vessels formation in the liver of patients with NASH [224–226]. In animal models of NASH, mice exhibit a disrupted liver vasculature and hepatic expression of VEGF and CD105 is increased [221].

Several mechanisms trigger angiogenesis during NASH. First, the chronic inflammation sustains tissue hypoxia and promotes angiogenesis by inducing the transcription of angiogenic genes modulated by HIF-1α [219,247]. Pro-inflammatory mediators also elicit direct angiogenic response through the induction of HIF-1α transcriptional activity and

VEGF production [219]. Moreover, cytokines and ROS can activate the MAPK/ERK pathway, a signaling pathway involved in cell migration and angiogenesis [219]. Second, mice fed the methionine and choline deficient diet have high circulating levels of hepatocytes derived microvesicles which replicate the angiogenic effect of VEGF *in vitro*. *In vitro* experiments showed that hepatocytes exposed to excessive amounts of saturated FFA, that mimics steatosis, release microvesicles with pro-angiogenic activity on human umbilical vein endothelial cells mimicking the cellular response to VEGF [248] thus linking hepatocyte lipotoxicity to angiogenesis. Third, Angiopoietins are also key regulators of angiogenesis. Although angiopoietins-1 and 2 contributes to vascular stability and quiescence in physiological conditions, angiopoietin-2 promotes pathological angiogenesis in inflammatory conditions [249]. Interestingly, Lefere and coworkers recently showed that serum angiopoietin-2 levels were increased in patients with NASH and correlates with the severity of the disease but not with fibrosis [226]. This was confirmed in two murine models of NASH, namely the methionine and choline deficient diet and the neonatal streptozotocin and 16 weeks of western diet [226]. Importantly, LSECs have been shown to be the main source of hepatic angiopoietin-2 in NASH [226]. Angiopoeitin-2 levels increase during the progression of NASH and promote angiogenesis [226].

In turn, angiogenesis promotes inflammation as the inhibition of angiogenesis by different manner improves liver inflammation (Figure 8). Coulon and colleagues showed in a mouse models of NASH that treatment with anti-VEGFR2 antibody improves liver vasculature and decreases inflammatory gene expression, both in a preventive and therapeutic manner [221]. Lefere and colleagues showed that blocking angiopoietin-2/Tie2 interaction with L1-10 peptibody also inhibits pathologic angiogenesis, improves hepatic vasculature and alleviates liver injury and inflammation in methionine and choline deficient diet-fed mice [226]. Importantly, this effect of L1-10 therapy is at least mediated by an improvement of LSECs since L1-10 treatment downregulates VCAM-1, ICAM-1 and MCP-1 expression in liver endothelial cells isolated from methionine and choline deficient diet-fed mice [226]. This last result support the major proinflammatory role of LSECs in NASH. Taken together, these results indicate that blocking pathologic angiogenesis improve inflammation in NASH. Consistently, this anti-inflammatory effect of anti-angiogenic treatment is not specific for NASH since it is observed in most models of chronic liver disease (carbon tetrachloride, bile duct ligation and partial portal vein ligation) [250–255].

To summarize, inflammation stimulates angiogenesis that in turn worsens it as attested by anti-inflammatory effect of anti-angiogenic therapies (Figure 8).

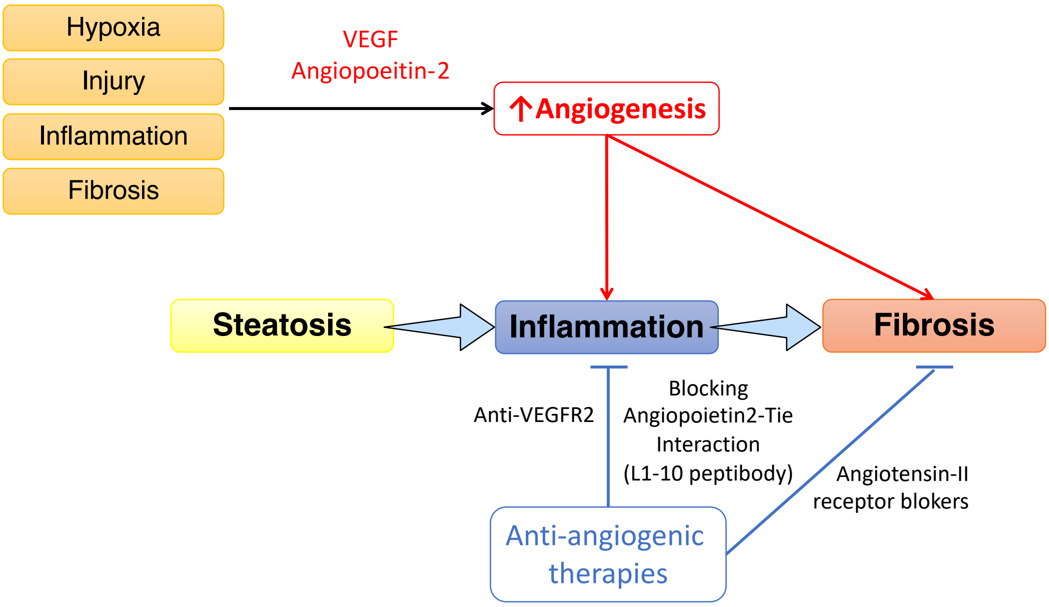
Hypoxia
Injury
Inflammation
Fibrosis
VEGF
Angiopoeitin-2
↑Angiogenesis
Steatosis
Inflammation
Fibrosis
Anti-VEGFR2
Blocking
Angiopoietin2-Tie
Interaction
(L1-10 peptibody)
Angiotensin-II
receptor blokers
Anti-angiogenic
therapies

Figure 8: Angiogenesis in NASH

4. Role of LSECs in NASH-related fibrosis

Liver fibrosis is defined as the excessive deposition of extracellular matrix in hepatic parenchyma as a result of a long-standing wound healing process caused by hepatocellular injury and inflammation and mediated by hepatic stellate cells activation [14]. Hepatic stellate cells are nonparenchymal cells close to LSECs in the space of Disse which store retinoids in physiological conditions and shift their phenotype to an activated myofibroblastic state during liver injury to secret large amounts of extracellular matrix compounds [127]. It is well established that liver inflammation triggers hepatic stellate cells activation and consequently liver fibrosis [14,127]. As detailed above, LSECs are major effectors of liver inflammation in NASH. Therefore, LSECs are key players of hepatic fibrosis by promoting liver inflammation. For example, LSECs overexpress VAP-1 during inflammation which, in addition to its pro-inflammatory functions in NASH, is directly involved in hepatic stellate cells activation [234]. VAP-1 is a strong profibrogenic stimulus as demonstrated in methionine and choline deficient diet and high-fat diet-induced NASH. VAP-1 inhibition or deficiency also attenuates liver fibrosis [234]. Another important process that links endothelial cells to organ fibrosis is the endothelial-to-mesenchymal transition which is the mechanism by which endothelial cells convert into myofibroblasts and contributes to extracellular matrix deposition [256,257]. Endothelial-to-mesenchymal transition occurs in various fibrotic cardiovascular and pulmonary diseases [256–258]. This might happen during liver fibrosis but has been overlooked in NASH. Only one study reported that endothelial-to-mesenchymal transitions occurs in alcohol and hepatitis C virus-related cirrhosis [259]. Furthermore, LSECs contribute to liver fibrosis through other mechanisms including capillarization and endothelial dysfunction.

- *LSECs capillarization promotes liver fibrosis*

Capillarization is the main morphological change of LSECs considered as an integral part of liver fibrosis. This phenotypic alteration is observed in patients and animal models of NASH and precedes fibrosis [163,179,197,260–263]. Capillarization of LSECs not only precedes fibrosis but also promotes its development. This is supported by the study of Herrnberger and colleagues in which they demonstrated that PLVAP deficient mice, that have a pronounced reduction in the number of *fenestrae* in LSECs, spontaneously develop perisinusoidal liver fibrosis [185]. It is important to mention that PLVAP deficient mice exhibit hyperlipidemia and severe steatosis that mimics NASH setting [185].

Most of the mechanistic knowledge about the role of LSECs in liver fibrosis *in vivo* comes from chemical hepatotoxic models (such as carbon tetrachloride or thioacetamide treatment) or from the bile duct ligation cirrhosis model. However, these models did not reproduce the pathophysiology of NASH. Further studies are needed to better characterize the role of LSECs in NASH-related fibrosis *in vivo*. Meanwhile, a wide body of evidence based on *in vitro* studies allowed to understand the links between LSECs and hepatic stellate cells. An important cross-talk occurs between LSECs and hepatic stellate cells to regulate each other their phenotype. Healthy LSECs maintains hepatic stellate cells quiescent while capillarized LSECs lose this ability [163,164] (Figure 9). A vicious cycle between LSECs capillarization and hepatic stellate cells activation is likely to occur during the fibrotic process. For example, *in vitro* experiments showed that capillarization is a Hedgehog-dependent mechanism [264]. LSECs are both Hedgehog-sensitive and producing cells. Ballooned hepatocytes increasingly produces hedgehog molecules [265]. Quiescent hepatic stellate cells are Hedgehog-sensitive cells while activated hepatic stellate cells become Hedgehog-producing cells [266]. Activated hepatic stellate cells can release microvesicules loaded with Hedgehog signaling molecules that interact with LSECs [267]. Inhibition of Hedgehog signaling prevents capillarization and partially reverts LSECs phenotype from dedifferentiated to their differentiated state [264]. It is tempting to speculate that during liver injury, Hedgehog ligands are released by epithelial cells and LSECs thus activating LSECs and quiescent hepatic stellate cells by autocrine and paracrine effects. Activated hepatic stellate cells can secrete Hedgehog molecules promoting LSECs injury which in turn favors hepatic stellate cells activation promoting the fibrogenic process. Moreover, healthy LSECs produce a modest amount of collagen and fibronectin [268] while capillarized LSECs secrete fibrogenic factors such as TGF-β1 and extracellular matrix proteins such as fibronectin and laminin that stimulate hepatic stellate cells activation [162,269,270].

- *LSECs dysfunction promotes liver fibrosis*

Endothelial dysfunction appears very early in the course of NAFLD and precedes fibrosis in animal models of NASH [189,197,199] suggesting that LSECs dysfunction is permissive for hepatic fibrogenesis. Here again, *in vivo* analyses to assess the effect of endothelial dysfunction on fibrosis in NASH-related fibrosis specifically are required. Meanwhile, *in vitro* studies demonstrated that differentiated LSECs keep hepatic stellate cells quiescent at least *via* nitric oxide production and can promote the reversal of activated hepatic stellate cells from an activated state to quiescence as previously reviewed [163,164]. VEGF production either by HSCs and hepatocytes maintains LSECs differentiation [163,164,271]. eNOS inhibition with L-NAME blocks the ability of LSECs to maintain hepatic stellate cells quiescence [272,273]. Of note, LSECs cultured in the presence of L-NAME capillarize and capillarized LSECs fail to maintain hepatic stellate cells quiescence [163,272]. Moreover, healthy LSECs can reverse hepatic stellate cells activation while dysfunctional LSECs lose this ability. Indeed, activated hepatic stellate cells revert to quiescence when they are cultivated with differentiated LSECs if endothelial function is maintained with a soluble guanylate cyclase activator [168]. The mediator for this paracrine effect on activated hepatic stellate cells has not been identified since nitric oxide alone does not promote the reversion of activated hepatic stellate cells to quiescence [168]. Interestingly, improving LSECs health with simvastatin ameliorates high-fat diet-induced fibrosis in rats through increased eNOS expression in the liver [218].

To summarize, these data demonstrate that capillarization and LSECs dysfunction not only precedes fibrosis, but are also permissive for it (Figure 9). LSECs are able to maintain hepatic stellate cells quiescent as long they are differentiated so that differentiated LSECs are gatekeepers of fibrosis.

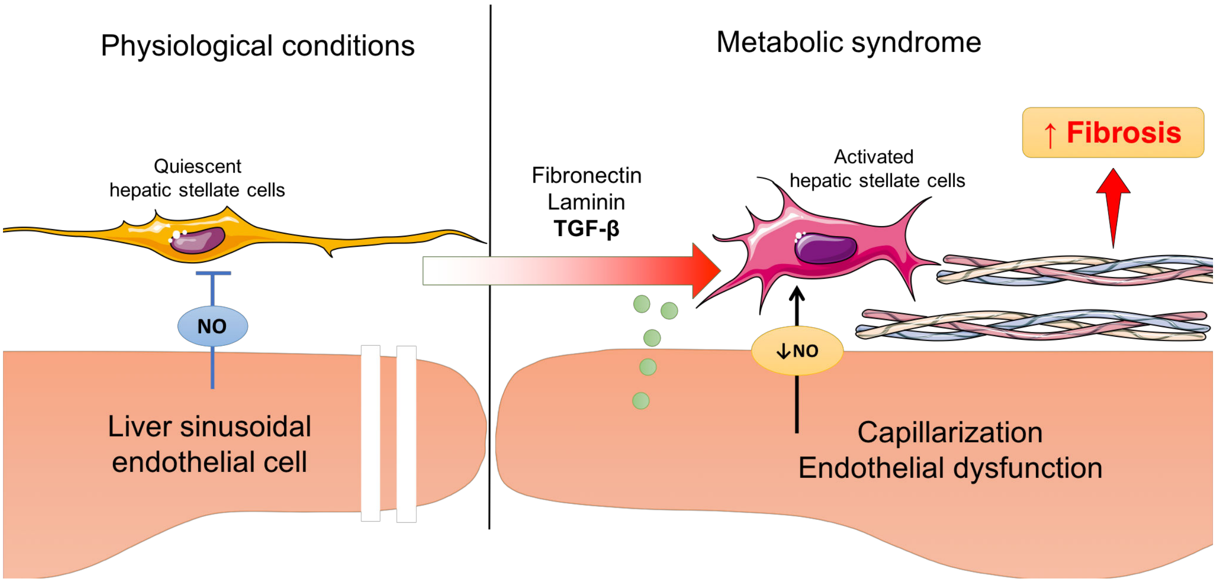
Physiological conditions
Metabolic syndrome
↑ Fibrosis
Quiescent hepatic stellate cells
Fibronectin
Laminin
TGF-β
Activated hepatic stellate cells
NO
↓NO
Liver sinusoidal endothelial cell
Capillarization
Endothelial dysfunction

Figure 9: Role of LSECs in NASH-related fibrosis.

- *Angiogenesis in NASH-related fibrosis*

Angiogenesis is a key pathological feature closely associated with fibrosis in NASH [224,225,244,274,245]. Kitade and colleagues described an up-regulation of hepatic CD34 expression, which is a widely used marker of angiogenesis, in patients with NASH and showed that angiogenesis is correlated with the grade of fibrosis [224,225]. The same group demonstrated in rats that leptin-mediated neovascularization in the liver, coordinated by VEGF, plays an important role in the progression of NASH and fibrosis [274].

In NASH setting, angiogenesis is first stimulated by the progressive increase of tissue hypoxia which is worsened by the fibrotic scar tissue thus activating the transcription of hypoxia-sensitive pro-angiogenic genes modulated by HIF [219]. Second, leptin is an adipocytokine increased in the serum of NAFLD patients [275] which, in addition to its pro-angiogenic effect [274], exhibits direct pro-fibrogenic effect through the upregulation of TGF-β in LSECs and Kupffer cells [276]. Third, fat-laden hepatocytes derived microvesicles were found to act on endothelial cells and to promote pathologic angiogenesis after their internalization as shown *in vitro* and *in vivo* in mice exposed to a murine model of NASH [248,277]. Finally, angiopoietin-2 levels increase in NASH and drive pathologic angiogenesis [226].

In turn, angiogenesis promotes fibrosis since the inhibition of angiogenesis prevents NASH-related fibrosis (Figure 8). Indeed, pathologic angiogenesis can be inefficient to correct liver hypoxia due to the immaturity and impermeability of neovessels [278] thereby worsening liver fibrosis. First, in the study of Kitade and colleagues, neither angiogenesis nor fibrosis was observed in the absence of leptin signaling in a rat model of NASH [274]. Second, the blockage of the release of pro-angiogenic fat laden-derived microvesicles or the inhibition of their binding to their target cells protects mice from steatohepatitis-induced pathologic angiogenesis and results in a reduction of liver fibrosis [248]. Third, Zhou and coworkers recently showed that specific deletion of prolyl-hydroxylase-2 in endothelial cells promotes dietary-induced liver fibrosis in mice [279].

Prolyl-hydroxylases are physiological inhibitors of angiogenesis by inducing HIFs degradation [280]. Whether this pro-fibrotic effect of endothelial prolyl-hydroxylase-2 deficiency is induced by promoting angiogenesis remains to be determined. Meanwhile, the authors showed that prolyl-hydroxylase-2 deficiency in endothelial cells also results in angiopoietin-2 and TGF-β1 overexpression in the liver [279]. Fourth, two studies reported that angiotensin-II receptor inhibition with telmisartan or candesartan inhibits angiogenesis and fibrosis in the liver of choline-deficient, L-amino acid-defined diet-fed rats [244,245]. Finally, Lefere and colleague demonstrated that blocking angiogenesis by inhibiting angiopoietin-2/Tie2 interaction improves liver fibrosis in a preventive and therapeutic manner in methionine and choline deficient diet-fed mice. Therapeutic application of L1-10 peptibody also prevents liver fibrosis in diabetic mice with NASH (streptozotocin and western diet model) [226]. Moreover, this anti-fibrotic effect of anti-angiogenic treatments is not specific for NASH since it also prevents fibrosis in hepatotoxic models of advanced liver fibrosis [250–255,281–287].

5. Role of LSECs in cirrhosis in NAFLD setting

Cirrhosis develops from liver fibrosis and is the severe pathological stage of all chronic liver disease including NAFLD. It is estimated that 10–25% of steatohepatitis progress into cirrhosis over 8–14 years with an increased risk of developing portal hypertension liver failure, and hepatocellular carcinoma [288]. Liver fibrosis and cirrhosis involve excessive production of extracellular matrix, which is closely related to LSECs injury. Importantly, a gap in our knowledge exist about the mechanistic specifities underlying the clinical outcomes of cirrhosis in NASH background since experimental models of NASH-related cirrhosis are lacking. Indeed, available strategies to study cirrhosis in NAFLD/NASH setting involve either long-term high-fat diet feeding (over 36 weeks) or require the use of chemicals hepatotoxic insults combined with dietary measures thus bringing an “artificial pathophysiology” [289–292]. Therefore, most of the knowledge about the role of LSEC in NASH-related cirrhosis is based on carbon tetrachloride, thioacetamide and bile duct ligation models, as reviewed elsewhere [293,294]. We will here focus on what is known about the role of LSECs in NAFLD-related cirrhosis.

Portal hypertension is the clinical manifestation of increased portal venous pressure and a major complication of cirrhosis. It is responsible for most complications associated with advanced NAFLD thus representing a leading cause of death [295]. Splanchnic vasodilation is commonly associated with PHT in cirrhosis. Given that this review focuses on the role of LSECs in NAFLD, this point will not be discussed. As stated above, sinusoidal architecture becomes distorted in NAFLD and cirrhosis leading to increased intrahepatic vascular resistance [219]. Observations made in clinical and experimental models of NAFLD provide evidences that increase portal venous pressure may occur in NAFLD when severe steatosis is either the only histological feature or minimal/mild fibrosis is present [188,191,296–298]. Mechanisms responsible for the increase in sinusoids resistance were addressed above and include a mechanic factor (consequent to fat and fibrosis deposition), and a dynamic component related to capillarization, endothelial dysfunction and increased vasoconstrictor production [219,298,299]. Strategies improving LSECs demonstrated their benefits in alcoholic, hepatitis B and C and biliary-related cirrhosis and portal hypertension as well as in experimental models of chemically and bile duct ligation-induced cirrhosis and portal hypertension [300–305]. Further studies are needed to investigate this potential in NASH-related cirrhosis. Interestingly, the gut microbiota is an emerging factor which directly influences portal hypertension in NASH. Garcia-Lezana and colleagues recently demonstrated that healthy microbiota restoration *via* fecal transplantation improves NASH-induced PHT in rats through improvement of eNOS signaling in the liver [306].

- *Angiogenesis in cirrhosis*

The progression from fibrosis to cirrhosis, the end-point of chronic liver diseases, is distinguished by an abnormal angioarchitecture distinctive for cirrhosis. Vascular structural changes are well established pathological hallmarks of cirrhosis [307]. The analysis of cirrhotic livers indicates an increased number of vessels in the fibrotic septa and surrounding regenerative nodules [307]. Angiogenesis contributes to progression of fibrosis to cirrhosis in patients with chronic liver diseases [219] and cellular crosstalk between LSECs, hepatic stellate cells and hepatocytes plays an important role in the angiogenic process during the development of cirrhosis [253,282,308–310]. Anti-angiogenic treatments have shown beneficial effects in bile duct ligation and carbon tetrachloride-induced cirrhosis [250,251,253,286,287,311,312]. Here again, further studies in NAFLD setting are required.

6. Role of LSECs in hepatocellular carcinoma in NAFLD setting

Hepatocellular carcinoma (HCC) is the most common primary liver malignancy and is a leading cause death making it the third most frequent cause of cancer-related death. In most cases, hepatocellular carcinoma develops within an established background of chronic liver disease (70–90% of all patients). NASH is increasingly recognized as risk factor for HCC and patients with cirrhosis are at highest risk of developing this malignant disease [313,314]. Importantly, patients with metabolic syndrome and NAFLD also develop HCC in the absence of underlying cirrhosis, suggesting oncogenic pathways specific for NASH [16,315,316].

- *LSECs phenotype in hepatocellular carcinoma*

As previously review, and regardless of the cause of the underlying liver disease, LSECs within HCC are phenotypically and functionally different and the vascular changes associated with HCC are characterized by sinusoidal capillarization and arterialization [162,317]. First, endothelial cells present within HCC sequentially lose during tumor progression their specific markers including stabilin-1, stabilin-2, LYVE-1 and CD32b (SE-1), as observed in both human and murine HCC models [318]. Endothelial cells derived from human HCC have a higher expression of integrins and a lower expression of ICAM-1 [319]. In the peritumoral tissue, LSECs also undergo changes including the loss of Stabilin-2 and CD32b (SE-1) [318]. Second, healthy LSECs and LSECs derived from cancerous liver exhibits different adhesive capacities. As compared to LSECs isolated from healthy human liver, endothelial cells derived from human HCC exhibit a higher adherence capacity with the human liver cancer cell line Bel-7402 *in vitro* and this adherence activity is inhibited by antibodies against integrins (αvβ3 and αvβ5) [319]. Furthermore, leukocyte adherence is lower on LSECs from cancerous liver than on control LSECs [319]. These data suggest that LSECs in HCC environment may promote cancerous cells recruitment through integrins and inhibit inflammatory cells recruitment in the cancerous tissue, while normal LSECs do the opposite, suggesting that LSECs may be permissive for HCC development. Finally, LSECs can alter tumor-associated immune responses *via* their ability to confer T cell tolerance towards cancer-associated antigens and to create an immunosuppressive environment towards circulating antigen tumors cells [320,321]. However, the significance of these pathways in NAFLD-related HCC remains to be confirmed since the experimental available data does not include this setting. Indeed, little is known about the role of LSECs in this setting despite the fact that LSECs are among the first cells in contact with visceral adipose tissue-derived adipocytokines which may play a key role in this setting [276,322]. For example, a link between leptin, angiogenesis, NASH and HCC development can be made since HCC does not develop in the absence of leptin signaling in rats [274]. Additional adipocytokines, such as FABP4 are increased in patients with NAFLD, and correlates with liver inflammation and fibrosis [323]. Interestingly, Laouirem and colleagues highlighted that FABP4 is upregulated in HCC samples from patients with metabolic syndrome and that tumor cell-lining endothelial cells are the main source of FABP4 in human HCC. FABP4 from LSECs contributes to HCC development since its specific inhibition reduces tumor growth in a xenograft mouse model submitted to high-fat diet [324] (*unpublished data*).

- *Angiogenesis in hepatocellular carcinoma*

HCC is one of the most vascular solid tumors in which angiogenesis plays an important role in its development, progression, and metastasis. Angiogenesis is required to provide the nutrient and oxygen for tumor cells. HCC develops blood supply predominantly from the arterial system because of its high need of oxygen. The expression of markers for microvessel density has been reported to be associated with the development and progression of HCC. In established HCC, microvessel density has been shown to impact on prognosis of patients [325].

In NAFLD setting, angiogenesis is highly stimulated and promotes NAFLD-associated HCC since the inhibition of angiogenesis by different manner prevents HCC development. First, leptin-mediated angiogenesis has been demonstrated to be involved in HCC development since neither angiogenesis nor HCC develop in the absence of leptin signaling in choline-deficient, L-amino acid-defined diet-fed Zucker rats [274]. Second, Yoshiji and colleagues showed that the conventional anti-angiogenic treatment with sorafenib inhibits preneoplastic lesions apparition in choline-deficient, L-amino acid-defined diet-fed rats [326]. In this study, the authors also demonstrated that the combined treatment with low doses of sorafenib and the angiotensin-II receptor inhibitor losartan successfully inhibits preneoplastic lesions [326]. Third, Tamaki and colleagues demonstrated that angiotensin-II receptor inhibition with telmisartan inhibits HIF-1α activity and VEGF expression in the liver of 48 weeks choline-deficient, L-amino acid-defined diet-fed rats [244]. In this study, telmisartan inhibited preneoplastic lesions and prevented HCC development [244]. Finally, Lefere and coworkers recently showed that therapeutic inhibition of angiopoietin-2 alleviates steatohepatitis and prevents NASH-associated HCC progression in mice [226]. However, a recent study showed that trebananib treatment, which sequesters both angiopeitin1 and 2 and blocks their interaction with Tie2, in addition to standard sorafenib treatment, did not improve the survival of patients with advanced HCC [327].

C. Autophagy

1. Definition

Autophagy (from the Greek, “auto” oneself, “phagy” to eat) is an intracellular catabolic process by which the dysfunctional cytoplasmic material joins lysosomes to be degraded [328]. The term "autophagy" was first introduced more than 50 years ago by Christian De Duve and was based on observations of the degradation of mitochondria and other intracellular structures within lysosomes in the liver of rats [329]. Three types of autophagy exist (chaperone-mediated autophagy, microautophagy and macroautophagy, Figure 10) that are distinguished by their physiological functions and the mode of delivery of the cytoplasmic material to lysosomes [330] (Figure 10).

The scientific knowledge about autophagy has made significant progress in recent years with major contributions from many scientific groups to our understanding of the physiological significance of autophagy and the molecular events regulating this process. Autophagy is involved in the removal of misfolded or aggregated proteins, damaged organelles, such as mitochondria, endoplasmic reticulum and peroxisomes, and the clearance of intracellular pathogens [331]. Autophagy is also important for the regulation of the cellular energetic balance at critical times in response to nutrient stresses [331]. Autophagy occurs physiologically at basal level in all cell types and is rapidly activated in conditions of nutrient deficiency or cellular stresses such as hypoxia or endoplasmic reticulum stress. Under basal conditions, autophagy controls organelle and protein quality to maintain cellular homeostasis. Under conditions of stress, autophagy acts as a survival mechanism, maintaining cellular integrity by regenerating metabolic precursors and clearing subcellular debris [332]. The physiologic importance of autophagy as a source of energy is highlighted by the death of total autophagy-deficient mice during the neonatal period [333]. At birth, the placental nutrient supply is suddenly interrupted confronting neonates to sever starvation up until lactation. Autophagy is immediately activated at this time in various tissue, including the liver, the heart and muscles, and maintained at high level for twelve hours to allows neonates to face the severe starvation. This primordial role of autophagy in nutrient intake is supported by the fact that the survival of autophagy deficient mice at birth can be prolonged by forced milk feeding that provides amino-acids required for neonates' survival [333].

During this physiological process, a portion of the cytoplasm is sequestered in a vacuole to be degraded and recycled [334]. Autophagy primarily acts as a protective mechanism preventing cell death and senescence [332]. In aging organisms, autophagy becomes insufficient, threatening cell functionality and survival [332]. However, in some specific conditions, autophagy can lead to autophagic cell death or autosis which is distinguished from apoptosis by the absence of chromatin condensation, DNA oligonucleosomal fragmentation, and caspase activation [335–337].

2. Types of autophagy

a. Chaperone-mediated autophagy

Chaperone-mediated autophagy (CMA) was discovered later in 1981 [338]. CMA is a selective form of autophagy where substrates bind to a cytosolic chaperone protein, heat shock cognate 70 (HSC70) (Figure 10). Once bound to the chaperone, the substrate is directed to the lysosomal surface where the interaction with the LAMP-2A protein allows its internalization into the lysosomal lumen. The recognition of the substrates by HSC70 requires a pentapeptide pattern KFERQ or a KFERQ-like motif [339]. HSC70 recognizes and binds to proteins with this sequence and directly targets them to the lysosomal membrane where they interact with the cytoplasmic tail of LAMP-2A. The KFERQ motif become accessible for recognition by chaperones after the unfolding of the protein in the case of masked motifs in the core of the protein, after the separation of the proteins from multiprotein complexes if the motif is masked in the protein-protein interaction region, or when the proteins are released from the subcellular membranes in the case where the motif is in the membrane binding region [340] (Figure 10).

LAMP-2A is present in the lysosomal membrane as monomers combined with other proteins to form a multi-protein complex required for the translocation of the substrate. The binding of the substrate induces the multimerization of LAMP-2A. During the transition from monomers to multimers, the stability of LAMP-2A is maintained by its interaction with HSP90 located at the luminal side of the lysosomal membrane [341]. The native substrate binds to LAMP-2A but cannot cross the lysosomal membrane without unfolding. This unfolding step seems to be mediated by HSC70 [340]. Once the substrate translocated into the lysosomal lumen, LAMP-2A multimers are rapidly disassembled into monomers which will be available for new substrates [341]. Assembly / disassembly of LAMP-2A is regulated by the interaction of GFAP and EF1α proteins in a GTP-dependent manner [342].

CMA plays an important role in pathophysiology since disturbances of this process are associated with various pathologies. For example, a decrease in CMA is observed in aging and neurodegenerative diseases (Alzheimer's and Parkinson's), while it is abnormally increased in some cancers. The modulation of this process has therefore high therapeutic potential [340].

b. Microautophagy

De Duve and Wattiaux described the phenomena of macro and microautophagy in 1966 [343] in the liver of rats but the proper term “microautophagy” was introduced for the first time in 1983 [344]. Microautophagy is a non-selective lysosomal degradative process that involves the direct engulfment of the cytoplasmic cargo by autophagic tubes in the lysosomal/late endosomal compartment. While the original observations of microautophagy were made in the liver, most of our knowledge originates from studies in yeast where its selectivity for lipids, organelles and nuclear portions has been reported [345,346]. During the microautophagy process, the lysosomal membrane is randomly invaginated and forms an autophagic tube to sequester portions of the cytosol. In microautophagy, proteins carrying a KFERQ-like motif are also recognized by HSC70. Contrary to CMA, the protein/chaperone complex directly binds to lipids at the lysosomal/late endosomal membrane and are internalized in small vesicles. Vesicles form at the top of this tube, fuse and then bud to be founded in the lysosomal lumen and degraded with their content by lysosomal hydrolases [344] (Figure 10). Microautophagy allows the cell survival under nitrogen restriction conditions and the maintenance of membrane homeostasis [344]. In yeast, microautophagy allows the degradation of various organelles such as peroxisomes, mitochondria, lipid droplets and the nucleus, but its contribution to organellophagy in mammals remains to be elucidated [347]. In addition to the degradation of autophagic substrates, microautophagy also regulates the size of lysosomes, *via* the consumption of excess membrane, which can come from the fusion with autophagosomes during macroautophagy for example (see below paragraph III-B.2.c: Macroautophagy) [344].

c. Macroautophagy

Macroautophagy is the main form of autophagy in cells. It allows non-selective degradation of dysfunctional cytoplasmic material. My thesis is focused on macroautophagy which will be referred to as autophagy thereafter.

Autophagy is initiated by the nucleation of a double membrane structure called the phagophore. The phagophore extremities extend and fuse to form an autophagic vacuole called the autophagosome that sequester the dysfunctional cytoplasmic material. The autophagosome then fuses with lysosomes to form an autolysosome in which the dysfunctional material is degraded by the lysosomal hydrolases and then recycled to cytosol for synthesis of macromolecules or energy production [348] (Figure 10). Research on yeast allowed to identify more than thirty proteins involved in the autophagic cascade (ATG proteins), most of which have an orthologue in mammals [349,350]. The autophagic process can be summarized in three stages: initiation/nucleation, elongation-closure and maturation-fusion with lysosomes [348] (Figure 10).

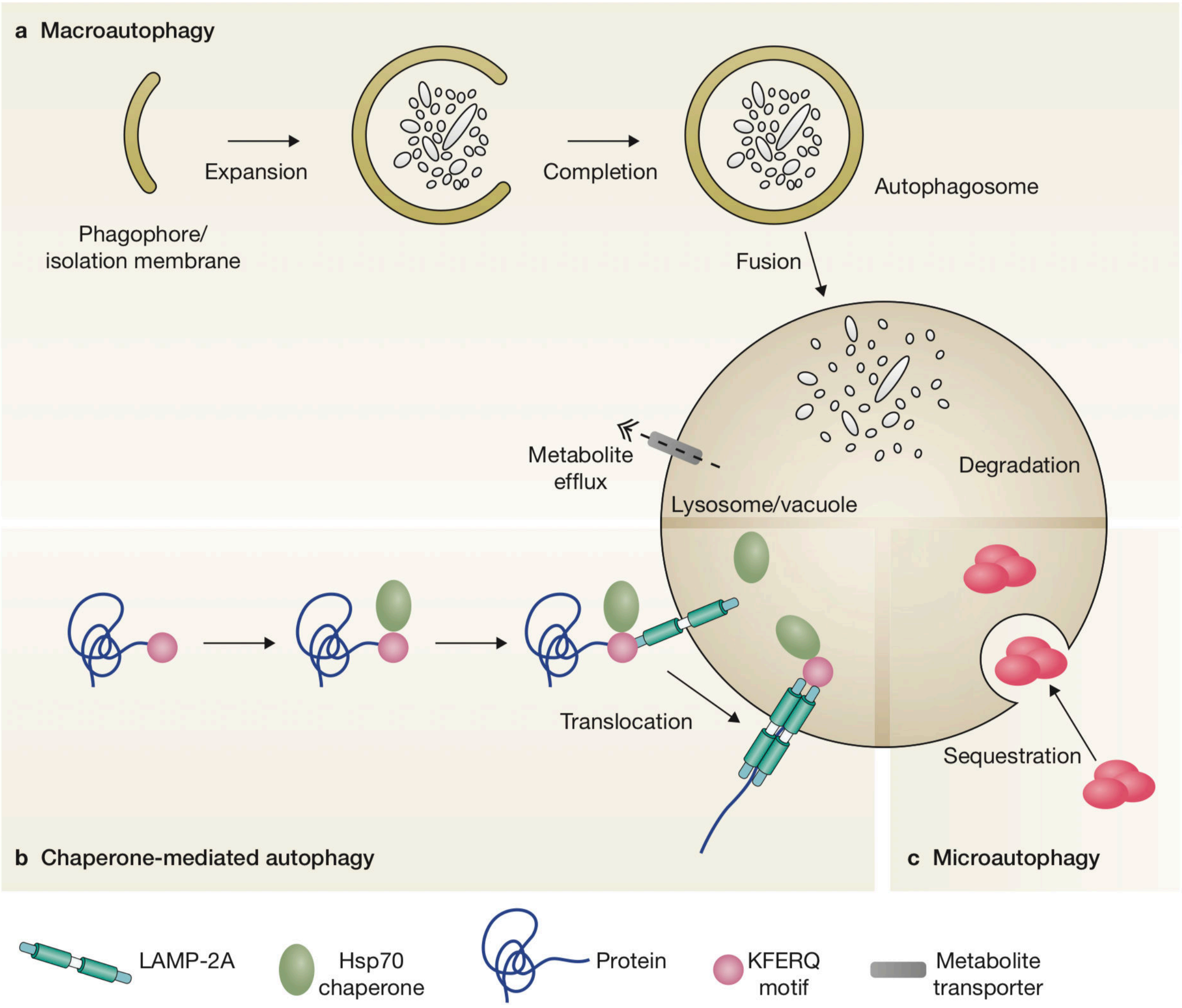
a Macroautophagy
Phagophore/
isolation membrane
Expansion
Completion
Autophagosome
Fusion
Metabolite
efflux
Lysosome/vacuole
Degradation
Translocation
Sequestration
b Chaperone-mediated autophagy
c Microautophagy
LAMP-2A
Hsp70
chaperone
Protein
KFERQ
motif
Metabolite
transporter

Figure 10: Types of autophagy (From Boya P et al., *Nat Cell Biol*, 2013) [351]

3. Molecular machinery of macroautophagy

a- Initiation/Nucleation

The process of autophagosome formation begins at the site of assembly of the phagophore where ULK complex proteins (ULK1 or ULK2, ATG13, FIP200 and ATG101) assemble to initiate the formation of autophagosomes [348] (Figure 11).

The phagophore originates through the assembly of proteins and lipids from different organelles such as the endoplasmic reticulum, Golgi, mitochondria, endocytic system, or plasma membrane. The cargoes are selectively recognized by autophagy adaptors, such as p62, which interacts with autophagic proteins, such as LC3, and allows selective degradation of the ubiquitinated cargo by autophagy. Following a pro-autophagic stimulus such as nutrient starvation, ULK1 and ULK2, which are functionally redundant, dissociate from their negative regulator mTORC1, anchor to the membranes and phosphorylate their targets ATG13 and FIP200 [348].

During the nucleation, the activated ULK complex targets the class III PI3K complex constituted by Beclin 1, VPS15, VPS34 and ATG14 which produces a pool of phosphatidylinositol 3-phosphate (PI3P) specific for autophagosomes. The regulation of the Class III PI3K complex is mediated by proteins essential for macroautophagy that interact with Beclin-1.

The anti-apoptotic protein BCL-2 binds to Beclin-1 and thus prevents its interaction with PIK3C3, thereby inhibiting macroautophagy [352]. Rubicon, another protein that binds to Beclin-1, inhibits PIK3C3 activity in the class III PI3K complex *via* UVRAG [353]. Two major positive regulators of class III PI3K complex are AMBRA1, that directly binds to Beclin-1 [354], and SH3GLB1 / Bif-1, that interacts with Beclin-1 *via* UVRAG [355].

b- Elongation and closure

During the phagophore extension phase, the ATG12-ATG5-ATG16 complex is recruited to the phagophore membrane where it performs E3 ligase activity to mediate the lipidation of the soluble form of LC3, LC3I, with phosphatidyl-ethanolamine to generate the insoluble lipidated form, LC3II, which is involved in the autophagosome membrane extension [348]. Recent studies indicate that LC3 deacetylation as well as cytosolic translocation of a nuclear pool are required for its lipidation, especially in starvation induced autophagy [356].

LC3 is first synthesized as pro-LC3 and rapidly cleaved to give the soluble form LC3-I. Upon autophagy activation, LC3I is cleaved by a protease, ATG4, that induces the exposure of a C-terminus glycine residue which conjugates to the polar head of the phosphatidyl-ethanolamine in a reaction that involves ATG3, ATG7 and the ATG12-ATG5-ATG16L complex. ATG12 is activated by ATG7 and then conjugated to ATG5 by ATG10 (Figure 11). Before the closure of the autophagosome, the ATG proteins dissociate from the membrane but LC3II remains fixed and founded in the inner side of the autophagosome membrane [357]. LC3II is commonly used as a marker of autophagy [358].

Another protein involved in the phagophore extension is the transmembrane protein ATG9. In nutrient-rich conditions, ATG9 is localized in the trans-Golgi network and multivesicular bodies (late endosomes) [359]. In starvation conditions, ATG9 colocalizes with autophagic markers [359]. The delocalization of ATG9 to autophagosomes depends on class III PI3K and ULK1 activity while it is negatively regulated by p38α [359,360]. The precise role of ATG9 and the mechanisms of ATG9 vesicles trafficking are not fully understood although current knowledge suggests a role of ATG9 vesicles as a source of membrane for autophagic machinery [361].

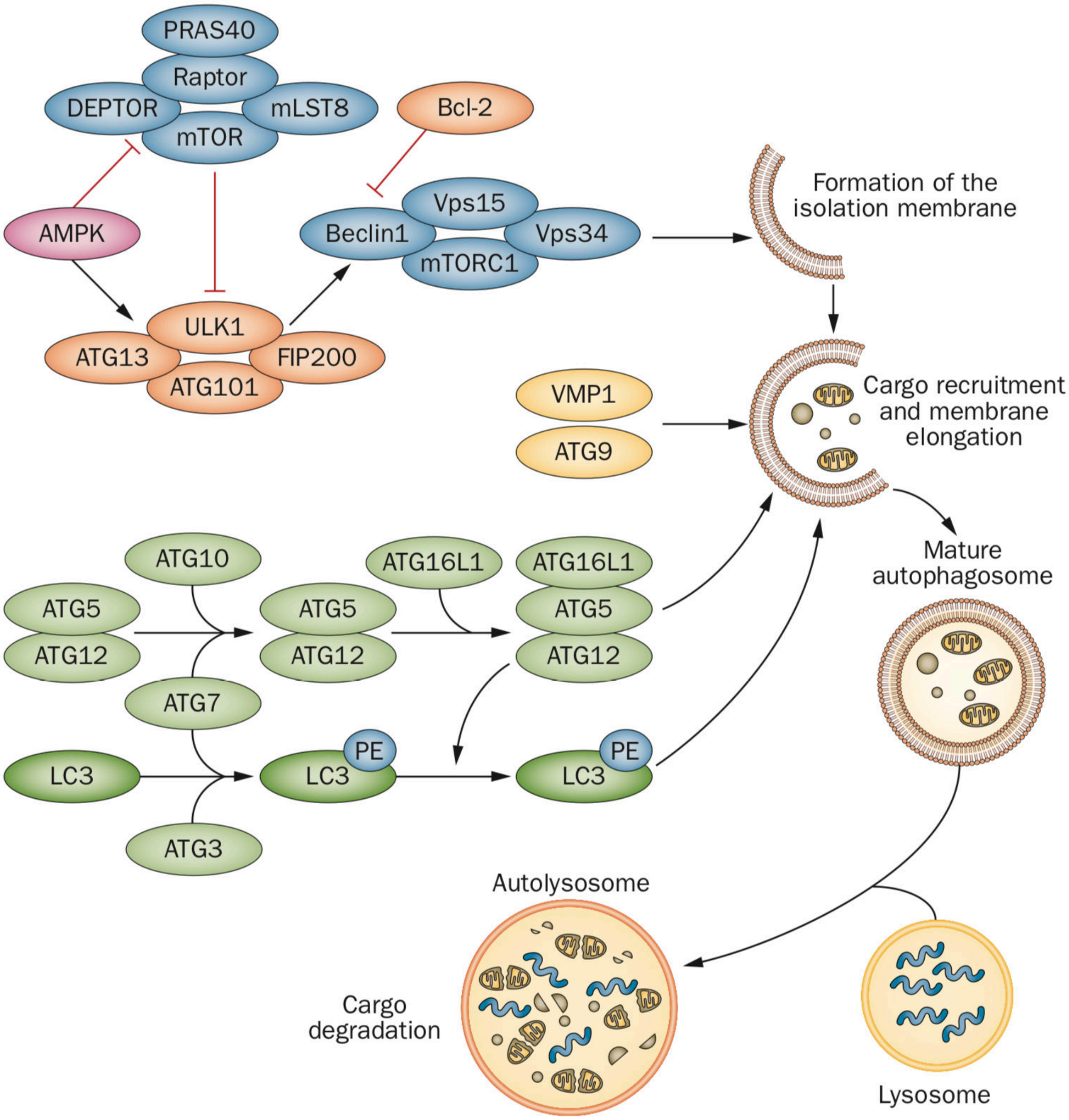
PRAS40
Raptor
DEPTOR
mLST8
mTOR
Bcl-2
AMPK
Vps15
Beclin1
Vps34
mTORC1
Formation of the isolation membrane
ULK1
ATG13
FIP200
ATG101
VMP1
ATG9
Cargo recruitment and membrane elongation
ATG10
ATG16L1
ATG16L1
ATG5
ATG5
ATG5
ATG12
ATG12
ATG12
ATG7
Mature autophagosome
LC3
PE
LC3
PE
LC3
ATG3
Autolysosome
Cargo degradation
Lysosome

Figure 11: Signaling pathways involved in autophagosomes formation (From Fougeray S et al., *Nat Rev Nephrol*, 2015) [362]

c- Maturation/Fusion

Once formed, the autophagosome is directed to the lysosomal compartment to fuse and deliver the cytoplasmic material for degradation. This succession of events is very important and the fusion must occur only once the phagophore closed. If the fusion machinery is recruited and activated before the closure of the phagophore, the material to be sequestered could be released or attached to the cytosolic side of the lysosomal membrane. The fusion factors must therefore recognize only mature autophagosomes. A potential signal could come from the LC3 protein. The deconjugation of Atg8 (LC3 homologue in yeast) from the outer autophagosome membrane is a fusion signal that induces the removal of autophagy initiation machinery [363,364]. Indeed, the majority of Atg8 is present on the inner membrane of mature autophagosomes [365] and the proteins associated to the phagophore, such as ATG16 and ULK1 complex, are absent from the mature autophagosome suggesting that they are removed before its fusion with lysosomes [366].

The mature autophagosomes cross along the microtubule network in the direction of the lysosomal compartment, fusing on their way with early and/or late endosomes (multivesicular bodies) to form hybrid structures called amphisomes. These structures progressively acidify, either because of the pH of the structures with which they fuse, or due to the action of proton pumps on their surface [366].

The fusion process involves multiple protein complexes. For example, UVRAG can bind to the endosomal attachment complex C-VPS (composed by VPS11, VPS16, VPS18 and VPS33) to induce the fusion of autophagosomes with endosomes and/or lysosomes [367]. This process involves a positive regulation of the small GTPase Rab7 [367] which is involved for the fusion process [368]. The ESCRT complex (Endosomal Sorting Complexes Required for Transport), initially identified for its involvement in multivesicular bodies biogenesis and the sorting of ubiquitylated proteins towards multivesicular bodies and lysosomes [369], seems to be involved in the final steps of autophagosomes maturation. Indeed, ESCRT is necessary for the autophagosome-lysosome fusion in human cells [370].

Chen and colleagues demonstrated that TECPR1 (Tectonin beta-Propeller Repeat Containing protein 1) is localized in mature autophagosomes and lysosomes. The loss of TECPR1 induces the accumulation of autophagosomes. TECPR1 binds to PI3P, the enzymatic product of VPS34 complex in an ATG5-ATG12 dependent manner. This binding seems to be crucial for its function [371]. The fusion between autophagosome and lysosome is mediated by SNAREs proteins. Syntaxin 17 is translocated to the outer membrane of mature autophagosomes where it mediates the fusion with the lysosome by interacting with its partners such as SNAP-29 and VAMP8 [372] (Figure 12).

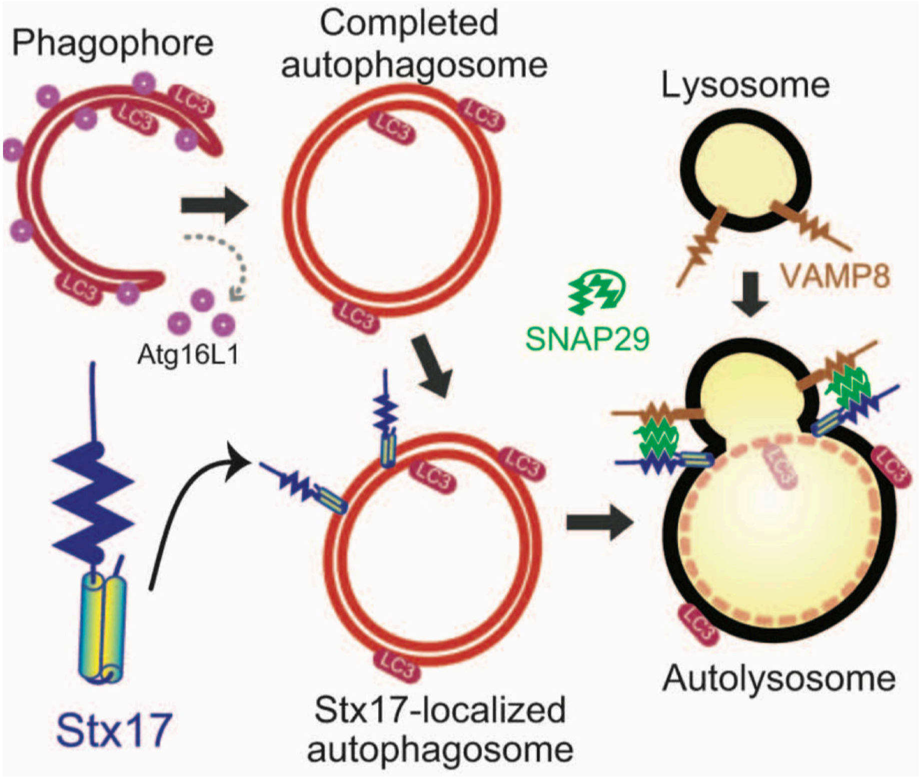
Phagophore
Completed autophagosome
Lysosome
LC3
Atg16L1
VAMP8
SNAP29
Stx17
Stx17-localized autophagosome
Autolysosome

Figure 12: Role of syntaxin 17 (Stx17) in autophagosome-lysosome fusion (From Itakura E et al., *Autophagy*, 2013) [373]

The lysosomal proteins LAMP-1 and LAMP-2 play a key role in autophagosomes maturation. LAMP-1 and LAMP-2 deficient mouse embryonic fibroblasts accumulate immature and mature autophagosomes [374]. This effect is due to a defect in autophagosomes trafficking through microtubules [375]. Moreover, a recent study demonstrated that LAMP-2 is necessary for the expression of Syntaxin 17 by autophagosomes [376].

In addition to the acquisition of the correct fusion machinery, the spatial organization of autophagosomes and lysosomes seems to be a supplemental factor involved in the maturation and the fusion steps. The effective fusion between lysosomes and autophagosomes requires a coordinated positioning of these two organelles in the perinuclear zone [377,378].

4. Signaling pathways and macroautophgy regulation

a. mTOR

mTOR (mammalian Target Of Rapamycin) is a major negative regulator of autophagy through its serine/threonine kinase activity (Figure 13). Three independent groups demonstrated that mTOR inhibits the ULK complex which initiates autophagy by phosphorylating ATG13 and ULK1/2 in their inhibitory sites. mTOR inhibition induces an increase of ULK1/2 kinase activity that phosphorylate ATG13 and FIP2000 inducing ULK complex activation [379–381].

mTOR phosphorylates ULK1 at serine 758 residue and blocks its interaction with AMPK which is necessary for ULK1 activation [382]. Moreover, mTOR may inhibit the stability of ULK1 through the inhibitory phosphorylation of AMBRA1 [383].

mTOR also regulates the VPS34 complex activity which is involved in the formation of autophagosomes. VPS34 forms multiple complexes and plays a major role in vesicles trafficking and autophagy induction. mTOR phosphorylates ATG14L in the VPS34 complex and inhibits the lipid-kinase activity of VPS34 thus inhibiting autophagy [384].

mTOR also regulates autophagy at transcriptional level since it modulates the subcellular localization of TFEB (Transcription Factor EB), a major transcriptional regulator of lysosomal and autophagic genes [385]. mTOR directly phosphorylates TFEB at serine 142 and 211 residues inducing its cytoplasmic sequestration [386,387].

b. Class I PI3K

Upstream of mTOR, the PI3K/AKT pathway modulates mTOR activity (Figure 13). Among the numerous signaling pathways that activates mTOR, the class I PI3K is the key element in the response to growth factors such as insulin [388]. The class I PI3K is a heterodimeric complex composed by a regulatory subunit (p85) and a catalytic subunit (p110) that activates AKT/PKB signaling through the PDK1 kinase activity. Once activated, AKT promotes mTOR activity by suppressing the repressive action of TSC complex (tuberous sclerosis complex, which is composed by TSC1 and TSC2) by phosphorylating TSC2 at serine residue 939 [389]. TSC2 inhibition is associated with the activation of Rheb (Ras homolog enriched in brain) that stimulates mTOR activity [390] which in turn inhibits autophagy. Class I PI3K signaling is a major inhibitory pathway of autophagy (Figure 13).

c. AMPK

AMPK is an intracellular energy sensor involved in the regulation of the energetic homeostasis in response to variations of the ATP/AMP ratio in the cells [391]. AMPK activation is allowed by upstream regulators such as LKB1 [392]. AMPK is a major positive regulator of autophagy (Figure 13). Many studies linked AMPK activation to autophagy induction in response to energetic stresses through its ability to suppress the repressive action of mTOR [382]. AMPK directly phosphorylates TSC2 at threonine 1227 and serine 1345 residues inducing TSC complex activation. Activated TSC complex inhibits Rheb, which is an mTOR activator, thus inducing autophagy [393]. Moreover, AMPK phosphorylates Raptor inducing its sequestration via its binding to 14-3-3 protein and mTOR inhibition [394].

AMPK also interacts with ULK1 and this interaction has been shown to be necessary for autophagy induction [382]. This interaction is increased in cells treated with rapamycin (which inhibits mTOR) suggesting that mTOR negatively regulates this interaction [382]. In addition to its direct interaction with ULK1, AMPK also induces ULK1 activation through its kinase activity at multiple residues. Four AMPK phosphorylation sites have been identified in ULK1 that mediates its activation. Egan and coworkers demonstrated that the phosphorylation at serine 467 and 555 residues is essential for autophagic activity [395] while Kim and colleagues shown that the activation of autophagy induced by glucose starvation depends on the phosphorylation of ULK1 at serine 317 and 777 residues [382].

d. FOXO

The Forkhead transcription factors are a group that includes about hundred members in humans and have various biological functions. In this group, the FOXO family includes four members: FOXO1, FOXO3, FOXO4 and FOXO6 that exhibit positive regulatory effects on autophagy. In response to insulin or growth factors such as IGF1 (Insulin Growth Factor 1), Akt/PKB is activated and directly phosphorylates FOXO members at three regulatory sites (Threonine 32, Serine 253 and Serine 315 for FOXO3) inducing the cytoplasmic sequestration of these transcription factors that become inactive [396]. Inversely, when insulin or growth factors are absent, Akt/PKB is inactive and FOXO members are translocated to the nuclear compartment where they are transcriptionally active [397–399]. Moreover, the cytoplasmic FOXO1 seems to positively regulate autophagy independently of its transcriptional activity [400].

XBP1 negatively regulates autophagy through its action on FOXO1 [401,402]. The stress sensor IRE1α (also called ERN1) is involved in the unfolded protein response (UPR) and catalyzes the splicing of *Xbp1* mRNA to generate the XBP1 protein. XBP1 binds to FOXO1 and regulates it negatively by inducing its proteasomal degradation [401,402]. FOXO3 also stimulates autophagy in diverse cell types via the upregulation of several autophagic genes but its functions on autophagy seems to depend on FOXO1 [403].

e. p53

The tumor suppressor gene p53 plays a dual role in the induction of the autophagic process [404]. In genotoxic stress conditions or when oncogenes are activated, p53 activation induces autophagy. P53 activates AMPK which in turn activates the TSC complex that inhibits mTOR pathway [405]. P53 can also induce autophagy via its positive regulation of DRAM which is a key lysosomal protein that mediates the pro-autophagic and pro-apoptotic effects of p53 [406]. However, the pharmacological inhibition of p53, the downregulation of its expression as well as its genetic deletion lead to autophagy activation [407]. Interestingly, it has been established that it is the cytoplasmic form of p53 that exerts the inhibitory functions on autophagy while the nuclear form of p53, which is transcriptionally active, promotes autophagy [407]. Indeed, the reintroduction in p53 deficient cells of a cytoplasmic restricted p53 mutant inhibits autophagy while the p53 mutants that accumulate in the nucleus fail to block autophagy [407]. Moreover, a recent high throughput sequencing study showed that several genes involved in the different steps of the autophagy are targets for transcriptional activation by p53 [408].

f. E2F1 and NFκB

E2F1 transcription factors are known for their roles in the regulation of genes involved in the regulation of the cell cycle [409]. E2F1 activation also positively regulates autophagy mainly through the induction of autophagy essential genes such as LC3, ULK1, ATG5 and DRAM. E2F1 induces a direct transcriptional upregulation of LC3, ULK1 and DRAM by its binding to the promoter of these genes while the regulation of ATG5 by E2F1 seems to be indirect [410]. E2F1 can also binds to the promoter of Beclin-1 but its transcriptional regulatory effect remains to be demonstrated [411]. BNIP3 is another E2F1 target gene that positively regulates autophagy by disrupting the inhibitory binding of BCL-2 to Beclin-1 [412].

NFκB also exerts regulatory functions on autophagy through its transcriptional activity. NFκB can inhibits autophagy because it is constitutively fixed to the promoter of BNIP3 and blocks the recruitment of E2F1 transcription factor thus preventing BNIP3 gene expression [413]. Inversely, when autophagy is activated, NFκB is removed from the BNIP3 promoter that allows the binding of E2F1 and the expression of BNIP3 protein [413]. Moreover, E2F1 also stabilizes the NFκB inhibitor IκB, thus inhibiting NFκB activation [414]. To summarize, E2F1 and NFκB regulate autophagy by their competitive functions for the binding to the promoter of BNIP3. However, NFκB can also induces some key autophagy genes such as Beclin-1 and SQSTM1 and positively regulates this process [414]. Therefore, NFκB has a dual role in the regulation of autophagy.

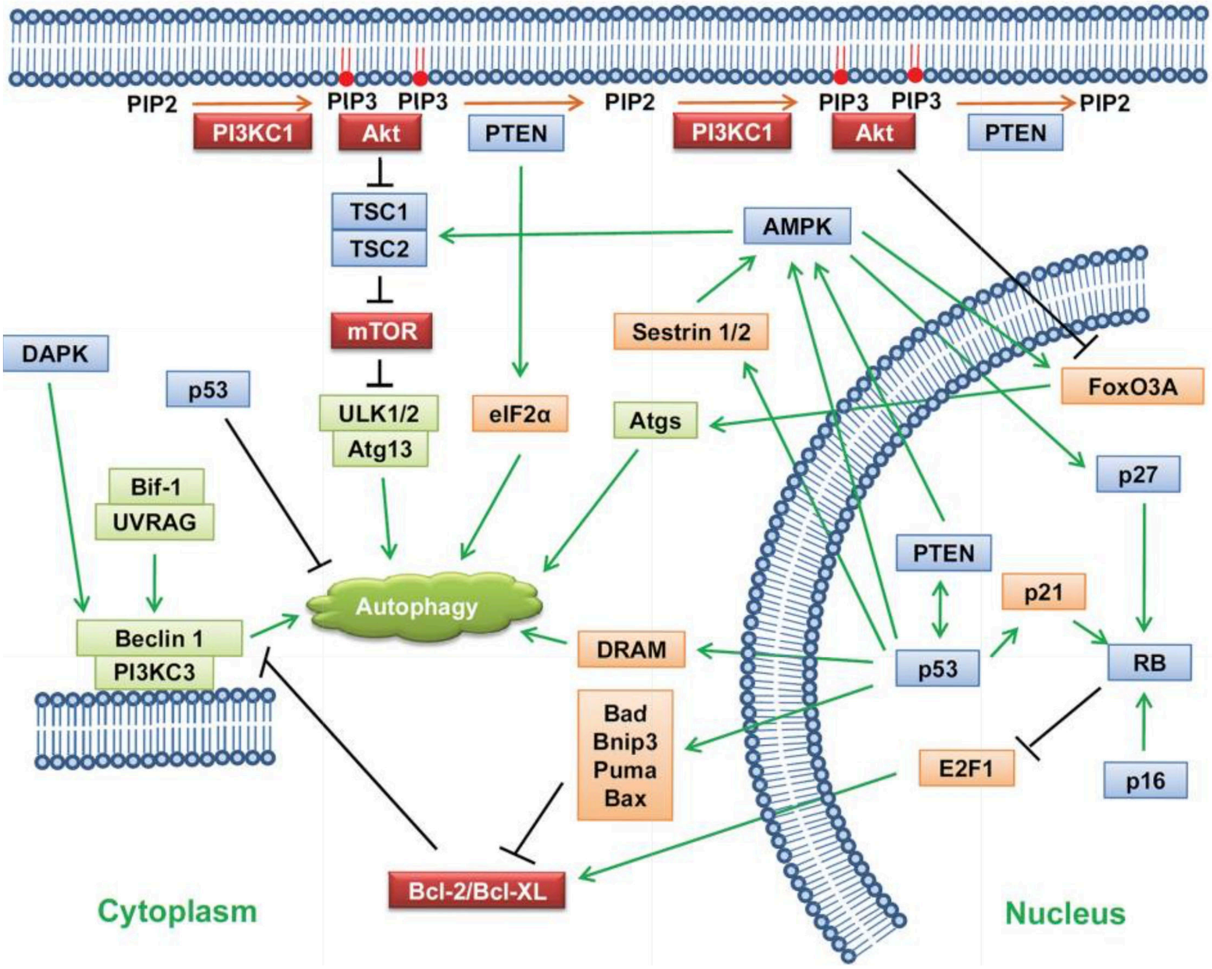
PIP2
PI3KC1
PIP3
PIP3
Akt
PTEN
PIP2
PI3KC1
PIP3
PIP3
Akt
PTEN
PIP2
TSC1
TSC2
AMPK
mTOR
Sestrin 1/2
DAPK
p53
ULK1/2
Atg13
eIF2α
Atgs
FoxO3A
p27
Bif-1
UVRAG
PTEN
p21
Autophagy
Beclin 1
PI3KC3
DRAM
p53
RB
Bad
Bnip3
Puma
Bax
E2F1
p16
Bcl-2/Bcl-XL
Cytoplasm
Nucleus

Figure 13: Regulatory mechanisms of autophagy (From White EJ et al., *Am J Cancer Res*, 2011) [415]

D. Autophagy in the liver

1. Autophagy in liver metabolism and homeostasis

The three types of autophagy (macroautophagy, microautophagy and CMA) co-exist in hepatocytes. Macroautophagy and CMA have been largely studied and are involved in liver metabolism. While the first observations of microautophagy were made in the liver, the molecular mechanism and its physiological relevance in this organ remains poorly evaluated.

Hepatic autophagy provides amino acids, lipids and carbohydrates required for the cellular energetic balance. Autophagy also modulates hepatic metabolism by controlling the levels of enzymes involved in glycolysis and lipolysis. Finally, a key role is attributed to autophagy in the liver to control the number and the functionality of mitochondria, which are essential players of energy homeostasis, *via* a selective form of autophagy called mitophagy [416]. In these conditions, autophagy acts as a survival mechanism, maintaining cellular integrity by regenerating metabolic precursors and clearing subcellular debris. However, in some extreme conditions such as anorexia nervosa, hepatocytes autophagy can lead to autophagic cell death also known as autosis which is distinguished from apoptosis [337].

Starvation is the best-characterized trigger for both macroautophagy and CMA in the liver. Starvation directly inactivates mTOR leading to macroautophagy activation in hepatocytes which degrades in first-line proteins and organelles in bulk [416]. The resulting amino acids are directly used for new protein synthesis or directed to the Krebs cycle for ATP and glucose production [417] (Figure 14).

In addition to protein breakdown, hepatic autophagy can restore the energetic homeostasis through lipids and carbohydrates hydrolysis since lysosomes contain a large repertoire of hydrolases able to degrade these molecules [416]. Indeed, the type of cargo enrolled in the autophagic process in the liver depends on the duration of the starvation. Initially, macroautophagy degrades cytosolic proteins and organelles in bulk to restore the pool of amino acids. When nutrient starvation persists, the cargo is shifted toward glycogen (glycophagy) and lipid droplets (lipophagy) to overcome the nutrient deficiency [416] (Figure 14).

Therefore, in long-term starvation conditions, hepatic glycogen stock thus become an important source of glucose that can be used to sustain a positive energetic balance in absence of nutrients. Autophagy activation can mobilize this glycogen stocks in hepatocytes to be hydrolyzed in lysosomes by α-glucosidase *via* glycophagy which is a selective form of macroautophagy [416]. Glycogen breakdown during starvation may also be processed after its delivery to lysosomes by microautophagy [418] (Figure 14).

Lipophagy is another selective form of macroautophagy that degrades triglycerides and cholesterol stored in lipid droplets (Figure 14) to generates free fatty acids which can be used as cellular fuel in prolonged nutrient starvation [90]. Importantly, lipophagy is also activated when high levels of dietary lipids arrive to the liver. By this way, lipophagy protects the liver against fatty acids-induced lipotoxicity [90]. This mechanism seems to be regulated by the FFA sensor PPARα [419]. Interestingly, both lipophagy and CMA are activated in response to acute increases in intracellular lipids. In contrast, the chronic exposure to lipids inhibit both lipophagy and CMA via changes in lipid composition of the autophagosomes and lysosomes membranes [420,421].

If starvation persists, the contribution of macroautophagy progressively decreases and replaced by CMA [422]. Another way by which autophagy regulates cellular energetic balance is the selective regulation of enzymes involved in metabolic pathways. In this case, CMA seems to be a major mechanism for this process both in basal and starvation-induced turnover of enzymes involved in lipid, carbohydrate and amino acid metabolism [416] (Figure 14). Indeed, CMA deficiency in the liver leads to an increase of basal glycolysis through increased basal expression of glycolytic enzymes including glyceraldehyde-3-phosphate dehydrogenase, pyruvate kinase, aldolase A, malate dehydrogenase 1 or enolase 1 [423]. In the same line, CMA deficiency in hepatocytes leads to the increase of lipogenic enzymes levels (which normally undergo degradation by CMA). This may contribute to the pronounced steatosis observed in the liver of these hepatic CMA-deficient mice which accumulate lipids because of the failure to perform lipolysis [424]. CMA involvement in liver metabolic homeostasis seems to be crucial for the adaptation to nutritional changes. Interestingly, CMA is activated both in starvation conditions (to mobilize liver lipids) and in nutrient rich conditions (such as high fat diet feeding) to protect the liver against lipotoxicity [416,424].

Finally, a key role is attributed to autophagy in the liver for the regulation of mitochondria homeostasis. Mitochondria are key regulators of cellular metabolism through ATP productions, FFA β-oxidation, calcium storage and biosynthesis of phospholipids and heme. Damaged mitochondria produce ROS that generates oxidative stress responsible for cellular injuries and death. Maintenance of mitochondria health is therefore essential for cellular homeostasis [416].

Damaged mitochondria can be removed via a selective form of macroautophagy known as mitophagy [416]. Mitochondria damages induces PINK1 (PTEN Induced Putative Kinase 1) accumulation on the mitochondrial membrane, which induces the recruitment of the ubiquitin ligase PARKIN. In turn, PARKIN allows the ubiquitination of proteins present in the outer mitochondrial membrane allowing their recognition by ATGs and the subsequent mitochondria engulfment in autophagosomes [425]. The regulation of mitochondria turnover is at least regulated by ULK1 phosphorylation which is mediated by AMPK [395]. By this way, mitophagy contributes to restore cellular homeostasis, protecting hepatocytes against oxidative stress, preventing futile consumption of ATP by damaged organelles, therefore reducing cellular damage and cell death pathways activation [416] (Figure 14).

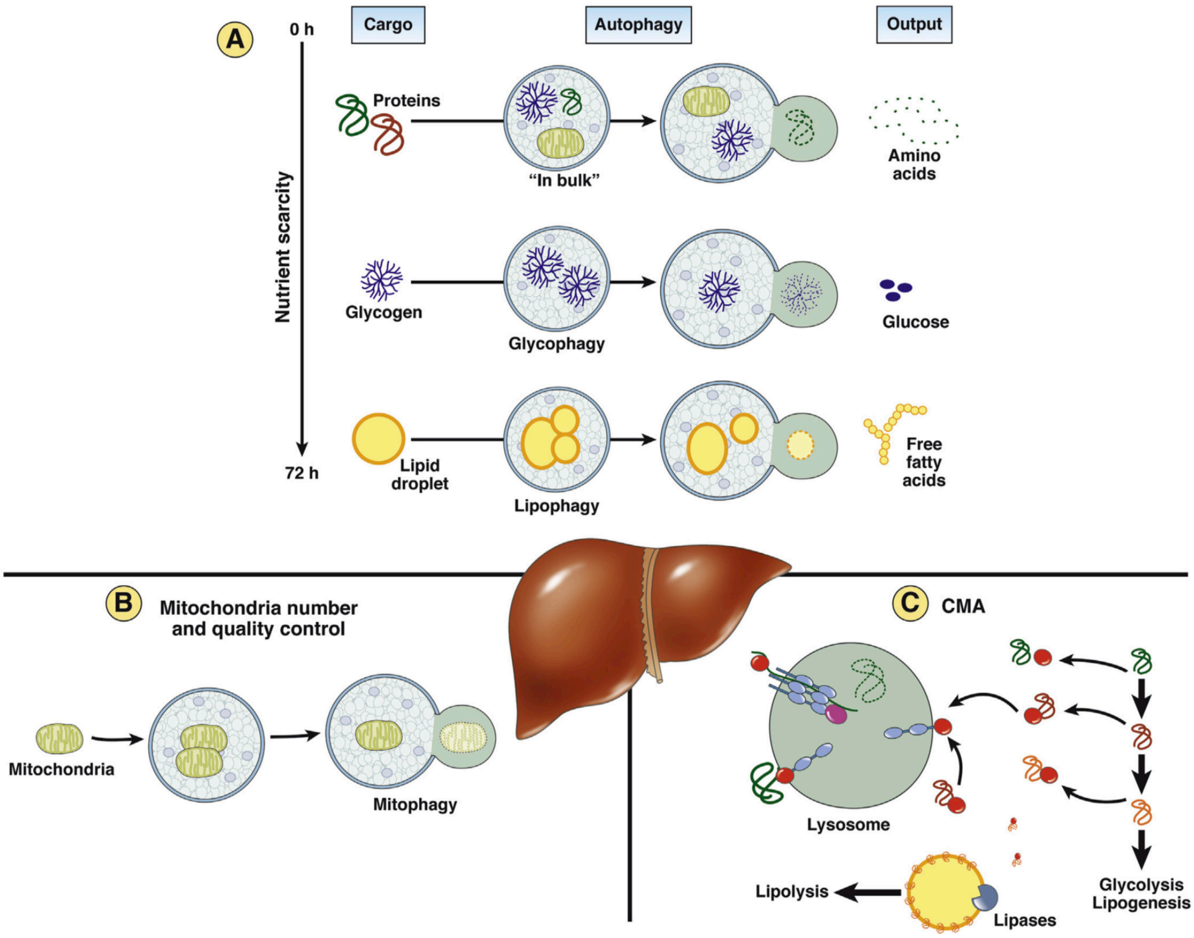
A
0 h
Cargo
Autophagy
Output
Proteins
"In bulk"
Amino acids
Nutrient scarcity
Glycogen
Glycophagy
Glucose
72 h
Lipid droplet
Lipophagy
Free fatty acids
B
Mitochondria number and quality control
Mitochondria
Mitophagy
C
CMA
Lysosome
Lipolysis
Lipases
Glycolysis
Lipogenesis

Figure 14: Main functions of autophagy in the regulation of liver homeostasis (From Madrigal-Matute J and Cuervo AM, *Gastroenterology*, 2016) [416]. **A**: Protein, organelles, glycogen (glycophagy) and lipids (lipophagy) recycling by macroautophagy. **B**: Mitochondrial turnover through mitophagy. **C**: chaperone-mediated autophagy (CMA).

Once amino acids levels and/or energetic balance have been restored, mTOR reactivation induces the phosphorylation of TFEB, preventing its nuclear translocation, thus inhibiting the transcriptional program of autophagy [386]. Moreover, bile acids, which are the end products of lipid metabolism, have an inhibitory effect on lipophagy both at the transcriptional level, through the nuclear sensor FXR [419], and by reducing the autophagosome-lysosome fusion in hepatocytes [426].

2. Autophagy in nonalcoholic steatohepatitis

Given that autophagy is involved in liver metabolism and particularly in lipid droplets breakdown, studies rapidly focused on its role in NASH which is characterized by chronic lipid overload, liver injury with inflammation and varying degree of fibrosis. Accumulating body evidence indicates that autophagy regulates the major steps of NASH progression that highlights its high potential for therapeutic purposes.

NASH is associated with the metabolic syndrome which includes obesity, hyperglycemia and/or type 2 diabetes, dyslipidemia and systemic hypertension. All these features of the metabolic syndrome may have a negative effect on autophagy. For example, autophagy is suppressed by hyperinsulinemia and insulin resistance in the liver of high-fat diet fed mice and in hepatocytes *in vitro*. This effect is mediated by the inhibition of FOXO1 which normally up-regulates key autophagy proteins [398].

It is now well established that autophagy is decreased in fatty livers [416,427]. Indeed, an increase in LC3II and p62 expression in the liver of obese patients with NAFLD and NASH has been reported [428]. LC3II and p62 are both degraded at the end of the autophagic process. Although LC3II accumulation suggests an activation of autophagy, p62 accumulation suggests a blockage of the final step of autophagy, *i.e.* the degradation phase. Taken together, LC3II and p62 accumulation suggests a blockage of the autophagic flux. This hepatic LC3II and p62 accumulation has been positively correlated with the severity of the disease suggesting a progressive blockade of autophagic flux during NAFLD progression [428]. Analyzes in patients with NAFLD and obese mice have shown that liver steatosis impairs autophagic degradation and lysosomal activity *via* an impairment of autophagosomes acidification and the inhibition of cathepsin-L expression, resulting in a decrease of lysosomal degradation of cargo delivered by all types of autophagy [429,430].

The increase in intracellular lipids reduces both macroautophagy and CMA as a result of changes in intracellular membrane composition [420,421]. Changes in the lipid compositions of the autophagosome membrane decrease their ability to fuse with lysosomes thus reducing macroautophagic flux and the clearance of autophagosomes [421]. This may explain the accumulation of LC3II and P62 seen in the liver of patients with NAFL and NASH [428]. Moreover, high dietary lipids can alter the lysosomal stability of CMA receptors such as LAMP-2A, leading to the reduction of CMA activity [420].

Other mechanisms have been proposed in murine models of NASH to explain the decrease in macroautophagic flux in fatty hepatocytes such as 1) the overactivation of mTOR in fatty livers, which is a major inhibitor of autophagy [431]; 2) increased expression of calpain-2 (a calcium-dependent protease), which leads to the degradation of key autophagy proteins such as ATG7 [432]; 3) elevated levels of methionine and S-adenosylmethionine, which inhibit the autophagic lipids catabolism by modulating lipophagy [433]. Impairment of macroautophagy and CMA in the liver both result in marked steatosis [416].

In NASH, the effect of autophagy depends on the cell type. In hepatocytes and Kuppfer cells, autophagy protects against fat accumulation, organelles injury, and displays anti-inflammatory and anti-fibrogenic properties thus inhibiting NASH. By contrast, autophagy in hepatic stellate cell enhances their fibrogenic functions [416,427] (Figure 15). Nothing is known about the role of autophagy in liver sinusoidal endothelial cells

(LSECs) in chronic liver diseases including NASH despite the fact that these cells are among the first liver cells in contact with products derived from the visceral adipose tissue. In acute liver injury, indirect evidences suggest that autophagy in LSECs plays a protective role against ischemia/reperfusion-induced liver injury [434].

a- Autophagy in hepatocytes

As stated above, autophagy impairment in hepatocytes first results in liver steatosis. Several studies reported that macroautophagy alteration results in lipid breakdown dysfunction and lipid droplets accumulation. This was highlighted in genetic models of macroautophagy deficiency (*Atg5* and *Atg7* deficient mice) or by using pharmacological inhibitors of autophagy (3-methyladenine) resulting in steatosis in both cases [90,432]. Macroautophagy inhibition also leads to mitochondrial damage, abnormalities in proteostasis [432] and ER stress in hepatocytes [90,433]. Mitophagy is also impaired in NASH resulting in a reduction of mitochondria turnover leading to altered mitochondria quality control. This promotes oxidative stress through ROS generation and activation of downstream inflammatory pathways such as NF-kB and inflammasome activation [435].

Conversely, autophagy overactivation by adenoviral-induced *Atg7* overexpression or hepatocyte-specific inhibition of Rubicon (a negative regulator of autophagosome fusion through its interaction with Beclin-1) or treatment with pharmacological activators of macroautophagy (carbamazepine or rapamycin) suppresses hepatic steatosis, ER stress and insulin resistance in high fat diet fed mice [433,436,437].

In addition to macroautophagy, CMA is a major regulator of lipid metabolism and has been shown to be altered in NAFLD [416]. Mice deficient in LAMP-2 specifically in hepatocytes spontaneously develop massive steatosis as a result to an increase in lipogenic enzymes levels [423]. Steatosis may also result from reduced mitochondrial β-oxidation and reduced secretion of VLDL (involved in lipids export from the liver), as demonstrated in isolated hepatocytes from CMA-deficient animals [423]. Defects in proteostasis is also observed when hepatic CMA is blocked and promotes the accumulation of oxidized proteins thus contributing to perpetuate the chronic oxidative stress in the liver [438].

To summarize, a defect in hepatocytes autophagy is observed in NASH. Defective hepatocytes autophagy perpetuates the dysfunctional lipid metabolism and promotes oxidative stress, ER stress, inflammatory pathways activation and insulin resistance, lipotoxicity and hepatocytes cell death which is a hallmark of NASH that distinguishes it from NAFL. Therefore, autophagy in hepatocytes prevents from steatosis, oxidative stress, inflammation and liver injury (Figure 15).

b- Autophagy in macrophages

Autophagy is a master regulator of inflammatory functions and immunity and can be modulated by inflammatory mediators such as cytokines [439]. Autophagy controls the differentiation of monocyte into macrophages and can regulate phagocytosis of pathogens by macrophages [440]. When autophagy is inhibited in macrophages, these cells exhibit a proinflammatory profile characterized the accumulation of ROS-producing mitochondria that stimulate NRLP3 inflammasome pathway activation and consequent IL-1β secretion [435,441].

Accumulating body evidence demonstrates that autophagy in liver macrophages is a potent anti-inflammatory process protecting the liver against inflammation and consequent fibrosis. Bone marrow-derived macrophages and peritoneal macrophages from high-fat diet fed mice exhibit a decreased autophagy suggesting a generalized impairment of macrophage autophagy in obese mice [442]. ATG5 deficiency in macrophages specifically exacerbates liver inflammation induced by high fat diet feeding and low doses LPS administration. This effect on liver inflammation is mediated through the regulation of macrophages polarization since autophagy deficiency promotes the polarization of hepatic macrophages into pro-inflammatory M1 phenotype on the one hand, and reduces the M2 polarization in the other hand [442].

Moreover, experiments performed in *Atg5* deficient mice in the myeloid lineage specifically submitted to the carbon tetrachloride induced-hepatotoxicity model showed that these mice exhibit a higher inflammatory response in the liver as compared to littermate controls mice [443]. Inflammation in the liver generated by loss of macrophage autophagy is sufficient to trigger liver injury and mediates fibrogeneis. Interestingly, mice deficient in autophagy in the myeloid lineage show enhanced accumulation of liver fibrogenic cells and an exacerbated fibrosis in the CCl4 fibrosis model [443]. *In vitro*, hepatic myofibroblasts exposed to the culture supernatant of autophagy deficient macrophages display a higher fibrogenic potential as a result of higher release of IL-1α and β from autophagy deficient macrophages [443]. Inhibition of macrophage-dependent inflammation by autophagy also prevents hepatic fibrosis [427]. Therefore, macrophage autophagy is an anti-inflammatory and anti-fibrogenic pathway in the liver (Figure 15).

c- Autophagy in hepatic stellate cells

Hepatic stellate cells are the main players of liver fibrosis. Hepatic stellate cells store retinoids in physiological conditions and shift their phenotype to an activated myofibroblastic state in liver injury to secret large amounts of extracellular matrix components. Contrary to other liver cell types, autophagy in hepatic stellate cells is deleterious (Figure 15).

Human and murine hepatic stellate cells display an increase in LC3II and a decrease in p62 expression during their activation suggestive of an activated autophagic flux. This is confirmed by the presence of a high number of autophagic vacuoles in these cells [444,445]. *Atg7* deficiency in hepatic stellate cells specifically (*Atg7*$^{lox/lox}$/glial fibrillary acidic proteinCre mice) reduces hepatic stellate cells activation and liver fibrosis. Autophagy activation in hepatic stellate cells contributes to their activation. Increased autophagic flux in activated hepatic stellate cells induces the loss of lipid droplets containing retinoids which is associated with the transdifferentiation of quiescent hepatic stellate cells into myofibroblastic cells [444,445]. Lipid droplets breakdown *via* autophagy generates FFA that increase ATP availability thus providing the cellular energy required for hepatic stellate cells activation and transdifferentiation [444]. Potential autophagy inducers favoring hepatic stellate cells activations include oxidative stress and ER stress [444,445].

In addition to the lipogenic activity, autophagy also regulates the fibrogenic properties of hepatic stellate cells through the regulation of their proliferation and their expression of fibrogenic genes including *Collagen1α1*, *Collagen1α2*, *Mmp2*, *Pdgf receptor* and *α-SMA*. Pharmacological inhibition of autophagy in hepatic stellate cells upon CCl4 or thioacetamide treatment downregulates their proliferation and the expression of fibrogenic markers in addition to avoid the loss of lipid droplets [444,445]. Taken together, these results demonstrate that autophagy in hepatic stellate cells contributes to fibrogenesis through lipophagic activity in the one hand, and by enhancing hepatic stellate cells fibrogenic properties in the other hand. Therefore, hepatic stellate cells autophagy is a pro-fibrogenic pathway in the liver (Figure 15).

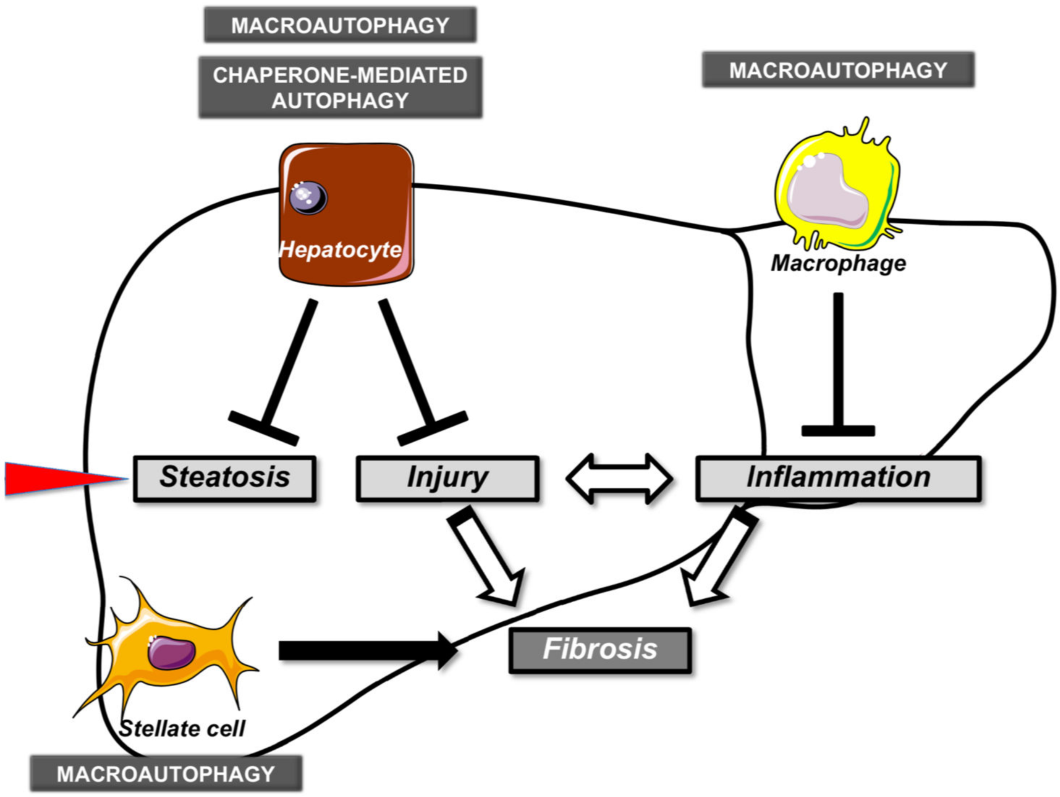
MACROAUTOPHAGY
CHAPERONE-MEDIATED AUTOPHAGY
MACROAUTOPHAGY
Hepatocyte
Macrophage
Steatosis
Injury
Inflammation
Fibrosis
Stellate cell
MACROAUTOPHAGY

Figure 15: Role of autophagy in the liver depending on the cell type (Adapted from Gual P et al., *Am J Physiol Cell Physiol*, 2017) [427].

IV- THESIS WORK

A- Background, hypothesis and aims

Background:

The pathophysiology of NASH is not fully understood. Understanding how simple steatosis evolves to NASH is some patients particularly is of utmost importance. Recent studies demonstrated that endothelial alterations precede inflammation and fibrosis and promote NASH [179,197]. The precise mechanisms triggering these endothelial alterations remain to be determined.

Autophagy is a key process involved in the regulation of cellular homeostasis. Studies demonstrated the role of autophagy in hepatocytes, macrophages and hepatic stellate cells. In hepatocytes and macrophages, autophagy prevents liver injury and displays anti-inflammatory and anti-fibrogenic properties. By contrast, in hepatic stellate cell autophagy enhances fibrogenic functions [427]. Nothing is known about the role of autophagy in LSECs in NASH specifically.

We recently demonstrated that autophagy in endothelial cells of large arteries is crucial for endothelial cell homeostasis. Endothelial autophagy deficiency induces apoptosis and endothelial activation and promotes atherosclerosis in mice [446].

Hypothesis:

Given that autophagy is a key process for endothelial cells integrity and that endothelial alterations promotes NASH development, we hypothesized that autophagy in LSECs could be impaired in NASH thus inducing endothelial alterations and promoting NASH.

Aims:

To test our hypothesis, we divided the project into 2 aims:

1. Evaluate autophagy in LSECs in NASH setting
    a- Evaluate autophagy level in LSECs of patients without liver histological abnormalities, with steatosis or with NASH.
    b- Identify which mediators could modulate autophagy in LSECs in NASH setting.

2. Evaluate the consequences of endothelial autophagy deficiency
    a- Evaluate the consequences of autophagy deficiency on the phenotype of LSECs.
    b- Evaluate the effect of endothelial autophagy deficiency on the development of NASH and advanced fibrosis in mice.

B- Role of autophagy in LSECs in NASH

Article: A defect in autophagy in liver sinusoidal endothelial cells occurs in nonalcoholic steatohepatitis and promotes liver inflammation and fibrosis

A defect in autophagy in liver sinusoidal endothelial cells occurs in NASH and promotes inflammation and fibrosis

Authors: Adel Hammoutene[1,2], Juliette Lasselin[1,2], Marouane Kheloufi[1,2], Anne-Clémence Vion[1,2], Jules Mérian[1,2], Nathalie Colnot[3,5], Xavier Loyer[1,2], Patrice Codogno[2,6,7], Sophie Lotersztajn[4,5], Valérie Paradis[4,5,8], Alain Tedgui[1,2], Chantal M. Boulanger[1,2], Pierre-Emmanuel Rautou[1,3,4]

1- Inserm, UMR-970, Paris Cardiovascular Research Center, PARCC, Paris, France
2- University Paris Descartes, Paris, France
3- Service d'Hépatologie, Centre de Référence des Maladies Vasculaires du Foie, DHU Unity, Pôle des Maladies de l'Appareil Digestif, Hôpital Beaujon, AP-HP, Clichy, France
4- University Paris Diderot, Paris, France
5- INSERM, UMR1149, Centre de Recherche sur l'Inflammation, Paris, France
6- Inserm U1151, Institut Necker-Enfants Malades-INEM, Paris, France
7- CNRS UMR 8253, 75014 Paris, France
8- Service d'Anatomie Pathologique, Hôpital Beaujon, Assistance Publique-Hôpitaux de Paris, Clichy, France.

Original article (to be submitted)

Key words: autophagy, LSECs, NASH, inflammation, fibrosis

Abbreviations: AMPK, AMP-activated protein kinase; CCl4, carbon tetrachloride; IL6, Interleukin 6; LSECs, liver sinusoidal endothelial cells; MCP1, monocyte chemoattractant protein-1; NASH, nonalcoholic steatohepatitis; TGF-β1, transforming growth factor-β1; TNF, tumor necrosis factor; VCAM-1 vascular cell adhesion molecule 1.

Words: 7093 inclunding abstract, references and figure legends

Figures: 6

References: 49

Financial support: This work was supported by the "Institut National de la Santé et de la Recherche Médicale", Paris Descartes University, the "Fondation pour la Recherche Médicale" (FRM, DPC20111122979), the "Agence Nationale pour la Recherche" (ANR-14-CE12-0011, ANR-14-CE35-0022, ANR-18-CE14-0006-01) and by the "Association Française pour l'Etude du foie" (AFEF 2014), A.H. and M.K. by the "Ministère de l'Enseignement Supérieur et de la Recherche", A-C.V. by CODDIM Ile de France, and M.K. by the "Fondation pour la Recherche Médicale" (FDT20160435690).

Conflict of interest: none

Authors' contributions: A.H., and P-E.R. designed the experiments and wrote the manuscript. A.H., J.L., M.K, A-C.V., J.M., and N.C. performed the experiments. P-E.R. obtained funding for the project. All authors discussed and critically revised the manuscript.

Acknowledgment: We thank members of the INSERM UMR-970 animal facility (ERI) for animal handling and breeding. We thank Michèle Souyri for having provided *VE-cadherin-Cre* transgenic mice and Noburo Mizushima for having provided *Atg5flox/flox* mice.

Highlights

- Autophagy is defective in LSECs from patients with NASH
- Inflammatory mediators present in the portal blood could be responsible for this defect
- Deficiency in autophagy induces LSECs inflammation, endothelial to mesenchymal transition and apoptosis
- Deficiency in endothelial autophagy promotes liver inflammation and liver fibrosis

Abstract: (250/250)

Background and aims: Previous studies demonstrated that autophagy is protective in hepatocytes and macrophages, but detrimental in hepatic stellate cells in chronic liver diseases. Nothing is known about the role of autophagy in liver sinusoidal endothelial cells (LSECs) in nonalcoholic steatohepatitis (NASH). Our aim was to analyze the potential implication of autophagy in LSECs in NASH and liver fibrosis.

Methods: We analyzed autophagy in LSECs from patients using transmission electron microscopy. We determined the consequences of a deficiency in autophagy on LSECs phenotype using cultured liver endothelial cells transduced with an Atg5 shRNA. We analyzed the effect of a deficiency in endothelial autophagy on early stages of NASH and on advanced stages of liver fibrosis, using transgenic mice deficient in autophagy specifically in endothelial cells and fed a high fat diet or treated with carbon tetrachloride, respectively.

Results: Patients with NASH had twice less LSECs containing autophagic vacuoles than patient without liver histological abnormalities, or with simple steatosis. *In vitro*, deficiency in autophagy enhanced endothelial inflammation, endothelial-to-mesenchymal transition and apoptosis. In mice fed a high fat diet, deficiency in endothelial autophagy induced liver expression of inflammatory markers and perisinusoidal liver fibrosis. Mice deficient in endothelial autophagy treated with carbon tetrachloride developed more perisinusoidal liver fibrosis.

Conclusions: A defect in autophagy in LSECs occurs in the liver of patients with NASH. Deficiency in endothelial autophagy promotes to the development of liver inflammation, endothelial-to-mesenchymal transition and liver fibrosis at early stages of NASH, but also favors more advanced stages of liver fibrosis.

Nonalcoholic fatty liver disease is an expanding health problem with an estimated global prevalence of 25% [1]. Nonalcoholic fatty liver disease is associated with obesity, insulin resistance or type 2 diabetes and other metabolic abnormalities collectively termed the metabolic syndrome [2]. Nonalcoholic fatty liver disease encompasses a spectrum of conditions including simple steatosis and nonalcoholic steatohepatitis (NASH) which includes in addition to steatosis, hepatocellular injury and inflammation with varying degree of fibrosis [2]. NASH can progress to both cirrhosis and hepatocellular carcinoma and is projected to become the most common indication for liver transplantation in the next decade [3]. Despite its prevalence and severity, there is no approved therapy for NASH and available treatments only aim to control associated conditions [4]. Understanding the pathophysiology of NASH and in particular how simple steatosis progresses to NASH is thus of utmost importance.

Liver sinusoidal endothelial cells (LSECs) are highly specialized endothelial cells representing an interface between the blood derived from organs involved in NASH pathogenesis, namely the visceral adipose tissue and the gut, and other liver cells including hepatocytes and hepatic stellate cells [5–7]. Recent studies suggested that alterations in LSECs precede the onset of NASH and promote its development. First, several groups reported disruption of vascular architecture in nonalcoholic fatty liver disease [8–10]. Second, LSECs capillarization and endothelial dysfunction precede inflammation and fibrogenesis in murine models of nonalcoholic fatty liver disease [10–15]. Third, angiogenesis plays a key role in the progression of NASH [8,16–19]. The mechanisms underlying LSECs alterations in NASH remain unknown.

Macroautophagy (hereafter referred to as autophagy) is a major intracellular recycling system. Under basal conditions, autophagy controls organelle and protein quality to maintain cellular homeostasis. Under conditions of stress, autophagy acts as a survival mechanism, maintaining cellular integrity by regenerating metabolic precursors and clearing subcellular debris [20]. This process modulates an expanding list of disease processes [20]. In NASH and chronic liver diseases, the effect of autophagy depends on the cell type [21]. In hepatocytes, autophagy protects against fat accumulation and prevents liver injury by removing altered mitochondria and decreasing cellular stresses [21,22]. Importantly, hepatocyte autophagy is reduced in NASH [21,23]. In macrophages, autophagy displays anti-inflammatory properties and prevents hepatic inflammation and fibrosis [21,24]. By contrast, autophagy in hepatic stellate cell enhances fibrogenic functions [21,25]. Nothing is known about the role of autophagy in LSECs in chronic liver diseases including NASH. In mild and severe acute liver injury, endothelial autophagy plays a protective role [26,27].

This led us to test the hypothesis that autophagy in LSECs could be involved in NASH development.

Material and methods

Human samples.

Twenty-five patients who underwent a percutaneous or transjugular liver biopsy were selected from a pathological database: 7 had no or mild abnormalities at liver histological examination, 4 had simple steatosis and 12 had NASH. None of the patients had detectable anti-hepatitis C virus antibodies or HBs antigen. Alcohol consumption was below 21 drinks on average per week in men and 14 drinks on average per week in women. Patients' metabolic parameters are described in supplementary table 1. All patients gave their consent. This study was approved by the Institutional Review Board of Paris North Hospitals, Paris 7 University, AP-HP (N° 2017-013). The study conformed to the ethical guidelines of the 1975 Declaration of Helsinki. For transmission electron microscopy (TEM) analysis, liver biopsies were fixed with 1.7% glutaraldehyde dehydrated in ethanol, cuted (90ηm) with an ultramicrotome and embedded in grids. Observations were performed at Cochin institute (Paris, France) with a transmission electron microscope (JEOL 1011) equipped with a tungsten filament. Images were captured with digital camera and Digital Micrograph software. For morphometric analysis, a minimum of 11 random LSECs per patient were taken in a blinded manner at a magnification of 40000x. Electron microscopy pictures were assessed in a blinded manner. For TEM experiments, the term autophagic vacuole was defined as vacuoles with an electron-dense content and referred to autophagosome or autolysosome since it is often not possible to determine from TEM images whether an autophagosome has fused or not with a lysosome [28,29].

Animal Models: All mice were on a C57BL/6 background (male and female) and were housed on a 12 hrs light/dark cycle with *ad-libitum* access to food and water. All experiments were conducted in accordance with the European Community guidelines for the care and use of laboratory animals. Animal studies were approved by the institutional ethics committee and authorized by the French education and research ministry (# 12943 - 2017070617179577). Mice constitutively deficient in endothelial autophagy were obtained by crossing *VE-cadherin-Cre* transgenic mice provided by M. Souyri [30], with *Atg5*$^{lox/lox}$ mice provided by N. Mizushima [31]. VE-cadherin is expressed during embryonic development in hemangioblast, which is common progenitor to endothelial myeloid cells [32]. To avoid the leak of ATG5 deletion in myeloid cells, all mice used in this study were irradiated and transplanted with a bone marrow from *Atg5*$^{lox/lox}$ mice. For the study of initial steps of NASH development, 12-week-old *Atg5*$^{lox/lox}$ and *Atg5*$^{lox/lox}$; *VE-cadherin-Cre* mice were fed a control chow diet or a high-fat diet (Safe U8220 version 16) containing 1.25% of cholesterol and 15% of cocoa butter (45% Kcal derived from lipids) for 16 weeks (supplemental Figure 4). For the study of advanced stages of liver fibrosis, *Atg5*$^{lox/lox}$ and *Atg5*$^{lox/lox}$; *VE- cadherin-Cre* mice received a single injection of clodronate (clodronateliposomes.org) in addition to the bone marrow transplant. Mice were then intraperitoneally injected with carbon tetrachloride (CCl4, Sigma Aldrich 319961) suspended in peanut oil (Sigma Aldrich P2144) at 0.24mL/Kg, three times a week for 6 consecutive weeks (supplemental Figure 6). Control mice received intraperitoneal injection of vehicle. At the end of each protocol, blood was collected from inferior vena cava under isofluorane anesthesia. Mice fed a high fat diet were fasted for 6 hrs before blood collection. Mice were humanely euthanized. Animals were then perfused with 10 mL of saline and organs (liver, spleen and heart) were harvested. One part of the liver was fixed in 10% formalin and the remaining tissue was immediately frozen in liquid nitrogen and stored at -80°C until processing for western blot experiments, as described below.

Blood pressure measurement: Arterial blood pressure was measured every 30 seconds at the tail of conscious mice using a CODA non-invasive blood pressure device (Kent Scientific Corporation) (mean value of 15 measurements). Blood pressure was measured for 3 consecutive days after 2 days of acclimation in the chamber.

Plasma preparation: On the day of euthanasia, mice were sedated with 2% isofluorane. Blood was collected from the inferior vena cava using a 25-gauge x 1' needle in a 1 mL syringe pre-coated with 3.8% sodium citrate. Blood was centrifuged at 2500 g for 15 minutes at 18°C in order to pellet cells. Then, plasma was centrifuged a second time at 2500 g for 15 minutes at 18°C to pellet platelets and cell debris. Platelet free plasma was aliquoted and stored at -80°C for biochemical measurements, as described below.

Plasma biochemical measurements: plasma alanine aminotransferase (ALT) and aspartate aminotransferase (AST) levels, fasting glucose, total cholesterol, high-density lipoprotein (HDL)-cholesterol and triglyceride levels were measured in PFP by standard methods with a multiparametric automate Olympus AU400 at the institute Claude Bernard (Paris 7 University).

Hepatic lipid analysis: About fifty micrograms of frozen liver tissue were homogenized by sonication in 1 mL of acetone. After overnight incubation at 4°C, samples were centrifuged at 4000 g for 10 min. Triglyceride (Diasys, Holzheim, Germany) and total cholesterol (Biomérieux, Craponne, France) contents were then measured in the supernatant using enzymatic kits according to manufacturers' instructions. Triglycerides and total cholesterol content were normalized to the weight of the liver tissue used for the lipid extraction.

Histopathology: Liver samples were fixed in 10% formalin and embedded in paraffin. 3 μm thickness sections were made and stained with Hematoxylin and Eosin and Sirius red. Images were taken using a light microscope (Nikon Eclipse E600) equipped with a digital camera by using Archimed software. The Sirius red positive area was measured in at least 12 fields without vessels or capsule and quantified with ImageJ software. Steatosis was scored on HE staining according to the following scoring system that assesses the proportion of large or medium fat droplets containing hepatocytes: S0: <5%; S1: 5–33%; S2: 34–66%; S3: >67%.

Transformed liver sinusoidal Endothelial Cells culture: The immortalized murine LSECs cell line TSECs [33] was provided by Dr. Vijay Shah (Mayo Clinic, Rochester, MN) and cultured on 0.2 % gelatin-coated slides (Menzel Glazer; Braunschweig, Germany) in Dulbecco's modified Eagle medium (DMEM) containing 1% endothelial cell growth supplement (ECGS, Sciencell 1052), 5% fetal bovine serum, streptomycin (100 IU/mL), penicillin (100 IU/mL) and Amphotericin B (10 μg/L) (Gibco).

Lentiviral transduction: Lentiviruses expressing inducible shRNA (Sigma Aldrich, MISSION® inducible shRNA Vectors) were used to silence ATG5. TSECs were infected in the presence of hexadimethrine bromide at 8 μg/mL (Sigma Aldrich H9268) with lentiviruses at multiplicity of infection (MOI) 2.5. Negative controls were lentiviruses expressing a non-target shRNA used at the same MOI. Transduced cells were amplified and selected using puromycine (Sigma Aldrich P9620) at 1 μg/mL during the amplification period. shRNA expression was induced by treating the transduced cells with Isopropyl β-D-1-thiogalactopyranoside (IPTG, Sigma Aldrich; I6758) for 5 consecutive days at 0.1 mmol/L. ATG5 knockdown was verified in all experiments. Experiments in which ATG5 extinction was lower than 30% were systematically excluded.

Shear stress experiment *in vitro*: A unidirectional steady laminar and peristaltic shear stress was applied to confluent TSECs to mimic physiological conditions using a parallel plate chamber system as described elsewhere [34]. Endothelial cell medium was perfused for 24 hrs. Local shear stress was calculated using Poiseuille's law and was 20 dynes/cm^2. To analyze the effect of mediators present in the portal blood on autophagy level, TSECs were treated during the 24 hrs of shear stress with MCP1 (100 pg/mL, R&D systems), or insulin (1 nmol/L, Sigma Aldrich), or TNFα (10 pg/mL, Peprotech), or IL6 (10 pg/mL, Peprotech) or with the combination of TNFα and IL6 (10 pg/mL for each) at concentrations similar to those reported in the portal venous blood in metabolic syndrome [35–38]. In some experiments, cells were treated with chloroquine (300 µmol/L) for 30 minutes before the end of the shear stress experiment in order to assess autophagic flux. Effect of the deficiency in autophagy in TSECs on endothelial inflammation, endothelial-to-mesenchymal transition and endothelial apoptosis was tested in basal conditions as well as after exposure of TSECs to TNFα (1 ng/mL) for 12 hrs before the end of the shear stress experiment. TSECs were then collected for Western blot or RT-qPCR or flow cytometry, as detailed below.

Western blot: For *in vivo* experiments, about 50 mg of frozen mouse liver tissues were homogenized in 650 µL RIPA buffer containing 150 mmol/L NaCl, 50 mmol/L TrisHCl, pH 7.4, 2 mmol/L EDTA, 0.5% sodium deoxycholate, 0.2% sodium dodecyl sulfate, 2 mmol/L activated orthovanadate, complete protease inhibitor cocktail tablet (Complet mini, Roche, France) and complete phosphatase inhibitor cocktail tablet (Roche, France). The homogenates were then incubated at 4°C for 45 minutes. For *in vitro* experiments, TSECs were washed with cold PBS and scraped off in RIPA buffer. Lysates from liver samples and TSECs were sonicated (15 seconds, 40 watts, Vibra Cell, Bioblock) and then centrifuged at

12000 g for 5 min. Supernatants were collected and protein content was quantified using the Lowry protein assay (Bio-Rad; Hercules, CA). Lysates were mixed with the reducing sample buffer for electrophoresis and subsequently transferred onto nitrocellulose membrane (Bio-Rad). Equal loading was checked using Ponceau red solution. Membranes were incubated with primary antibodies (primary antibodies used are described in supplementary table 2). After secondary antibody incubation (anti-goat, Santa Cruz Biotechnology, INC, 1/5000; anti-rabbit or anti-mouse, Amersham, GE Healthcare, UK 1/3000), immunodetection was performed using an enhanced chemiluminescence kit (Immun-Star Western C kit, Bio-Rad). Bands were revealed using the LAS-4000 imaging system. Values reported from Western blots were obtained by band density analysis using Image Gauge software (Fujifilm, Tokyo, Japan) and expressed as the ratio protein of interest compared to GAPDH for whole cell extract.

Quantitative reverse transcription-PCR: mRNA from liver samples and TSECs were extracted in TRIzol® reagent (Life technologies) according to manufacturers' instructions. cDNA synthesis was performed with QuantiTect Reverse Transcription Kit (Qiagen). Quantitative polymerase chain reaction (PCR) was performed on Real-Time PCR System StepOne Plus (Applied Biosystems) with Power SYBR Green PCR Master Mix (Eurogentec) with the following parameters: 1 cycle at 95°C for 10s followed by 45 cycles at 95°C for 15s, 57°C–65°C (depending on each primer couple) for 30s and finally 72°C for 30s. Primers sequences and corresponding annealing temperatures used are described in supplementary table 3. Melt curve analysis was employed to confirm the presence of a single PCR product. Liver expression of all genes has been normalized to *Gapdh* expression for the high fat diet protocol. Gene expression in the CCl4 protocol and in TSECs has been normalized using three housekeeping genes (*Gapdh, Hprt* and *Ppia*).

Relative expression was calculated using the 2-delta-delta CT method. Geometric average of normalization to each housekeeping gene was calculated for TSECs gene expression analysis.

Flow cytometry: TSECs were washed with cold PBS and incubated with anti-VCAM-1 (R&D AF643, 0.25 μg/10^6 cells) antibody for 30 minutes at 4°C. After washing, cells were incubated with an anti-goat AlexaFluor®594 secondary antibody (Invitrogen, 1/400) for 30 minutes and analyzed using a LSRII flow cytometer (BD Biosciences). Results were expressed as mean fluorescent intensity.

Statistical analysis: Data are expressed as median ± IQR for human data and *in vivo* experiments and as mean ± SEM for *in vitro* experiments. Comparisons were performed using the Mann-Whitney U-test. Statistical analyses and figures were performed using GraphPad Prism 6 software for Mac OS X. All tests were two-sided and used a significance level of 0.05.

Results

Autophagy is defective in LSECs in NASH

We first investigated liver endothelial autophagy in nonalcoholic fatty liver disease by performing transmission electron microscopy on liver biopsies from patients. In patients with NASH, LSECs contained autophagic vacuoles twice less frequently than in patients with no or mild abnormalities at liver histological examination or in patients with simple steatosis (Figure 1A and B), suggesting that NASH is associated with a defect in liver endothelial autophagy.

We then sought to identify the mediators present in the portal blood accounting for such a possible defect in liver endothelial autophagy. We used immortalized liver endothelial cells, called TSECs [33], exposed to shear stress to mimic *in vivo* conditions. As presented in Supplemental Figure 1, shear stress activated autophagic flux since LC3II/GAPDH ratio was increased by shear stress and further augmented when the inhibitor of autophagic flux, chloroquine, was added (Supplemental Figure 1). We observed that MCP1, insulin, TNFα or IL6 alone, at concentrations similar to those found in the portal vein in rodents and patients with metabolic syndrome [35–38], did not change LC3II/GAPDH ratio (Supplemental Figure 2). Interestingly, the combination of TNFα and IL6 decreased LC3II/GAPDH ratio ($p=0.0002$) (Figure 1C). Similar results were obtained in the presence of chloroquine demonstrating that the combination of TNFα and IL6 decreased autophagic flux (Supplemental Figure 2).

We then investigated the pathways by which TNFα and IL6 regulate autophagy in TSECs and analyzed the AMPKα pathway, a master positive regulator of autophagy [39]. We observed that the combination of TNFα and IL6 reduced p-AMPKα/GAPDH ratio ($p=0.01$) (Figure 1D).

Taken together, these results suggest that a defect in liver endothelial autophagy occurs in NASH, following an inhibition of AMPKα activity induced by TNFα and IL6.

Deficiency in liver endothelial autophagy leads to endothelial inflammation, endothelial-to-mesenchymal transition and endothelial apoptosis

To assess the consequences of a deficiency in autophagy on liver endothelial cell phenotype, we inhibited autophagy in TSECs using a genetic approach (transduction with a lentivirus expressing an ATG5 shRNA; Figure 2A; Supplemental Figure 3 A-C).

We first tested whether autophagy regulates endothelial inflammatory responses. In basal conditions, *Rantes* gene expression was higher in TSECs deficient in autophagy than in control cells ($p<0.0001$), while *Mcp1* gene expression was unchanged (Supplemental Figure 3D). After exposure to the proinflammatory stimulus TNFα, TSECs deficient in autophagy expressed 1.5-fold more *Mcp1* ($p=0.002$) and 2.5-fold more *Rantes* ($p=0.002$) than control TSECs (Figure 2B). Moreover, VCAM-1 expression at cell surface, evaluated using flow cytometry, was higher in TSECs deficient in ATG5 than in TSECs transduced with a control shRNA ($p=0.001$) (Figure 2C).

We also evaluated features of endothelial-to-mesenchymal transition. In basal conditions, *α-SMA*, *Tgf-β1* and *Collagen1α2* gene expression was not affected by autophagy level (Supplemental Figure 3E). After exposure to the proinflammatory stimulus TNFα, *α-SMA*, *Tgf-β1* and *Collagen1α2* gene expression were higher in TSECs deficient in autophagy than in control cells ($p=0.002$) (Figure 2D).

Finally, we assessed the effect of a deficiency in endothelial autophagy on endothelial apoptosis. We observed that cleaved Caspase-3/GAPDH ratio was increased in TSECs deficient in autophagy in basal conditions (Supplemental Figure 3F) as well as after exposure to the proinflammatory stimulus TNFα ($p=0.0002$) (Figure 2E).

Taken together, these results show that a deficiency in autophagy in liver endothelial cells induces features of endothelial inflammation, of endothelial-to-mesenchymal transition and endothelial apoptosis.

Deficiency in endothelial autophagy promotes NASH development

To assess the role of endothelial autophagy at early stages of NASH, *Atg5*$^{lox/lox}$ and *Atg5*$^{lox/lox}$*; VE-cadherin-Cre* mice were fed a chow diet or a high fat diet for 16 weeks (Supplementary Figure 4).

As expected in this mouse model reproducing early stages of NASH [40], steatosis, markers of liver injury (plasma AST and ALT levels), and of liver inflammation (liver *Mcp1* and VCAM-1 expression) were higher in *Atg5*$^{lox/lox}$ mice fed a high fat diet than in *Atg5*$^{lox/lox}$ mice fed a chow diet (Figure 3 B-F), and markers of liver fibrosis were similar (Figure 4).

When fed a chow diet, mice deficient in endothelial autophagy had similar markers of liver injury, of liver inflammation and of liver fibrosis as littermate controls (Figures 3 and 4). When fed a high fat diet, mice deficient in endothelial autophagy had more frequently a nodular liver surface (20% *vs.* 78% respectively, $p<0.0001$) (Figure 3A), higher markers of liver inflammation (liver *Mcp1* and *Rantes* gene expression and liver VCAM-1 protein expression; Figure 3 D-F), and of liver fibrogenesis (liver α-SMA protein expression, liver *Tgf-β1* and *Collagen1α2* gene expression, liver collagen staining with Sirius red) than littermate controls, (Figure 4). Of note, liver fibrosis was mainly perisinusoidal in mice deficient in endothelial autophagy (Figure 4E). In mice fed a high fat diet, deficiency in endothelial autophagy had no impact on markers of liver injury (AST and ALT levels) (Figure 3C), or on liver steatosis assessed by histology (Figure 3B) or by liver triglyceride content (Supplement Figure 5A). Liver cholesterol content was slightly lower in *Atg5*$^{lox/lox}$*; VE-cadherin-Cre* mice than in *Atg5*$^{lox/lox}$ mice (Supplement Figure 5B).

Deficiency in endothelial ATG5 had no effect on body weight, organs weight, blood cell count, arterial blood pressure, plasma cholesterol, triglycerides and glucose levels (Supplemental Table 4). Only liver weight/body weight ratio was slightly lower in mice deficient in endothelial autophagy fed a high fat diet than in littermate controls (p=0.01) (Supplemental Table 4).

Taken together, these findings indicate that deficiency in endothelial autophagy induces liver inflammation and promotes liver fibrogenesis.

Deficiency in endothelial autophagy promotes liver fibrosis deposition in mice treated with carbon tetrachloride

To determine whether endothelial autophagy is also involved at more advanced stages of chronic liver diseases progression, we treated *Atg5*$^{lox/lox}$ and *Atg5*$^{lox/lox}$*; VE-cadherin-Cre* mice with carbon tetrachloride (CCl4) or its vehicle for 6 weeks (Supplemental Figure 6).

As expected, markers of liver injury (plasma AST and ALT levels), of liver inflammation (liver *Rantes* gene expression) and of liver fibrogenesis (liver α-*SMA*, *Tgf-β1* and *Collagen1α2* gene expression, and liver collagen staining with Sirius red) were higher in *Atg5*$^{lox/lox}$ treated with CCl4 than in *Atg5*$^{lox/lox}$ treated with vehicle (Figure 5, Supplemental Figure 7B-D).

When compared with littermate controls, mice deficient in endothelial autophagy had higher levels of markers of liver fibrogenesis (liver α-*SMA*, *Tgf-β1* and *Collagen1α2* gene expression, and liver collagen staining with Sirius red) (Figures 5). Of note, liver fibrosis was mainly perisinusoidal in mice deficient in endothelial autophagy (Figure 5D).

Deficiency in endothelial ATG5 had no effect on body and organ weight, on blood cell count (Supplemental Table 5), on markers of liver injury (plasma AST and ALT levels) (Supplemental Figure 7B) nor on markers of liver inflammation (liver *Mcp1* and *Rantes* gene expression) (Supplemental Figure 7C).

These findings demonstrate that deficiency in endothelial autophagy promotes liver fibrosis development in more advanced stages of chronic liver diseases progression.

Discussion

This study provides strong evidence suggesting that NASH is associated with a defect in liver endothelial autophagy, while simple steatosis is not. This defect was reproduced by low concentrations of inflammatory mediators present in the portal blood of patients with metabolic syndrome. Such a defect in autophagy promoted liver endothelial cell inflammation, endothelial-to-mesenchymal transition and apoptosis, favoring the development of NASH and liver fibrosis.

The first major finding in this study was the observation that LSECs from patients with NASH display less autophagic vacuoles than those from patients with a simple steatosis or with a normal liver. Although such a low number of autophagic vacuoles could result from increased autophagic flux [41], this hypothesis seems very unlikely. Indeed, we observed that cultured TSECs exposed to shear stress -to mimic induction of autophagy existing *in vivo*- and to a combination of TNFα and IL6 at concentrations similar to those observed in the portal blood of patients with metabolic syndrome [35–38] displayed a decreased autophagic flux, as ascertained by chloroquine experiments. Moreover, we showed that inhibiting autophagy in liver endothelial cells reproduces the increased expression of *Mcp1* and VCAM-1 reported in LSECs in mouse models of NASH [42]. These results are a step forward in our view of liver autophagy, since autophagy had not been assessed in liver endothelial cells in patients with liver disease. More generally, the impact of metabolic syndrome on endothelial autophagy level has not been investigated in any vascular bed, neither in patients nor in animals. If we and others showed that a defect in endothelial autophagy favors atherosclerosis development, the impact of metabolic syndrome on endothelial autophagy level is unknown [34,43].

The second major finding in the present study was that a defect in endothelial autophagy promotes NASH and liver fibrosis in mice. The effects we observed in this study were not mediated by an effect of the defect in endothelial autophagy on metabolic risk factors, as body weight, arterial blood pressure, plasma cholesterol and triglycerides as well as fasting glucose levels were not different between mice deficient or not in endothelial autophagy in basal conditions or when fed a high fat diet. This observation of a protective role of endothelial autophagy completes the picture of the role of autophagy in chronic liver diseases, since previous studies demonstrated that hepatocyte autophagy protects against fat accumulation and liver injury during fatty liver disease [21,22], that macrophages autophagy is an anti-inflammatory pathway in the liver, with protective anti-fibrogenic effects [21,24], and that, by contrast, autophagy is profibrogenic in hepatic stellate cells [21,25]. It should be stressed that we included in this study both male and female patients and animals, implying that the observed regulation and effect of endothelial autophagy is a general process, not restricted to one gender.

In the present study, the main effect of the deficiency in endothelial autophagy was an increase in liver fibrosis, an effect observed in a mouse model of fatty liver disease and of liver fibrosis. It should be stressed that in both models, liver fibrosis was mainly perisinusoidal, a feature typically observed in patients with NASH related fibrosis [44]. Classically, it is considered that liver fibrosis results from hepatic stellate cells activation which is associated with the acquisition of a myofibroblastic phenotype characterized by α-SMA expression by these cells [45]. The increase in α-SMA expression we observed in the liver of high fat diet and CCl4-treated mice likely results in part from an activation of hepatic stellate cells, possibly by the inflammatory mediators, including Rantes and Mcp1, released by LSECs. However, we also provide evidence for an original complementary hypothesis that could account for the perisinusoidal location of liver fibrosis we observed, namely the fact that α-SMA overexpression could also result from endothelial-to mesenchymal transition. Indeed, we demonstrated, using cultured TSECs, that a defect in autophagy is associated with an overexpression of α-SMA in TSECs, together with an overexpression of *Tgf-β1* and *Collagen1α2, i.e.* typical features of endothelial-to-mesenchymal transition. This suggests that the pool of hepatic myofibroblast in NASH may not only originate from hepatic stellate cells, but also from endothelial-to-mesenchymal transition, and might explain the typical perisinusoidal fibrosis associated with this disease. While this phenomenon has been well described in fibrotic cardiovascular and pulmonary diseases [46–48], rare studies described endothelial-to-mesenchymal transition in the liver [49] and suggested that this process is marginal in fibrosis induced by chronic toxic injury. However, endothelial-to-mesenchymal transition might be more prominent in NASH than in other chronic liver diseases, as suggested by the frequent perisinusoidal fibrosis in this disease.

In conclusion, this study provides new insights into our understanding of the role of liver endothelial cells in the development of NASH and liver fibrosis. Autophagy is defective in LSECs in NASH and this defect can be attributed, at least in part, to inflammatory mediators present in the portal venous blood. Deficiency in autophagy in LSECs induces endothelial inflammation, endothelial-to-mesenchymal transition and apoptosis, thus promoting liver inflammation and fibrosis at early and advanced stages of NASH (Figure 6). Liver endothelial autophagy level might be the missing link explaining why some patients with simple steatosis progress to NASH and liver fibrosis while others do not. Targeting specifically liver endothelial autophagy may be an attractive strategy for NASH treatment.

References

[1] Estes C, Razavi H, Loomba R, Younossi Z, Sanyal AJ. Modeling the epidemic of nonalcoholic fatty liver disease demonstrates an exponential increase in burden of disease. Hepatology 2018;67:123–33. doi:10.1002/hep.29466.

[2] Friedman SL, Neuschwander-Tetri BA, Rinella M, Sanyal AJ. Mechanisms of NAFLD development and therapeutic strategies. Nat Med 2018;24:908–22. doi:10.1038/s41591-018-0104-9.

[3] Wong RJ, Aguilar M, Cheung R, Perumpail RB, Harrison SA, Younossi ZM, et al. Nonalcoholic steatohepatitis is the second leading etiology of liver disease among adults awaiting liver transplantation in the United States. Gastroenterology 2015;148:547–55. doi:10.1053/j.gastro.2014.11.039.

[4] Schuppan D, Schattenberg JM. Non-alcoholic steatohepatitis: pathogenesis and novel therapeutic approaches. J Gastroenterol Hepatol 2013;28 Suppl 1:68–76. doi:10.1111/jgh.12212.

[5] Marra F, Svegliati-Baroni G. Lipotoxicity and the gut-liver axis in NASH pathogenesis. J Hepatol 2018;68:280–95. doi:10.1016/j.jhep.2017.11.014.

[6] Wu J, Meng Z, Jiang M, Zhang E, Trippler M, Broering R, et al. Toll-like receptor-induced innate immune responses in non-parenchymal liver cells are cell type-specific. Immunology 2010;129:363–74. doi:10.1111/j.1365-2567.2009.03179.x.

[7] Poisson J, Lemoinne S, Boulanger C, Durand F, Moreau R, Valla D, et al. Liver sinusoidal endothelial cells: Physiology and role in liver diseases. J Hepatol 2017;66:212–27. doi:10.1016/j.jhep.2016.07.009.

[8] Coulon S, Legry V, Heindryckx F, Van Steenkiste C, Casteleyn C, Olievier K, et al. Role of vascular endothelial growth factor in the pathophysiology of nonalcoholic steatohepatitis in two rodent models. Hepatology 2013;57:1793–805. doi:10.1002/hep.26219.

[9] McCuskey RS, Ito Y, Robertson GR, McCuskey MK, Perry M, Farrell GC. Hepatic microvascular dysfunction during evolution of dietary steatohepatitis in mice. Hepatology 2004;40:386–93. doi:10.1002/hep.20302.

[10] Francque S, Laleman W, Verbeke L, Van Steenkiste C, Casteleyn C, Kwanten W, et al. Increased intrahepatic resistance in severe steatosis: endothelial dysfunction, vasoconstrictor overproduction and altered microvascular architecture. Lab Invest 2012;92:1428–39. doi:10.1038/labinvest.2012.103.

[11] Gonzalez-Paredes FJ, Hernández Mesa G, Morales Arraez D, Marcelino Reyes R, Abrante B, Diaz-Flores F, et al. Contribution of Cyclooxygenase End Products and Oxidative Stress to Intrahepatic Endothelial Dysfunction in Early Non-Alcoholic Fatty Liver Disease. PLoS ONE 2016;11:e0156650. doi:10.1371/journal.pone.0156650.

[12] Miyao M, Kotani H, Ishida T, Kawai C, Manabe S, Abiru H, et al. Pivotal role of liver sinusoidal endothelial cells in NAFLD/NASH progression. Lab Invest 2015;95:1130–44. doi:10.1038/labinvest.2015.95.

[13] Pasarín M, La Mura V, Gracia-Sancho J, García-Calderó H, Rodríguez-Vilarrupla A, García-Pagán JC, et al. Sinusoidal endothelial dysfunction precedes inflammation and fibrosis in a model of NAFLD. PLoS ONE 2012;7:e32785. doi:10.1371/journal.pone.0032785.

[14] DeLeve LD, Wang X, Kanel GC, Atkinson RD, McCuskey RS. Prevention of hepatic fibrosis in a murine model of metabolic syndrome with nonalcoholic steatohepatitis. Am J Pathol 2008;173:993–1001. doi:10.2353/ajpath.2008.070720.

[15] DeLeve LD. Liver sinusoidal endothelial cells in hepatic fibrosis. Hepatology

2015;61:1740–6. doi:10.1002/hep.27376.
[16] Kitade M, Yoshiji H, Kojima H, Ikenaka Y, Noguchi R, Kaji K, et al. Leptin-mediated neovascularization is a prerequisite for progression of nonalcoholic steatohepatitis in rats. Hepatology 2006;44:983–91. doi:10.1002/hep.21338.
[17] Kitade M, Yoshiji H, Noguchi R, Ikenaka Y, Kaji K, Shirai Y, et al. Crosstalk between angiogenesis, cytokeratin-18, and insulin resistance in the progression of non-alcoholic steatohepatitis. World J Gastroenterol 2009;15:5193–9.
[18] Tarantino G, Conca P, Pasanisi F, Ariello M, Mastrolia M, Arena A, et al. Could inflammatory markers help diagnose nonalcoholic steatohepatitis? Eur J Gastroenterol Hepatol 2009;21:504–11. doi:10.1097/MEG.0b013e3283229b40.
[19] Cayón A, Crespo J, Guerra AR, Pons-Romero F. [Gene expression in obese patients with non-alcoholic steatohepatitis]. Rev Esp Enferm Dig 2008;100:212–8.
[20] Choi AMK, Ryter SW, Levine B. Autophagy in human health and disease. N Engl J Med 2013;368:651–62. doi:10.1056/NEJMra1205406.
[21] Gual P, Gilgenkrantz H, Lotersztajn S. Autophagy in chronic liver diseases: the two faces of Janus. Am J Physiol, Cell Physiol 2017;312:C263–73. doi:10.1152/ajpcell.00295.2016.
[22] Madrigal-Matute J, Cuervo AM. Regulation of Liver Metabolism by Autophagy. Gastroenterology 2016;150:328–39. doi:10.1053/j.gastro.2015.09.042.
[23] Gracia-Sancho J, Guixé-Muntet S. The many-faced role of autophagy in liver diseases. J Hepatol 2018;68:593–4. doi:10.1016/j.jhep.2017.09.015.
[24] Lodder J, Denaës T, Chobert M-N, Wan J, El-Benna J, Pawlotsky J-M, et al. Macrophage autophagy protects against liver fibrosis in mice. Autophagy 2015;11:1280–92. doi:10.1080/15548627.2015.1058473.
[25] Hernández-Gea V, Ghiassi-Nejad Z, Rozenfeld R, Gordon R, Fiel MI, Yue Z, et al. Autophagy releases lipid that promotes fibrogenesis by activated hepatic stellate cells in mice and in human tissues. Gastroenterology 2012;142:938–46. doi:10.1053/j.gastro.2011.12.044.
[26] Guixé-Muntet S, de Mesquita FC, Vila S, Hernández-Gea V, Peralta C, García-Pagán JC, et al. Cross-talk between autophagy and KLF2 determines endothelial cell phenotype and microvascular function in acute liver injury. J Hepatol 2017;66:86–94. doi:10.1016/j.jhep.2016.07.051.
[27] Ruart M, Chavarria L, Campreciós G, Suárez-Herrera N, Montironi C, Guixé-Muntet S, et al. Impaired Endothelial Autophagy Promotes Liver Fibrosis By Aggravating The Oxidative Stress Response During Acute Liver Injury. Journal of Hepatology 2018. doi:10.1016/j.jhep.2018.10.015.
[28] Eskelinen E-L. Maturation of autophagic vacuoles in Mammalian cells. Autophagy 2005;1:1–10.
[29] Rautou P-E, Cazals-Hatem D, Feldmann G, Mansouri A, Grodet A, Barge S, et al. Changes in autophagic response in patients with chronic hepatitis C virus infection. Am J Pathol 2011;178:2708–15. doi:10.1016/j.ajpath.2011.02.021.
[30] Oberlin E, Fleury M, Clay D, Petit-Cocault L, Candelier J-J, Mennesson B, et al. VE-cadherin expression allows identification of a new class of hematopoietic stem cells within human embryonic liver. Blood 2010;116:4444–55. doi:10.1182/blood-2010-03-272625.
[31] Hara T, Nakamura K, Matsui M, Yamamoto A, Nakahara Y, Suzuki-Migishima R, et al. Suppression of basal autophagy in neural cells causes neurodegenerative disease in mice. Nature 2006;441:885–9. doi:10.1038/nature04724.
[32] Oberlin E, El Hafny B, Petit-Cocault L, Souyri M. Definitive human and mouse

hematopoiesis originates from the embryonic endothelium: a new class of HSCs based on VE-cadherin expression. Int J Dev Biol 2010;54:1165–73. doi:10.1387/ijdb.103121eo.
[33] Huebert RC, Jagavelu K, Liebl AF, Huang BQ, Splinter PL, LaRusso NF, et al. Immortalized liver endothelial cells: a cell culture model for studies of motility and angiogenesis. Lab Invest 2010;90:1770–81. doi:10.1038/labinvest.2010.132.
[34] Vion A-C, Kheloufi M, Hammoutene A, Poisson J, Lasselin J, Devue C, et al. Autophagy is required for endothelial cell alignment and atheroprotection under physiological blood flow. Proc Natl Acad Sci USA 2017;114:E8675–84. doi:10.1073/pnas.1702223114.
[35] Peiris AN, Mueller RA, Smith GA, Struve MF, Kissebah AH. Splanchnic insulin metabolism in obesity. Influence of body fat distribution. J Clin Invest 1986;78:1648–57. doi:10.1172/JCI112758.
[36] Fontana L, Eagon JC, Trujillo ME, Scherer PE, Klein S. Visceral fat adipokine secretion is associated with systemic inflammation in obese humans. Diabetes 2007;56:1010–3. doi:10.2337/db06-1656.
[37] Magkos F, Fabbrini E, Patterson BW, Eagon JC, Klein S. Portal vein and systemic adiponectin concentrations are closely linked with hepatic glucose and lipoprotein kinetics in extremely obese subjects. Metab Clin Exp 2011;60:1641–8. doi:10.1016/j.metabol.2011.03.019.
[38] Liu RH, Kurose T, Matsukura S. Oral nicotine administration decreases tumor necrosis factor-alpha expression in fat tissues in obese rats. Metab Clin Exp 2001;50:79–85.
[39] Gatica D, Chiong M, Lavandero S, Klionsky DJ. Molecular mechanisms of autophagy in the cardiovascular system. Circ Res 2015;116:456–67. doi:10.1161/CIRCRESAHA.114.303788.
[40] Santhekadur PK, Kumar DP, Sanyal AJ. Preclinical models of non-alcoholic fatty liver disease. J Hepatol 2018;68:230–7. doi:10.1016/j.jhep.2017.10.031.
[41] Loos B, du Toit A, Hofmeyr J-HS. Defining and measuring autophagosome flux—concept and reality. Autophagy 2014;10:2087–96. doi:10.4161/15548627.2014.973338.
[42] Lefere S, Van de Velde F, Hoorens A, Raevens S, Van Campenhout S, Vandierendonck A, et al. Angiopoietin-2 promotes pathological angiogenesis and is a novel therapeutic target in murine non-alcoholic fatty liver disease. Hepatology 2018. doi:10.1002/hep.30294.
[43] Torisu K, Singh KK, Torisu T, Lovren F, Liu J, Pan Y, et al. Intact endothelial autophagy is required to maintain vascular lipid homeostasis. Aging Cell 2016;15:187–91. doi:10.1111/acel.12423.
[44] Bedossa P, Poitou C, Veyrie N, Bouillot J-L, Basdevant A, Paradis V, et al. Histopathological algorithm and scoring system for evaluation of liver lesions in morbidly obese patients. Hepatology 2012;56:1751–9. doi:10.1002/hep.25889.
[45] Tsuchida T, Friedman SL. Mechanisms of hepatic stellate cell activation. Nat Rev Gastroenterol Hepatol 2017;14:397–411. doi:10.1038/nrgastro.2017.38.
[46] Li Y, Lui KO, Zhou B. Reassessing endothelial-to-mesenchymal transition in cardiovascular diseases. Nat Rev Cardiol 2018;15:445–56. doi:10.1038/s41569-018-0023-y.
[47] Piera-Velazquez S, Mendoza FA, Jimenez SA. Endothelial to Mesenchymal Transition (EndoMT) in the Pathogenesis of Human Fibrotic Diseases. J Clin Med 2016;5. doi:10.3390/jcm5040045.
[48] Singh KK, Lovren F, Pan Y, Quan A, Ramadan A, Matkar PN, et al. The essential autophagy gene ATG7 modulates organ fibrosis via regulation of endothelial-to-

mesenchymal transition. J Biol Chem 2015;290:2547–59. doi:10.1074/jbc.M114.604603.
[49] Ribera J, Pauta M, Melgar-Lesmes P, Córdoba B, Bosch A, Calvo M, et al. A small population of liver endothelial cells undergoes endothelial-to-mesenchymal transition in response to chronic liver injury. Am J Physiol Gastrointest Liver Physiol 2017;313:G492–504. doi:10.1152/ajpgi.00428.2016.

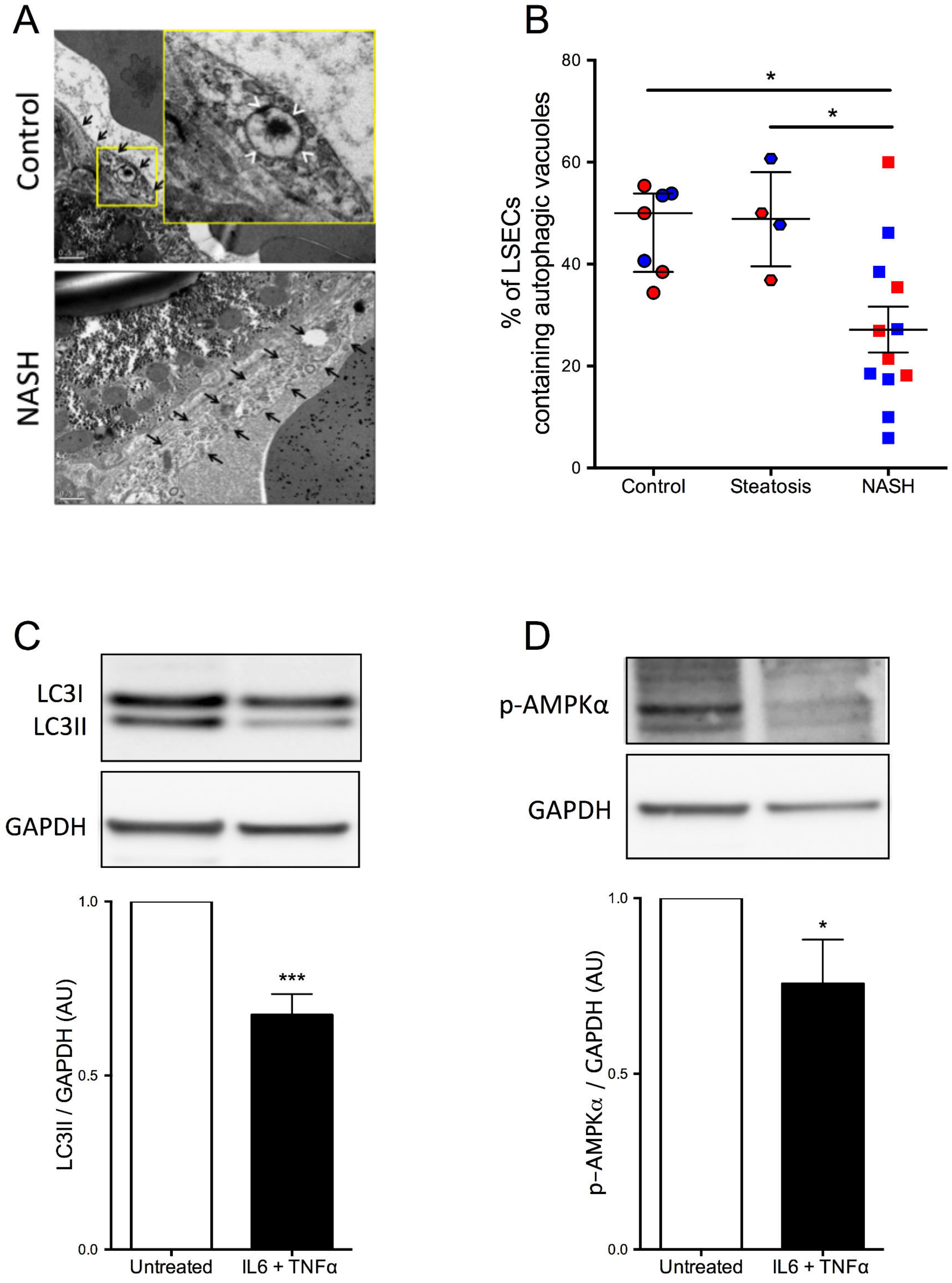

Figure 1: Autophagy is defective in LSECs in NASH. (A) Representative images of transmission electron microscopy pictures of the liver from patients without abnormalities at liver histological examination (control), or from patients with NASH. Arrows indicate LSECs. Arrowheads indicate autophagic vacuoles. Scale bar 0.5 µm. (B) Quantification of the percentage of LSECs containing autophagic vacuoles in the liver of

patients without abnormalities at liver histological examination (n=7) or patients with simple steatosis (n=4) or patients with NASH (n=12). Blue and red dots indicate males and females respectively. Data are expressed as median ± IQR. (C) Western blot analysis of LC3II expression in TSECs exposed to shear stress and treated or not with TNFα and IL6 (10 pg/mL each) for 24 hrs. n=8 independent experiments. (D) Western blot analysis of p-AMPKα expression in TSECs exposed to shear stress and treated or not with TNFα and IL6 (10 pg/mL each) for 24 hrs. n=7 independent experiments. *In vitro* data are normalized to the untreated condition for each experiment and expressed as mean ± SEM. *p<0.05; ***p<0.001. TSECs, transformed sinusoidal endothelial cells.

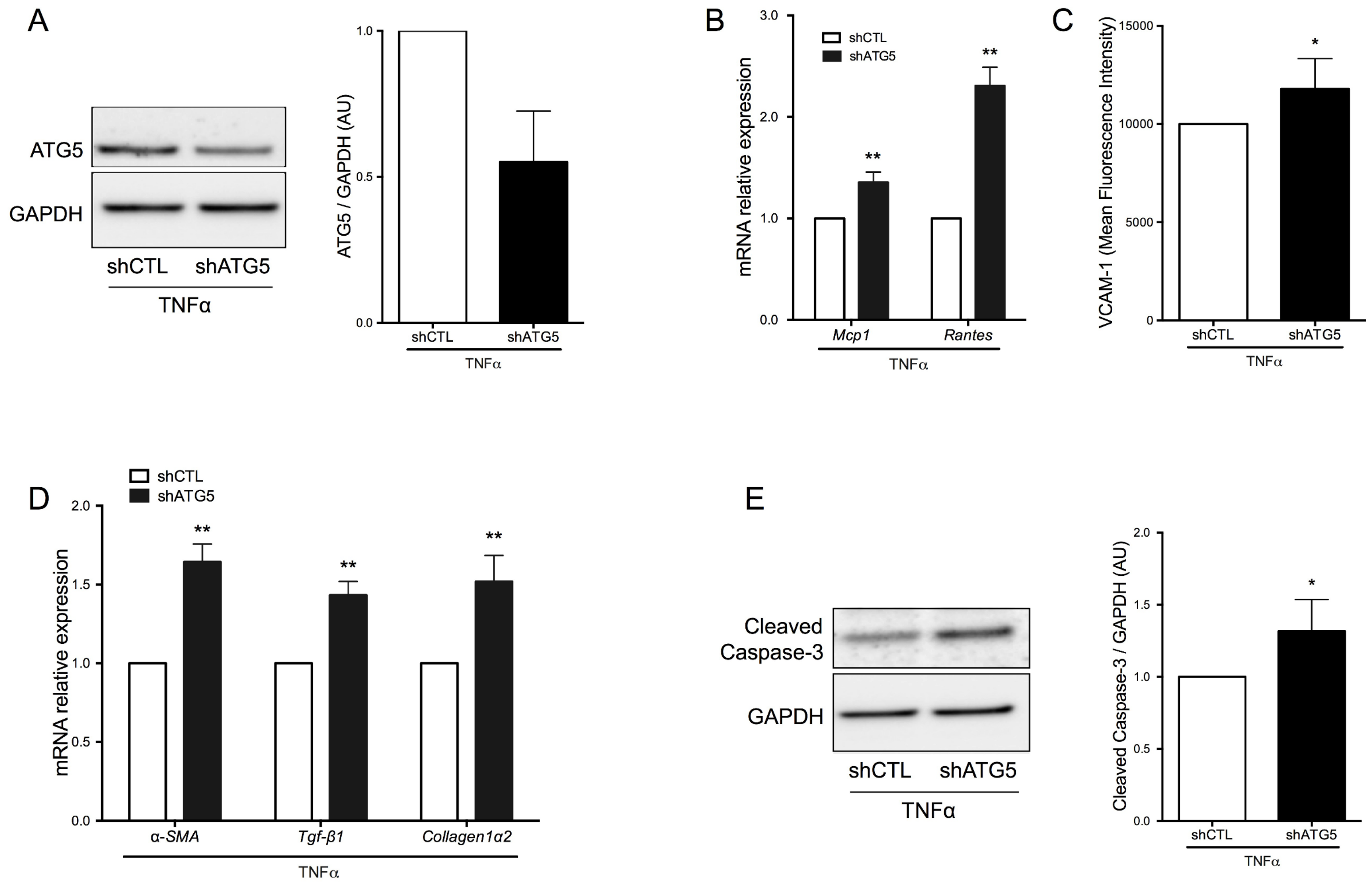

Figure 2: Deficiency in autophagy in TSECs impairs endothelial phenotype. TSECs were transduced with a lentivirus expressing an *Atg5* or a control (CTL) shRNA and exposed to shear stress for 24 hrs with TNFα (1 ng/mL) for the last 12 hrs. (A) Western blot analysis

of ATG5 expression in TSECs (n=9). (B) *Mcp1* and *Rantes* gene expression in TSECs (n=6). (C) Flow cytometry analysis of VCAM-1 expression in TSECs (n=9). (D) α-*SMA*, *Tgf-β1* and *Collagen1*α*2* gene expression in TSECs (n=6). cleaved Caspase-3 expression in TSECs (n=9). (E) Western blot analysis of cleaved-caspase-3 expression in TSECs (n=9). Data are normalized to the shCTL condition for each experiment and expressed as mean ± SEM. *$p<0.05$; **$p<0.01$. TSECs, transformed sinusoidal endothelial cells.

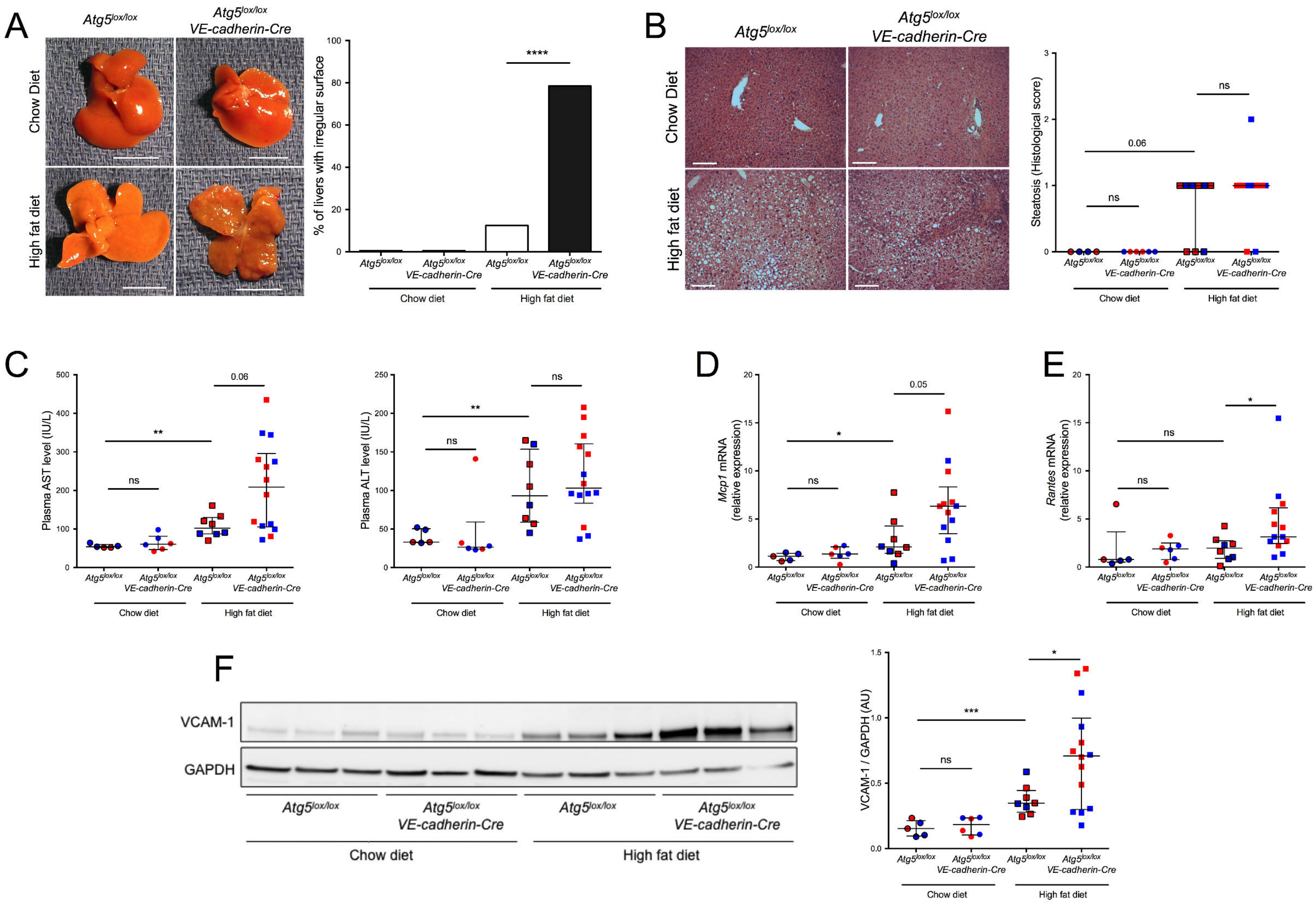

Figure 3: Deficiency in endothelial autophagy increases liver inflammation in mice fed a high fat diet. Twelve weeks old mice were fed a chow diet or a high fat diet for 16 weeks. (A) Representative images of the liver of *Atg5*$^{lox/lox}$ and *Atg5*$^{lox/lox}$*;VE-cadherin-cre* fed a chow

diet or a high fat diet and quantification of the percentage of livers with nodular surface. Scale bar, 1 cm. (B) Histological analysis of liver steatosis on Hematoxylin and Eosin stained liver sections. Scale bar 150 µm. (C) Plasma AST and ALT levels. (D) Liver gene expression of *Mcp1* and (E) *Rantes*. (F) Western blot analysis of VCAM-1 expression in the liver. *Atg5*$^{lox/lox}$, chow diet: n=5; *Atg5*$^{lox/lox}$*;VE-cadherin-cre,* chow diet: n=6; *Atg5*$^{lox/lox}$, high-fat diet: n=8; *Atg5*$^{lox/lox}$*;VE-cadherin-cre,* high-fat diet: n=14. Blue and red dots indicate males and females respectively. Data are expressed as median ± IQR. *p<0.05; **p<0.01; ****p<0.0001; ns, not significant.

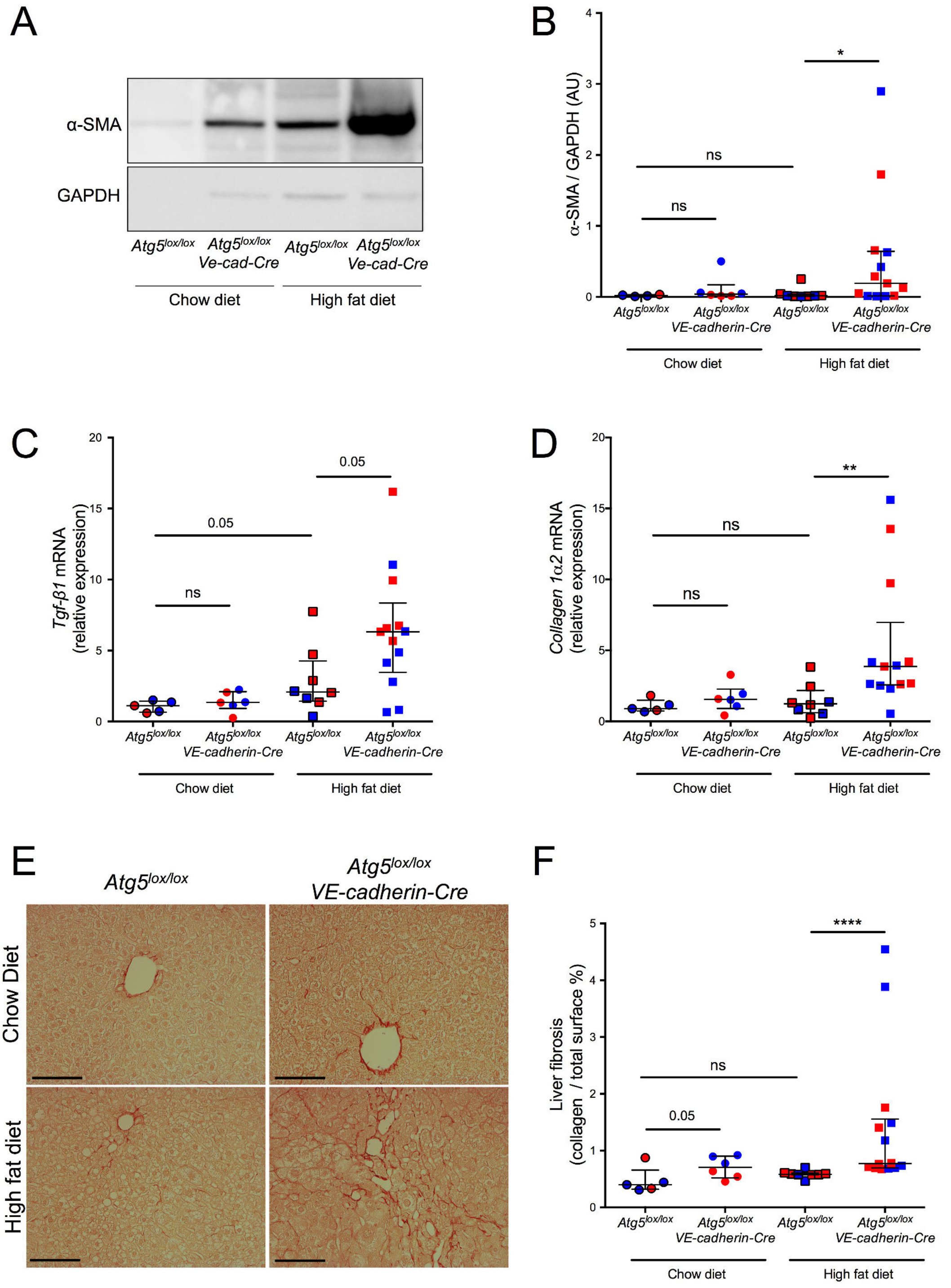

Figure 4: Deficiency in endothelial autophagy induces liver fibrosis in mice fed a high fat diet. Twelve weeks mice were fed a chow diet or a high fat diet for 16 weeks. (A) Liver gene expression of *Collagen1α2* and (B) *Tgf-β1.* (C) Representative image of western blot analysis of liver α-SMA expression. (D) Quantification of α-SMA/GAPDH ratio. (E) Representative images of Sirius red staining of liver sections. Scale bar 100 µm. (F)

Histological quantification of liver fibrosis. *Atg5*$^{lox/lox}$, chow diet: n=5; *Atg5*$^{lox/lox}$*;VE-cadherin-cre,* chow diet: n=6; *Atg5*$^{lox/lox}$, high fat diet: n=8; *Atg5*$^{lox/lox}$*;VE-cadherin-cre,* high fat diet: n=14. Blue and red dots indicate males and females respectively. Data are expressed as median ± IQR. *$p<0.05$; **$p<0.01$; ****$p<0.0001$; ns, not significant.

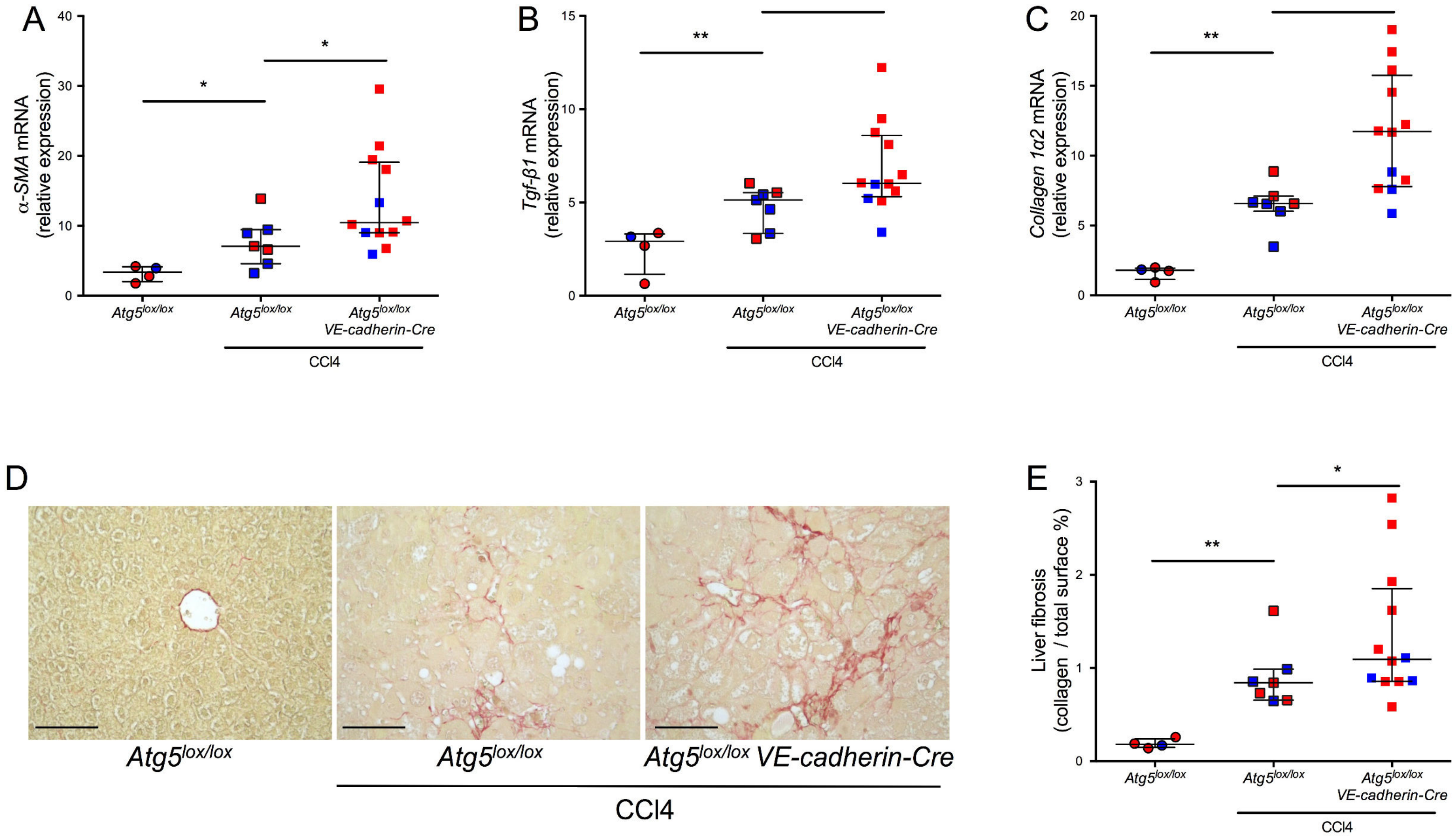

Figure 5: Deficiency in endothelial autophagy increases CCl4-induced liver fibrosis. Twelve weeks mice were intraperitoneally injected with carbon tetrachloride (CCl4, 0.24 mL/kg, 3 times a week) for 6 weeks. (A) Liver gene expression of α-*SMA,* (B) *Tgf-β1* and (C) *Collagen1α2*. (D) Representative images of liver sections stained with Sirius red. Scale bar 100 µm. (E) Histological quantification of liver

fibrosis. *Atg5*$^{lox/lox}$, vehicle: n=4; *Atg5*$^{lox/lox}$, CCl_4: n=7; *Atg5*$^{lox/lox}$*;VE-cadherin-cre,* high-fat diet: n=12. Blue and red dots indicate males and females respectively. Data are expressed as median ± IQR. *$p<0.05$; **$p<0.01$.

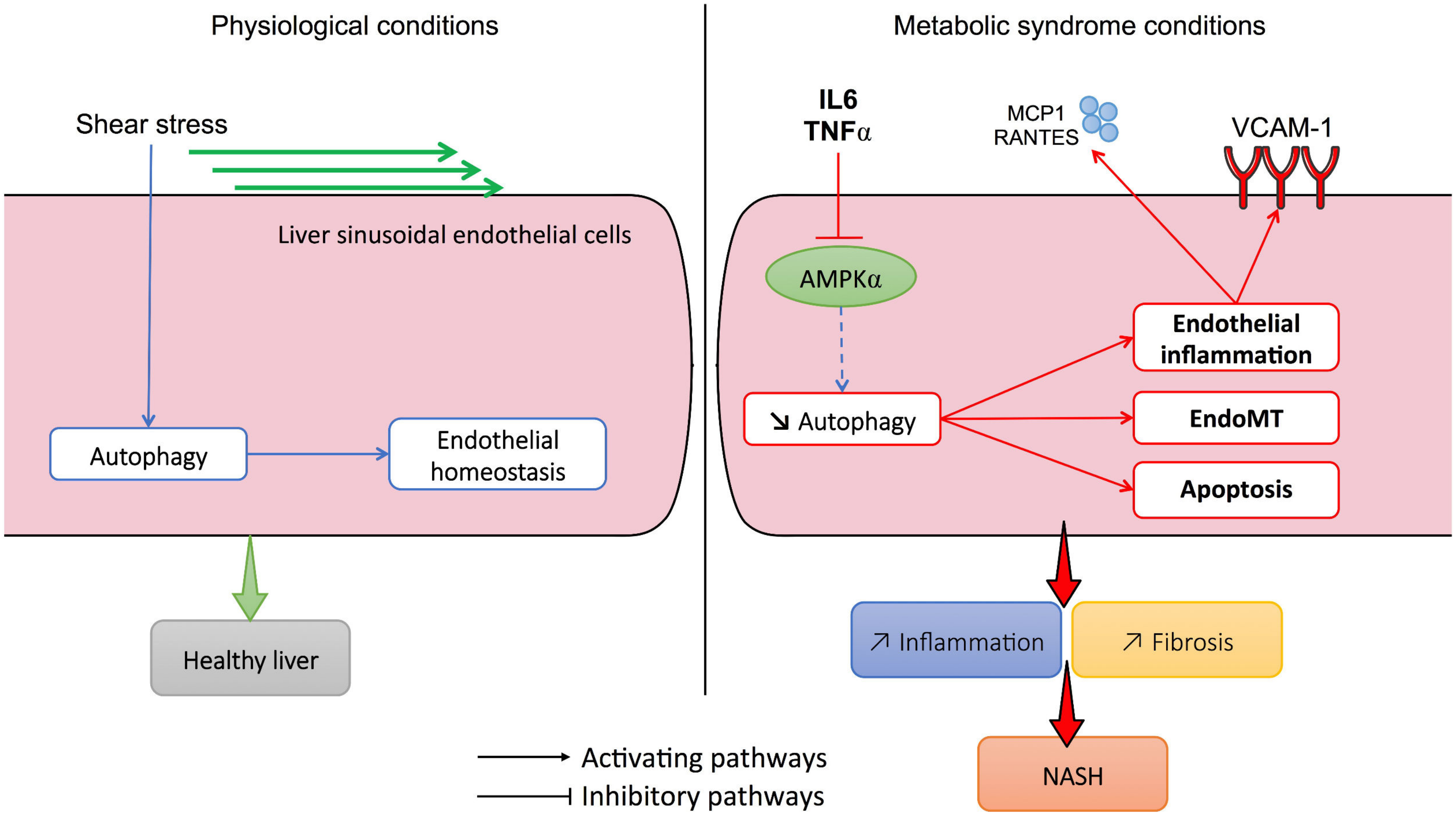
Physiological conditions
Metabolic syndrome conditions
Shear stress
Liver sinusoidal endothelial cells
Autophagy
Endothelial homeostasis
Healthy liver
IL6
TNFα
MCP1
RANTES
VCAM-1
AMPKα
↘ Autophagy
Endothelial inflammation
EndoMT
Apoptosis
↗ Inflammation
↗ Fibrosis
NASH
Activating pathways
Inhibitory pathways

Figure 6: Schematic illustration depicting the links between autophagy in LSECs and NASH development. In physiological conditions, autophagy is activated in LSECs by shear stress and maintains endothelial homeostasis and liver health. In metabolic syndrome conditions, TNFα and IL6 impair autophagy in LSECs by inhibiting AMPKα activity. Deficiency in autophagy in LSECs induces liver

endothelial cell inflammation (release of MCP1 and RANTES and overexpression of VCAM-1), endothelial-to-mesenchymal transition and endothelial apoptosis, and eventually perisinusoidal liver fibrosis.

Abbreviations: AMPKα, AMP activated protein kinase; EndoMT, endothelial-to-mesenchymal transition; HSCs, hepatic stellate cells; MCP1, monocyte chemoattractant protein 1; VCAM-1, vascular cell adhesion molecule 1.

Supplemental Figures

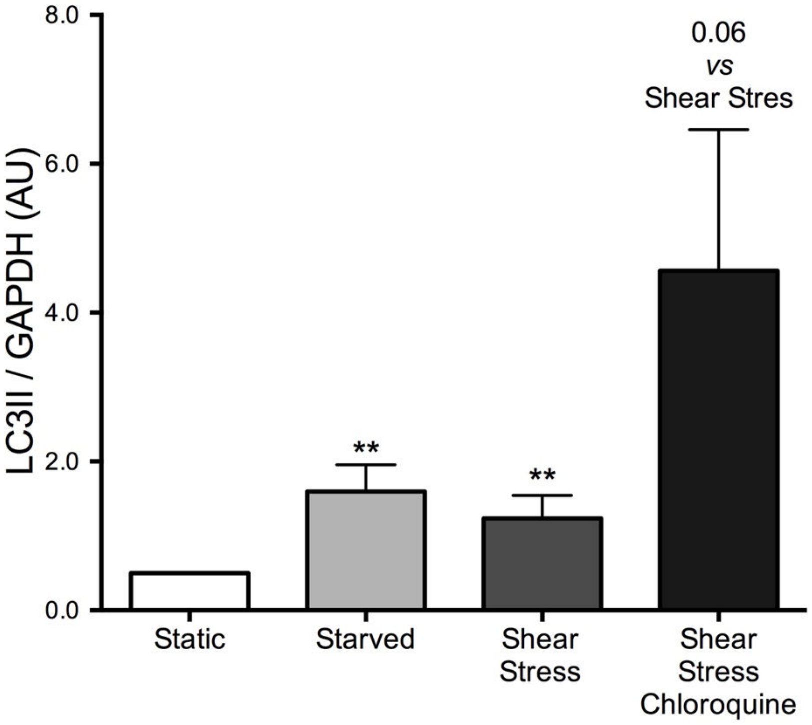

Sup Figure 1: TSECs exhibits autophagy under shear stress conditions. Western blot analysis of autophagy in TSECs in static conditions or exposed to shear stress (20 dyn/cm^2) for 2 4hrs. Starvation was used as a positive control for autophagy stimulation. Chloroquine (300 μM) was added to the culture medium for the last 30 minutes. n=6 independent experiments. Data are normalized to the static condition for each experiment and are expressed as mean ± SEM. *$p<0.05$ *vs* static; **$p<0.01$ *vs* static \$ $p<0.05$ *vs* static.

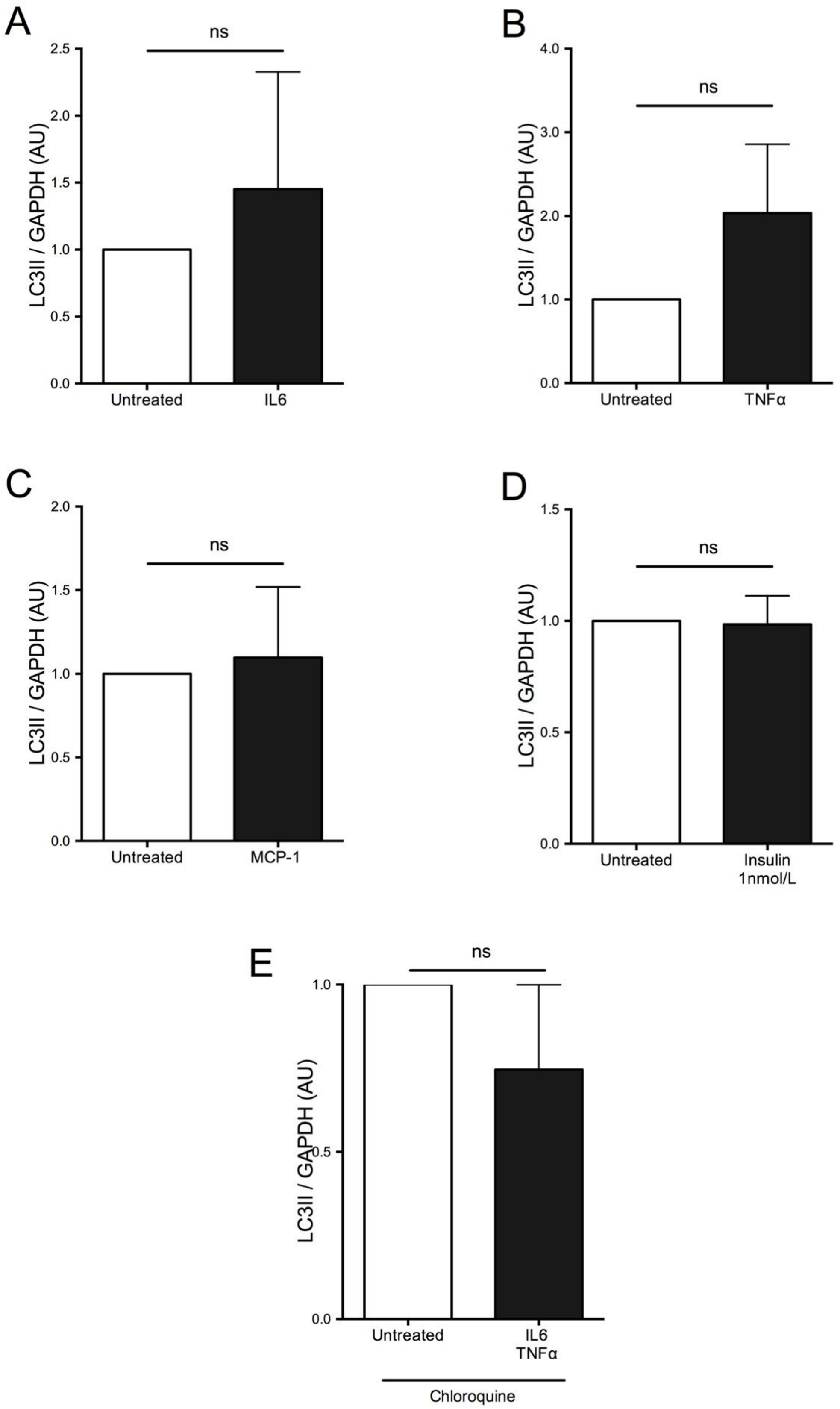

Sup Figure 2: The combination of TNFα and IL6 impair autophagic flux in TSECs but each cytokine alone does not alter autophagy. Western blot analysis of autophagy in TSECs exposed to shear stress (20 dyn/cm^2) for 24hrs and treated or not either with (A)

IL6 (10 pg/mL, n=3), (B) TNFα (10 pg/mL, n=2), (C) MCP1 (100 pg/mL, n=6) or (D) Insulin (1 ηmol/L, n=6) alone. (E) Western blot analysis of autophagy in TSECs exposed to shear stress (20 dyn/cm^2) for 24 hrs and treated or not with the combination of IL-6 and TNFα (10 pg/mL for each, n=2). Chloroquine (300 μM) was added to the culture medium for the last 30 minutes (n=2). Data are normalized to the untreated condition for each experiment and are expressed as mean ± SEM. ns: not significant.

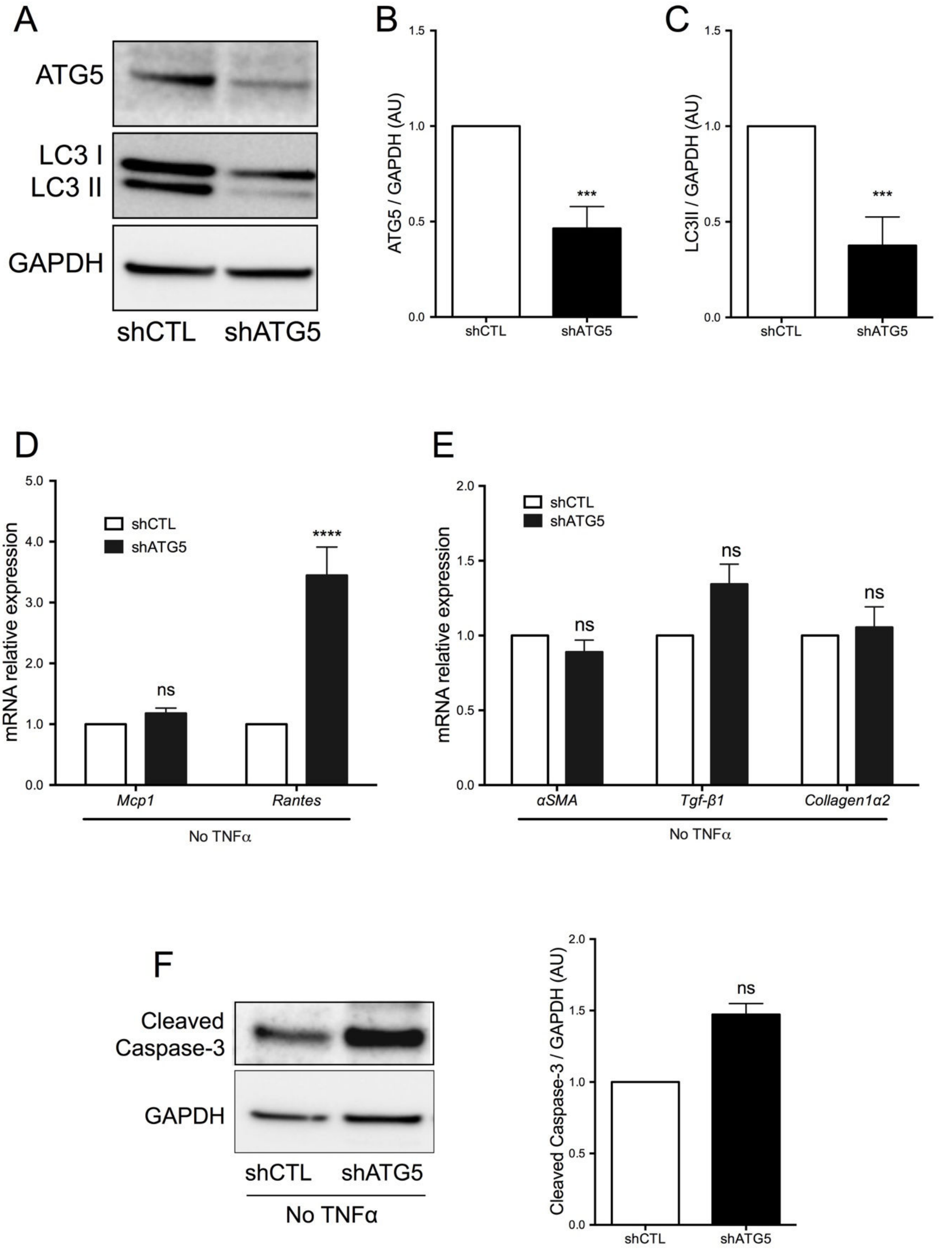

Sup Figure 3: Autophagy deficiency in TSECs induces *Rantes* overexpression in basal conditions. TSECs were transduced with a lentivirus expressing an *Atg5* or a control (CTL) shRNA and exposed to shear stress for 24 hrs. (A) Representative images of western blot analysis of ATG5 and LC3 expression in TSECs. (B) Quantification of ATG5/GAPDH and (C) LC3-II/GAPDH ration. (D) *Mcp1* and *Rantes* gene expression analysis in TSECs (n=13). (E) α-*SMA*, *Tgf-β1* and *Collagen1α2* gene expression analysis in TSECs (n=13). (F) Western blot analysis of Cleaved-caspase 3 expression in TSECs (n=3). Data are normalized to the shCTL condition for each experiment and expressed as mean ± SEM. ***p<0.001; ****p<0.0001 *vs* shCTL; ns: not significant *vs* shCTL.

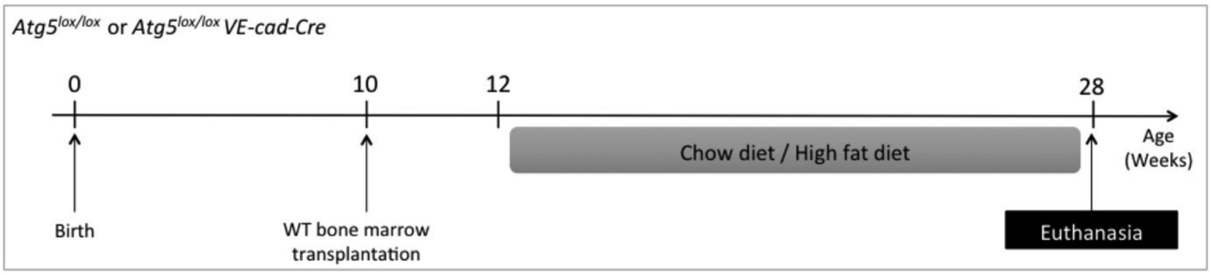
Atg5lox/lox or Atg5lox/lox VE-cad-Cre
0
10
12
28
Age (Weeks)
Chow diet / High fat diet
Birth
WT bone marrow transplantation
Euthanasia

Sup Figure 4: Experimental procedure: protocol to investigate NASH development in *Atg5*$^{lox/lox}$ and *Atg5*$^{lox/lox}$*;VE-cadherin-Cre* mice fed a chow diet or a high-fat diet for 16 weeks.

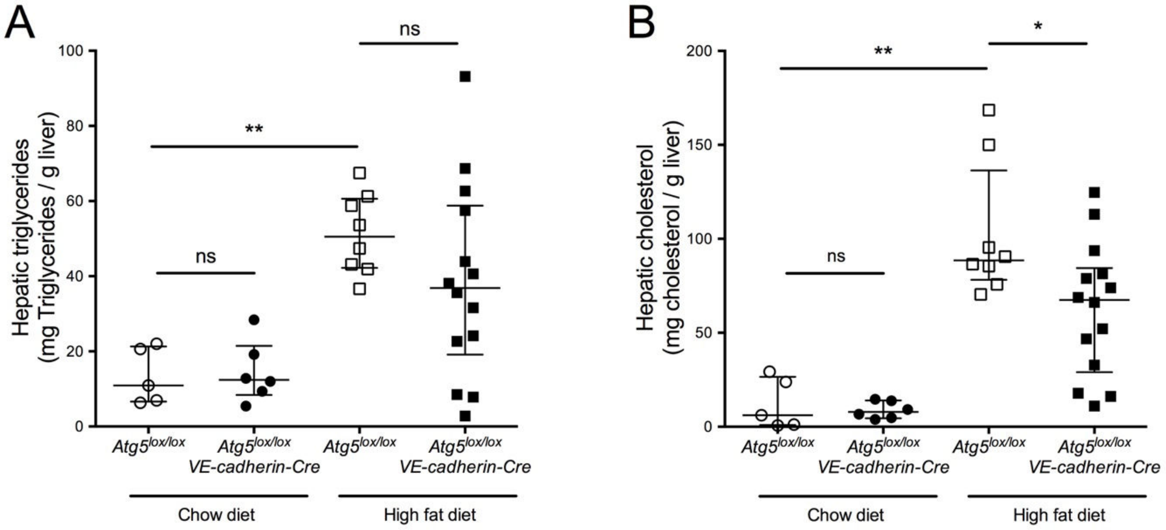

Sup Figure 5: Deficiency in endothelial autophagy does not change liver steatosis. Twelve weeks mice were fed a chow diet or a high-fat diet for 16 weeks. (A) Hepatic (A) triglycerides and (B) cholesterol content in *Atg5*$^{lox/lox}$ and *Atg5*$^{lox/lox}$*;VE-cadherin-Cre* mice fed a chow diet or a high-fat diet for 16 weeks.

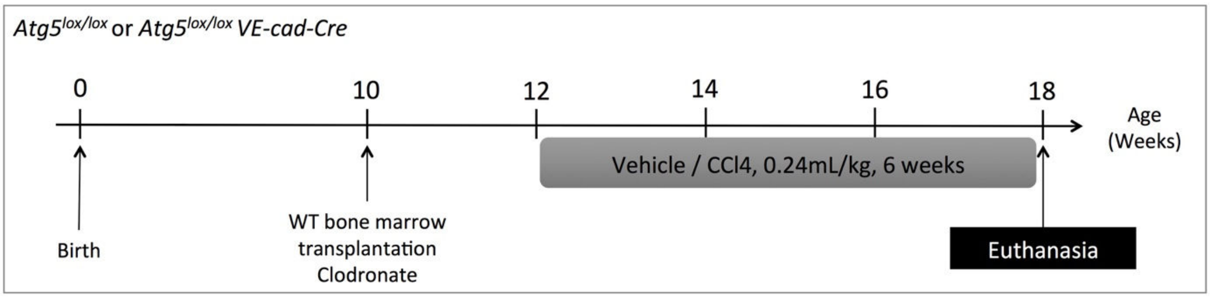
Atg5lox/lox or Atg5lox/lox VE-cad-Cre
0
10
12
14
16
18
Age (Weeks)
Vehicle / CCl4, 0.24mL/kg, 6 weeks
Birth
WT bone marrow transplantation Clodronate
Euthanasia

Sup Figure 6: Experimental procedure: protocol to investigate fibrosis development in *Atg5*$^{lox/lox}$ and *Atg5*$^{lox/lox}$*;VE-cadherin-Cre* treated with carbon tetrachloride (CCl4) or its vehicle. CCl4 was administered by itraperitoneal injection at 0.24 mL/kg 3 times a week for 6 weeks.

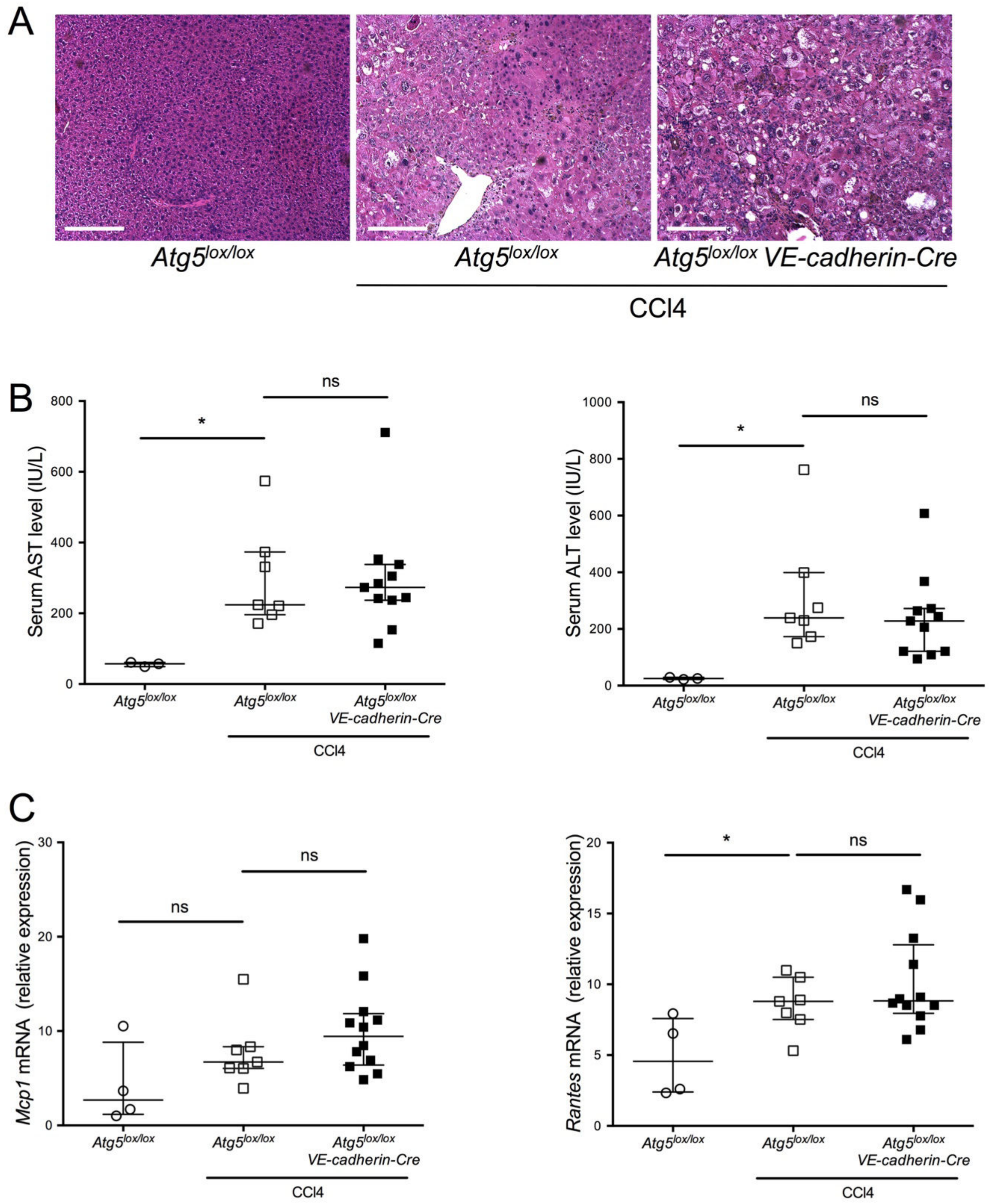

Sup Figure 7: Deficiency in endothelial autophagy does not change liver injury and inflammation in CCl4 treated mice. Twelve weeks mice were injected with CCl4 (0.24 mL/kg, 3 times a week) for 6 weeks. (A) Representative images of hematoxyline and eosin staining. Scale bare 100 µm. (B) Serum AST and ALT levels. (C) Hepatic gene expression of *Mcp1* and *Rantes*. *Atg5*$^{lox/lox}$, vehicle: n=4; *Atg5*$^{lox/lox}$, CCl4: n=7; *Atg5*$^{lox/lox}$*;VE-cadherin-cre,* high-fat diet: n=12. Data are expressed as median ± IQR. *p<0.05; ns: not significant.

Supplemental Tables

Supplemental Table 1. Patients' characteristics

Metabolic and morphological features	**Healthy controls (n=7)**	**Steatosis (n=4)**	**NASH (n=12)**
Age (years)	41 (34 – 45)	46 (33 – 62)	51 (39 – 59)
Male gender	3 (43%)	2 (50%)	7 (58%)
BMI (kg/m^2)	23.2 (19.7 – 27.4)	25.3 (23.6 – 35.0)	28.4 (26.2 – 34.8) *
Fasting serum glucose (mg/dL)	88 (76 – 108)	92 (86 – 115)	101 (88 – 130)
Serum cholesterol (g/L)	2.2 (1.9 – 2.3)	1.5 (1.2 – 2.2)	2.1 (1.7 – 2.4)
Serum HDL cholesterol (g/L)	0.6 (0.4 – 0.7)	0.3 (0.3 – 0.5)	0.4 (0.3 – 0.4)
Serum LDL cholesterol (g/L)	1.4 (1.3 – 1.6)	0.9 (0.6 – 1.3)	1.0 (0.8 – 1.3)
Serum triglycerides (g/L)	0.9 (0.7 – 2.0)	1.3 (1.1 – 1.7)	1.3 (0.9 – 2.7)
Serum AST (x ULN)	1.1 (0.8 – 1.5)	0.9 (0.7 – 1.9)	1.2 (1.0 – 1.9)
Serum ALT (x ULN)	1.8 (1.4 – 2.2)	1.6 (0.7 – 3.6)	1.3 (1.0 – 2.2)

Data are expressed as median ± IQR or frequency (%) for the gender.

*$p<0.05$ *vs* healthy controls.

Abbreviations: ALT, alanine aminotransferases; AST, aspartate aminotransferase; BMI, body mass index; HDL, high density lipoprotein; LDL, low density lipoprotein; ULN, upper limit of the normal.

Supplemental Table 2. List of antibodies used for western blots analyses

Antibody anti-	Raised in	Reference	Dilution	WB buffer
α-SMA	Mouse	Sigma Aldrich A 2547	1/1000	TBST milk
ATG5	Rabbit	CST 8540	1/1000	TBST milk
Cleaved Caspase-3	Rabbit	CST 9662	1/1000	TBST milk
GAPDH	Mouse	Millipore MAB374	1/20000	TBST milk
LC3B	Rabbit	CST 2775	1/1000	TBST milk
p-AMPKα (Thr172)	Rabbit	CST 2535	1/1000	TBST BSA

Abbreviations: BSA, bovine serum albumin; CST, cell signaling technology; TBST, tris buffer salin 0.05 tween; WB, western blot.

Supplemental Table 3. List and sequences of primers used for gene expression analyses.

Gene	Primer	Sequence	Annealing Temperature (°C)
α-***SMA***	Forward	5' GAA CCC TAA GGC CAA CCG GGA GAA A 3’	59.3
	Reverse	5' CCA CAT ACA TGG CGG GGA CAT TGA 3’	
Atg5	Forward	5' TTC CGC AGT CGC CCC TGA AGA T 3'	62.4
	Reverse	5' TCT GTT GGC TGG GGG ACA ATG CTA AT 3’	
Collagene1α2	Forward	5’ GCT GAG GGC AAC AGC AGG TTC ACC TA 3’	61.3
	Reverse	5’ GGA ACG GCA GGC GAG ATG GCT TAT T 3’	
Gapdh	Forward	5’ CGT CCC GTA GAC AAA ATG GTG AA 3’	61.9
	Reverse	5’ GCC GTG AGT GGA GTC ATA CTG GAA CA 3’	
Hprt	Forward	5’ TGT GCT CAA GGG GGG CTA TAA GTT 3’	57.4
	Reverse	5’ ACT TTT ATG TCC CCC GTT GAC TGA 3’	
Mcp1	Forward	5’ ATG CTT CTG GGC CTG CTG CTG TTC A 3’	61.6
	Reverse	5’ GAG TGG GGC GTT AAC TGC ATC TG 3’	
Ppia	Forward	5’ CAC-CGT-GTT-CTT-CGA-CAT-CA 3’	60
	Reverse	5’ CAG-TGC-TCA-GAG-CTC-GAA-AGT 3’	
Rantes	Forward	5’ CCC CCG CAC CTG CCT CAC CAT A 3’	64.1
	Reverse	5’ AGG CAG CGC GAG GGA GAG GTA 3’	
Tgf-β1	Forward	5’ CGG AGA GCC CTG GAT ACC AAC TA 3’	58.8
	Reverse	5’ GCC GCA CAC AGC AGT TCT TCT CT 3’	

Supplemental Table 4. Metabolic and blood cell count of 28 weeks old *Atg5*$^{lox/lox}$ *vs.* *Atg5*$^{lox/lox}$*;VE-cadherin-Cre* mice fed a chow diet or a high-fat diet

	***Atg5*$^{lox/lox}$** **Chow diet** **(n=5)**	***Atg5*$^{lox/lox}$** ***VE-cad-Cre*** **Chow diet** **(n=6)**	***Atg5*$^{lox/lox}$** **High fat diet** **(n=8)**	***Atg5*$^{lox/lox}$** ***VE-cad-Cre*** **High fat diet** **(n=14)**
Morphological features				
Body weight (g)	28 (26 – 36)	31 (28.5 – 34)	26 (22 – 29)	26 (23 – 30)
Male gender	3 (60%)	3 (50%)	3 (37.5%)	7 (50%)
Liver weight/body weight (%)	4.5 (4.3 – 4.7)	3.6 (3.2 – 4.8)	4.5 (4.1 – 5.0)	3.3 (2.5 – 4.4) $
Spleen weight/body weight (%)	0.1 (0.1 – 0.3)	0.2 (0.1 – 0.2)	0.2 (0.1 – 0.4)	0.4 (0.2 – 0.5)
Kidney weight/body weight (%)	0.6 (0.5 – 0.7)	0.6 (0.4 – 0.7)	0.5 (0.4 – 0.7)	0.5 (0.5 – 0.6)
Heart weight/body weight (%)	0.4 (0.4 – 0.5)	0.5 (0.4 – 0.5)	0.4 (0.4 – 0.5)	0.4 (0.4 – 0.5)
Metabolic features				
Arterial blood pressure (mm Hg)	NA	NA	114 (103 – 118)	102 (97 – 112)
Fasting plasma glucose (mg/dL)	143 (124 – 159)	129 (104 – 145)	131 (119 – 150)	128 (75 – 137)
Plasma cholesterol (g/L)	0.7 (0.6 – 0.7)	0.8 (0.5 – 0.9)	1.3 (1.1 – 1.6) **	1.1 (0.9 – 1.3)
Plasma HDL cholesterol (g/L)	0.5 (0.4 – 0.5)	0.5 (0.3 – 0.6)	0.7 (0.5 – 0.9)	0.5 (0.1 – 0.8)
Plasma triglycerides (g/L)	0.6 (0.3 – 1.0)	0.8 (0.5 – 0.9)	0.3 (0.2 – 0.4) **	0.4 (0.3 – 0.5)
Blood cell count				
RBC ($10^3/mm^3$)	4.3 (3.4 – 7.2)	6.7 (4.7 – 7.3)	5.0 (4.7 – 6.3)	5.1 (4.0 – 6.3)
Hemoglobin (g/dL)	6.1 (4.9 – 10.3)	9.5 (6.5 – 10.7)	7.0 (6.3 – 9.3)	7.5 (5.8 – 9.2)
WBC ($10^3/mm^3$)	3.2 (1.7 – 5.3)	5.7 (3.9 – 6.8)	4.8 (3.2 – 11.2)	5.9 (4.0 – 9.0)
Neutrophils ($10^3/mm^3$)	0.3 (0.2 – 1.4)	0.7 (0.5 – 1.5)	0.7 (0.5 – 2.2)	0.9 (0.7 – 2.2)
Lymphocytes ($10^3/mm^3$)	2.8 (1.4 – 3.7)	4.5 (3.3 – 5.8)	4.0 (2.4 – 8.6)	5.0 (3.2 – 6.6)
Monocytes ($10^3/mm^3$)	0.1 (0.0 – 0.1)	0.0 (0.0 – 0.0)	0.0 (0.0 – 0.2)	0.0 (0.0 – 0.1)
Platelets ($10^3/mm^3$)	508 (371 – 760)	635 (512 – 746)	738 (643 – 839)	625 (445 – 724)

Data are expressed as median ± IQR or number (%) for the gender.

** $p<0.01$ *vs.* $Atg5^{lox/lox}$, chow diet; \$ $p<0.05$ *vs.* $Atg5^{lox/lox}$, high-fat diet.

Abbreviations: HDL, high density lipoprotein; NA, not available; RBC, red blood cells; WBC, white blood cells.

Supplemental Table 5. Metabolic and blood cell count of 28 weeks old *Atg5*$^{lox/lox}$ *vs.* *Atg5*$^{lox/lox}$*;VE-cadherin-Cre* mice treated with vehicle or carbon tetrachloride (CCl4)

	Atg5$^{lox/lox}$ **Vehicle** **(n=4)**	***Atg5***$^{lox/lox}$ **CCl4** **(n=8)**	***Atg5***$^{lox/lox}$ ***VE-cad-Cre*** **CCl4** **(n=12)**
Morphological features			
Body weight (g)	24 (23.1 – 24.5)	26 (20.7 – 30.5)	24 (21.8 – 25.3)
Male gender	1 (25%)	4 (50%)	3 (25%)
Liver weight/body weight (%)	4.6 (4.5 – 4.8)	4.4 (3.8 – 4.7)	3.9 (3.4 – 4.4)
Spleen weight/body weight (%)	0.2 (0.2 – 0.3)	0.5 (0.4 – 0.5) **	0.4 (0.4 – 0.5) **
Kidney weight/body weight (%)	0.6 (0.5 – 0.6)	0.7 (0.6 – 0.7) *	0.6 (0.5 – 0.7)
Heart weight/body weight (%)	0.5 (0.5 – 0.6)	0.5 (0.5 – 0.5)	0.5 (0.5 – 0.5)
Blood cell count			
RBC (10^3/mm^3)	7.8 (7.8 – 8.6)	8.1 (7.6 – 8.4)	7.6 (7.1 – 8.3)
Hemoglobin (g/dL)	9.7 (9.3– 12.2)	11.7 (11.5 – 12.5)	11.8 (11.1 – 12.6)
WBC (10^3/mm^3)	8.4 (6.3 – 9.0)	11.5 (8.5 – 13.7)	8.9 (6.1 – 11.6)
Neutrophils (10^3/mm^3)	2.6 (2.3 – 4.7)	6.1 (4.1 – 7.9)	4.4 (2.5 – 5.9)
Lymphocytes (10^3/mm^3)	4.0 (3.6 – 5.6)	5.3 (3.9 – 5.5)	3.8 (3.0 – 5.8)
Monocytes (10^3/mm^3)	0.2 (0.1 – 0.2)	0.3 (0.2 – 0.3)	0.2 (0.1 – 0.3)
Platelets (10^3/mm^3)	581(524 – 673)	460 (394 – 528) *	423 (288 – 517) *

Data are expressed as median ± IQR or number (%) for the gender.

* p<0.05 *vs.* *Atg5*$^{lox/lox}$, vehicle; ** p<0.01 *vs.* *Atg5*$^{lox/lox}$, vehicle.

Abbreviations: CCl4, carbon tetrachloride; RBC, red blood cells; WBC, white blood cells.

V- DISCUSSION AND PROSPECTS

Nonalcoholic steatohepatitis is an expanding health issue owing to its close association with the worldwide epidemic of the metabolic syndrome. Its pathophysiology is still incompletely elucidated. Understanding how simple steatosis progress to NASH is of utmost importance. Several evidences have highlighted the pivotal role of LSECs in the pathogenesis of NASH. Indeed, studies demonstrated that sinusoidal endothelial alterations occur very early in the course of the disease, preceding the onset of NASH [179,185,189,197,221,224–226,263,274]. These alterations include 1) capillarization of LSECs, defined as the loss of the fenestrae and the formation of a basement membrane [179,263], 2) endothelial dysfunction, characterized by the blunted activation of eNOS and the reduction of NO bioavailability in the liver [189,197], 3) endothelial inflammation which strongly contributes to liver inflammation [226] and 4) pathologic angiogenesis [221,224–226,274]. All these alterations have been shown to promote NASH development. However, the precise mechanisms underlying these alterations remained elusive.

Autophagy is a gatekeeper of cellular homeostasis. Although the role of autophagy in the different liver cells types has been studied [427], nothing was known about autophagy in LSECs in chronic liver diseases. This led us to the first aim of this study which was to analyze autophagy in LSECs in NASH. We demonstrated using liver biopsies from patients that endothelial autophagy is defective in patients with NASH and that this defect occurs specifically in NASH but not in steatosis.

We first aimed to identify which mediators could regulate autophagy in LSECs in NAFLD setting. Because of LSECs are highly specialized endothelial cells that displays morphological and functional specificities compared to other endothelial cells from large vessels or other microvascular endothelial cells [162], we used a murine cell line of transformed LSECs (TSECs) that maintain some features of LSECs [447]. We exposed these cells to shear stress to mimic physiological conditions. Shear stress is a physiological mechanical stimulus which activates autophagy in endothelial cells in large vessels [446]. We confirmed that TSECs respond to shear stress stimulation. Indeed, TSECs exhibited a complete autophagic flux when stimulated with shear forces.

NAFLD is associated with hyperinsulinemia and systemic inflammation. This led us to test the effect of insulin and pro-inflammatory mediators (MCP1, TNFα and IL-6), involved in the pathogenesis of NASH [14], on autophagy level in TSECs. To be close to the pathophysiology of the disease, we treated the cells with each of these molecules at concentrations reported in the portal venous blood in metabolic syndrome conditions [448–451]. In this setting, none of these molecules had an effect on autophagy level in TSECs when incubated separately with TSECs. However, the pathophysiology of NASH is more complex and characterized by disturbances in a wide array of inflammatory and metabolic molecules that act simultaneously on the cells. This led us to test the effect of combined inflammatory mediators on autophagy level in TSECs. Interestingly, we founded that the combination of TNFα and IL-6 at concentrations in the range of those found in the portal vein of patients significantly impairs autophagy in TSECs.

Although a decrease in LC3II/GAPDH ratio is suggestive of a decrease autophagy initiation, this may also result from an increase of the autophagic flux with an increase in autolysosomal degradation since LC3II is degraded at the end of the autophagic process in autolysosomes [452]. This can be analyzed by blocking the autolysosomal degradation, *i.e.* the final step of autophagy, with chloroquine. In two independent experiments, LC3II/GAPDH ratio was decreased in TSECs treated with TNFα and IL-6 when autolysosomal degradation was blocked with chloroquine, comparatively to untreated cells (Supplemental Figure 2E). This suggests that TNFα and IL-6 inhibit autophagy initiation since less LC3II accumulates when autolysosomal degradation is blocked with chloroquine. This result did not reach the statistical significance due to the low number of experiments (n=2). Further experiments will be performed to validate this result. Furthermore, it would be interesting to test the effect of other combinations of metabolic mediators associated with NASH such as insulin, glucose or ox-LDL.

To better characterize the mechanisms triggering the defect in autophagy in LSECs in NASH, we aimed to identify which signaling pathways were modulated by TNFα and IL-6. We tested the AMPKα pathway since it is a major positive regulator of autophagy [453]. Moreover, AMPKα has been shown to mediate shear stress-induced autophagy in endothelial cells [446]. We founded that TNFα and IL-6 decrease the phosphorylation of AMPKα suggesting that these inflammatory mediators inhibit autophagy in TSECs by inhibiting AMPKα activation. This result further confirms that TNFα and IL-6 block the initiation of autophagy since AMPKα signaling pathway is involved in the initial steps of autophagy activation. Taken together, these results provide insights in the understanding of how autophagy in LSECs can be regulated in NASH setting. The power of these results is that they are based on pathophysiological concentrations of inflammatory mediators making them relevant regarding to the pathological setting of the disease.

Another powerful regulator of autophagy is mTOR which is a major negative regulator that blocks the initiation of autophagy [453]. As described in introduction, mTOR can be negatively regulated by AMPKα in certain conditions [394]. Given that TNFα and IL-6 inhibit autophagy initiation through the inhibition of the AMPKα pathway, it is tempting to speculate that mTOR pathway could be overactivated in these conditions. Further experiments will be performed to assess the effect of TNFα and IL-6 on mTOR signaling.

Finally, we generated a LSECs line deficient in autophagy by transducing TSECs with a short hairpin RNA targeting *Atg5*. As illustrated in supplemental Figure 3, the knockdown of ATG5 in TSECs blunted the activation of autophagy by shear stress. We used these cells to test the hypothesis that the deficiency in autophagy may induce alterations in LSECs since we previously described that the lack of autophagy in HUVECs induces endothelial inflammation [446]. We first conducted our experiments in unstimulating conditions. Interestingly, *Rantes* expression was three times higher in TSECs deficient in autophagy while *Mcp-1* was not modulated. We then decided to better mimic the pathophysiology of NASH by stimulating the cells. After exposure to the proinflammatory stimulus TNFα, deficiency in autophagy in TSECs was associated with an overexpression of *Mcp-1* and *Rantes* suggesting that autophagy prevents inflammatory genes expression in conditions of stress. It would be interesting to consolidate this result by measuring MCP-1 and RANTES levels in the culture supernatant of these cells. Moreover, deficiency in autophagy in TSECs also resulted in VCAM-1 which is a hallmark of endothelial inflammation involved in leukocytes recruitment. This result is reminiscent of the increased expression of cell adhesion molecules including VCAM-1 in dietary-induced steatohepatitis mouse models of NASH [226]. Taken together, these results indicate that deficiency in autophagy in LSECs induces endothelial inflammation. Activated endothelial cells can in turn contribute to liver inflammation.

In addition, deficiency in autophagy in TSECs also promoted the expression of endothelial-to-mesenchymal transition markers. This result in line with a previous study showing that ATG7 deficiency promotes endothelial-to-mesenchymal transition in

HUVECs [258]. Finally, deficiency in autophagy also promoted apoptosis in TSECs which is in accordance with a previous study in which we demonstrated that ATG5 deficiency promotes endothelial senescence and apoptosis in mice [446].

The second aim of this study was to analyze the consequences of the defect in endothelial autophagy on NASH and liver fibrosis.

We first used a model of early NASH induced by a high fat diet to study the role endothelial autophagy in NASH. This model presents the advantage that it resembles the pathophysiology of human NASH because it includes some of the key systemic metabolic disorders associated with the disease [289]. In mice fed a high fat diet, deficiency in endothelial autophagy promoted NASH development, as attested by *Mcp-1*, *Rantes* and VCAM-1 liver overexpression. Interestingly, these markers were also overexpressed by TSECs deficient in autophagy.

Liver fibrosis was also increased in endothelial autophagy deficient mice in both high fat diet model and CCl4-induced fibrosis. Liver fibrosis develops as a result of hepatic stellate cells activation. Interestingly, we observed an overexpression of α-SMA in the liver of endothelial autophagy deficient mice in both models suggestive of an overactivation of hepatic stellate cells. The mechanisms linking endothelial autophagy to hepatic stellate cells activation deserve further studies but we can speculate that defective endothelial autophagy could promote endothelial dysfunction, which is permissive for hepatic stellate cells activation. Indeed, healthy LSECs maintain hepatic stellate cells quiescence through nitric oxide but lose this ability when endothelial dysfunction appears [454]. Interestingly, autophagy deficiency has been linked to endothelial dysfunction in HUVECs [455]. Measuring endothelial function in the liver of endothelial autophagy deficient mice would be of great interest. Furthermore, we also provide evidence that α-SMA overexpression could also result from endothelial-to-mesenchymal transition. We demonstrated *in vitro* that autophagy deficiency is associated with α-SMA overexpression in TSECs. This was associated with the overexpression of *Tgf-β1* and *Collagen1α2* consistent with endothelial-to-mesenchymal transition. This suggests that the pool of hepatic myofibroblast may also originate from endothelial-to-mesenchymal transition in NASH and liver fibrosis. While this phenomenon has been poorly described in the liver [259], it occurs in fibrotic cardiovascular and pulmonary diseases [256,257]. Moreover, deficiency in endothelial autophagy has been shown to promote endothelial-to-mesenchymal transition and associated with pulmonary fibrosis in mice suggesting that endothelial autophagy prevents organ fibrosis [258]. Altogether, these evidences indicate that endothelial-to-mesenchymal transition is likely to occur in the liver in NASH thus contributing to liver fibrosis.

Taken together, our *in vivo* and *in vitro* findings indicate that liver endothelial autophagy displays anti-inflammatory and anti-fibrogenic properties and complete the picture of the role of autophagy in chronic liver diseases. In physiological conditions, autophagy is activated in LSECs and maintains endothelial homeostasis and the liver health while in metabolic syndrome conditions, inflammatory and/or metabolic mediators present in the portal venous blood induce a defect in autophagy in LSECs. The defect in autophagy in LSECs induces in turn endothelial alterations. Altered endothelial cells strongly contribute to liver inflammation and fibrosis thus promoting NASH and liver fibrosis.

This study could in part explain how patients with simple steatosis progress to NASH. It is tempting to speculate that patients with steatosis in whom autophagy in LSECs is effective remain stable while patients with steatosis in whom autophagy in LSECs becomes defective progress to NASH.

These findings extend the available knowledge about the role of LSECs in NAFLD showing that endothelial cell alterations including capillarization, endothelial dysfunction, endothelial inflammation and angiogenesis promote NASH development. Our results indicate that the defect in autophagy in LSECs occurring in NASH is a mechanism triggering endothelial inflammation and endothelial-to-mesenchymal transition (Figure 16). Further studies are required to assess the role of autophagy in LSECs in sinusoidal capillarization, endothelial dysfunction, angiogenesis and vascular architecture.

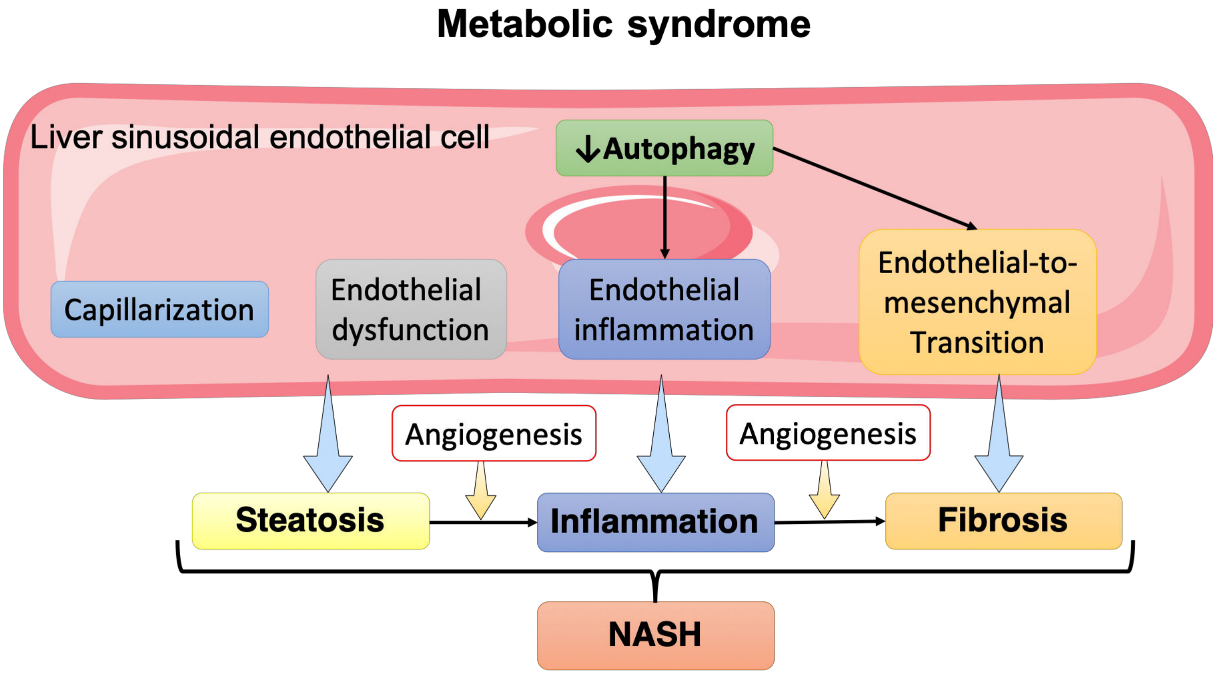
Metabolic syndrome
Liver sinusoidal endothelial cell
↓Autophagy
Capillarization
Endothelial dysfunction
Endothelial inflammation
Endothelial-to-mesenchymal Transition
Angiogenesis
Angiogenesis
Steatosis
Inflammation
Fibrosis
NASH

Figure 16: Schematic illustration depicting the role of LSECs in NASH development.

The ultimate challenge of this project will be to test the therapeutic potential of endothelial autophagy in NASH and liver fibrosis. This could be done *in vivo* in mice challenged with high fat diet in which autophagy in liver endothelial cells will have been overactivated. This ambitious objective could be achieved by using adeno-associated viruses (AAV) displaying a hepatic and endothelial tropism in which key autophagy genes, such as *Beclin-1*, *Atg5*, *Atg7* or *Tfeb* [456] will be inserted. The serotype AAV-5 is a good candidate for this purpose since it displays hepatic tropism and has been shown to be uptaken by LSECs [457,458]. Moreover, the challenge of targeting specifically LSECs could be accomplished by submitting autophagic genes to the control of an endothelial specific promoter. In this case, in addition to the uptake by LSECs in majority, autophagy gene will be expressed only in endothelial cells. This therapeutic strategy could be tested both in a preventive setting, by treating the mice concomitantly with the beginning of the high fat diet administration, before the establishment of the disease, or in a curative manner, by treating the mice after a long period of high fat diet administration, once the disease established.

VI- REFERENCES

[1] Eckel RH, Alberti KGMM, Grundy SM, Zimmet PZ. The metabolic syndrome. Lancet 2010;375:181–3. doi:10.1016/S0140-6736(09)61794-3.

[2] Zelman S. The liver in obesity. AMA Arch Intern Med 1952;90:141–56.

[3] Kern WH, Heger AH, Payne JH, DeWind LT. Fatty metamorphosis of the liver in morbid obesity. Arch Pathol 1973;96:342–6.

[4] Galambos JT, Wills CE. Relationship between 505 paired liver tests and biopsies in 242 obese patients. Gastroenterology 1978;74:1191–5.

[5] Adler M, Schaffner F. Fatty liver hepatitis and cirrhosis in obese patients. Am J Med 1979;67:811–6.

[6] Creutzfeldt W, Frerichs H, Sickinger K. Liver diseases and diabetes mellitus. Prog Liver Dis 1970;3:371–407.

[7] Itoh S, Tsukada Y, Motomura Y, Ichinoe A. Five patients with nonalcoholic diabetic cirrhosis. Acta Hepatogastroenterol (Stuttg) 1979;26:90–7.

[8] Falchuk KR, Fiske SC, Haggitt RC, Federman M, Trey C. Pericentral hepatic fibrosis and intracellular hyalin in diabetes mellitus. Gastroenterology 1980;78:535–41.

[9] DeWind LT, Payne JH. Intestinal bypass surgery for morbid obesity. Long-term results. JAMA 1976;236:2298–301.

[10] Campbell JM, Hunt TK, Karam JH, Forsham PH. Jejunoileal bypass as a treatment of morbid obesity. Arch Intern Med 1977;137:602–10.

[11] Ludwig J, Viggiano TR, McGill DB, Oh BJ. Nonalcoholic steatohepatitis: Mayo Clinic experiences with a hitherto unnamed disease. Mayo Clin Proc 1980;55:434–8.

[12] Ratziu V, Bellentani S, Cortez-Pinto H, Day C, Marchesini G. A position statement on NAFLD/NASH based on the EASL 2009 special conference. J Hepatol 2010;53:372–84. doi:10.1016/j.jhep.2010.04.008.

[13] Chalasani N, Younossi Z, Lavine JE, Diehl AM, Brunt EM, Cusi K, et al. The diagnosis and management of non-alcoholic fatty liver disease: practice Guideline by the American Association for the Study of Liver Diseases, American College of Gastroenterology, and the American Gastroenterological Association. Hepatology 2012;55:2005–23. doi:10.1002/hep.25762.

[14] Friedman SL, Neuschwander-Tetri BA, Rinella M, Sanyal AJ. Mechanisms of NAFLD development and therapeutic strategies. Nat Med 2018;24:908–22. doi:10.1038/s41591-018-0104-9.

[15] Vernon G, Baranova A, Younossi ZM. Systematic review: the epidemiology and natural history of non-alcoholic fatty liver disease and non-alcoholic steatohepatitis in adults. Aliment Pharmacol Ther 2011;34:274–85. doi:10.1111/j.1365-2036.2011.04724.x.

[16] Paradis V, Zalinski S, Chelbi E, Guedj N, Degos F, Vilgrain V, et al. Hepatocellular carcinomas in patients with metabolic syndrome often develop without significant liver fibrosis: a pathological analysis. Hepatology 2009;49:851–9. doi:10.1002/hep.22734.

[17] European Association for the Study of the Liver (EASL), European Association for the Study of Diabetes (EASD), European Association for the Study of Obesity (EASO). EASL-EASD-EASO Clinical Practice Guidelines for the management of non-alcoholic fatty liver disease. J Hepatol 2016;64:1388–402. doi:10.1016/j.jhep.2015.11.004.

[18] White DL, Kanwal F, El-Serag HB. Association between nonalcoholic fatty liver disease and risk for hepatocellular cancer, based on systematic review. Clin Gastroenterol Hepatol 2012;10:1342-1359.e2. doi:10.1016/j.cgh.2012.10.001.

[19] Wong RJ, Aguilar M, Cheung R, Perumpail RB, Harrison SA, Younossi ZM, et al. Nonalcoholic steatohepatitis is the second leading etiology of liver disease among adults awaiting liver transplantation in the United States. Gastroenterology 2015;148:547–55. doi:10.1053/j.gastro.2014.11.039.

[20] Lindenmeyer CC, McCullough AJ. The Natural History of Nonalcoholic Fatty Liver Disease-An Evolving View. Clin Liver Dis 2018;22:11–21. doi:10.1016/j.cld.2017.08.003.
[21] Rinella ME, Sanyal AJ. Management of NAFLD: a stage-based approach. Nat Rev Gastroenterol Hepatol 2016;13:196–205. doi:10.1038/nrgastro.2016.3.
[22] Adams LA, Anstee QM, Tilg H, Targher G. Non-alcoholic fatty liver disease and its relationship with cardiovascular disease and other extrahepatic diseases. Gut 2017;66:1138–53. doi:10.1136/gutjnl-2017-313884.
[23] Targher G, Byrne CD. Non-alcoholic fatty liver disease: an emerging driving force in chronic kidney disease. Nat Rev Nephrol 2017;13:297–310. doi:10.1038/nrneph.2017.16.
[24] Drew L. Fatty liver disease: turning the tide. Nature 2017;550:S101. doi:10.1038/550S101a.
[25] Cohen JC, Horton JD, Hobbs HH. Human fatty liver disease: old questions and new insights. Science 2011;332:1519–23. doi:10.1126/science.1204265.
[26] Satapathy SK, Sanyal AJ. Epidemiology and Natural History of Nonalcoholic Fatty Liver Disease. Semin Liver Dis 2015;35:221–35. doi:10.1055/s-0035-1562943.
[27] Estes C, Razavi H, Loomba R, Younossi Z, Sanyal AJ. Modeling the epidemic of nonalcoholic fatty liver disease demonstrates an exponential increase in burden of disease. Hepatology 2018;67:123–33. doi:10.1002/hep.29466.
[28] Hyysalo J, Männistö VT, Zhou Y, Arola J, Kärjä V, Leivonen M, et al. A population-based study on the prevalence of NASH using scores validated against liver histology. J Hepatol 2014;60:839–46. doi:10.1016/j.jhep.2013.12.009.
[29] McPherson S, Hardy T, Henderson E, Burt AD, Day CP, Anstee QM. Evidence of NAFLD progression from steatosis to fibrosing-steatohepatitis using paired biopsies: implications for prognosis and clinical management. J Hepatol 2015;62:1148–55. doi:10.1016/j.jhep.2014.11.034.
[30] Singh S, Allen AM, Wang Z, Prokop LJ, Murad MH, Loomba R. Fibrosis progression in nonalcoholic fatty liver vs nonalcoholic steatohepatitis: a systematic review and meta-analysis of paired-biopsy studies. Clin Gastroenterol Hepatol 2015;13:643-654.e1-9; quiz e39-40. doi:10.1016/j.cgh.2014.04.014.
[31] Younossi ZM, Blissett D, Blissett R, Henry L, Stepanova M, Younossi Y, et al. The economic and clinical burden of nonalcoholic fatty liver disease in the United States and Europe. Hepatology 2016;64:1577–86. doi:10.1002/hep.28785.
[32] Loomba R, Sanyal AJ. The global NAFLD epidemic. Nat Rev Gastroenterol Hepatol 2013;10:686–90. doi:10.1038/nrgastro.2013.171.
[33] Mittal S, El-Serag HB, Sada YH, Kanwal F, Duan Z, Temple S, et al. Hepatocellular Carcinoma in the Absence of Cirrhosis in United States Veterans is Associated With Nonalcoholic Fatty Liver Disease. Clin Gastroenterol Hepatol 2016;14:124-131.e1. doi:10.1016/j.cgh.2015.07.019.
[34] Choudhury J, Sanyal AJ. Insulin resistance and the pathogenesis of nonalcoholic fatty liver disease. Clin Liver Dis 2004;8:575–94, ix. doi:10.1016/j.cld.2004.04.006.
[35] Ballestri S, Zona S, Targher G, Romagnoli D, Baldelli E, Nascimbeni F, et al. Nonalcoholic fatty liver disease is associated with an almost twofold increased risk of incident type 2 diabetes and metabolic syndrome. Evidence from a systematic review and meta-analysis. J Gastroenterol Hepatol 2016;31:936–44. doi:10.1111/jgh.13264.
[36] Lorbeer R, Bayerl C, Auweter S, Rospleszcz S, Lieb W, Meisinger C, et al. Association between MRI-derived hepatic fat fraction and blood pressure in participants without history of cardiovascular disease. J Hypertens 2017;35:737–44. doi:10.1097/HJH.0000000000001245.
[37] Sorrentino P, Terracciano L, D’Angelo S, Ferbo U, Bracigliano A, Vecchione R. Predicting fibrosis worsening in obese patients with NASH through parenchymal fibronectin,

HOMA-IR, and hypertension. Am J Gastroenterol 2010;105:336–44. doi:10.1038/ajg.2009.587.

[38] Pelusi S, Petta S, Rosso C, Borroni V, Fracanzani AL, Dongiovanni P, et al. Renin-Angiotensin System Inhibitors, Type 2 Diabetes and Fibrosis Progression: An Observational Study in Patients with Nonalcoholic Fatty Liver Disease. PLoS ONE 2016;11:e0163069. doi:10.1371/journal.pone.0163069.

[39] Namisaki T, Noguchi R, Moriya K, Kitade M, Aihara Y, Douhara A, et al. Beneficial effects of combined ursodeoxycholic acid and angiotensin-II type 1 receptor blocker on hepatic fibrogenesis in a rat model of nonalcoholic steatohepatitis. J Gastroenterol 2016;51:162–72. doi:10.1007/s00535-015-1104-x.

[40] Eslam M, Valenti L, Romeo S. Genetics and epigenetics of NAFLD and NASH: Clinical impact. J Hepatol 2018;68:268–79. doi:10.1016/j.jhep.2017.09.003.

[41] Romeo S, Kozlitina J, Xing C, Pertsemlidis A, Cox D, Pennacchio LA, et al. Genetic variation in PNPLA3 confers susceptibility to nonalcoholic fatty liver disease. Nat Genet 2008;40:1461–5. doi:10.1038/ng.257.

[42] Bruschi FV, Claudel T, Tardelli M, Caligiuri A, Stulnig TM, Marra F, et al. The PNPLA3 I148M variant modulates the fibrogenic phenotype of human hepatic stellate cells. Hepatology 2017;65:1875–90. doi:10.1002/hep.29041.

[43] Kozlitina J, Smagris E, Stender S, Nordestgaard BG, Zhou HH, Tybjærg-Hansen A, et al. Exome-wide association study identifies a TM6SF2 variant that confers susceptibility to nonalcoholic fatty liver disease. Nat Genet 2014;46:352–6. doi:10.1038/ng.2901.

[44] BasuRay S, Smagris E, Cohen JC, Hobbs HH. The PNPLA3 variant associated with fatty liver disease (I148M) accumulates on lipid droplets by evading ubiquitylation. Hepatology 2017;66:1111–24. doi:10.1002/hep.29273.

[45] Stender S, Kozlitina J, Nordestgaard BG, Tybjærg-Hansen A, Hobbs HH, Cohen JC. Adiposity amplifies the genetic risk of fatty liver disease conferred by multiple loci. Nat Genet 2017;49:842–7. doi:10.1038/ng.3855.

[46] Abul-Husn NS, Cheng X, Li AH, Xin Y, Schurmann C, Stevis P, et al. A Protein-Truncating HSD17B13 Variant and Protection from Chronic Liver Disease. N Engl J Med 2018;378:1096–106. doi:10.1056/NEJMoa1712191.

[47] Liu Y-L, Reeves HL, Burt AD, Tiniakos D, McPherson S, Leathart JBS, et al. TM6SF2 rs58542926 influences hepatic fibrosis progression in patients with non-alcoholic fatty liver disease. Nat Commun 2014;5:4309. doi:10.1038/ncomms5309.

[48] Sookoian S, Castaño GO, Scian R, Mallardi P, Fernández Gianotti T, Burgueño AL, et al. Genetic variation in transmembrane 6 superfamily member 2 and the risk of nonalcoholic fatty liver disease and histological disease severity. Hepatology 2015;61:515–25. doi:10.1002/hep.27556.

[49] Hashimoto E, Tokushige K. Prevalence, gender, ethnic variations, and prognosis of NASH. J Gastroenterol 2011;46 Suppl 1:63–9. doi:10.1007/s00535-010-0311-8.

[50] Frith J, Day CP, Henderson E, Burt AD, Newton JL. Non-alcoholic fatty liver disease in older people. Gerontology 2009;55:607–13. doi:10.1159/000235677.

[51] Wong VW-S, Chu WC-W, Wong GL-H, Chan RS-M, Chim AM-L, Ong A, et al. Prevalence of non-alcoholic fatty liver disease and advanced fibrosis in Hong Kong Chinese: a population study using proton-magnetic resonance spectroscopy and transient elastography. Gut 2012;61:409–15. doi:10.1136/gutjnl-2011-300342.

[52] Browning JD, Szczepaniak LS, Dobbins R, Nuremberg P, Horton JD, Cohen JC, et al. Prevalence of hepatic steatosis in an urban population in the United States: impact of ethnicity. Hepatology 2004;40:1387–95. doi:10.1002/hep.20466.

[53] Dowman JK, Tomlinson JW, Newsome PN. Systematic review: the diagnosis and staging of non-alcoholic fatty liver disease and non-alcoholic steatohepatitis. Aliment

Pharmacol Ther 2011;33:525–40. doi:10.1111/j.1365-2036.2010.04556.x.
[54] Adams LA, Feldstein AE. Non-invasive diagnosis of nonalcoholic fatty liver and nonalcoholic steatohepatitis. J Dig Dis 2011;12:10–6. doi:10.1111/j.1751-2980.2010.00471.x.
[55] Pratt DS, Kaplan MM. Evaluation of abnormal liver-enzyme results in asymptomatic patients. N Engl J Med 2000;342:1266–71. doi:10.1056/NEJM200004273421707.
[56] Yan E, Durazo F, Tong M, Hong K. Nonalcoholic fatty liver disease: pathogenesis, identification, progression, and management. Nutr Rev 2007;65:376–84.
[57] Adams LA, Angulo P, Lindor KD. Nonalcoholic fatty liver disease. CMAJ 2005;172:899–905. doi:10.1503/cmaj.045232.
[58] Angulo P, Keach JC, Batts KP, Lindor KD. Independent predictors of liver fibrosis in patients with nonalcoholic steatohepatitis. Hepatology 1999;30:1356–62. doi:10.1002/hep.510300604.
[59] Kleiner DE, Brunt EM, Van Natta M, Behling C, Contos MJ, Cummings OW, et al. Design and validation of a histological scoring system for nonalcoholic fatty liver disease. Hepatology 2005;41:1313–21. doi:10.1002/hep.20701.
[60] Bedossa P, Poitou C, Veyrie N, Bouillot J-L, Basdevant A, Paradis V, et al. Histopathological algorithm and scoring system for evaluation of liver lesions in morbidly obese patients. Hepatology 2012;56:1751–9. doi:10.1002/hep.25889.
[61] Musso G, Cassader M, Gambino R. Non-alcoholic steatohepatitis: emerging molecular targets and therapeutic strategies. Nat Rev Drug Discov 2016;15:249–74. doi:10.1038/nrd.2015.3.
[62] Machado MV, Diehl AM. Pathogenesis of Nonalcoholic Steatohepatitis. Gastroenterology 2016;150:1769–77. doi:10.1053/j.gastro.2016.02.066.
[63] Greuter T, Malhi H, Gores GJ, Shah VH. Therapeutic opportunities for alcoholic steatohepatitis and nonalcoholic steatohepatitis: exploiting similarities and differences in pathogenesis. JCI Insight 2017;2. doi:10.1172/jci.insight.95354.
[64] Day CP, James OF. Steatohepatitis: a tale of two “hits”? Gastroenterology 1998;114:842–5.
[65] Bril F, Barb D, Portillo-Sanchez P, Biernacki D, Lomonaco R, Suman A, et al. Metabolic and histological implications of intrahepatic triglyceride content in nonalcoholic fatty liver disease. Hepatology 2017;65:1132–44. doi:10.1002/hep.28985.
[66] Marra F, Bertolani C. Adipokines in liver diseases. Hepatology 2009;50:957–69. doi:10.1002/hep.23046.
[67] Donnelly KL, Smith CI, Schwarzenberg SJ, Jessurun J, Boldt MD, Parks EJ. Sources of fatty acids stored in liver and secreted via lipoproteins in patients with nonalcoholic fatty liver disease. J Clin Invest 2005;115:1343–51. doi:10.1172/JCI23621.
[68] Cusi K. Role of obesity and lipotoxicity in the development of nonalcoholic steatohepatitis: pathophysiology and clinical implications. Gastroenterology 2012;142:711-725.e6. doi:10.1053/j.gastro.2012.02.003.
[69] Boursier J, Mueller O, Barret M, Machado M, Fizanne L, Araujo-Perez F, et al. The severity of nonalcoholic fatty liver disease is associated with gut dysbiosis and shift in the metabolic function of the gut microbiota. Hepatology 2016;63:764–75. doi:10.1002/hep.28356.
[70] Gruben N, Shiri-Sverdlov R, Koonen DPY, Hofker MH. Nonalcoholic fatty liver disease: A main driver of insulin resistance or a dangerous liaison? Biochim Biophys Acta 2014;1842:2329–43. doi:10.1016/j.bbadis.2014.08.004.
[71] Guo S. Insulin signaling, resistance, and the metabolic syndrome: insights from mouse models into disease mechanisms. J Endocrinol 2014;220:T1–23. doi:10.1530/JOE-13-0327.
[72] Miao H, Zhang Y, Lu Z, Liu Q, Gan L. FOXO1 involvement in insulin resistance-related pro-inflammatory cytokine production in hepatocytes. Inflamm Res 2012;61:349–58.

doi:10.1007/s00011-011-0417-3.

[73] Svegliati-Baroni G, Ridolfi F, Di Sario A, Casini A, Marucci L, Gaggiotti G, et al. Insulin and insulin-like growth factor-1 stimulate proliferation and type I collagen accumulation by human hepatic stellate cells: differential effects on signal transduction pathways. Hepatology 1999;29:1743–51. doi:10.1002/hep.510290632.

[74] Begriche K, Massart J, Robin M-A, Bonnet F, Fromenty B. Mitochondrial adaptations and dysfunctions in nonalcoholic fatty liver disease. Hepatology 2013;58:1497–507. doi:10.1002/hep.26226.

[75] Schuppan D, Schattenberg JM. Non-alcoholic steatohepatitis: pathogenesis and novel therapeutic approaches. J Gastroenterol Hepatol 2013;28 Suppl 1:68–76. doi:10.1111/jgh.12212.

[76] Marra F, Svegliati-Baroni G. Lipotoxicity and the gut-liver axis in NASH pathogenesis. J Hepatol 2018;68:280–95. doi:10.1016/j.jhep.2017.11.014.

[77] Walenbergh SMA, Koek GH, Bieghs V, Shiri-Sverdlov R. Non-alcoholic steatohepatitis: the role of oxidized low-density lipoproteins. J Hepatol 2013;58:801–10. doi:10.1016/j.jhep.2012.11.014.

[78] Klein S. The case of visceral fat: argument for the defense. J Clin Invest 2004;113:1530–2. doi:10.1172/JCI22028.

[79] Rytka JM, Wueest S, Schoenle EJ, Konrad D. The portal theory supported by venous drainage-selective fat transplantation. Diabetes 2011;60:56–63. doi:10.2337/db10-0697.

[80] Brady LJ, Brady PS, Romsos DR, Hoppel CL. Elevated hepatic mitochondrial and peroxisomal oxidative capacities in fed and starved adult obese (ob/ob) mice. Biochem J 1985;231:439–44.

[81] Koliaki C, Szendroedi J, Kaul K, Jelenik T, Nowotny P, Jankowiak F, et al. Adaptation of hepatic mitochondrial function in humans with non-alcoholic fatty liver is lost in steatohepatitis. Cell Metab 2015;21:739–46. doi:10.1016/j.cmet.2015.04.004.

[82] Serviddio G, Bellanti F, Tamborra R, Rollo T, Capitanio N, Romano AD, et al. Uncoupling protein-2 (UCP2) induces mitochondrial proton leak and increases susceptibility of non-alcoholic steatohepatitis (NASH) liver to ischaemia-reperfusion injury. Gut 2008;57:957–65. doi:10.1136/gut.2007.147496.

[83] Yang Y, Jiang G, Zhang P, Fan J. Programmed cell death and its role in inflammation. Mil Med Res 2015;2:12. doi:10.1186/s40779-015-0039-0.

[84] Wisely GB, Miller AB, Davis RG, Thornquest AD, Johnson R, Spitzer T, et al. Hepatocyte nuclear factor 4 is a transcription factor that constitutively binds fatty acids. Structure 2002;10:1225–34.

[85] Miura K, Ohnishi H. Role of gut microbiota and Toll-like receptors in nonalcoholic fatty liver disease. World J Gastroenterol 2014;20:7381–91. doi:10.3748/wjg.v20.i23.7381.

[86] Lee JY, Sohn KH, Rhee SH, Hwang D. Saturated fatty acids, but not unsaturated fatty acids, induce the expression of cyclooxygenase-2 mediated through Toll-like receptor 4. J Biol Chem 2001;276:16683–9. doi:10.1074/jbc.M011695200.

[87] Amir M, Czaja MJ. Autophagy in nonalcoholic steatohepatitis. Expert Rev Gastroenterol Hepatol 2011;5:159–66. doi:10.1586/egh.11.4.

[88] Feldstein AE, Canbay A, Angulo P, Taniai M, Burgart LJ, Lindor KD, et al. Hepatocyte apoptosis and fas expression are prominent features of human nonalcoholic steatohepatitis. Gastroenterology 2003;125:437–43.

[89] Ashraf NU, Sheikh TA. Endoplasmic reticulum stress and Oxidative stress in the pathogenesis of Non-alcoholic fatty liver disease. Free Radic Res 2015;49:1405–18. doi:10.3109/10715762.2015.1078461.

[90] Singh R, Kaushik S, Wang Y, Xiang Y, Novak I, Komatsu M, et al. Autophagy regulates lipid metabolism. Nature 2009;458:1131–5. doi:10.1038/nature07976.

[91] Ter Horst KW, Serlie MJ. Fructose Consumption, Lipogenesis, and Non-Alcoholic Fatty Liver Disease. Nutrients 2017;9. doi:10.3390/nu9090981.

[92] Peters KM, Wilson RB, Borradaile NM. Non-parenchymal hepatic cell lipotoxicity and the coordinated progression of non-alcoholic fatty liver disease and atherosclerosis. Curr Opin Lipidol 2018;29:417–22. doi:10.1097/MOL.0000000000000535.

[93] Min H-K, Maruyama H, Jang BK, Shimada M, Mirshahi F, Ren S, et al. Suppression of IGF binding protein-3 by palmitate promotes hepatic inflammatory responses. FASEB J 2016;30:4071–82. doi:10.1096/fj.201600427R.

[94] Huang W, Metlakunta A, Dedousis N, Zhang P, Sipula I, Dube JJ, et al. Depletion of liver Kupffer cells prevents the development of diet-induced hepatic steatosis and insulin resistance. Diabetes 2010;59:347–57. doi:10.2337/db09-0016.

[95] Navarro LA, Wree A, Povero D, Berk MP, Eguchi A, Ghosh S, et al. Arginase 2 deficiency results in spontaneous steatohepatitis: a novel link between innate immune activation and hepatic de novo lipogenesis. J Hepatol 2015;62:412–20. doi:10.1016/j.jhep.2014.09.015.

[96] Teratani T, Tomita K, Suzuki T, Oshikawa T, Yokoyama H, Shimamura K, et al. A high-cholesterol diet exacerbates liver fibrosis in mice via accumulation of free cholesterol in hepatic stellate cells. Gastroenterology 2012;142:152-164.e10. doi:10.1053/j.gastro.2011.09.049.

[97] Natarajan SK, Ingham SA, Mohr AM, Wehrkamp CJ, Ray A, Roy S, et al. Saturated free fatty acids induce cholangiocyte lipoapoptosis. Hepatology 2014;60:1942–56. doi:10.1002/hep.27175.

[98] Li Z, Berk M, McIntyre TM, Gores GJ, Feldstein AE. The lysosomal-mitochondrial axis in free fatty acid-induced hepatic lipotoxicity. Hepatology 2008;47:1495–503. doi:10.1002/hep.22183.

[99] Hamlin AN, Basford JE, Jaeschke A, Hui DY. LRP1 Protein Deficiency Exacerbates Palmitate-induced Steatosis and Toxicity in Hepatocytes. J Biol Chem 2016;291:16610–9. doi:10.1074/jbc.M116.717744.

[100] Aubert J, Begriche K, Knockaert L, Robin MA, Fromenty B. Increased expression of cytochrome P450 2E1 in nonalcoholic fatty liver disease: mechanisms and pathophysiological role. Clin Res Hepatol Gastroenterol 2011;35:630–7. doi:10.1016/j.clinre.2011.04.015.

[101] Begriche K, Igoudjil A, Pessayre D, Fromenty B. Mitochondrial dysfunction in NASH: causes, consequences and possible means to prevent it. Mitochondrion 2006;6:1–28. doi:10.1016/j.mito.2005.10.004.

[102] Angulo P, Machado MV, Diehl AM. Fibrosis in nonalcoholic Fatty liver disease: mechanisms and clinical implications. Semin Liver Dis 2015;35:132–45. doi:10.1055/s-0035-1550065.

[103] Machado MV, Diehl AM. Liver renewal: detecting misrepair and optimizing regeneration. Mayo Clin Proc 2014;89:120–30. doi:10.1016/j.mayocp.2013.10.009.

[104] Marra F, Svegliati-Baroni G. Lipotoxicity and the gut-liver axis in NASH pathogenesis. J Hepatol 2018;68:280–95. doi:10.1016/j.jhep.2017.11.014.

[105] Ralston JC, Lyons CL, Kennedy EB, Kirwan AM, Roche HM. Fatty Acids and NLRP3 Inflammasome-Mediated Inflammation in Metabolic Tissues. Annu Rev Nutr 2017;37:77–102. doi:10.1146/annurev-nutr-071816-064836.

[106] Csak T, Ganz M, Pespisa J, Kodys K, Dolganiuc A, Szabo G. Fatty acid and endotoxin activate inflammasomes in mouse hepatocytes that release danger signals to stimulate immune cells. Hepatology 2011;54:133–44. doi:10.1002/hep.24341.

[107] Guy CD, Suzuki A, Zdanowicz M, Abdelmalek MF, Burchette J, Unalp A, et al. Hedgehog pathway activation parallels histologic severity of injury and fibrosis in human nonalcoholic fatty liver disease. Hepatology 2012;55:1711–21. doi:10.1002/hep.25559.

[108] Choi SS, Omenetti A, Syn W-K, Diehl AM. The role of Hedgehog signaling in fibrogenic liver repair. Int J Biochem Cell Biol 2011;43:238–44. doi:10.1016/j.biocel.2010.10.015.

[109] Witek RP, Yang L, Liu R, Jung Y, Omenetti A, Syn W-K, et al. Liver cell-derived microparticles activate hedgehog signaling and alter gene expression in hepatic endothelial cells. Gastroenterology 2009;136:320-330.e2. doi:10.1053/j.gastro.2008.09.066.

[110] Povero D, Eguchi A, Li H, Johnson CD, Papouchado BG, Wree A, et al. Circulating extracellular vesicles with specific proteome and liver microRNAs are potential biomarkers for liver injury in experimental fatty liver disease. PLoS ONE 2014;9:e113651. doi:10.1371/journal.pone.0113651.

[111] Nojima H, Freeman CM, Schuster RM, Japtok L, Kleuser B, Edwards MJ, et al. Hepatocyte exosomes mediate liver repair and regeneration via sphingosine-1-phosphate. J Hepatol 2016;64:60–8. doi:10.1016/j.jhep.2015.07.030.

[112] Wang R, Ding Q, Yaqoob U, de Assuncao TM, Verma VK, Hirsova P, et al. Exosome Adherence and Internalization by Hepatic Stellate Cells Triggers Sphingosine 1-Phosphate-dependent Migration. J Biol Chem 2015;290:30684–96. doi:10.1074/jbc.M115.671735.

[113] Syn W-K, Agboola KM, Swiderska M, Michelotti GA, Liaskou E, Pang H, et al. NKT-associated hedgehog and osteopontin drive fibrogenesis in non-alcoholic fatty liver disease. Gut 2012;61:1323–9. doi:10.1136/gutjnl-2011-301857.

[114] Xie G, Choi SS, Syn W-K, Michelotti GA, Swiderska M, Karaca G, et al. Hedgehog signalling regulates liver sinusoidal endothelial cell capillarisation. Gut 2013;62:299–309. doi:10.1136/gutjnl-2011-301494.

[115] Matz-Soja M, Gebhardt R. The many faces of Hedgehog signalling in the liver: recent progress reveals striking cellular diversity and the importance of microenvironments. J Hepatol 2014;61:1449–50. doi:10.1016/j.jhep.2014.06.041.

[116] Omenetti A, Choi S, Michelotti G, Diehl AM. Hedgehog signaling in the liver. J Hepatol 2011;54:366–73. doi:10.1016/j.jhep.2010.10.003.

[117] Betrapally NS, Gillevet PM, Bajaj JS. Changes in the Intestinal Microbiome and Alcoholic and Nonalcoholic Liver Diseases: Causes or Effects? Gastroenterology 2016;150:1745-1755.e3. doi:10.1053/j.gastro.2016.02.073.

[118] Jandhyala SM, Talukdar R, Subramanyam C, Vuyyuru H, Sasikala M, Nageshwar Reddy D. Role of the normal gut microbiota. World J Gastroenterol 2015;21:8787–803. doi:10.3748/wjg.v21.i29.8787.

[119] Loomba R, Seguritan V, Li W, Long T, Klitgord N, Bhatt A, et al. Gut Microbiome-Based Metagenomic Signature for Non-invasive Detection of Advanced Fibrosis in Human Nonalcoholic Fatty Liver Disease. Cell Metab 2017;25:1054-1062.e5. doi:10.1016/j.cmet.2017.04.001.

[120] Frasinariu OE, Ceccarelli S, Alisi A, Moraru E, Nobili V. Gut-liver axis and fibrosis in nonalcoholic fatty liver disease: an input for novel therapies. Dig Liver Dis 2013;45:543–51. doi:10.1016/j.dld.2012.11.010.

[121] Rahman K, Desai C, Iyer SS, Thorn NE, Kumar P, Liu Y, et al. Loss of Junctional Adhesion Molecule A Promotes Severe Steatohepatitis in Mice on a Diet High in Saturated Fat, Fructose, and Cholesterol. Gastroenterology 2016;151:733-746.e12. doi:10.1053/j.gastro.2016.06.022.

[122] Pendyala S, Walker JM, Holt PR. A high-fat diet is associated with endotoxemia that originates from the gut. Gastroenterology 2012;142:1100-1101.e2. doi:10.1053/j.gastro.2012.01.034.

[123] Peterson LW, Artis D. Intestinal epithelial cells: regulators of barrier function and immune homeostasis. Nat Rev Immunol 2014;14:141–53. doi:10.1038/nri3608.

[124] Szabo G, Iracheta-Vellve A. Inflammasome activation in the liver: Focus on alcoholic

and non-alcoholic steatohepatitis. Clin Res Hepatol Gastroenterol 2015;39 Suppl 1:S18-23. doi:10.1016/j.clinre.2015.06.012.

[125] Zhu L, Baker SS, Gill C, Liu W, Alkhouri R, Baker RD, et al. Characterization of gut microbiomes in nonalcoholic steatohepatitis (NASH) patients: a connection between endogenous alcohol and NASH. Hepatology 2013;57:601–9. doi:10.1002/hep.26093.

[126] Mallat A, Lotersztajn S. Cellular mechanisms of tissue fibrosis. 5. Novel insights into liver fibrosis. Am J Physiol, Cell Physiol 2013;305:C789-799. doi:10.1152/ajpcell.00230.2013.

[127] Tsuchida T, Friedman SL. Mechanisms of hepatic stellate cell activation. Nat Rev Gastroenterol Hepatol 2017;14:397–411. doi:10.1038/nrgastro.2017.38.

[128] Hellerbrand C, Stefanovic B, Giordano F, Burchardt ER, Brenner DA. The role of TGFbeta1 in initiating hepatic stellate cell activation in vivo. J Hepatol 1999;30:77–87.

[129] Breitkopf K, Godoy P, Ciuclan L, Singer MV, Dooley S. TGF-beta/Smad signaling in the injured liver. Z Gastroenterol 2006;44:57–66. doi:10.1055/s-2005-858989.

[130] Huang G, Brigstock DR. Regulation of hepatic stellate cells by connective tissue growth factor. Front Biosci (Landmark Ed) 2012;17:2495–507.

[131] Henderson NC, Arnold TD, Katamura Y, Giacomini MM, Rodriguez JD, McCarty JH, et al. Targeting of αv integrin identifies a core molecular pathway that regulates fibrosis in several organs. Nat Med 2013;19:1617–24. doi:10.1038/nm.3282.

[132] Olaso E, Ikeda K, Eng FJ, Xu L, Wang LH, Lin HC, et al. DDR2 receptor promotes MMP-2-mediated proliferation and invasion by hepatic stellate cells. J Clin Invest 2001;108:1369–78. doi:10.1172/JCI12373.

[133] Martin K, Pritchett J, Llewellyn J, Mullan AF, Athwal VS, Dobie R, et al. PAK proteins and YAP-1 signalling downstream of integrin beta-1 in myofibroblasts promote liver fibrosis. Nat Commun 2016;7:12502. doi:10.1038/ncomms12502.

[134] Thoma C, Day CP, Trenell MI. Lifestyle interventions for the treatment of non-alcoholic fatty liver disease in adults: a systematic review. J Hepatol 2012;56:255–66. doi:10.1016/j.jhep.2011.06.010.

[135] Zelber-Sagi S, Ratziu V, Oren R. Nutrition and physical activity in NAFLD: an overview of the epidemiological evidence. World J Gastroenterol 2011;17:3377–89. doi:10.3748/wjg.v17.i29.3377.

[136] Wong VW-S, Chan RS-M, Wong GL-H, Cheung BH-K, Chu WC-W, Yeung DK-W, et al. Community-based lifestyle modification programme for non-alcoholic fatty liver disease: a randomized controlled trial. J Hepatol 2013;59:536–42. doi:10.1016/j.jhep.2013.04.013.

[137] Ricci G, Bersani G, Rossi A, Pigò F, De Fabritiis G, Alvisi V. Bariatric therapy with intragastric balloon improves liver dysfunction and insulin resistance in obese patients. Obes Surg 2008;18:1438–42. doi:10.1007/s11695-008-9487-x.

[138] Lassailly G, Caiazzo R, Buob D, Pigeyre M, Verkindt H, Labreuche J, et al. Bariatric Surgery Reduces Features of Nonalcoholic Steatohepatitis in Morbidly Obese Patients. Gastroenterology 2015;149:379–88; quiz e15-16. doi:10.1053/j.gastro.2015.04.014.

[139] Sjöström L, Narbro K, Sjöström CD, Karason K, Larsson B, Wedel H, et al. Effects of bariatric surgery on mortality in Swedish obese subjects. N Engl J Med 2007;357:741–52. doi:10.1056/NEJMoa066254.

[140] Hafeez S, Ahmed MH. Bariatric surgery as potential treatment for nonalcoholic fatty liver disease: a future treatment by choice or by chance? J Obes 2013;2013:839275. doi:10.1155/2013/839275.

[141] Mathurin P, Hollebecque A, Arnalsteen L, Buob D, Leteurtre E, Caiazzo R, et al. Prospective study of the long-term effects of bariatric surgery on liver injury in patients without advanced disease. Gastroenterology 2009;137:532–40.

doi:10.1053/j.gastro.2009.04.052.
[142] Caiazzo R, Lassailly G, Leteurtre E, Baud G, Verkindt H, Raverdy V, et al. Roux-en-Y gastric bypass versus adjustable gastric banding to reduce nonalcoholic fatty liver disease: a 5-year controlled longitudinal study. Ann Surg 2014;260:893–8; discussion 898-899. doi:10.1097/SLA.0000000000000945.
[143] Haukeland JW, Konopski Z, Eggesbø HB, von Volkmann HL, Raschpichler G, Bjøro K, et al. Metformin in patients with non-alcoholic fatty liver disease: a randomized, controlled trial. Scand J Gastroenterol 2009;44:853–60. doi:10.1080/00365520902845268.
[144] Ratziu V, Caldwell S, Neuschwander-Tetri BA. Therapeutic trials in nonalcoholic steatohepatitis: insulin sensitizers and related methodological issues. Hepatology 2010;52:2206–15. doi:10.1002/hep.24042.
[145] Sanyal AJ, Chalasani N, Kowdley KV, McCullough A, Diehl AM, Bass NM, et al. Pioglitazone, vitamin E, or placebo for nonalcoholic steatohepatitis. N Engl J Med 2010;362:1675–85. doi:10.1056/NEJMoa0907929.
[146] Aithal GP, Thomas JA, Kaye PV, Lawson A, Ryder SD, Spendlove I, et al. Randomized, placebo-controlled trial of pioglitazone in nondiabetic subjects with nonalcoholic steatohepatitis. Gastroenterology 2008;135:1176–84. doi:10.1053/j.gastro.2008.06.047.
[147] Armstrong MJ, Gaunt P, Aithal GP, Parker R, Barton D, Hull D, et al. G01 : Liraglutide is effective in the histological clearance of non-alcoholic steatohepatitis in a multicentre, doubleblinded, randomised, placebo-controlled phase II trial. Journal of Hepatology 2015;62:S187. doi:10.1016/S0168-8278(15)30002-7.
[148] Svegliati-Baroni G, Saccomanno S, Rychlicki C, Agostinelli L, De Minicis S, Candelaresi C, et al. Glucagon-like peptide-1 receptor activation stimulates hepatic lipid oxidation and restores hepatic signalling alteration induced by a high-fat diet in nonalcoholic steatohepatitis. Liver Int 2011;31:1285–97. doi:10.1111/j.1478-3231.2011.02462.x.
[149] Iwasaki T, Yoneda M, Inamori M, Shirakawa J, Higurashi T, Maeda S, et al. Sitagliptin as a novel treatment agent for non-alcoholic Fatty liver disease patients with type 2 diabetes mellitus. Hepatogastroenterology 2011;58:2103–5. doi:10.5754/hge11263.
[150] Olaywi M, Bhatia T, Anand S, Singhal S. Novel anti-diabetic agents in non-alcoholic fatty liver disease: a mini-review. HBPD INT 2013;12:584–8.
[151] Ma Y-Y, Li L, Yu C-H, Shen Z, Chen L-H, Li Y-M. Effects of probiotics on nonalcoholic fatty liver disease: a meta-analysis. World J Gastroenterol 2013;19:6911–8. doi:10.3748/wjg.v19.i40.6911.
[152] Loscalzo J. Gut microbiota, the genome, and diet in atherogenesis. N Engl J Med 2013;368:1647–9. doi:10.1056/NEJMe1302154.
[153] Ferolla SM, Armiliato GNA, Couto CA, Ferrari TCA. The role of intestinal bacteria overgrowth in obesity-related nonalcoholic fatty liver disease. Nutrients 2014;6:5583–99. doi:10.3390/nu6125583.
[154] Adorini L, Pruzanski M, Shapiro D. Farnesoid X receptor targeting to treat nonalcoholic steatohepatitis. Drug Discov Today 2012;17:988–97. doi:10.1016/j.drudis.2012.05.012.
[155] Neuschwander-Tetri BA, Loomba R, Sanyal AJ, Lavine JE, Van Natta ML, Abdelmalek MF, et al. Farnesoid X nuclear receptor ligand obeticholic acid for non-cirrhotic, non-alcoholic steatohepatitis (FLINT): a multicentre, randomised, placebo-controlled trial. Lancet 2015;385:956–65. doi:10.1016/S0140-6736(14)61933-4.
[156] Federico A, Zulli C, de Sio I, Del Prete A, Dallio M, Masarone M, et al. Focus on emerging drugs for the treatment of patients with non-alcoholic fatty liver disease. World J Gastroenterol 2014;20:16841–57. doi:10.3748/wjg.v20.i45.16841.
[157] Bojic LA, Huff MW. Peroxisome proliferator-activated receptor δ: a multifaceted

metabolic player. Curr Opin Lipidol 2013;24:171–7. doi:10.1097/MOL.0b013e32835cc949.
[158] Staels B, Rubenstrunk A, Noel B, Rigou G, Delataille P, Millatt LJ, et al. Hepatoprotective effects of the dual peroxisome proliferator-activated receptor alpha/delta agonist, GFT505, in rodent models of nonalcoholic fatty liver disease/nonalcoholic steatohepatitis. Hepatology 2013;58:1941–52. doi:10.1002/hep.26461.
[159] Ratziu V, Harrison SA, Francque S, Bedossa P, Lehert P, Serfaty L, et al. Elafibranor, an Agonist of the Peroxisome Proliferator-Activated Receptor-α and -δ, Induces Resolution of Nonalcoholic Steatohepatitis Without Fibrosis Worsening. Gastroenterology 2016;150:1147-1159.e5. doi:10.1053/j.gastro.2016.01.038.
[160] Friedman SL, Ratziu V, Harrison SA, Abdelmalek MF, Aithal GP, Caballeria J, et al. A randomized, placebo-controlled trial of cenicriviroc for treatment of nonalcoholic steatohepatitis with fibrosis. Hepatology 2018;67:1754–67. doi:10.1002/hep.29477.
[161] Zapotoczny B, Szafranska K, Kus E, Braet F, Wisse E, Chlopicki S, et al. Tracking Fenestrae Dynamics in Live Murine Liver Sinusoidal Endothelial Cells. Hepatology 2018. doi:10.1002/hep.30232.
[162] Poisson J, Lemoinne S, Boulanger C, Durand F, Moreau R, Valla D, et al. Liver sinusoidal endothelial cells: Physiology and role in liver diseases. J Hepatol 2017;66:212–27. doi:10.1016/j.jhep.2016.07.009.
[163] DeLeve LD. Liver sinusoidal endothelial cells in hepatic fibrosis. Hepatology 2015;61:1740–6. doi:10.1002/hep.27376.
[164] Maslak E, Gregorius A, Chlopicki S. Liver sinusoidal endothelial cells (LSECs) function and NAFLD; NO-based therapy targeted to the liver. Pharmacol Rep 2015;67:689–94. doi:10.1016/j.pharep.2015.04.010.
[165] Seternes T, Sørensen K, Smedsrød B. Scavenger endothelial cells of vertebrates: a nonperipheral leukocyte system for high-capacity elimination of waste macromolecules. Proc Natl Acad Sci USA 2002;99:7594–7. doi:10.1073/pnas.102173299.
[166] Le Couteur DG, Cogger VC, Markus AM, Harvey PJ, Yin ZL, Ansselin AD, et al. Pseudocapillarization and associated energy limitation in the aged rat liver. Hepatology 2001;33:537–43. doi:10.1053/jhep.2001.22754.
[167] Le Couteur DG, Warren A, Cogger VC, Smedsrød B, Sørensen KK, De Cabo R, et al. Old age and the hepatic sinusoid. Anat Rec (Hoboken) 2008;291:672–83. doi:10.1002/ar.20661.
[168] Xie G, Wang X, Wang L, Wang L, Atkinson RD, Kanel GC, et al. Role of differentiation of liver sinusoidal endothelial cells in progression and regression of hepatic fibrosis in rats. Gastroenterology 2012;142:918-927.e6. doi:10.1053/j.gastro.2011.12.017.
[169] Chiu J-J, Chien S. Effects of disturbed flow on vascular endothelium: pathophysiological basis and clinical perspectives. Physiol Rev 2011;91:327–87. doi:10.1152/physrev.00047.2009.
[170] Hilmer SN, Cogger VC, Fraser R, McLean AJ, Sullivan D, Le Couteur DG. Age-related changes in the hepatic sinusoidal endothelium impede lipoprotein transfer in the rat. Hepatology 2005;42:1349–54. doi:10.1002/hep.20937.
[171] Cogger VC, Hilmer SN, Sullivan D, Muller M, Fraser R, Le Couteur DG. Hyperlipidemia and surfactants: the liver sieve is a link. Atherosclerosis 2006;189:273–81. doi:10.1016/j.atherosclerosis.2005.12.025.
[172] Carpenter B, Lin Y, Stoll S, Raffai RL, McCuskey R, Wang R. VEGF is crucial for the hepatic vascular development required for lipoprotein uptake. Development 2005;132:3293–303. doi:10.1242/dev.01902.
[173] Fraser R, Bosanquet AG, Day WA. Filtration of chylomicrons by the liver may influence cholesterol metabolism and atherosclerosis. Atherosclerosis 1978;29:113–23.
[174] Hagberg CE, Falkevall A, Wang X, Larsson E, Huusko J, Nilsson I, et al. Vascular

endothelial growth factor B controls endothelial fatty acid uptake. Nature 2010;464:917–21. doi:10.1038/nature08945.

[175] May D, Djonov V, Zamir G, Bala M, Safadi R, Sklair-Levy M, et al. A transgenic model for conditional induction and rescue of portal hypertension reveals a role of VEGF-mediated regulation of sinusoidal fenestrations. PLoS ONE 2011;6:e21478. doi:10.1371/journal.pone.0021478.

[176] Van Berkel TJ, De Rijke YB, Kruijt JK. Different fate in vivo of oxidatively modified low density lipoprotein and acetylated low density lipoprotein in rats. Recognition by various scavenger receptors on Kupffer and endothelial liver cells. J Biol Chem 1991;266:2282–9.

[177] Blomhoff R, Drevon CA, Eskild W, Helgerud P, Norum KR, Berg T. Clearance of acetyl low density lipoprotein by rat liver endothelial cells. Implications for hepatic cholesterol metabolism. J Biol Chem 1984;259:8898–903.

[178] Qiuxian Peng, Zhang Q, Xiao W, Shao M, Fan Q, Zhang H, et al. Protective effects of Sapindus mukorossi Gaertn against fatty liver disease induced by high fat diet in rats. Biochem Biophys Res Commun 2014;450:685–91. doi:10.1016/j.bbrc.2014.06.035.

[179] Miyao M, Kotani H, Ishida T, Kawai C, Manabe S, Abiru H, et al. Pivotal role of liver sinusoidal endothelial cells in NAFLD/NASH progression. Lab Invest 2015;95:1130–44. doi:10.1038/labinvest.2015.95.

[180] Cogger VC, Mohamad M, Solon-Biet SM, Senior AM, Warren A, O’Reilly JN, et al. Dietary macronutrients and the aging liver sinusoidal endothelial cell. Am J Physiol Heart Circ Physiol 2016;310:H1064-1070. doi:10.1152/ajpheart.00949.2015.

[181] Zhang Q, Liu J, Liu J, Huang W, Tian L, Quan J, et al. oxLDL induces injury and defenestration of human liver sinusoidal endothelial cells via LOX1. J Mol Endocrinol 2014;53:281–93. doi:10.1530/JME-14-0049.

[182] Hang T-C, Lauffenburger DA, Griffith LG, Stolz DB. Lipids promote survival, proliferation, and maintenance of differentiation of rat liver sinusoidal endothelial cells in vitro. Am J Physiol Gastrointest Liver Physiol 2012;302:G375-388. doi:10.1152/ajpgi.00288.2011.

[183] Feng R, Luo C, Li C, Du S, Okekunle AP, Li Y, et al. Free fatty acids profile among lean, overweight and obese non-alcoholic fatty liver disease patients: a case - control study. Lipids Health Dis 2017;16:165. doi:10.1186/s12944-017-0551-1.

[184] Dobbs BR, Rogers GW, Xing HY, Fraser R. Endotoxin-induced defenestration of the hepatic sinusoidal endothelium: a factor in the pathogenesis of cirrhosis? Liver 1994;14:230–3.

[185] Herrnberger L, Hennig R, Kremer W, Hellerbrand C, Goepferich A, Kalbitzer HR, et al. Formation of fenestrae in murine liver sinusoids depends on plasmalemma vesicle-associated protein and is required for lipoprotein passage. PLoS ONE 2014;9:e115005. doi:10.1371/journal.pone.0115005.

[186] Chung C, Iwakiri Y. The lymphatic vascular system in liver diseases: its role in ascites formation. Clin Mol Hepatol 2013;19:99–104. doi:10.3350/cmh.2013.19.2.99.

[187] Fraser R, Cogger VC, Dobbs B, Jamieson H, Warren A, Hilmer SN, et al. The liver sieve and atherosclerosis. Pathology 2012;44:181–6. doi:10.1097/PAT.0b013e328351bcc8.

[188] Francque S, Verrijken A, Mertens I, Hubens G, Van Marck E, Pelckmans P, et al. Noncirrhotic human nonalcoholic fatty liver disease induces portal hypertension in relation to the histological degree of steatosis. Eur J Gastroenterol Hepatol 2010;22:1449–57. doi:10.1097/MEG.0b013e32833f14a1.

[189] Francque S, Laleman W, Verbeke L, Van Steenkiste C, Casteleyn C, Kwanten W, et al. Increased intrahepatic resistance in severe steatosis: endothelial dysfunction, vasoconstrictor overproduction and altered microvascular architecture. Lab Invest 2012;92:1428–39. doi:10.1038/labinvest.2012.103.

[190] Seifalian AM, Chidambaram V, Rolles K, Davidson BR. In vivo demonstration of impaired microcirculation in steatotic human liver grafts. Liver Transpl Surg 1998;4:71–7.
[191] Seifalian AM, Piasecki C, Agarwal A, Davidson BR. The effect of graded steatosis on flow in the hepatic parenchymal microcirculation. Transplantation 1999;68:780–4.
[192] Ijaz S, Yang W, Winslet MC, Seifalian AM. The role of nitric oxide in the modulation of hepatic microcirculation and tissue oxygenation in an experimental model of hepatic steatosis. Microvasc Res 2005;70:129–36. doi:10.1016/j.mvr.2005.08.001.
[193] Farrell GC, Teoh NC, McCuskey RS. Hepatic microcirculation in fatty liver disease. Anat Rec (Hoboken) 2008;291:684–92. doi:10.1002/ar.20715.
[194] Caldwell S, Lackner C. Perspectives on NASH Histology: Cellular Ballooning. Ann Hepatol 2017;16:182–4. doi:10.5604/16652681.1231550.
[195] Ijaz S, Yang W, Winslet MC, Seifalian AM. Impairment of hepatic microcirculation in fatty liver. Microcirculation 2003;10:447–56. doi:10.1038/sj.mn.7800206.
[196] Flammer AJ, Anderson T, Celermajer DS, Creager MA, Deanfield J, Ganz P, et al. The assessment of endothelial function: from research into clinical practice. Circulation 2012;126:753–67. doi:10.1161/CIRCULATIONAHA.112.093245.
[197] Pasarín M, La Mura V, Gracia-Sancho J, García-Calderó H, Rodríguez-Vilarrupla A, García-Pagán JC, et al. Sinusoidal endothelial dysfunction precedes inflammation and fibrosis in a model of NAFLD. PLoS ONE 2012;7:e32785. doi:10.1371/journal.pone.0032785.
[198] Gonzalez-Paredes FJ, Hernández Mesa G, Morales Arraez D, Marcelino Reyes R, Abrante B, Diaz-Flores F, et al. Contribution of Cyclooxygenase End Products and Oxidative Stress to Intrahepatic Endothelial Dysfunction in Early Non-Alcoholic Fatty Liver Disease. PLoS ONE 2016;11:e0156650. doi:10.1371/journal.pone.0156650.
[199] Tateya S, Rizzo NO, Handa P, Cheng AM, Morgan-Stevenson V, Daum G, et al. Endothelial NO/cGMP/VASP signaling attenuates Kupffer cell activation and hepatic insulin resistance induced by high-fat feeding. Diabetes 2011;60:2792–801. doi:10.2337/db11-0255.
[200] Matsumoto M, Zhang J, Zhang X, Liu J, Jiang JX, Yamaguchi K, et al. The NOX1 isoform of NADPH oxidase is involved in dysfunction of liver sinusoids in nonalcoholic fatty liver disease. Free Radic Biol Med 2018;115:412–20. doi:10.1016/j.freeradbiomed.2017.12.019.
[201] Montagnani M, Chen H, Barr VA, Quon MJ. Insulin-stimulated activation of eNOS is independent of Ca2+ but requires phosphorylation by Akt at Ser(1179). J Biol Chem 2001;276:30392–8. doi:10.1074/jbc.M103702200.
[202] Pasarín M, Abraldes JG, Rodríguez-Vilarrupla A, La Mura V, García-Pagán JC, Bosch J. Insulin resistance and liver microcirculation in a rat model of early NAFLD. J Hepatol 2011;55:1095–102. doi:10.1016/j.jhep.2011.01.053.
[203] Pasarín M, Abraldes JG, Liguori E, Kok B, La Mura V. Intrahepatic vascular changes in non-alcoholic fatty liver disease: Potential role of insulin-resistance and endothelial dysfunction. World J Gastroenterol 2017;23:6777–87. doi:10.3748/wjg.v23.i37.6777.
[204] Gunnett CA, Lund DD, Chu Y, Brooks RM, Faraci FM, Heistad DD. NO-dependent vasorelaxation is impaired after gene transfer of inducible NO-synthase. Arterioscler Thromb Vasc Biol 2001;21:1281–7.
[205] Chauhan SD, Seggara G, Vo PA, Macallister RJ, Hobbs AJ, Ahluwalia A. Protection against lipopolysaccharide-induced endothelial dysfunction in resistance and conduit vasculature of iNOS knockout mice. FASEB J 2003;17:773–5. doi:10.1096/fj.02-0668fje.
[206] Saavedra JE, Billiar TR, Williams DL, Kim YM, Watkins SC, Keefer LK. Targeting nitric oxide (NO) delivery in vivo. Design of a liver-selective NO donor prodrug that blocks tumor necrosis factor-alpha-induced apoptosis and toxicity in the liver. J Med Chem 1997;40:1947–54. doi:10.1021/jm9701031.
[207] Kus E, Jasiński K, Skórka T, Czyzynska-Cichon I, Chlopicki S. Short-term treatment

with hepatoselective NO donor V-PYRRO/NO improves blood flow in hepatic microcirculation in liver steatosis in mice. Pharmacol Rep 2018;70:463–9. doi:10.1016/j.pharep.2017.11.019.

[208] Schild L, Dombrowski F, Lendeckel U, Schulz C, Gardemann A, Keilhoff G. Impairment of endothelial nitric oxide synthase causes abnormal fat and glycogen deposition in liver. Biochim Biophys Acta 2008;1782:180–7. doi:10.1016/j.bbadis.2007.12.007.

[209] Schild L, Jaroscakova I, Lendeckel U, Wolf G, Keilhoff G. Neuronal nitric oxide synthase controls enzyme activity pattern of mitochondria and lipid metabolism. FASEB J 2006;20:145–7. doi:10.1096/fj.05-3898fje.

[210] Roediger WE, Hems R, Wiggins D, Gibbons GF. Inhibition of hepatocyte lipogenesis by nitric oxide donor: could nitric oxide regulate lipid synthesis? IUBMB Life 2004;56:35–40. doi:10.1080/15216540310001649822.

[211] Winder WW, Hardie DG. Inactivation of acetyl-CoA carboxylase and activation of AMP-activated protein kinase in muscle during exercise. Am J Physiol 1996;270:E299-304. doi:10.1152/ajpendo.1996.270.2.E299.

[212] Fu WJ, Haynes TE, Kohli R, Hu J, Shi W, Spencer TE, et al. Dietary L-arginine supplementation reduces fat mass in Zucker diabetic fatty rats. J Nutr 2005;135:714–21. doi:10.1093/jn/135.4.714.

[213] Zou M-H, Hou X-Y, Shi C-M, Kirkpatick S, Liu F, Goldman MH, et al. Activation of 5'-AMP-activated kinase is mediated through c-Src and phosphoinositide 3-kinase activity during hypoxia-reoxygenation of bovine aortic endothelial cells. Role of peroxynitrite. J Biol Chem 2003;278:34003–10. doi:10.1074/jbc.M300215200.

[214] Park H, Kaushik VK, Constant S, Prentki M, Przybytkowski E, Ruderman NB, et al. Coordinate regulation of malonyl-CoA decarboxylase, sn-glycerol-3-phosphate acyltransferase, and acetyl-CoA carboxylase by AMP-activated protein kinase in rat tissues in response to exercise. J Biol Chem 2002;277:32571–7. doi:10.1074/jbc.M201692200.

[215] Muoio DM, Seefeld K, Witters LA, Coleman RA. AMP-activated kinase reciprocally regulates triacylglycerol synthesis and fatty acid oxidation in liver and muscle: evidence that sn-glycerol-3-phosphate acyltransferase is a novel target. Biochem J 1999;338 (Pt 3):783–91.

[216] Maslak E, Zabielski P, Kochan K, Kus K, Jasztal A, Sitek B, et al. The liver-selective NO donor, V-PYRRO/NO, protects against liver steatosis and improves postprandial glucose tolerance in mice fed high fat diet. Biochem Pharmacol 2015;93:389–400. doi:10.1016/j.bcp.2014.12.004.

[217] Kus K, Walczak M, Maslak E, Zakrzewska A, Gonciarz-Dytman A, Zabielski P, et al. Hepatoselective Nitric Oxide (NO) Donors, V-PYRRO/NO and V-PROLI/NO, in Nonalcoholic Fatty Liver Disease: A Comparison of Antisteatotic Effects with the Biotransformation and Pharmacokinetics. Drug Metab Dispos 2015;43:1028–36. doi:10.1124/dmd.115.063388.

[218] Wang W, Zhao C, Zhou J, Zhen Z, Wang Y, Shen C. Simvastatin ameliorates liver fibrosis via mediating nitric oxide synthase in rats with non-alcoholic steatohepatitis-related liver fibrosis. PLoS ONE 2013;8:e76538. doi:10.1371/journal.pone.0076538.

[219] Coulon S, Heindryckx F, Geerts A, Van Steenkiste C, Colle I, Van Vlierberghe H. Angiogenesis in chronic liver disease and its complications. Liver Int 2011;31:146–62. doi:10.1111/j.1478-3231.2010.02369.x.

[220] Coulon S, Francque S, Colle I, Verrijken A, Blomme B, Heindryckx F, et al. Evaluation of inflammatory and angiogenic factors in patients with non-alcoholic fatty liver disease. Cytokine 2012;59:442–9. doi:10.1016/j.cyto.2012.05.001.

[221] Coulon S, Legry V, Heindryckx F, Van Steenkiste C, Casteleyn C, Olievier K, et al. Role of vascular endothelial growth factor in the pathophysiology of nonalcoholic steatohepatitis in two rodent models. Hepatology 2013;57:1793–805. doi:10.1002/hep.26219.

[222] Iwakiri Y, Shah V, Rockey DC. Vascular pathobiology in chronic liver disease and cirrhosis - current status and future directions. J Hepatol 2014;61:912–24. doi:10.1016/j.jhep.2014.05.047.
[223] Tarantino G, Conca P, Pasanisi F, Ariello M, Mastrolia M, Arena A, et al. Could inflammatory markers help diagnose nonalcoholic steatohepatitis? Eur J Gastroenterol Hepatol 2009;21:504–11. doi:10.1097/MEG.0b013e3283229b40.
[224] Kitade M, Yoshiji H, Kojima H, Ikenaka Y, Noguchi R, Kaji K, et al. Neovascularization and oxidative stress in the progression of non-alcoholic steatohepatitis. Mol Med Rep 2008;1:543–8.
[225] Kitade M, Yoshiji H, Noguchi R, Ikenaka Y, Kaji K, Shirai Y, et al. Crosstalk between angiogenesis, cytokeratin-18, and insulin resistance in the progression of non-alcoholic steatohepatitis. World J Gastroenterol 2009;15:5193–9.
[226] Lefere S, Van de Velde F, Hoorens A, Raevens S, Van Campenhout S, Vandierendonck A, et al. Angiopoietin-2 promotes pathological angiogenesis and is a novel therapeutic target in murine non-alcoholic fatty liver disease. Hepatology 2018. doi:10.1002/hep.30294.
[227] Peters KM, Wilson RB, Borradaile NM. Non-parenchymal hepatic cell lipotoxicity and the coordinated progression of non-alcoholic fatty liver disease and atherosclerosis. Curr Opin Lipidol 2018. doi:10.1097/MOL.0000000000000535.
[228] Seki S, Kitada T, Yamada T, Sakaguchi H, Nakatani K, Wakasa K. In situ detection of lipid peroxidation and oxidative DNA damage in non-alcoholic fatty liver diseases. J Hepatol 2002;37:56–62.
[229] Sutter AG, Palanisamy AP, Lench JH, Esckilsen S, Geng T, Lewin DNB, et al. Dietary Saturated Fat Promotes Development of Hepatic Inflammation Through Toll-Like Receptor 4 in Mice. J Cell Biochem 2016;117:1613–21. doi:10.1002/jcb.25453.
[230] Brun P, Castagliuolo I, Di Leo V, Buda A, Pinzani M, Palù G, et al. Increased intestinal permeability in obese mice: new evidence in the pathogenesis of nonalcoholic steatohepatitis. Am J Physiol Gastrointest Liver Physiol 2007;292:G518-525. doi:10.1152/ajpgi.00024.2006.
[231] Wu J, Meng Z, Jiang M, Zhang E, Trippler M, Broering R, et al. Toll-like receptor-induced innate immune responses in non-parenchymal liver cells are cell type-specific. Immunology 2010;129:363–74. doi:10.1111/j.1365-2567.2009.03179.x.
[232] Ip E, Farrell G, Hall P, Robertson G, Leclercq I. Administration of the potent PPARalpha agonist, Wy-14,643, reverses nutritional fibrosis and steatohepatitis in mice. Hepatology 2004;39:1286–96. doi:10.1002/hep.20170.
[233] Dela Peña A, Leclercq I, Field J, George J, Jones B, Farrell G. NF-kappaB activation, rather than TNF, mediates hepatic inflammation in a murine dietary model of steatohepatitis. Gastroenterology 2005;129:1663–74. doi:10.1053/j.gastro.2005.09.004.
[234] Weston CJ, Shepherd EL, Claridge LC, Rantakari P, Curbishley SM, Tomlinson JW, et al. Vascular adhesion protein-1 promotes liver inflammation and drives hepatic fibrosis. J Clin Invest 2015;125:501–20. doi:10.1172/JCI73722.
[235] Tomita K, Tamiya G, Ando S, Ohsumi K, Chiyo T, Mizutani A, et al. Tumour necrosis factor alpha signalling through activation of Kupffer cells plays an essential role in liver fibrosis of non-alcoholic steatohepatitis in mice. Gut 2006;55:415–24. doi:10.1136/gut.2005.071118.
[236] Feder LS, Todaro JA, Laskin DL. Characterization of interleukin-1 and interleukin-6 production by hepatic endothelial cells and macrophages. J Leukoc Biol 1993;53:126–32.
[237] Braunersreuther V, Viviani GL, Mach F, Montecucco F. Role of cytokines and chemokines in non-alcoholic fatty liver disease. World J Gastroenterol 2012;18:727–35. doi:10.3748/wjg.v18.i8.727.

[238] Marra F, Tacke F. Roles for chemokines in liver disease. Gastroenterology 2014;147:577-594.e1. doi:10.1053/j.gastro.2014.06.043.
[239] Roh Y-S, Seki E. Chemokines and Chemokine Receptors in the Development of NAFLD. Adv Exp Med Biol 2018;1061:45–53. doi:10.1007/978-981-10-8684-7_4.
[240] Shetty S, Lalor PF, Adams DH. Lymphocyte recruitment to the liver: molecular insights into the pathogenesis of liver injury and hepatitis. Toxicology 2008;254:136–46. doi:10.1016/j.tox.2008.08.003.
[241] Lalor PF, Shields P, Grant A, Adams DH. Recruitment of lymphocytes to the human liver. Immunol Cell Biol 2002;80:52–64. doi:10.1046/j.1440-1711.2002.01062.x.
[242] Lalor PF, Edwards S, McNab G, Salmi M, Jalkanen S, Adams DH. Vascular adhesion protein-1 mediates adhesion and transmigration of lymphocytes on human hepatic endothelial cells. J Immunol 2002;169:983–92.
[243] Edwards S, Lalor PF, Nash GB, Rainger GE, Adams DH. Lymphocyte traffic through sinusoidal endothelial cells is regulated by hepatocytes. Hepatology 2005;41:451–9. doi:10.1002/hep.20585.
[244] Tamaki Y, Nakade Y, Yamauchi T, Makino Y, Yokohama S, Okada M, et al. Angiotensin II type 1 receptor antagonist prevents hepatic carcinoma in rats with nonalcoholic steatohepatitis. J Gastroenterol 2013;48:491–503. doi:10.1007/s00535-012-0651-7.
[245] Yoshiji H, Kuriyama S, Noguchi R, Ikenaka Y, Kitade M, Kaji K, et al. Angiotensin-II and vascular endothelial growth factor interaction plays an important role in rat liver fibrosis development. Hepatol Res 2006;36:124–9. doi:10.1016/j.hepres.2006.07.003.
[246] Cayón A, Crespo J, Guerra AR, Pons-Romero F. [Gene expression in obese patients with non-alcoholic steatohepatitis]. Rev Esp Enferm Dig 2008;100:212–8.
[247] Kietzmann T, Görlach A. Reactive oxygen species in the control of hypoxia-inducible factor-mediated gene expression. Semin Cell Dev Biol 2005;16:474–86. doi:10.1016/j.semcdb.2005.03.010.
[248] Povero D, Eguchi A, Niesman IR, Andronikou N, de Mollerat du Jeu X, Mulya A, et al. Lipid-induced toxicity stimulates hepatocytes to release angiogenic microparticles that require Vanin-1 for uptake by endothelial cells. Sci Signal 2013;6:ra88. doi:10.1126/scisignal.2004512.
[249] Kim M, Allen B, Korhonen EA, Nitschké M, Yang HW, Baluk P, et al. Opposing actions of angiopoietin-2 on Tie2 signaling and FOXO1 activation. J Clin Invest 2016;126:3511–25. doi:10.1172/JCI84871.
[250] Tugues S, Fernandez-Varo G, Muñoz-Luque J, Ros J, Arroyo V, Rodés J, et al. Antiangiogenic treatment with sunitinib ameliorates inflammatory infiltrate, fibrosis, and portal pressure in cirrhotic rats. Hepatology 2007;46:1919–26. doi:10.1002/hep.21921.
[251] Mejias M, Garcia-Pras E, Tiani C, Miquel R, Bosch J, Fernandez M. Beneficial effects of sorafenib on splanchnic, intrahepatic, and portocollateral circulations in portal hypertensive and cirrhotic rats. Hepatology 2009;49:1245–56. doi:10.1002/hep.22758.
[252] Van Steenkiste C, Ribera J, Geerts A, Pauta M, Tugues S, Casteleyn C, et al. Inhibition of placental growth factor activity reduces the severity of fibrosis, inflammation, and portal hypertension in cirrhotic mice. Hepatology 2011;53:1629–40. doi:10.1002/hep.24238.
[253] Thabut D, Routray C, Lomberk G, Shergill U, Glaser K, Huebert R, et al. Complementary vascular and matrix regulatory pathways underlie the beneficial mechanism of action of sorafenib in liver fibrosis. Hepatology 2011;54:573–85. doi:10.1002/hep.24427.
[254] Öztürk Akcora B, Storm G, Prakash J, Bansal R. Tyrosine kinase inhibitor BIBF1120 ameliorates inflammation, angiogenesis and fibrosis in CCl4-induced liver fibrogenesis mouse model. Sci Rep 2017;7:44545. doi:10.1038/srep44545.
[255] Yang L, Kwon J, Popov Y, Gajdos GB, Ordog T, Brekken RA, et al. Vascular

endothelial growth factor promotes fibrosis resolution and repair in mice. Gastroenterology 2014;146:1339-1350.e1. doi:10.1053/j.gastro.2014.01.061.
[256] Li Y, Lui KO, Zhou B. Reassessing endothelial-to-mesenchymal transition in cardiovascular diseases. Nat Rev Cardiol 2018;15:445–56. doi:10.1038/s41569-018-0023-y.
[257] Piera-Velazquez S, Mendoza FA, Jimenez SA. Endothelial to Mesenchymal Transition (EndoMT) in the Pathogenesis of Human Fibrotic Diseases. J Clin Med 2016;5. doi:10.3390/jcm5040045.
[258] Singh KK, Lovren F, Pan Y, Quan A, Ramadan A, Matkar PN, et al. The essential autophagy gene ATG7 modulates organ fibrosis via regulation of endothelial-to-mesenchymal transition. J Biol Chem 2015;290:2547–59. doi:10.1074/jbc.M114.604603.
[259] Ribera J, Pauta M, Melgar-Lesmes P, Córdoba B, Bosch A, Calvo M, et al. A small population of liver endothelial cells undergoes endothelial-to-mesenchymal transition in response to chronic liver injury. Am J Physiol Gastrointest Liver Physiol 2017;313:G492–504. doi:10.1152/ajpgi.00428.2016.
[260] Schaffner F, Poper H. Capillarization of hepatic sinusoids in man. Gastroenterology 1963;44:239–42.
[261] Xu B, Broome U, Uzunel M, Nava S, Ge X, Kumagai-Braesch M, et al. Capillarization of hepatic sinusoid by liver endothelial cell-reactive autoantibodies in patients with cirrhosis and chronic hepatitis. Am J Pathol 2003;163:1275–89. doi:10.1016/S0002-9440(10)63487-6.
[262] Sørensen KK, Simon-Santamaria J, McCuskey RS, Smedsrød B. Liver Sinusoidal Endothelial Cells. Compr Physiol 2015;5:1751–74. doi:10.1002/cphy.c140078.
[263] DeLeve LD, Wang X, Kanel GC, Atkinson RD, McCuskey RS. Prevention of hepatic fibrosis in a murine model of metabolic syndrome with nonalcoholic steatohepatitis. Am J Pathol 2008;173:993–1001. doi:10.2353/ajpath.2008.070720.
[264] Xie G, Choi SS, Syn W-K, Michelotti GA, Swiderska M, Karaca G, et al. Hedgehog signalling regulates liver sinusoidal endothelial cell capillarisation. Gut 2013;62:299–309. doi:10.1136/gutjnl-2011-301494.
[265] Rangwala F, Guy CD, Lu J, Suzuki A, Burchette JL, Abdelmalek MF, et al. Increased production of sonic hedgehog by ballooned hepatocytes. J Pathol 2011;224:401–10. doi:10.1002/path.2888.
[266] Matz-Soja M, Gebhardt R. The many faces of Hedgehog signalling in the liver: recent progress reveals striking cellular diversity and the importance of microenvironments. J Hepatol 2014;61:1449–50. doi:10.1016/j.jhep.2014.06.041.
[267] Witek RP, Yang L, Liu R, Jung Y, Omenetti A, Syn W-K, et al. Liver cell-derived microparticles activate hedgehog signaling and alter gene expression in hepatic endothelial cells. Gastroenterology 2009;136:320-330.e2. doi:10.1053/j.gastro.2008.09.066.
[268] Smedsrød B, De Bleser PJ, Braet F, Lovisetti P, Vanderkerken K, Wisse E, et al. Cell biology of liver endothelial and Kupffer cells. Gut 1994;35:1509–16.
[269] Wang R, Ding Q, Yaqoob U, de Assuncao TM, Verma VK, Hirsova P, et al. Exosome Adherence and Internalization by Hepatic Stellate Cells Triggers Sphingosine 1-Phosphate-dependent Migration. J Biol Chem 2015;290:30684–96. doi:10.1074/jbc.M115.671735.
[270] Wells RG. Cellular sources of extracellular matrix in hepatic fibrosis. Clin Liver Dis 2008;12:759–68, viii. doi:10.1016/j.cld.2008.07.008.
[271] DeLeve LD, Wang X, Hu L, McCuskey MK, McCuskey RS. Rat liver sinusoidal endothelial cell phenotype is maintained by paracrine and autocrine regulation. Am J Physiol Gastrointest Liver Physiol 2004;287:G757-763. doi:10.1152/ajpgi.00017.2004.
[272] Deleve LD, Wang X, Guo Y. Sinusoidal endothelial cells prevent rat stellate cell activation and promote reversion to quiescence. Hepatology 2008;48:920–30. doi:10.1002/hep.22351.

[273] Marrone G, Russo L, Rosado E, Hide D, García-Cardeña G, García-Pagán JC, et al. The transcription factor KLF2 mediates hepatic endothelial protection and paracrine endothelial-stellate cell deactivation induced by statins. J Hepatol 2013;58:98–103. doi:10.1016/j.jhep.2012.08.026.
[274] Kitade M, Yoshiji H, Kojima H, Ikenaka Y, Noguchi R, Kaji K, et al. Leptin-mediated neovascularization is a prerequisite for progression of nonalcoholic steatohepatitis in rats. Hepatology 2006;44:983–91. doi:10.1002/hep.21338.
[275] Huang X-D, Fan Y, Zhang H, Wang P, Yuan J-P, Li M-J, et al. Serum leptin and soluble leptin receptor in non-alcoholic fatty liver disease. World J Gastroenterol 2008;14:2888–93.
[276] Marra F, Bertolani C. Adipokines in liver diseases. Hepatology 2009;50:957–69. doi:10.1002/hep.23046.
[277] Lemoinne S, Thabut D, Housset C, Moreau R, Valla D, Boulanger CM, et al. The emerging roles of microvesicles in liver diseases. Nat Rev Gastroenterol Hepatol 2014;11:350–61. doi:10.1038/nrgastro.2014.7.
[278] McCuskey RS, Ito Y, Robertson GR, McCuskey MK, Perry M, Farrell GC. Hepatic microvascular dysfunction during evolution of dietary steatohepatitis in mice. Hepatology 2004;40:386–93. doi:10.1002/hep.20302.
[279] Zhou L-Y, Zeng H, Wang S, Chen J-X. Regulatory Role of Endothelial PHD2 in the Hepatic Steatosis. Cell Physiol Biochem 2018;48:1003–11. doi:10.1159/000491968.
[280] Ozer A, Bruick RK. Regulation of HIF by prolyl hydroxylases: recruitment of the candidate tumor suppressor protein ING4. Cell Cycle 2005;4:1153–6. doi:10.4161/cc.4.9.2040.
[281] Kantari-Mimoun C, Castells M, Klose R, Meinecke A-K, Lemberger UJ, Rautou P-E, et al. Resolution of liver fibrosis requires myeloid cell-driven sinusoidal angiogenesis. Hepatology 2015;61:2042–55. doi:10.1002/hep.27635.
[282] Taura K, De Minicis S, Seki E, Hatano E, Iwaisako K, Osterreicher CH, et al. Hepatic stellate cells secrete angiopoietin 1 that induces angiogenesis in liver fibrosis. Gastroenterology 2008;135:1729–38. doi:10.1053/j.gastro.2008.07.065.
[283] Yoshiji H, Kuriyama S, Yoshii J, Ikenaka Y, Noguchi R, Hicklin DJ, et al. Vascular endothelial growth factor and receptor interaction is a prerequisite for murine hepatic fibrogenesis. Gut 2003;52:1347–54.
[284] Zhao S, Zhang Z, Yao Z, Shao J, Chen A, Zhang F, et al. Tetramethylpyrazine attenuates sinusoidal angiogenesis via inhibition of hedgehog signaling in liver fibrosis. IUBMB Life 2017;69:115–27. doi:10.1002/iub.1598.
[285] Hennenberg M, Trebicka J, Kohistani Z, Stark C, Nischalke H-D, Krämer B, et al. Hepatic and HSC-specific sorafenib effects in rats with established secondary biliary cirrhosis. Lab Invest 2011;91:241–51. doi:10.1038/labinvest.2010.148.
[286] Coch L, Mejias M, Berzigotti A, Garcia-Pras E, Gallego J, Bosch J, et al. Disruption of negative feedback loop between vasohibin-1 and vascular endothelial growth factor decreases portal pressure, angiogenesis, and fibrosis in cirrhotic rats. Hepatology 2014;60:633–47. doi:10.1002/hep.26995.
[287] Chatterjee S. Reversal of vasohibin-driven negative feedback loop of vascular endothelial growth factor/angiogenesis axis promises a novel antifibrotic therapeutic strategy for liver diseases. Hepatology 2014;60:458–60. doi:10.1002/hep.27061.
[288] Goh GB-B, McCullough AJ. Natural History of Nonalcoholic Fatty Liver Disease. Dig Dis Sci 2016;61:1226–33. doi:10.1007/s10620-016-4095-4.
[289] Santhekadur PK, Kumar DP, Sanyal AJ. Preclinical models of non-alcoholic fatty liver disease. J Hepatol 2018;68:230–7. doi:10.1016/j.jhep.2017.10.031.
[290] Farrell G, Schattenberg JM, Leclercq I, Yeh MM, Goldin R, Teoh N, et al. Mouse

models of nonalcoholic steatohepatitis Towards optimization of their relevance to human NASH. Hepatology 2018. doi:10.1002/hep.30333.
[291] Tsuchida T, Lee YA, Fujiwara N, Ybanez M, Allen B, Martins S, et al. A simple diet- and chemical-induced murine NASH model with rapid progression of steatohepatitis, fibrosis and liver cancer. J Hepatol 2018;69:385–95. doi:10.1016/j.jhep.2018.03.011.
[292] Van Herck MA, Vonghia L, Francque SM. Animal Models of Nonalcoholic Fatty Liver Disease-A Starter's Guide. Nutrients 2017;9. doi:10.3390/nu9101072.
[293] García-Pagán J-C, Gracia-Sancho J, Bosch J. Functional aspects on the pathophysiology of portal hypertension in cirrhosis. J Hepatol 2012;57:458–61. doi:10.1016/j.jhep.2012.03.007.
[294] Ni Y, Li J-M, Liu M-K, Zhang T-T, Wang D-P, Zhou W-H, et al. Pathological process of liver sinusoidal endothelial cells in liver diseases. World J Gastroenterol 2017;23:7666–77. doi:10.3748/wjg.v23.i43.7666.
[295] Bosch J, García-Pagán JC. Complications of cirrhosis. I. Portal hypertension. J Hepatol 2000;32:141–56.
[296] Mendes FD, Suzuki A, Sanderson SO, Lindor KD, Angulo P. Prevalence and indicators of portal hypertension in patients with nonalcoholic fatty liver disease. Clin Gastroenterol Hepatol 2012;10:1028-1033.e2. doi:10.1016/j.cgh.2012.05.008.
[297] Vonghia L, Magrone T, Verrijken A, Michielsen P, Van Gaal L, Jirillo E, et al. Peripheral and Hepatic Vein Cytokine Levels in Correlation with Non-Alcoholic Fatty Liver Disease (NAFLD)-Related Metabolic, Histological, and Haemodynamic Features. PLoS ONE 2015;10:e0143380. doi:10.1371/journal.pone.0143380.
[298] Baffy G. Origins of Portal Hypertension in Nonalcoholic Fatty Liver Disease. Dig Dis Sci 2018;63:563–76. doi:10.1007/s10620-017-4903-5.
[299] McConnell M, Iwakiri Y. Biology of portal hypertension. Hepatol Int 2018;12:11–23. doi:10.1007/s12072-017-9826-x.
[300] Abraldes JG, Albillos A, Bañares R, Turnes J, González R, García-Pagán JC, et al. Simvastatin lowers portal pressure in patients with cirrhosis and portal hypertension: a randomized controlled trial. Gastroenterology 2009;136:1651–8. doi:10.1053/j.gastro.2009.01.043.
[301] Zafra C, Abraldes JG, Turnes J, Berzigotti A, Fernández M, Garca-Pagán JC, et al. Simvastatin enhances hepatic nitric oxide production and decreases the hepatic vascular tone in patients with cirrhosis. Gastroenterology 2004;126:749–55.
[302] Abraldes JG, Villanueva C, Aracil C, Turnes J, Hernandez-Guerra M, Genesca J, et al. Addition of Simvastatin to Standard Therapy for the Prevention of Variceal Rebleeding Does Not Reduce Rebleeding but Increases Survival in Patients With Cirrhosis. Gastroenterology 2016;150:1160-1170.e3. doi:10.1053/j.gastro.2016.01.004.
[303] Verbeke L, Farre R, Trebicka J, Komuta M, Roskams T, Klein S, et al. Obeticholic acid, a farnesoid X receptor agonist, improves portal hypertension by two distinct pathways in cirrhotic rats. Hepatology 2014;59:2286–98. doi:10.1002/hep.26939.
[304] Schwabl P, Hambruch E, Seeland BA, Hayden H, Wagner M, Garnys L, et al. The FXR agonist PX20606 ameliorates portal hypertension by targeting vascular remodelling and sinusoidal dysfunction. J Hepatol 2017;66:724–33. doi:10.1016/j.jhep.2016.12.005.
[305] Li J, Kuruba R, Wilson A, Gao X, Zhang Y, Li S. Inhibition of endothelin-1-mediated contraction of hepatic stellate cells by FXR ligand. PLoS ONE 2010;5:e13955. doi:10.1371/journal.pone.0013955.
[306] García-Lezana T, Raurell I, Bravo M, Torres-Arauz M, Salcedo MT, Santiago A, et al. Restoration of a healthy intestinal microbiota normalizes portal hypertension in a rat model of nonalcoholic steatohepatitis. Hepatology 2018;67:1485–98. doi:10.1002/hep.29646.
[307] Rappaport AM, MacPhee PJ, Fisher MM, Phillips MJ. The scarring of the liver acini

(Cirrhosis). Tridimensional and microcirculatory considerations. Virchows Arch A Pathol Anat Histopathol 1983;402:107–37.

[308] Iwakiri Y. Endothelial dysfunction in the regulation of cirrhosis and portal hypertension. Liver Int 2012;32:199–213. doi:10.1111/j.1478-3231.2011.02579.x.

[309] Lemoinne S, Cadoret A, Rautou P-E, El Mourabit H, Ratziu V, Corpechot C, et al. Portal myofibroblasts promote vascular remodeling underlying cirrhosis formation through the release of microparticles. Hepatology 2015;61:1041–55. doi:10.1002/hep.27318.

[310] Thabut D, Shah V. Intrahepatic angiogenesis and sinusoidal remodeling in chronic liver disease: new targets for the treatment of portal hypertension? J Hepatol 2010;53:976–80. doi:10.1016/j.jhep.2010.07.004.

[311] Hennenberg M, Trebicka J, Stark C, Kohistani AZ, Heller J, Sauerbruch T. Sorafenib targets dysregulated Rho kinase expression and portal hypertension in rats with secondary biliary cirrhosis. Br J Pharmacol 2009;157:258–70. doi:10.1111/j.1476-5381.2009.00158.x.

[312] Semela D, Das A, Langer D, Kang N, Leof E, Shah V. Platelet-derived growth factor signaling through ephrin-b2 regulates hepatic vascular structure and function. Gastroenterology 2008;135:671–9. doi:10.1053/j.gastro.2008.04.010.

[313] Forner A, Llovet JM, Bruix J. Hepatocellular carcinoma. Lancet 2012;379:1245–55. doi:10.1016/S0140-6736(11)61347-0.

[314] Balogh J, Victor D, Asham EH, Burroughs SG, Boktour M, Saharia A, et al. Hepatocellular carcinoma: a review. J Hepatocell Carcinoma 2016;3:41–53. doi:10.2147/JHC.S61146.

[315] White DL, Kanwal F, El-Serag HB. Association between nonalcoholic fatty liver disease and risk for hepatocellular cancer, based on systematic review. Clin Gastroenterol Hepatol 2012;10:1342-1359.e2. doi:10.1016/j.cgh.2012.10.001.

[316] Younossi ZM, Otgonsuren M, Henry L, Venkatesan C, Mishra A, Erario M, et al. Association of nonalcoholic fatty liver disease (NAFLD) with hepatocellular carcinoma (HCC) in the United States from 2004 to 2009. Hepatology 2015;62:1723–30. doi:10.1002/hep.28123.

[317] Yang ZF, Poon RTP. Vascular changes in hepatocellular carcinoma. Anat Rec (Hoboken) 2008;291:721–34. doi:10.1002/ar.20668.

[318] Géraud C, Mogler C, Runge A, Evdokimov K, Lu S, Schledzewski K, et al. Endothelial transdifferentiation in hepatocellular carcinoma: loss of Stabilin-2 expression in peri-tumourous liver correlates with increased survival. Liver Int 2013;33:1428–40. doi:10.1111/liv.12262.

[319] Wu LQ, Zhang WJ, Niu JX, Ye LY, Yang ZH, Grau GE, et al. Phenotypic and functional differences between human liver cancer endothelial cells and liver sinusoidal endothelial cells. J Vasc Res 2008;45:78–86. doi:10.1159/000109079.

[320] Berg M, Wingender G, Djandji D, Hegenbarth S, Momburg F, Hämmerling G, et al. Cross-presentation of antigens from apoptotic tumor cells by liver sinusoidal endothelial cells leads to tumor-specific CD8+ T cell tolerance. Eur J Immunol 2006;36:2960–70. doi:10.1002/eji.200636033.

[321] Höchst B, Schildberg FA, Böttcher J, Metzger C, Huss S, Türler A, et al. Liver sinusoidal endothelial cells contribute to CD8 T cell tolerance toward circulating carcinoembryonic antigen in mice. Hepatology 2012;56:1924–33. doi:10.1002/hep.25844.

[322] Sharma D, Wang J, Fu PP, Sharma S, Nagalingam A, Mells J, et al. Adiponectin antagonizes the oncogenic actions of leptin in hepatocellular carcinogenesis. Hepatology 2010;52:1713–22. doi:10.1002/hep.23892.

[323] Milner K-L, van der Poorten D, Xu A, Bugianesi E, Kench JG, Lam KSL, et al. Adipocyte fatty acid binding protein levels relate to inflammation and fibrosis in nonalcoholic fatty liver disease. Hepatology 2009;49:1926–34. doi:10.1002/hep.22896.

[324] Laouirem S, Albuquerque M, Lagadec F, Cros J, Soubrane O, Bedossa P, et al. Fatty liver binding protein 4: a targetable adipokine in hepatocellular carcinoma related to metabolic syndrome. Journal of Hepatology 2017;66:S635–6. doi:10.1016/S0168-8278(17)31722-1.
[325] Poon RT-P, Ng IO-L, Lau C, Yu W-C, Yang Z-F, Fan S-T, et al. Tumor microvessel density as a predictor of recurrence after resection of hepatocellular carcinoma: a prospective study. J Clin Oncol 2002;20:1775–85. doi:10.1200/JCO.2002.07.089.
[326] Yoshiji H, Noguchi R, Namisaki T, Moriya K, Kitade M, Aihara Y, et al. Combination of sorafenib and angiotensin-II receptor blocker attenuates preneoplastic lesion development in a non-diabetic rat model of steatohepatitis. J Gastroenterol 2014;49:1421–9. doi:10.1007/s00535-013-0906-y.
[327] Abou-Alfa GK, Blanc J-F, Miles S, Ganten T, Trojan J, Cebon J, et al. Phase II Study of First-Line Trebananib Plus Sorafenib in Patients with Advanced Hepatocellular Carcinoma. Oncologist 2017;22:780-e65. doi:10.1634/theoncologist.2017-0058.
[328] Levine B, Kroemer G. Autophagy in the pathogenesis of disease. Cell 2008;132:27–42. doi:10.1016/j.cell.2007.12.018.
[329] Deter RL, De Duve C. Influence of glucagon, an inducer of cellular autophagy, on some physical properties of rat liver lysosomes. J Cell Biol 1967;33:437–49.
[330] Kaur J, Debnath J. Autophagy at the crossroads of catabolism and anabolism. Nat Rev Mol Cell Biol 2015;16:461–72. doi:10.1038/nrm4024.
[331] Glick D, Barth S, Macleod KF. Autophagy: cellular and molecular mechanisms. J Pathol 2010;221:3–12. doi:10.1002/path.2697.
[332] Choi AMK, Ryter SW, Levine B. Autophagy in human health and disease. N Engl J Med 2013;368:651–62. doi:10.1056/NEJMra1205406.
[333] Kuma A, Hatano M, Matsui M, Yamamoto A, Nakaya H, Yoshimori T, et al. The role of autophagy during the early neonatal starvation period. Nature 2004;432:1032–6. doi:10.1038/nature03029.
[334] Martinet W, De Meyer GRY. Autophagy in atherosclerosis: a cell survival and death phenomenon with therapeutic potential. Circ Res 2009;104:304–17. doi:10.1161/CIRCRESAHA.108.188318.
[335] Codogno P, Meijer AJ. Autophagy and signaling: their role in cell survival and cell death. Cell Death Differ 2005;12 Suppl 2:1509–18. doi:10.1038/sj.cdd.4401751.
[336] Liu Y, Levine B. Autosis and autophagic cell death: the dark side of autophagy. Cell Death Differ 2015;22:367–76. doi:10.1038/cdd.2014.143.
[337] Kheloufi M, Boulanger CM, Codogno P, Rautou P-E. Autosis occurs in the liver of patients with severe anorexia nervosa. Hepatology 2015;62:657–8. doi:10.1002/hep.27597.
[338] Neff NT, Bourret L, Miao P, Dice JF. Degradation of proteins microinjected into IMR-90 human diploid fibroblasts. J Cell Biol 1981;91:184–94.
[339] Dice JF. Peptide sequences that target cytosolic proteins for lysosomal proteolysis. Trends Biochem Sci 1990;15:305–9.
[340] Cuervo AM, Wong E. Chaperone-mediated autophagy: roles in disease and aging. Cell Res 2014;24:92–104. doi:10.1038/cr.2013.153.
[341] Bandyopadhyay U, Kaushik S, Varticovski L, Cuervo AM. The chaperone-mediated autophagy receptor organizes in dynamic protein complexes at the lysosomal membrane. Mol Cell Biol 2008;28:5747–63. doi:10.1128/MCB.02070-07.
[342] Bandyopadhyay U, Sridhar S, Kaushik S, Kiffin R, Cuervo AM. Identification of regulators of chaperone-mediated autophagy. Mol Cell 2010;39:535–47. doi:10.1016/j.molcel.2010.08.004.
[343] De Duve C, Wattiaux R. Functions of lysosomes. Annu Rev Physiol 1966;28:435–92. doi:10.1146/annurev.ph.28.030166.002251.

[344] Li W, Li J, Bao J. Microautophagy: lesser-known self-eating. Cell Mol Life Sci 2012;69:1125–36. doi:10.1007/s00018-011-0865-5.
[345] Suzuki K. Selective autophagy in budding yeast. Cell Death Differ 2013;20:43–8. doi:10.1038/cdd.2012.73.
[346] van Zutphen T, Todde V, de Boer R, Kreim M, Hofbauer HF, Wolinski H, et al. Lipid droplet autophagy in the yeast Saccharomyces cerevisiae. Mol Biol Cell 2014;25:290–301. doi:10.1091/mbc.E13-08-0448.
[347] Okamoto K. Organellophagy: eliminating cellular building blocks via selective autophagy. J Cell Biol 2014;205:435–45. doi:10.1083/jcb.201402054.
[348] Lamb CA, Yoshimori T, Tooze SA. The autophagosome: origins unknown, biogenesis complex. Nat Rev Mol Cell Biol 2013;14:759–74. doi:10.1038/nrm3696.
[349] Nakatogawa H, Suzuki K, Kamada Y, Ohsumi Y. Dynamics and diversity in autophagy mechanisms: lessons from yeast. Nat Rev Mol Cell Biol 2009;10:458–67. doi:10.1038/nrm2708.
[350] Yang Z, Klionsky DJ. An overview of the molecular mechanism of autophagy. Curr Top Microbiol Immunol 2009;335:1–32. doi:10.1007/978-3-642-00302-8_1.
[351] Boya P, Reggiori F, Codogno P. Emerging regulation and functions of autophagy. Nat Cell Biol 2013;15:713–20. doi:10.1038/ncb2788.
[352] Pattingre S, Tassa A, Qu X, Garuti R, Liang XH, Mizushima N, et al. Bcl-2 antiapoptotic proteins inhibit Beclin 1-dependent autophagy. Cell 2005;122:927–39. doi:10.1016/j.cell.2005.07.002.
[353] Zhong Y, Wang QJ, Li X, Yan Y, Backer JM, Chait BT, et al. Distinct regulation of autophagic activity by Atg14L and Rubicon associated with Beclin 1-phosphatidylinositol-3-kinase complex. Nat Cell Biol 2009;11:468–76. doi:10.1038/ncb1854.
[354] Fimia GM, Stoykova A, Romagnoli A, Giunta L, Di Bartolomeo S, Nardacci R, et al. Ambra1 regulates autophagy and development of the nervous system. Nature 2007;447:1121–5. doi:10.1038/nature05925.
[355] Takahashi Y, Coppola D, Matsushita N, Cualing HD, Sun M, Sato Y, et al. Bif-1 interacts with Beclin 1 through UVRAG and regulates autophagy and tumorigenesis. Nat Cell Biol 2007;9:1142–51. doi:10.1038/ncb1634.
[356] Huang R, Xu Y, Wan W, Shou X, Qian J, You Z, et al. Deacetylation of nuclear LC3 drives autophagy initiation under starvation. Mol Cell 2015;57:456–66. doi:10.1016/j.molcel.2014.12.013.
[357] Klionsky DJ. The molecular machinery of autophagy: unanswered questions. J Cell Sci 2005;118:7–18. doi:10.1242/jcs.01620.
[358] Klionsky DJ, Abdelmohsen K, Abe A, Abedin MJ, Abeliovich H, Acevedo Arozena A, et al. Guidelines for the use and interpretation of assays for monitoring autophagy (3rd edition). Autophagy 2016;12:1–222. doi:10.1080/15548627.2015.1100356.
[359] Young ARJ, Chan EYW, Hu XW, Köchl R, Crawshaw SG, High S, et al. Starvation and ULK1-dependent cycling of mammalian Atg9 between the TGN and endosomes. J Cell Sci 2006;119:3888–900. doi:10.1242/jcs.03172.
[360] Webber JL, Tooze SA. Coordinated regulation of autophagy by p38alpha MAPK through mAtg9 and p38IP. EMBO J 2010;29:27–40. doi:10.1038/emboj.2009.321.
[361] Yamamoto H, Kakuta S, Watanabe TM, Kitamura A, Sekito T, Kondo-Kakuta C, et al. Atg9 vesicles are an important membrane source during early steps of autophagosome formation. J Cell Biol 2012;198:219–33. doi:10.1083/jcb.201202061.
[362] Fougeray S, Pallet N. Mechanisms and biological functions of autophagy in diseased and ageing kidneys. Nat Rev Nephrol 2015;11:34–45. doi:10.1038/nrneph.2014.201.
[363] Yu Z-Q, Ni T, Hong B, Wang H-Y, Jiang F-J, Zou S, et al. Dual roles of Atg8-PE deconjugation by Atg4 in autophagy. Autophagy 2012;8:883–92. doi:10.4161/auto.19652.

[364] Nair U, Yen W-L, Mari M, Cao Y, Xie Z, Baba M, et al. A role for Atg8-PE deconjugation in autophagosome biogenesis. Autophagy 2012;8:780–93. doi:10.4161/auto.19385.

[365] Kirisako T, Baba M, Ishihara N, Miyazawa K, Ohsumi M, Yoshimori T, et al. Formation process of autophagosome is traced with Apg8/Aut7p in yeast. J Cell Biol 1999;147:435–46.

[366] Ganley IG. Autophagosome maturation and lysosomal fusion. Essays Biochem 2013;55:65–78. doi:10.1042/bse0550065.

[367] Liang C, Lee J, Inn K, Gack MU, Li Q, Roberts EA, et al. Beclin1-binding UVRAG targets the class C Vps complex to coordinate autophagosome maturation and endocytic trafficking. Nat Cell Biol 2008;10:776–87. doi:10.1038/ncb1740.

[368] Ganley IG, Wong P-M, Gammoh N, Jiang X. Distinct autophagosomal-lysosomal fusion mechanism revealed by thapsigargin-induced autophagy arrest. Mol Cell 2011;42:731–43. doi:10.1016/j.molcel.2011.04.024.

[369] Hurley JH. The ESCRT complexes. Crit Rev Biochem Mol Biol 2010;45:463–87. doi:10.3109/10409238.2010.502516.

[370] Metcalf D, Isaacs AM. The role of ESCRT proteins in fusion events involving lysosomes, endosomes and autophagosomes. Biochem Soc Trans 2010;38:1469–73. doi:10.1042/BST0381469.

[371] Chen D, Fan W, Lu Y, Ding X, Chen S, Zhong Q. A mammalian autophagosome maturation mechanism mediated by TECPR1 and the Atg12-Atg5 conjugate. Mol Cell 2012;45:629–41. doi:10.1016/j.molcel.2011.12.036.

[372] Itakura E, Kishi-Itakura C, Mizushima N. The hairpin-type tail-anchored SNARE syntaxin 17 targets to autophagosomes for fusion with endosomes/lysosomes. Cell 2012;151:1256–69. doi:10.1016/j.cell.2012.11.001.

[373] Itakura E, Mizushima N. Syntaxin 17: the autophagosomal SNARE. Autophagy 2013;9:917–9. doi:10.4161/auto.24109.

[374] Eskelinen E-L. Roles of LAMP-1 and LAMP-2 in lysosome biogenesis and autophagy. Mol Aspects Med 2006;27:495–502. doi:10.1016/j.mam.2006.08.005.

[375] Huynh KK, Eskelinen E-L, Scott CC, Malevanets A, Saftig P, Grinstein S. LAMP proteins are required for fusion of lysosomes with phagosomes. EMBO J 2007;26:313–24. doi:10.1038/sj.emboj.7601511.

[376] Hubert V, Peschel A, Langer B, Gröger M, Rees A, Kain R. LAMP-2 is required for incorporating syntaxin-17 into autophagosomes and for their fusion with lysosomes. Biol Open 2016;5:1516–29. doi:10.1242/bio.018648.

[377] Korolchuk VI, Saiki S, Lichtenberg M, Siddiqi FH, Roberts EA, Imarisio S, et al. Lysosomal positioning coordinates cellular nutrient responses. Nat Cell Biol 2011;13:453–60. doi:10.1038/ncb2204.

[378] Poüs C, Codogno P. Lysosome positioning coordinates mTORC1 activity and autophagy. Nat Cell Biol 2011;13:342–4. doi:10.1038/ncb0411-342.

[379] Hosokawa N, Hara T, Kaizuka T, Kishi C, Takamura A, Miura Y, et al. Nutrient-dependent mTORC1 association with the ULK1-Atg13-FIP200 complex required for autophagy. Mol Biol Cell 2009;20:1981–91. doi:10.1091/mbc.e08-12-1248.

[380] Ganley IG, Lam DH, Wang J, Ding X, Chen S, Jiang X. ULK1.ATG13.FIP200 complex mediates mTOR signaling and is essential for autophagy. J Biol Chem 2009;284:12297–305. doi:10.1074/jbc.M900573200.

[381] Jung CH, Jun CB, Ro S-H, Kim Y-M, Otto NM, Cao J, et al. ULK-Atg13-FIP200 complexes mediate mTOR signaling to the autophagy machinery. Mol Biol Cell 2009;20:1992–2003. doi:10.1091/mbc.e08-12-1249.

[382] Kim J, Kundu M, Viollet B, Guan K-L. AMPK and mTOR regulate autophagy

through direct phosphorylation of Ulk1. Nat Cell Biol 2011;13:132–41. doi:10.1038/ncb2152.
[383] Nazio F, Strappazzon F, Antonioli M, Bielli P, Cianfanelli V, Bordi M, et al. mTOR inhibits autophagy by controlling ULK1 ubiquitylation, self-association and function through AMBRA1 and TRAF6. Nat Cell Biol 2013;15:406–16. doi:10.1038/ncb2708.
[384] Yuan H-X, Russell RC, Guan K-L. Regulation of PIK3C3/VPS34 complexes by MTOR in nutrient stress-induced autophagy. Autophagy 2013;9:1983–95.
[385] Settembre C, Fraldi A, Medina DL, Ballabio A. Signals from the lysosome: a control centre for cellular clearance and energy metabolism. Nat Rev Mol Cell Biol 2013;14:283–96. doi:10.1038/nrm3565.
[386] Settembre C, Zoncu R, Medina DL, Vetrini F, Erdin S, Erdin S, et al. A lysosome-to-nucleus signalling mechanism senses and regulates the lysosome via mTOR and TFEB. EMBO J 2012;31:1095–108. doi:10.1038/emboj.2012.32.
[387] Martina JA, Chen Y, Gucek M, Puertollano R. MTORC1 functions as a transcriptional regulator of autophagy by preventing nuclear transport of TFEB. Autophagy 2012;8:903–14. doi:10.4161/auto.19653.
[388] Cantley LC. The phosphoinositide 3-kinase pathway. Science 2002;296:1655–7. doi:10.1126/science.296.5573.1655.
[389] Heras-Sandoval D, Pérez-Rojas JM, Hernández-Damián J, Pedraza-Chaverri J. The role of PI3K/AKT/mTOR pathway in the modulation of autophagy and the clearance of protein aggregates in neurodegeneration. Cell Signal 2014;26:2694–701. doi:10.1016/j.cellsig.2014.08.019.
[390] Long X, Lin Y, Ortiz-Vega S, Yonezawa K, Avruch J. Rheb binds and regulates the mTOR kinase. Curr Biol 2005;15:702–13. doi:10.1016/j.cub.2005.02.053.
[391] Hardie DG, Ross FA, Hawley SA. AMPK: a nutrient and energy sensor that maintains energy homeostasis. Nat Rev Mol Cell Biol 2012;13:251–62. doi:10.1038/nrm3311.
[392] Shackelford DB, Shaw RJ. The LKB1-AMPK pathway: metabolism and growth control in tumour suppression. Nat Rev Cancer 2009;9:563–75. doi:10.1038/nrc2676.
[393] Inoki K, Zhu T, Guan K-L. TSC2 mediates cellular energy response to control cell growth and survival. Cell 2003;115:577–90.
[394] Gwinn DM, Shackelford DB, Egan DF, Mihaylova MM, Mery A, Vasquez DS, et al. AMPK phosphorylation of raptor mediates a metabolic checkpoint. Mol Cell 2008;30:214–26. doi:10.1016/j.molcel.2008.03.003.
[395] Egan DF, Shackelford DB, Mihaylova MM, Gelino S, Kohnz RA, Mair W, et al. Phosphorylation of ULK1 (hATG1) by AMP-activated protein kinase connects energy sensing to mitophagy. Science 2011;331:456–61. doi:10.1126/science.1196371.
[396] Tran H, Brunet A, Griffith EC, Greenberg ME. The many forks in FOXO's road. Sci STKE 2003;2003:RE5. doi:10.1126/stke.2003.172.re5.
[397] Sengupta A, Molkentin JD, Yutzey KE. FoxO transcription factors promote autophagy in cardiomyocytes. J Biol Chem 2009;284:28319–31. doi:10.1074/jbc.M109.024406.
[398] Liu H-Y, Han J, Cao SY, Hong T, Zhuo D, Shi J, et al. Hepatic autophagy is suppressed in the presence of insulin resistance and hyperinsulinemia: inhibition of FoxO1-dependent expression of key autophagy genes by insulin. J Biol Chem 2009;284:31484–92. doi:10.1074/jbc.M109.033936.
[399] Hariharan N, Maejima Y, Nakae J, Paik J, Depinho RA, Sadoshima J. Deacetylation of FoxO by Sirt1 Plays an Essential Role in Mediating Starvation-Induced Autophagy in Cardiac Myocytes. Circ Res 2010;107:1470–82. doi:10.1161/CIRCRESAHA.110.227371.
[400] Zhao Y, Yang J, Liao W, Liu X, Zhang H, Wang S, et al. Cytosolic FoxO1 is essential for the induction of autophagy and tumour suppressor activity. Nat Cell Biol 2010;12:665–75. doi:10.1038/ncb2069.
[401] Vidal RL, Hetz C. Unspliced XBP1 controls autophagy through FoxO1. Cell Res

2013;23:463–4. doi:10.1038/cr.2013.9.
[402] Zhao Y, Li X, Cai M-Y, Ma K, Yang J, Zhou J, et al. XBP-1u suppresses autophagy by promoting the degradation of FoxO1 in cancer cells. Cell Res 2013;23:491–507. doi:10.1038/cr.2013.2.
[403] Zhou J, Liao W, Yang J, Ma K, Li X, Wang Y, et al. FOXO3 induces FOXO1-dependent autophagy by activating the AKT1 signaling pathway. Autophagy 2012;8:1712–23. doi:10.4161/auto.21830.
[404] Levine B, Abrams J. p53: The Janus of autophagy? Nat Cell Biol 2008;10:637–9. doi:10.1038/ncb0608-637.
[405] Feng Z, Zhang H, Levine AJ, Jin S. The coordinate regulation of the p53 and mTOR pathways in cells. Proc Natl Acad Sci USA 2005;102:8204–9. doi:10.1073/pnas.0502857102.
[406] Crighton D, Wilkinson S, O'Prey J, Syed N, Smith P, Harrison PR, et al. DRAM, a p53-induced modulator of autophagy, is critical for apoptosis. Cell 2006;126:121–34. doi:10.1016/j.cell.2006.05.034.
[407] Tasdemir E, Maiuri MC, Galluzzi L, Vitale I, Djavaheri-Mergny M, D'Amelio M, et al. Regulation of autophagy by cytoplasmic p53. Nat Cell Biol 2008;10:676–87. doi:10.1038/ncb1730.
[408] Napoli M, Flores ER. The family that eats together stays together: new p53 family transcriptional targets in autophagy. Genes Dev 2013;27:971–4. doi:10.1101/gad.219147.113.
[409] DeGregori J, Johnson DG. Distinct and Overlapping Roles for E2F Family Members in Transcription, Proliferation and Apoptosis. Curr Mol Med 2006;6:739–48.
[410] Polager S, Ofir M, Ginsberg D. E2F1 regulates autophagy and the transcription of autophagy genes. Oncogene 2008;27:4860–4. doi:10.1038/onc.2008.117.
[411] Weinmann AS, Bartley SM, Zhang T, Zhang MQ, Farnham PJ. Use of chromatin immunoprecipitation to clone novel E2F target promoters. Mol Cell Biol 2001;21:6820–32. doi:10.1128/MCB.21.20.6820-6832.2001.
[412] Tracy K, Dibling BC, Spike BT, Knabb JR, Schumacker P, Macleod KF. BNIP3 is an RB/E2F target gene required for hypoxia-induced autophagy. Mol Cell Biol 2007;27:6229–42. doi:10.1128/MCB.02246-06.
[413] Shaw J, Yurkova N, Zhang T, Gang H, Aguilar F, Weidman D, et al. Antagonism of E2F-1 regulated Bnip3 transcription by NF-kappaB is essential for basal cell survival. Proc Natl Acad Sci USA 2008;105:20734–9. doi:10.1073/pnas.0807735105.
[414] Füllgrabe J, Klionsky DJ, Joseph B. The return of the nucleus: transcriptional and epigenetic control of autophagy. Nat Rev Mol Cell Biol 2014;15:65–74. doi:10.1038/nrm3716.
[415] White EJ, Martin V, Liu J-L, Klein SR, Piya S, Gomez-Manzano C, et al. Autophagy regulation in cancer development and therapy. Am J Cancer Res 2011;1:362–72.
[416] Madrigal-Matute J, Cuervo AM. Regulation of Liver Metabolism by Autophagy. Gastroenterology 2016;150:328–39. doi:10.1053/j.gastro.2015.09.042.
[417] Ezaki J, Matsumoto N, Takeda-Ezaki M, Komatsu M, Takahashi K, Hiraoka Y, et al. Liver autophagy contributes to the maintenance of blood glucose and amino acid levels. Autophagy 2011;7:727–36.
[418] Hers HG. alpha-Glucosidase deficiency in generalized glycogenstorage disease (Pompe's disease). Biochem J 1963;86:11–6.
[419] Lee JM, Wagner M, Xiao R, Kim KH, Feng D, Lazar MA, et al. Nutrient-sensing nuclear receptors coordinate autophagy. Nature 2014;516:112–5. doi:10.1038/nature13961.
[420] Rodriguez-Navarro JA, Kaushik S, Koga H, Dall'Armi C, Shui G, Wenk MR, et al. Inhibitory effect of dietary lipids on chaperone-mediated autophagy. Proc Natl Acad Sci USA 2012;109:E705-714. doi:10.1073/pnas.1113036109.
[421] Koga H, Kaushik S, Cuervo AM. Altered lipid content inhibits autophagic vesicular

fusion. FASEB J 2010;24:3052–65. doi:10.1096/fj.09-144519.
[422] Cuervo AM, Knecht E, Terlecky SR, Dice JF. Activation of a selective pathway of lysosomal proteolysis in rat liver by prolonged starvation. Am J Physiol 1995;269:C1200-1208. doi:10.1152/ajpcell.1995.269.5.C1200.
[423] Schneider JL, Suh Y, Cuervo AM. Deficient chaperone-mediated autophagy in liver leads to metabolic dysregulation. Cell Metab 2014;20:417–32. doi:10.1016/j.cmet.2014.06.009.
[424] Kaushik S, Cuervo AM. Degradation of lipid droplet-associated proteins by chaperone-mediated autophagy facilitates lipolysis. Nat Cell Biol 2015;17:759–70. doi:10.1038/ncb3166.
[425] Pickrell AM, Youle RJ. The roles of PINK1, parkin, and mitochondrial fidelity in Parkinson’s disease. Neuron 2015;85:257–73. doi:10.1016/j.neuron.2014.12.007.
[426] Manley S, Ni H-M, Kong B, Apte U, Guo G, Ding W-X. Suppression of autophagic flux by bile acids in hepatocytes. Toxicol Sci 2014;137:478–90. doi:10.1093/toxsci/kft246.
[427] Gual P, Gilgenkrantz H, Lotersztajn S. Autophagy in chronic liver diseases: the two faces of Janus. Am J Physiol, Cell Physiol 2017;312:C263–73. doi:10.1152/ajpcell.00295.2016.
[428] González-Rodríguez A, Mayoral R, Agra N, Valdecantos MP, Pardo V, Miquilena-Colina ME, et al. Impaired autophagic flux is associated with increased endoplasmic reticulum stress during the development of NAFLD. Cell Death Dis 2014;5:e1179. doi:10.1038/cddis.2014.162.
[429] Fukuo Y, Yamashina S, Sonoue H, Arakawa A, Nakadera E, Aoyama T, et al. Abnormality of autophagic function and cathepsin expression in the liver from patients with non-alcoholic fatty liver disease. Hepatol Res 2014;44:1026–36. doi:10.1111/hepr.12282.
[430] Inami Y, Yamashina S, Izumi K, Ueno T, Tanida I, Ikejima K, et al. Hepatic steatosis inhibits autophagic proteolysis via impairment of autophagosomal acidification and cathepsin expression. Biochem Biophys Res Commun 2011;412:618–25. doi:10.1016/j.bbrc.2011.08.012.
[431] Tremblay F, Krebs M, Dombrowski L, Brehm A, Bernroider E, Roth E, et al. Overactivation of S6 kinase 1 as a cause of human insulin resistance during increased amino acid availability. Diabetes 2005;54:2674–84.
[432] Yang L, Li P, Fu S, Calay ES, Hotamisligil GS. Defective hepatic autophagy in obesity promotes ER stress and causes insulin resistance. Cell Metab 2010;11:467–78. doi:10.1016/j.cmet.2010.04.005.
[433] Zubiete-Franco I, García-Rodríguez JL, Martínez-Uña M, Martínez-Lopez N, Woodhoo A, Juan VG-D, et al. Methionine and S-adenosylmethionine levels are critical regulators of PP2A activity modulating lipophagy during steatosis. J Hepatol 2016;64:409–18. doi:10.1016/j.jhep.2015.08.037.
[434] Guixé-Muntet S, de Mesquita FC, Vila S, Hernández-Gea V, Peralta C, García-Pagán JC, et al. Cross-talk between autophagy and KLF2 determines endothelial cell phenotype and microvascular function in acute liver injury. J Hepatol 2017;66:86–94. doi:10.1016/j.jhep.2016.07.051.
[435] Zhou R, Yazdi AS, Menu P, Tschopp J. A role for mitochondria in NLRP3 inflammasome activation. Nature 2011;469:221–5. doi:10.1038/nature09663.
[436] Lin C-W, Zhang H, Li M, Xiong X, Chen X, Chen X, et al. Pharmacological promotion of autophagy alleviates steatosis and injury in alcoholic and non-alcoholic fatty liver conditions in mice. J Hepatol 2013;58:993–9. doi:10.1016/j.jhep.2013.01.011.
[437] Tanaka S, Hikita H, Tatsumi T, Sakamori R, Nozaki Y, Sakane S, et al. Rubicon inhibits autophagy and accelerates hepatocyte apoptosis and lipid accumulation in nonalcoholic fatty liver disease in mice. Hepatology 2016;64:1994–2014.

doi:10.1002/hep.28820.
[438] Schneider JL, Villarroya J, Diaz-Carretero A, Patel B, Urbanska AM, Thi MM, et al. Loss of hepatic chaperone-mediated autophagy accelerates proteostasis failure in aging. Aging Cell 2015;14:249–64. doi:10.1111/acel.12310.
[439] Deretic V, Saitoh T, Akira S. Autophagy in infection, inflammation and immunity. Nat Rev Immunol 2013;13:722–37. doi:10.1038/nri3532.
[440] Jacquel A, Obba S, Boyer L, Dufies M, Robert G, Gounon P, et al. Autophagy is required for CSF-1-induced macrophagic differentiation and acquisition of phagocytic functions. Blood 2012;119:4527–31. doi:10.1182/blood-2011-11-392167.
[441] Chuang S-Y, Yang C-H, Chou C-C, Chiang Y-P, Chuang T-H, Hsu L-C. TLR-induced PAI-2 expression suppresses IL-1β processing via increasing autophagy and NLRP3 degradation. Proc Natl Acad Sci USA 2013;110:16079–84. doi:10.1073/pnas.1306556110.
[442] Liu K, Zhao E, Ilyas G, Lalazar G, Lin Y, Haseeb M, et al. Impaired macrophage autophagy increases the immune response in obese mice by promoting proinflammatory macrophage polarization. Autophagy 2015;11:271–84. doi:10.1080/15548627.2015.1009787.
[443] Lodder J, Denaës T, Chobert M-N, Wan J, El-Benna J, Pawlotsky J-M, et al. Macrophage autophagy protects against liver fibrosis in mice. Autophagy 2015;11:1280–92. doi:10.1080/15548627.2015.1058473.
[444] Hernández-Gea V, Ghiassi-Nejad Z, Rozenfeld R, Gordon R, Fiel MI, Yue Z, et al. Autophagy releases lipid that promotes fibrogenesis by activated hepatic stellate cells in mice and in human tissues. Gastroenterology 2012;142:938–46. doi:10.1053/j.gastro.2011.12.044.
[445] Thoen LFR, Guimarães ELM, Dollé L, Mannaerts I, Najimi M, Sokal E, et al. A role for autophagy during hepatic stellate cell activation. J Hepatol 2011;55:1353–60. doi:10.1016/j.jhep.2011.07.010.
[446] Vion A-C, Kheloufi M, Hammoutene A, Poisson J, Lasselin J, Devue C, et al. Autophagy is required for endothelial cell alignment and atheroprotection under physiological blood flow. Proc Natl Acad Sci USA 2017;114:E8675–84. doi:10.1073/pnas.1702223114.
[447] Huebert RC, Jagavelu K, Liebl AF, Huang BQ, Splinter PL, LaRusso NF, et al. Immortalized liver endothelial cells: a cell culture model for studies of motility and angiogenesis. Lab Invest 2010;90:1770–81. doi:10.1038/labinvest.2010.132.
[448] Peiris AN, Mueller RA, Smith GA, Struve MF, Kissebah AH. Splanchnic insulin metabolism in obesity. Influence of body fat distribution. J Clin Invest 1986;78:1648–57. doi:10.1172/JCI112758.
[449] Fontana L, Eagon JC, Trujillo ME, Scherer PE, Klein S. Visceral fat adipokine secretion is associated with systemic inflammation in obese humans. Diabetes 2007;56:1010–3. doi:10.2337/db06-1656.
[450] Magkos F, Fabbrini E, Patterson BW, Eagon JC, Klein S. Portal vein and systemic adiponectin concentrations are closely linked with hepatic glucose and lipoprotein kinetics in extremely obese subjects. Metab Clin Exp 2011;60:1641–8. doi:10.1016/j.metabol.2011.03.019.
[451] Liu RH, Kurose T, Matsukura S. Oral nicotine administration decreases tumor necrosis factor-alpha expression in fat tissues in obese rats. Metab Clin Exp 2001;50:79–85.
[452] Loos B, du Toit A, Hofmeyr J-HS. Defining and measuring autophagosome flux—concept and reality. Autophagy 2014;10:2087–96. doi:10.4161/15548627.2014.973338.
[453] Gatica D, Chiong M, Lavandero S, Klionsky DJ. Molecular mechanisms of autophagy in the cardiovascular system. Circ Res 2015;116:456–67. doi:10.1161/CIRCRESAHA.114.303788.
[454] DeLeve LD. Liver sinusoidal endothelial cells in hepatic fibrosis. Hepatology 2015;61:1740–6. doi:10.1002/hep.27376.
[455] LaRocca TJ, Henson GD, Thorburn A, Sindler AL, Pierce GL, Seals DR.

Translational evidence that impaired autophagy contributes to arterial ageing. J Physiol (Lond) 2012;590:3305–16. doi:10.1113/jphysiol.2012.229690.
[456] Levine B, Packer M, Codogno P. Development of autophagy inducers in clinical medicine. J Clin Invest 2015;125:14–24. doi:10.1172/JCI73938.
[457] Ganesan LP, Mohanty S, Kim J, Clark KR, Robinson JM, Anderson CL. Rapid and efficient clearance of blood-borne virus by liver sinusoidal endothelium. PLoS Pathog 2011;7:e1002281. doi:10.1371/journal.ppat.1002281.
[458] Sen D, Balakrishnan B, Gabriel N, Agrawal P, Roshini V, Samuel R, et al. Improved adeno-associated virus (AAV) serotype 1 and 5 vectors for gene therapy. Sci Rep 2013;3:1832. doi:10.1038/srep01832.

VII- APPENDIX

A. Co-authorship publications

1. Autophagy is required for endothelial cell alignment and atheroprotection under physiological blood flow

Autophagy is required for endothelial cell alignment and atheroprotection under physiological blood flow

Authors: Anne-Clemence Vion[a,b,1], Marouane Kheloufi[a,b,c,1], **Adel Hammoutene**[a,b], Johanne Poisson[a,b], Juliette Lasselin[a,b], Cecile Devue[a,b], Isabelle Pic[a,b], Nicolas Dupont[b,d,e], Johanna Busse[f], Konstantin Stark[f], Julie Lafaurie-Janvore[g], Abdul I. Barakat[g], Xavier Loyer[a,b], Michele Souyri[h], Benoit Viollet[b,i,j], Pierre Julia[b,k], Alain Tedgui[a,b], Patrice Codogno[b,d,e], Chantal M. Boulanger[a,b,2,3], and Pierre-Emmanuel Rautou[a,b,c,l,2]

Affiliations: [a] INSERM, U970, Paris Cardiovascular Research Center, 75015 Paris, France; [b] Université Paris Descartes, Sorbonne Paris Cité, 75006 Paris, France; [c] Université Paris Diderot, Sorbonne Paris Cité, 75013 Paris, France ; [d] INSERM U1151, Institut Necker-Enfants Malades-INEM, 75014 Paris, France ; [e] CNRS UMR 8253, 75014 Paris, France ; [f] Medizinische Klinik I, Klinikum der Universität München, 81377 Munich, Germany; [g] Mechanics & Living Systems, Cardiovascular Cellular Engineering, Laboratoire d'Hydrodynamique, Ecole Polytechnique, UMR 7646, 91128 Palaiseau, France; [h] INSERM UMR_S1131/IHU/Université Paris Diderot, 75013 Paris, France; [i] INSERM U1016, Institut Cochin, 75014 Paris, France; [j] CNRS, UMR 8104, 75014 Paris, France; [k] Service de Chirurgie Cardiaque et Vasculaire, Hôpital Européen Georges Pompidou, AP-HP, 75015 Paris, France; [l] Département Hospitalo-Universitaire Unity, Pôle des Maladies de l'Appareil Digestif, Service d'Hépatologie, Centre de Référence des Maladies Vasculaires du Foie, Hôpital Beaujon, Assistance Publique-Hopitaux de Paris, 92110 Clichy, France

Original article published in PNAS. 2017 Oct 10;114(41):E8675-E8684

Check for updates

Autophagy is required for endothelial cell alignment and atheroprotection under physiological blood flow

Anne-Clemence Vion[a,b,1], Marouane Kheloufi[a,b,c,1], Adel Hammoutene[a,b], Johanne Poisson[a,b], Juliette Lasselin[a,b], Cecile Devue[a,b], Isabelle Pic[a,b], Nicolas Dupont[b,d,e], Johanna Busse[f], Konstantin Stark[f], Julie Lafaurie-Janvore[g], Abdul I. Barakat[g], Xavier Loyer[a,b], Michele Souyri[h], Benoit Viollet[b,i,j], Pierre Julia[b,k], Alain Tedgui[a,b], Patrice Codogno[b,d,e], Chantal M. Boulanger[a,b,2,3], and Pierre-Emmanuel Rautou[a,b,c,l,2]

[a]INSERM, U970, Paris Cardiovascular Research Center, 75015 Paris, France; [b]Université Paris Descartes, Sorbonne Paris Cité, 75006 Paris, France; [c]Université Paris Diderot, Sorbonne Paris Cité, 75013 Paris, France; [d]INSERM U1151, Institut Necker-Enfants Malades-INEM, 75014 Paris, France; [e]CNRS UMR 8253, 75014 Paris, France; [f]Medizinische Klinik I, Klinikum der Universität München, 81377 Munich, Germany; [g]Mechanics & Living Systems, Cardiovascular Cellular Engineering, Laboratoire d'Hydrodynamique, Ecole Polytechnique, UMR 7646, 91128 Palaiseau, France; [h]INSERM UMR_S1131/IHU/Université Paris Diderot, 75013 Paris, France; [i]INSERM U1016, Institut Cochin, 75014 Paris, France; [j]CNRS, UMR 8104, 75014 Paris, France; [k]Service de Chirurgie Cardiaque et Vasculaire, Hôpital Européen Georges Pompidou, AP-HP, 75015 Paris, France; and [l]Département Hospitalo-Universitaire Unity, Pôle des Maladies de l'Appareil Digestif, Service d'Hépatologie, Centre de Référence des Maladies Vasculaires du Foie, Hôpital Beaujon, Assistance Publique-Hopitaux de Paris, 92110 Clichy, France

Edited by Beth Levine, The University of Texas Southwestern Medical Center, Dallas, TX, and approved August 23, 2017 (received for review February 10, 2017)

It has been known for some time that atherosclerotic lesions preferentially develop in areas exposed to low SS and are characterized by a proinflammatory, apoptotic, and senescent endothelial phenotype. Conversely, areas exposed to high SS are protected from plaque development, but the mechanisms have remained elusive. Autophagy is a protective mechanism that allows recycling of defective organelles and proteins to maintain cellular homeostasis. We aimed to understand the role of endothelial autophagy in the atheroprotective effect of high SS. Atheroprotective high SS stimulated endothelial autophagic flux in human and murine arteries. On the contrary, endothelial cells exposed to atheroprone low SS were characterized by inefficient autophagy as a result of mammalian target of rapamycin (mTOR) activation, AMPKα inhibition, and blockade of the autophagic flux. In hypercholesterolemic mice, deficiency in endothelial autophagy increased plaque burden only in the atheroresistant areas exposed to high SS; plaque size was unchanged in atheroprone areas, in which endothelial autophagy flux is already blocked. In cultured cells and in transgenic mice, deficiency in endothelial autophagy was characterized by defects in endothelial alignment with flow direction, a hallmark of endothelial cell health. This effect was associated with an increase in endothelial apoptosis and senescence in high-SS regions. Deficiency in endothelial autophagy also increased TNF-α–induced inflammation under high-SS conditions and decreased expression of the antiinflammatory factor KLF-2. Altogether, these results show that adequate endothelial autophagic flux under high SS limits atherosclerotic plaque formation by preventing endothelial apoptosis, senescence, and inflammation.

endothelial | autophagy | shear stress | atherosclerosis | inflammation

Atherosclerosis develops at arterial bifurcations and at the inner part of curvatures where blood flow is low or disturbed, whereas areas exposed to high blood flow, generating high laminar shear stress (SS) on the endothelium, remain lesion-free (1–4). Low SS is known to induce endothelial apoptosis, which in turn increases their procoagulant and proadhesive phenotype for platelets (5–7). Endothelial cells with senescence-associated phenotype are present in low-SS areas (8, 9). Senescent endothelial cells exhibit a proinflammatory phenotype that may contribute to the initiation and progression of atherosclerosis (9, 10). Low SS also stimulates endothelial expression of adhesion molecules and the release of chemokines that contribute to leukocyte recruitment, the early steps of atherosclerotic plaque formation (4, 11). However, the regulation of endothelial phenotypes by SS remains not fully elucidated.

Macroautophagy (hereafter referred to as autophagy) is a major intracellular recycling system. Under basal conditions, autophagy controls organelle and protein quality to maintain cellular homeostasis. Under conditions of stress, autophagy acts as a survival mechanism, maintaining cellular integrity by regenerating metabolic precursors and clearing subcellular debris (12). Autophagy primarily acts as a protective mechanism preventing cell death and senescence (12). This process modulates an expanding list of disease processes (12). Recent data indicate that mice deficient in endothelial Atg7, a key protein in autophagy process, develop more atherosclerotic plaques, but the mechanism remains elusive (13). Several groups have investigated the effect of SS on endothelial autophagy, with conflicting results. Most groups have found that SS activates autophagy in cultured endothelial cells (14–20), but a few investigators have compared the effects of different SS levels and reported paradoxical findings (14, 16–18, 21). The rare analyses of animal vessels did not help in drawing reliable conclusions (16, 18, 21). Importantly, the consequences of defective autophagy on endothelium health, i.e., apoptosis, senescence, and inflammatory phenotype, have not been thoroughly investigated (14). This led us to test the hypothesis that autophagy mediates the effect of SS on atherosclerosis development.

Significance

Atherosclerotic plaques tend to develop preferentially in areas of the vasculature exposed to low and disturbed shear stress (SS), but the mechanisms are not fully understood. In this study, we demonstrate that inefficient autophagy contributes to the development of atherosclerotic plaques in low-SS areas. Defective endothelial autophagy not only curbs endothelial alignment with the direction of blood flow, but also promotes an inflammatory, apoptotic, and senescent phenotype. Furthermore, genetic inactivation of endothelial autophagy in a murine model of atherosclerosis increases plaque burden exclusively in high-SS areas that are normally resistant to atherosclerotic plaque development. Altogether, these findings underline the role of endothelial autophagic flux activation by SS as an atheroprotective mechanism.

Author contributions: A.-C.V., M.K., C.M.B., and P.-E.R. designed research; A.-C.V., M.K., A.H., J.P., J.L., C.D., I.P., J.B., K.S., J.L.-J., X.L., and C.M.B. performed research; N.D., K.S., J.L.-J., A.I.B., M.S., B.V., P.J., and P.C. contributed new reagents/analytic tools; A.-C.V., M.K., X.L., A.T., P.C., C.M.B., and P.-E.R. analyzed data; and A.-C.V., M.K., A.T., P.C., C.M.B., and P.-E.R. wrote the paper.

The authors declare no conflict of interest.

This article is a PNAS Direct Submission.

[1] A.-C.V. and M.K. contributed equally to this work.

[2] C.M.B. and P.-E.R. contributed equally to this work.

[3] To whom correspondence should be addressed. Email: chantal.boulanger@inserm.fr.

This article contains supporting information online at www.pnas.org/lookup/suppl/doi:10.1073/pnas.1702223114/-/DCSupplemental.

Results

Autophagy Is Defective in Endothelial Cells Exposed to Low SS. Given the inconsistent in vitro results regarding the effect of SS on endothelial autophagy (14, 16–18, 21), we first examined endothelial autophagy level in isolated human and murine arteries by assessing LC3 punctae labeling (22). In human carotid arteries, LC3 staining was systematically less abundant in endothelial cells exposed to a disturbed low SS compared with those exposed to physiological high SS (7, 23, 24) (Fig. 1*A* and *SI Appendix*, Table S1). In murine arteries, en face LC3 staining of the inner part of the curvature of the aorta, exposed to a disturbed low SS, was significantly lower than that in the linear part of the descending thoracic aorta, exposed to a physiological high SS (Fig. 1*B*). This difference was observed in males as well as in females. Endothelial autophagy was then evaluated by measuring the LC3II/LC3I ratio in low-passage cultured human umbilical vein endothelial cells (HUVECs) exposed to 2 vs 20 dyn/cm^2 SS for as long as 24 h (Fig. 1*C*). A difference between low and high SS appeared after 12 h and was more pronounced at 24 h (Fig. 1*C*). Similar results were also observed when expressing LC3 as a ratio of LC3II to GAPDH (*SI Appendix*, Fig. S1*A*) and when measuring LC3 by flow cytometry analysis (*SI Appendix*, Fig. S1*B*). Finally, transmission EM analysis revealed a lower number of autophagic vacuoles in HUVECs exposed to low than to high SS ($n = 3$; Fig. 1*D*). Altogether, these results demonstrate that autophagy is reduced in endothelial cells exposed to low SS compared with high SS.

Complete autophagy requires the fusion of autophagosomes with lysosomes. To evaluate the autophagy flux, we treated HUVECs with bafilomycin A1, an inhibitor of autophagic flux. In HUVECs exposed to high SS for 6 h, bafilomycin A1 increased the LC3II/LC3I ratio, attesting to a functional autophagic flux under these conditions (Fig. 2*A*). On the contrary, bafilomycin A1 had no effect under low SS conditions, suggesting a blockade of the fusion between autophagosomes and lysosomes under these conditions (Fig. 2*A*). To confirm these data, we used a tandem monomeric red fluorescent protein (mRFP)-GFP-LC3 assay as a complementary strategy. In this assay, autophagosomes are labeled with a yellow signal (mRFP-GFP-LC3), and their maturation into autolysosomes is attested by a red signal as a result of the quenching of GFP fluorescence in lysosomes. As shown in Fig. 2*B*, RFP fluorescence was twofold lower in HUVECs exposed to low-SS compared with high-SS conditions, attesting to a blockade of autophagic flux under low SS. Similarly, colocalization of LC3 and the lysosomal marker LAMP2 was lower under low-SS than under high-SS conditions, confirming an impaired autophagic flux under low SS (Fig. 2*C*). We then investigated autophagic flux in vivo by injecting WT mice with chloroquine, an inhibitor of autophagic flux. As shown in

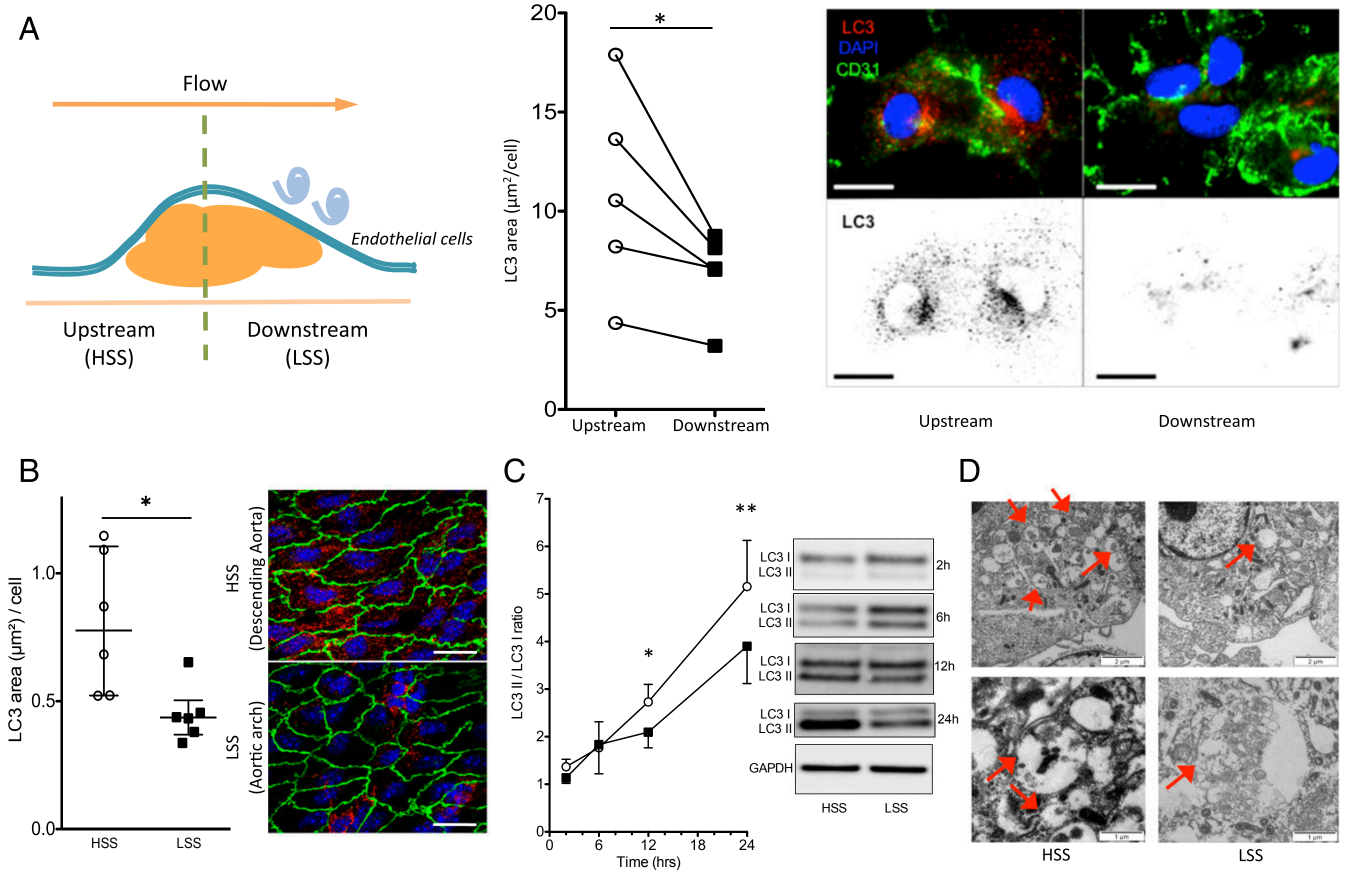

Fig. 1. Autophagy is defective in endothelial cells exposed to low SS (LSS). (*A*) LC3 en face staining of human endothelial cells isolated from endarterectomy specimen. (*Left*) Typical longitudinal section of a carotid atherosclerotic plaque showing upstream (exposed to high physiological SS) and downstream (exposed to low disturbed SS) parts. (*Middle*) Quantification. (*Right*) Representative images (green, CD31; red, LC3; blue, DAPI). (Scale bar, 10 μm.) Between 50 and 125 cells were counted per area for each patient. (*B*) LC3 en face staining of the aorta of 10-wk-old C57BL/6 mice ($n = 6$; green, CD31; red, LC3; blue, DAPI). (Scale bar, 20 μm). (*Left*) Quantification of LC3 area; data are given as median (horizontal bar) and interquartile range (error bar). (*Right*) Representative images. (*C*) Western blot analysis of LC3II/LC3I ratio in HUVECs exposed to high SS (HSS) and low SS. Data are normalized to static conditions for each time point ($n \geq 5$ per time point and per SS condition). Data are mean ± SEM. (*D*) Transmission EM analysis of HUVECs exposed to high and low SS for 24 h. Representative pictures of three independent experiments. Red arrows indicate autophagic vacuoles ($^*P < 0.05$ and $^{**}P < 0.01$).

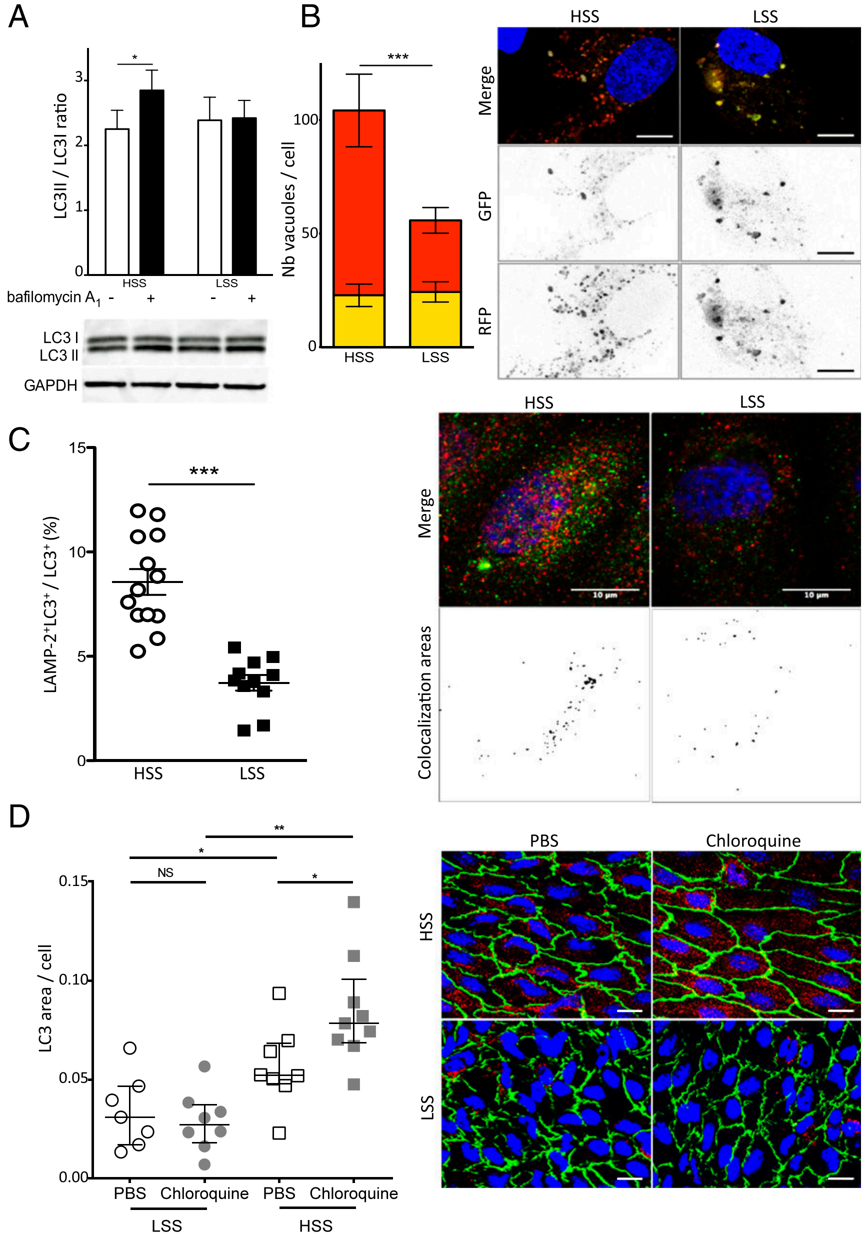

Fig. 2. Autophagic flux is blocked under low SS (LSS). (*A*) LC3 II/LC3 I ratio quantified by Western blot in HUVECs exposed to high SS (HSS) and low SS ($n = 5$; 6 h of SS including 4 h of bafilomycin A1, 100 nmol/L). (*B*) Quantification of HUVECs transfected with the tandem mRFP-GFP-LC3 plasmid and exposed for 24 h to high or low SS. Yellow bars represent autophagosomes, and red bars represent autolysosomes. Images are representative of three independent experiments in which more than 100 cells were observed. Autophagosomes are labeled with a yellow signal, whereas autolysosomes are labeled with a red signal. (Scale bar, 10 μm.) (*C*) Immunofluorescent LAMP2 and LC3 staining on HUVECs exposed to high or low SS for 24 h. (*Left*) Quantification. (*Right*) Representative images (red, LC3; green, LAMP2; blue, DAPI). Data are presented as mean ± SEM ($*P < 0.05$, $**P < 0.01$, and $***P < 0.001$). (*D*) LC3 en face staining of the aorta of 8-wk-old C57BL/6 male mice injected i.p. with PBS solution or chloroquine (60 mg/kg/d; 48 h, 24 h, and 4 h before euthanasia; $n = 7–9$ per group; green, CD144; red, LC3; blue, DAPI). (Scale bar, 20 μm.) (*Left*) Quantification of LC3 area. Data are given as median (horizontal bar) and interquartile range (error bar). (*Right*) Representative images.

Fig. 2*D*, chloroquine enhanced LC3 staining in high-SS areas but had no effect in low-SS areas, confirming the results obtained in vitro.

We then investigated the pathways responsible for this defect in endothelial autophagy under low SS. Exposure to SS for as long as 24 h did not alter endothelial expression of the key proteins of the autophagy pathway, namely Beclin1, ATG5, and ATG7 (*SI Appendix*, Fig. S1*C* and Table S3). LAMP2 expression was also unaffected (*SI Appendix*, Fig. S1*C*). The mammalian target of rapamycin (mTOR) and AMPK pathways are master negative and positive regulators of autophagy, respectively (25). Low SS increased 4EBP1 phosphorylation, confirming the activation of mTOR pathway under these experimental conditions (26) (*SI Appendix*, Fig. S1*D*). Inhibition of mTOR by using rapamycin increased autophagy level in HUVECs exposed to low-SS condition (Fig. 3*A*). Similarly, injection of rapamycin into WT mice increased LC3 staining in endothelial cells in low-SS areas (Fig. 3*B*). As previously described, we observed reduced phosphorylation of AMPKα and of its substrate, acetyl-CoA carboxylase, under low-SS conditions (26–28) (*SI Appendix*, Fig. S1 *E* and *F*). To ascertain the implication of AMPKα in the regulation of endothelial autophagy by SS, we evaluated LC3 staining in endothelial cells from the aorta of mice deficient in *Ampkα1* (Fig. 3*C*). Endothelial LC3 staining in high-SS areas was

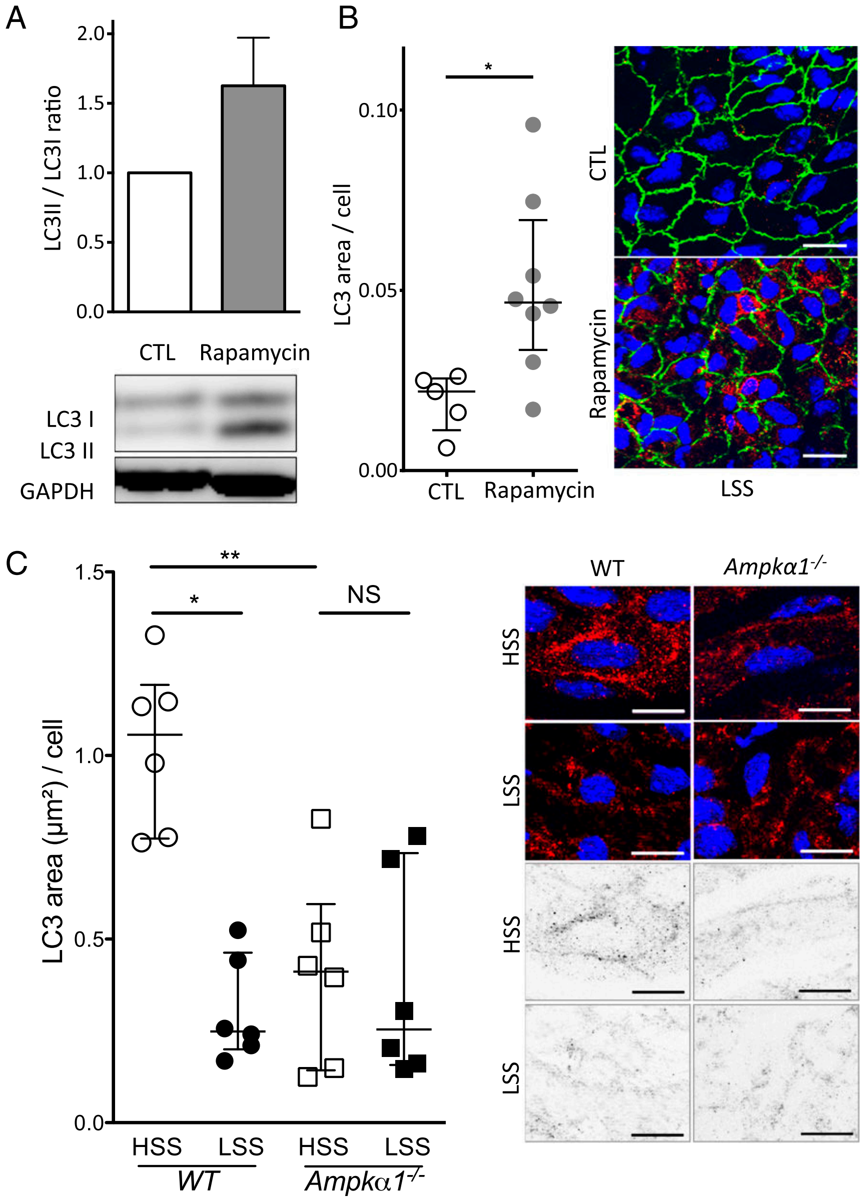

Fig. 3. Decreased AMPKα activity and increased mTOR activity concurrent with endothelial autophagy defect under low SS (LSS). (*A*) Western blot analysis of LC3II/LC3I ratio in HUVECs exposed to low SS for 24 h in the presence or absence of rapamycin (0.5 μmol/L; $n = 3$; data are normalized to static condition and are presented as mean ± SEM). (*B*) LC3 en face staining of the aorta of 9-wk-old C57BL/6 male mice injected i.p. with DMSO alone or with rapamycin (4 mg/kg/d 24 h and 4 h before euthanasia; $n = 5$ vs. $n = 8$, respectively; green, CD144; red, LC3; blue, DAPI). (Scale bar, 20 μm.) (*Left*) Quantification of LC3 area. Data are given as median (horizontal bar) and interquartile range (error bar). (*Right*) Representative images. (*C*) LC3 en face staining of the aorta of 12-wk-old *Ampkα1*-deficient and WT mice (red, LC3; blue, DAPI; $n = 6$). (Scale bar, 10 μm.) Data are given as median (horizontal bar) and interquartile range (error bar). HSS, high SS.

significantly lower in Ampkα1-deficient mice than in littermate WT mice. Moreover, endothelial LC3 labeling was not different between high- and low-SS areas of the aorta of *Ampkα1*-deficient mice, whereas it was significantly lesser in low-SS than in high-SS areas of WT mice. These results support the hypothesis that the AMPKα pathway mediates endothelial autophagy activation by high SS.

Taken together, these results demonstrate that the defect in endothelial autophagy under low-SS conditions results from an inhibition of the AMPKα and activation of the mTOR pathways and is associated with a blockade of the autophagic flux.

Atherosclerotic Lesions in Hypercholesterolemic Mice Deficient in Endothelial Autophagy. To assess the role of SS-induced autophagy on atherosclerotic plaque development, $Apoe^{-/-}$;$Atg5^{flox/flox}$;*VE-cadherin-cre* and littermate controls were fed a Western diet for 10 wk (*SI Appendix*, Fig. S2 *A* and *B*). In $Apoe^{-/-}$;$Atg5^{flox/flox}$ mice, atherosclerotic plaques formed preferentially in the curvature of the aorta, whereas the descending thoracic aorta was protected from lesion development (Fig. 4). Plaque size increased by approximately 100% in the descending thoracic aorta of mice deficient in endothelial autophagy compared with littermate controls (Fig. 4). This difference persisted even after excluding plaques at the ostia of branching arteries, which correspond to small areas of the descending thoracic aorta where SS is low (*SI Appendix*, Fig. S2*C*). Unlike the descending thoracic aorta, we observed no significant difference in plaque size in the aortic arch between the two strains (Fig. 4).

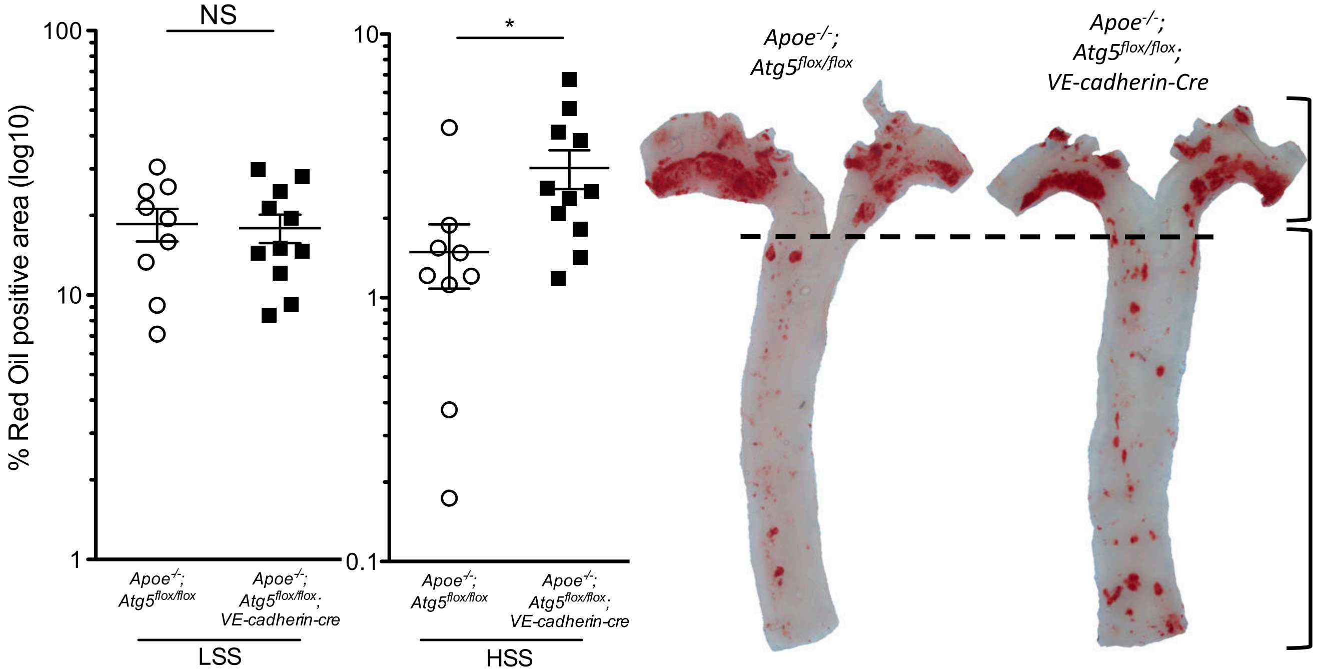

Fig. 4. Deficiency in endothelial autophagy promotes atherosclerosis. Twenty-three-week-old *Apoe*$^{-/-}$;*Atg5flox/flox* ($n = 9$) and *Apoe*$^{-/-}$;*Atg5flox/flox;VE-cadherin-cre* ($n = 11$) mice were fed a Western diet for 10 wk. Quantification of en face Oil Red O staining of atherosclerotic lesions in the aorta of these mice and representative images. (Scale bar, 1 mm.) Data are given as median (horizontal bar) and interquartile range (error bar; *$P < 0.05$, **$P < 0.01$, and ***$P < 0.001$; HSS, high SS; LSS, low SS).

Endothelial deficiency in ATG5 in the *Apoe*$^{-/-}$ mice had no effect on arterial blood pressure and cholesterol levels, body and organ weight, or blood cell count (*SI Appendix*, Table S4). Serum glucose level was significantly higher in *Apoe*$^{-/-}$;*Atg5*$^{flox/flox}$;*VE-cadherin-cre* mice than in littermate controls, but remained in the normal range, below 126 mg/dL. These data support a direct effect of endothelial autophagy on atherosclerotic plaque formation rather than an effect on systemic metabolic parameters.

Taken together, these findings demonstrate that deficiency in endothelial autophagy promotes atherosclerotic plaque formation in atheroresistant regions.

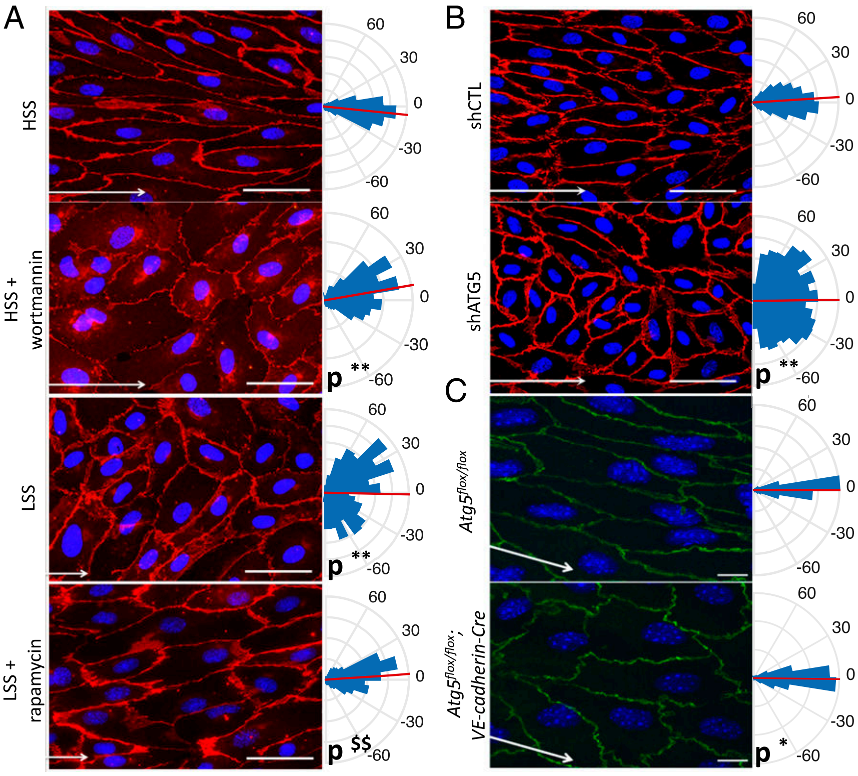

Fig. 5. Deficiency in endothelial autophagy impairs endothelial cells' ability to align in the direction of flow. (*A*) Quantification of cell alignment in the direction of flow on HUVECs treated with wortmannin [high SS (HSS)] or with rapamycin [low SS (LSS)] or not treated (red, CD144 staining; blue, DAPI; $n = 4$; more than 900 cells analyzed). (Scale bar, 50 mm.) Kuiper two-sample test: **$K_p < 0.01$ vs. WT or high-SS control, respectively; $^{\$\$}K_p < 0.01$ vs. low-SS control. White arrows represent flow direction. (*B*) Quantification of cell alignment in the direction of flow (high SS) on HUVECs infected with an shRNA control or with an shRNA targeting ATG5 (**$K_p < 0.01$). (*C*) Quantification of cell alignment in direction of flow in the linear part of the aorta (high SS) of *Atg5*$^{flox/flox}$ or *Atg5*$^{flox/flox}$;*VE-cadherin-Cre* mice (green, CD144 staining; blue, DAPI; $n = 6$; *$K_p < 0.05$). (Scale bar, 10 μm.) All panels display representative images (*Left*) and quantifications (*Right*), which are shown as rose-plot representations of endothelial axial polarity. Arcs represent cell angle with flow direction, red lines the mean of cell angle, and blue triangles the percentage of cells aligned in each direction. Each triangle represents a range of 10°.

Deficiency in Endothelial Autophagy Disturbs Endothelial Alignment in Response to Flow. The presence of lesions in areas that are normally resistant to atherosclerosis suggested a role for defective endothelial autophagy in the impairment of flow-dependent atheroprotective mechanisms. We first examined endothelial cell alignment, which is a hallmark of atheroresistant areas and plays an important role in the flow-dependent activation of antiinflammatory vs. proinflammatory pathways (3, 29, 30). We observed that HUVECs failed to align with the direction of flow under high SS when autophagy was inhibited by a pharmacological approach (i.e., wortmannin) or a genetic approach (i.e., a lentivirus expressing an ATG5 shRNA; Fig. 5 *A* and *B*). Conversely, activation of autophagy by using rapamycin in HUVECs exposed to low SS induced an alignment in flow direction (Fig. 5*A*). To investigate the relevance of these findings in vivo, we generated two models of mice deficient in endothelial autophagy, *Atg5*$^{flox/flox}$;*VE-cadherin-cre* and *Atg7*$^{flox/flox}$;*VE-cadherin-cre* mice (*SI Appendix*, Fig. S3). In these transgenic mice, deficiency in endothelial ATG5 or ATG7 had no effect on arterial blood pressure, serum glucose and cholesterol levels, or body weight, but spleen and heart weights were slightly higher in *Atg7*$^{flox/flox}$;*VE-cadherin-cre* mice but not in *Atg5*$^{flox/flox}$;*VE-cadherin-cre* (*SI Appendix*, Tables S5 and S6). In line with the observations made in vitro, endothelial alignment in the direction of flow was disturbed in high-SS areas of the aorta of mice deficient in ATG5 or ATG7 (Fig. 5*C* and *SI Appendix*, Fig. S4).

Role of PECAM-1 and of the Primary Cilium in SS Dependent Regulation of Endothelial Autophagy. One of the main flow sensors in endothelial cells is the complex formed by PECAM-1 (CD31), VE-cadherin, and VEGFR2 (31). As this complex is involved in cell orientation under flow, we evaluated its contribution to the regulation of endothelial autophagic flux. Decreasing PECAM-1 expression in HUVECs did not change the effect of high and low SS on the LC3II/LC3I ratio (*SI Appendix*, Fig. S5*A*). Similarly, LC3 en face staining of the aorta of *CD31*$^{-/-}$ mice showed the persistence of the enhanced autophagy level in high-SS areas compared with low-SS areas (*SI Appendix*, Fig. S5*B*). The primary cilium is another mechanosensor expressed by endothelial cells (32) and differentially regulated between high- and low-SS areas. Recent data indicate that the primary cilium can regulate autophagy in epithelial cells (33). To determine whether the primary cilium mediates the effect of SS on endothelial autophagy in HUVECs, we silenced KIF3a, a protein essential for primary cilium function, and exposed these cells to high and low SS. As shown in *SI Appendix*, Fig. S5*C*, the effect of SS on LC3II/LC3I ratio was not modified by the deficiency in KIF3a. Altogether, these data indicate that the mechanosensor mediating endothelial SS effect on autophagy is neither PECAM-1 nor the primary cilium.

Deficiency in Endothelial Autophagy Promotes Endothelial Inflammation. We then tested whether autophagy regulates endothelial inflammatory responses in high-SS conditions. Under control conditions, expression of KLF2 and ICAM-1 and release of MCP-1 were not different between HUVECs transduced with a lentivirus expressing an ATG5 shRNA and control cells (Fig. 6 *A*–*C*). By contrast, after exposure to the proinflammatory stimulus TNF-α, HUVECs deficient in autophagy expressed significantly less KLF2 and more ICAM-1 and released more MCP-1 than HUVECs transduced with a control shRNA (Fig. 6 *D*–*F*). This effect was not associated with an increase in autophagy level following TNF-α exposure (*SI Appendix*, Fig. S6). Altogether, these results establish that activation of endothelial autophagy by high SS is required for curbing the response to proinflammatory stimuli.

Deficiency in Endothelial Autophagy Leads to Endothelial Apoptosis. Previous in vitro data have suggested that high SS-induced autophagy could prevent apoptosis induced by H_2O_2 in endothelial cells (14). In WT mice, as expected, en face TUNEL staining showed more apoptotic nuclei in endothelial cells of the inner part of the curvature of the aortic arch exposed to low SS than in those of the linear part of the aorta exposed to high SS (7) (Fig. 7*A*). Interestingly, the linear part of the aorta of mice deficient in endothelial ATG5 contained fivefold more apoptotic cells than the same area of WT mice (Fig. 7*A*). As p53 controls apoptosis, we analyzed endothelial p53 expression in vivo. We exposed 13–17-wk-old mice deficient or not in ATG5 to a high-fat diet for 5 wk as reported previously (9) (*SI Appendix*, Fig. S7*A*). We observed that mice deficient in endothelial autophagy had twice as many p53-positive nuclei in the linear part of the aorta as the controls (Fig. 7*B*). These results show that activation of endothelial autophagy by high SS prevents apoptosis.

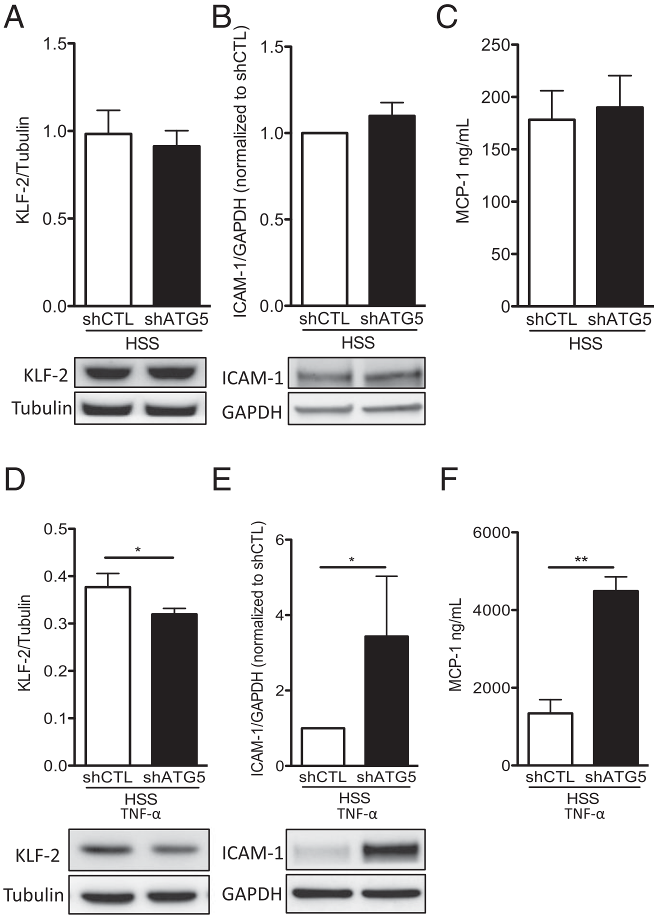

Fig. 6. Deficiency in endothelial autophagy promotes endothelial inflammation. HUVECs were transduced with a lentivirus expressing an Atg5 or a control (CTL) shRNA and exposed to high SS (HSS) for 24 h without (*A*–*C*) or with (*D*–*F*) TNF-α (1 ng/mL) for the last 12 h. (*A* and *D*) Western blot quantification of KLF-2 expression in HUVEC ($n = 6$ and $n = 5$, respectively). Data are given as mean (horizontal bar) and SEM (error bar). (*B* and *E*) Western blot quantification of ICAM-1 expression in HUVEC ($n = 4$ and $n = 6$, respectively). (*C* and *F*) Quantification of MCP1 in the supernatants of HUVECs by ELISA ($n = 8$ and $n = 6$, respectively; $^{*}P < 0.05$ and $^{**}P < 0.01$).

Deficiency in Endothelial Autophagy Leads to Endothelial Senescence. As p53 also regulates senescence, we thus evaluated the role of SS-induced autophagy on endothelial senescence in cultured cells and in mice. HUVECs exposed to low SS displayed higher senescence-associated (SA)–β-gal activity than those exposed to high SS, confirming that low SS induces senescence in endothelial cells (9) (Fig. 8*A*). Pharmacological inhibition of autophagy using wortmannin under high SS increased endothelial senescence to levels similar to

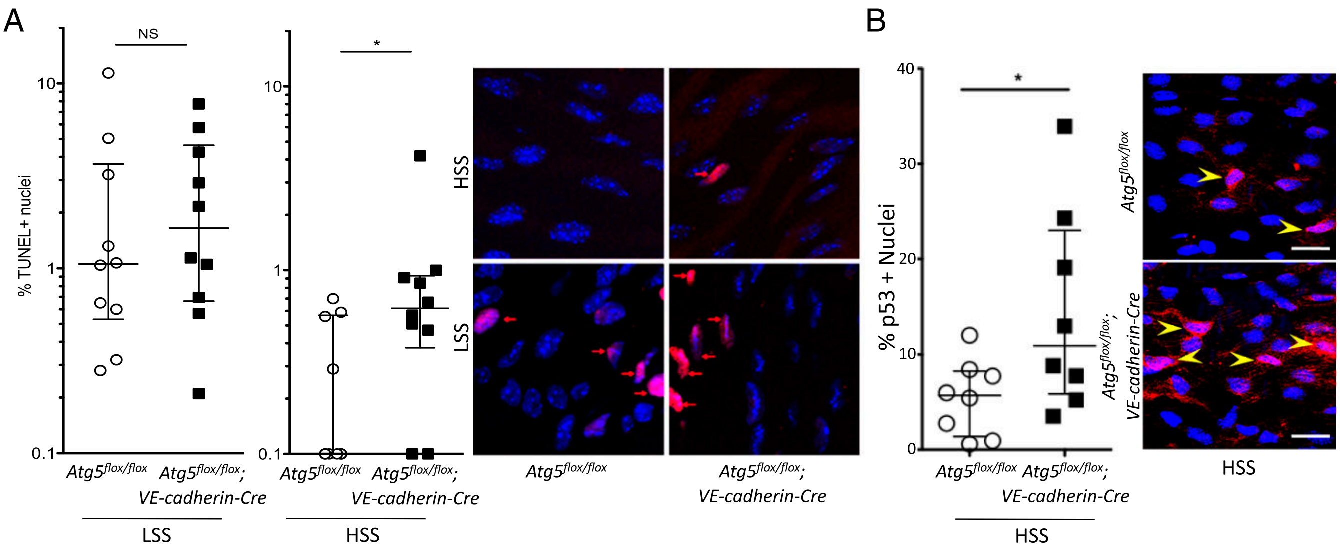

Fig. 7. Deficiency in endothelial autophagy increases apoptosis. (*A*) En face TUNEL staining of the aorta of 10-wk-old *Atg5*$^{flox/flox}$ vs. *Atg5*$^{flox/flox}$;*VE-cadherin-Cre* mice (red, TUNEL; blue, DAPI; $n = 10$). Data are given as median (horizontal bar) and interquartile range (error bar). (*B*) En face p53 staining of the descendant linear aorta [high SS (HSS)] of 13–17-wk-old *Atg5*$^{flox/flox}$ vs. *Atg5*$^{flox/flox}$;*VE-cadherin-Cre* mice fed a high-fat diet for 5 wk (red, p53; blue, DAPI; $n = 8$ per group). (Scale bar, 20 μm.) LSS, low SS; NS, not significant ($^*P < 0.05$).

those of HUVECs exposed to low-SS conditions (Fig. 8*A*). Similarly, inhibition of autophagy in HUVECs under high SS using a lentivirus expressing an ATG5 shRNA increased p16 protein expression by fourfold (Fig. 8*B*). Conversely, pharmacological activation of autophagy using rapamycin under low SS reduced senescence to a level similar to that of HUVECs exposed to high SS (Fig. 8*A*).

To assess senescence in vivo, we performed p16 en face staining on the thoracic descending part of the aorta of *Atg5*$^{flox/flox}$;*VE-cadherin-cre* vs. *Atg5*$^{flox/flox}$ mice, and observed that mice deficient in endothelial autophagy had twice as many p16-positive nuclei as the controls, attesting to a more senescent phenotype (Fig. 8*C*). To confirm these findings, we exposed 48-wk-old mice deficient in ATG5 or ATG7 and their littermate controls to a high-fat diet for 16 wk, a regimen used to better evidence endothelial senescence in vivo (34) (*SI Appendix*, Fig. S7*B*). There was no difference in serum glucose and cholesterol levels or in body and organ weight between mice deficient or not in endothelial autophagy for both models except for a slightly lower liver weight in *Atg5*$^{flox/flox}$;*VE-cadherin-cre* mice and a slightly higher heart weight in *Atg7*$^{flox/flox}$;*VE-cadherin-cre* than in littermate controls (*SI Appendix*, Tables S7 and S8). We evaluated senescence by en face SA–β-gal staining in both mouse models. As expected, in control animals, endothelial senescence was greater in the inner part of the curvature of the aortic cross, corresponding to a low-SS area, than in areas exposed to high SS (9) (Fig. 8*D* and *SI Appendix*, Fig. S7*C*). Interestingly, mice deficient in endothelial ATG5 as well as those deficient in endothelial ATG7 had 2.5 fold more senescent endothelial cells in high-SS areas of the aorta than littermate controls, whereas senescence in low-SS areas was unchanged (Fig. 8*D* and *SI Appendix*, Fig. S7*C*). Altogether, these data demonstrate that activation of endothelial autophagy by high SS protects against senescence and suggest that defective autophagy in low-SS areas is responsible for premature senescence in these regions.

Discussion

This study demonstrates that a defect in endothelial autophagy occurs in low-SS areas, impairing endothelial cell alignment in response to flow and causing endothelial inflammation, apoptosis, and senescence, thus favoring the development of atherosclerotic lesions.

The first major finding in this study was that low SS induces a defect in endothelial autophagy as a result of mTOR activation and AMPKα pathway inhibition. Conversely, high SS strongly activates autophagy. Previous analyses of the effect of various SS conditions on endothelial autophagy gave conflicting results in cultured cells (14, 16–18, 21). Fewer studies are available on blood vessels, but their results either lack sensitivity, as they were obtained with lysates from the entire arterial wall, where endothelial cells are quantitatively negligible (16, 18, 21), or used p62 immunohistochemistry, a molecule known to be regulated by SS (14, 16). Our results fill this gap in knowledge, as we observed, in human arteries, in aortas from mouse, and in cultured endothelial cells, a lower autophagy level in endothelial cells exposed to low compared with high SS. The difference in autophagic flux between the two conditions is even larger than that reflected by the LC3II/ LC3I ratio and the LC3 punctate signal we present. Indeed, under low SS, autophagic flux is blocked, leading to LC3II accumulation. Although sex differences in autophagy in various tissues have been reported in certain settings, we observed the same regulation of endothelial autophagy by SS in male and in female mice (35).

A second major finding in the present study was that a defect in endothelial autophagy enhances atherosclerotic plaque development specifically in high-SS areas where alignment of endothelial cells in the flow direction was impaired, and inflammation, apoptosis, and senescence were increased. We also tested major endothelial mechanosensors and found that neither PECAM-1, which is part of the PECAM-1/VE-cadherin/VEGFR2 complex, nor the primary cilium were implicated in signal transmission for autophagy regulation (3). The previously described endothelial dysfunction and lipid retention associated with endothelial autophagy deficiency may also contribute to atherosclerosis (13, 36). The effects we observed in the present study were not mediated by an impact on cardiovascular risk factors, as body weight, arterial blood pressure, and plasma cholesterol levels were not influenced by the deficiency in endothelial autophagy in basal conditions or under Western diet. Fasting serum glucose levels were only slightly higher in *Apoe*$^{-/-}$;*Atg5*$^{flox/flox}$;*VE-cadherin-cre* mice compared with littermate controls. However, such mild changes likely do not explain the effect we observed on atherosclerosis. Our observation that the increase in the proatherogenic phenotype and in plaque size in mice deficient in endothelial autophagy was restricted to high-SS areas implies that, under high atheroprotective SS, the autophagy level is high and prevents atherosclerosis development. Conversely, under low atherogenic SS,

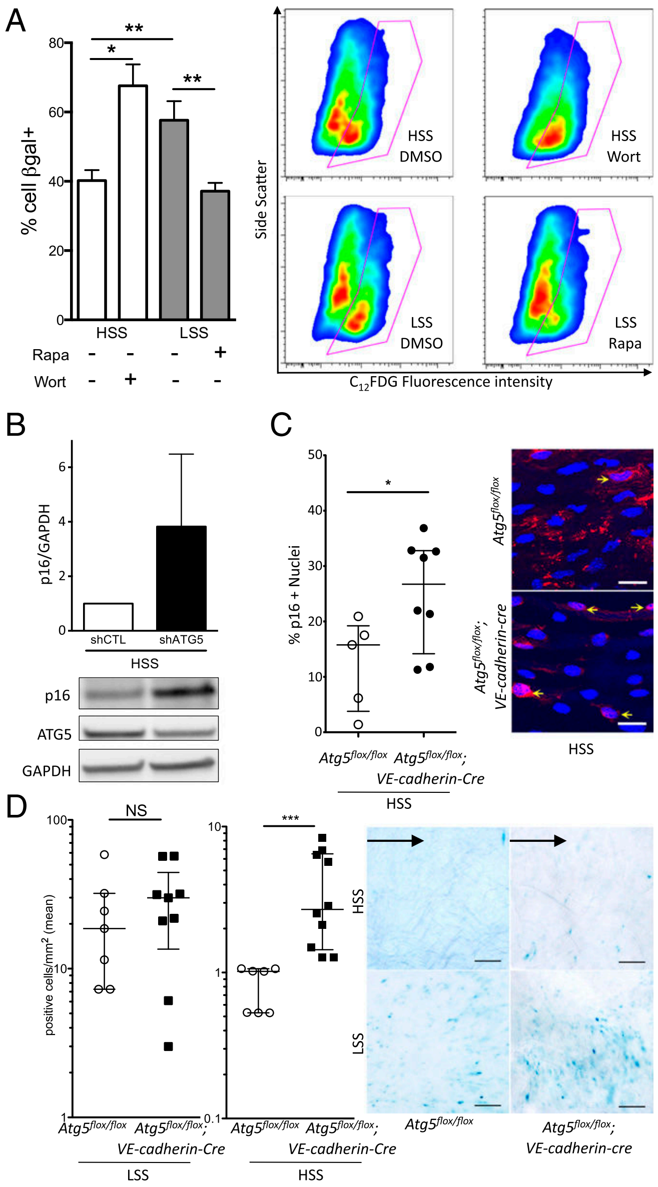

Fig. 8. Deficiency in endothelial autophagy increases senescence. (*A*) SA–β-gal activity evaluated by flow cytometry in HUVECs exposed for 24 h to high SS (HSS) with or without wortmannin (5 μmol/L) or to low SS (LSS) with or without rapamycin (0.5 μmol/L; $n \geq 6$ per condition). (*B*) Western blot analysis of p16 expression in HUVECs transduced with a lentivirus expressing an Atg5 or a control (CTL) shRNA and exposed to high SS for 24 h (shRNA induction by 1 mmol/L IPTG, $n = 5$). (*C*) En face p16 staining of the descendant linear aorta (high SS) of 48-wk-old *Atg5*$^{flox/flox}$ vs. *Atg5*$^{flox/flox}$;*VE-cadherin-Cre* mice fed a chow diet (red, p16; blue, DAPI; $n = 5$ and $n = 8$, respectively). (Scale bar, 20 μm.) (*D*) En face SA–β-gal staining of the aorta of 48-wk-old *Atg5*$^{flox/flox}$ vs. *Atg5*$^{flox/flox}$; *VE-cadherin-Cre* mice fed a high-fat diet ($n = 6$ and $n = 9$, respectively). (Scale bar, 100 μm.) Black arrow represents flow direction. The inner part of the curvature is exposed to low SS, and the descendant linear part is exposed to high SS. IPTG, isopropyl β-D-1-thiogalactopyranoside; NS, not significant ($^{*}P < 0.05$, $^{**}P < 0.01$, and $^{***}P < 0.001$).

endothelial autophagy is defective, resulting in cell death, senescence, and inflammation, which favor atherosclerosis development. The mechanisms linking SS-regulated endothelial autophagy with these various cell processes deserve further study. We can yet speculate that defective endothelial autophagy in low-SS areas induces the accumulation of damaged mitochondria, which causes increased formation of mitochondrial reactive oxygen species (37) and eventually apoptosis, senescence, and inflammation. Indeed, low or disturbed SS is known to decrease mitochondrial respiration rate and to increase mitochondrial membrane potential and superoxide anion production in endothelial cells, which can lead to endothelial apoptosis, senescence, and inflammation (11, 38, 39). Our results provide insights in the understanding of the mechanisms regulating plaque development preferentially in low- vs. high-SS areas. Our findings showing atheroprotective effects of endothelial autophagy are in line with previous studies showing that defective autophagy in vascular smooth muscle cells and macrophages promotes atherosclerosis formation and/or development (40–43). Altogether, these data indicate that inhibition of autophagy would be unfavorable as a therapeutic approach in the treatment of atherosclerosis, whereas stimulation of autophagy may be an attractive strategy.

In conclusion, low-SS atheroprone areas are characterized by low and inefficient endothelial autophagy, which triggers a defect in cell alignment as well as endothelial inflammation, apoptosis, and senescence, thereby setting the stage for the initial development of atherosclerotic lesions (Fig. 9). The defect in endothelial autophagy observed in low-SS areas may thus be the missing link between low SS and atherosclerosis development in these specific regions.

Materials and Methods

The *SI Appendix* includes further details of the study's materials and methods.

Endothelial Immunofluorescence in Human Carotid Arteries. Human atherosclerotic plaques obtained from five patients were remnants of the surgical specimens routinely processed for pathologic examination following en bloc carotid endarterectomy surgery, which was performed after patient consent (*SI Appendix*, Table S1). Institutional review board approval was not required for the human specimens at the time the work was done. The upstream part was identified from the downstream area of the lesion by using a silk thread. Endothelial cells from the upstream (i.e., high-SS) or downstream (i.e., low-SS) part of the plaque were collected separately (7, 44). Cells were fixed in 4% paraformaldehyde, permeabilized, incubated with an anti-LC3 antibody (*SI Appendix*, Table S2), and costaining with anti-CD31 antibody and DAPI.

HUVEC Culture. Confluent HUVECs (passage 2–4; 10 different primary cultures; Promocell) were cultured on 0.2% gelatin-coated slides in endothelial cell basal medium containing growth factors, 1% FCS (Promocell), streptomycin (100 IU/mL), penicillin (100 IU/mL), and amphotericin B (10 μg/L).

Plasmid Electroporation. DNA vector encoding the tandem mRFP-GFP-LC3 was used to transiently express the RFP-GFP–tagged LC3 protein to monitor the LC3 translocation and autophagosome fusion with lysosomes. In the absence of autophagy induction, the LC3 fluorescent signals are evenly distributed; upon autophagy induction, punctate fluorescent signals (i.e., yellow LC3 dots) appear as a result of LC3 accumulation on the membrane of autophagosomes; when fusion with lysosomes occurs, the punctate signal becomes red by acidic degradation of the GFP. Transfection efficacy was assessed by expression of fluorescent LC3 protein.

Lentiviral Transduction. Lentiviruses expressing inducible shRNA (Sigma-Aldrich) were used to silence Kinesin-like protein (i.e., KIF3A), ATG5, and CD31. HUVECs were infected in the presence of hexadimethrine bromide with lentiviruses. Negative controls were lentiviruses expressing a nontarget shRNA used at the same multiplicity of infection as for the protein of interest. Transduced cells were amplified and selected by using puromycin, and ShRNA expression was induced by using isopropyl β-D-1-thiogalactopyranoside.

SS Experiment in Vitro. A unidirectional steady laminar SS was applied to confluent HUVECs by using a parallel plate chamber system as described elsewhere (45). Endothelial cell medium previously filtered on a 0.1-μm membrane was perfused at different rates and for different times (1 min to 48 h). Local SS was calculated per Poiseuille's law and was 20, 2, or 0 dyn/cm^2, corresponding to high-SS, low-SS, or static conditions, respectively.

Immunofluorescent Staining and Immunofluorescence Microscopy in Vitro. To assess autophagy flux, permeabilized cells were incubated with an anti-LC3 antibody and an anti-LAMP2 antibody (*SI Appendix*, Table S2) and then with secondary antibody. For assessment of the morphology and orientation of

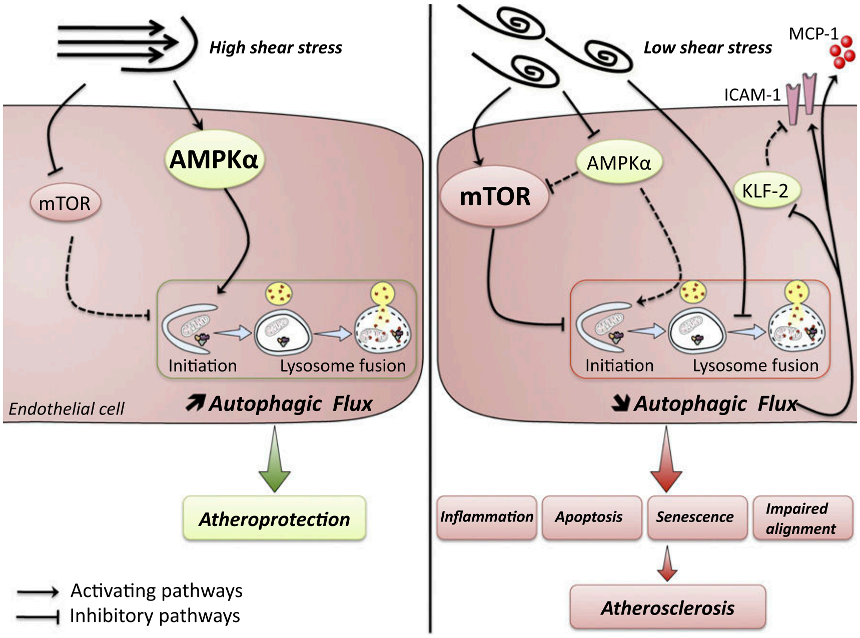

Fig. 9. Schematic illustration depicting the links between SS, autophagy, and atherosclerotic plaque formation. Under high laminar SS, endothelial autophagy is strongly induced and plays an antiapoptotic, antisenescent, antiinflammatory, and antiatherogenic role. Under low SS, a defect in endothelial autophagy occurs as a result of an inhibition of the AMPKα and activation of the mTOR pathways together with a blockade of the fusion between autophagosomes with lysosomes. This defect in endothelial autophagy leads to endothelial apoptosis, senescence, and inflammation, eventually increasing atherosclerosis development. ICAM-1, intercellular adhesion molecule 1; KLF-2, Krüppel-like factor 2; MCP-1, monocyte chemoattractant protein 1. Solid lines indicate up-regulated pathways. Dashed lines indicate down-regulated pathways.

endothelial cells under SS, HUVECs were stained with an anti-CD144 antibody. Samples were costained with DAPI to identify cell nuclei.

Transmission EM. For transmission EM experiments, the term "autophagic vesicle" refers to autophagosome or autolysosome, as it is often not possible to determine from transmission EM images whether an autophagosome has fused with a lysosome (46).

In Vitro LC3 Assessment Using Flow Cytometry. After exposure to SS, HUVECs were permeabilized by using 0.2% saponin, which specifically extracts the non–autophagosome-associated form of LC3 (47). Then, HUVECs were fixed in ethanol and incubated with an anti-LC3 antibody (47) (*SI Appendix*, Table S2). Costaining with propidium iodide for 5 min before flow-cytometry analysis was performed to identify live cells and exclude cell aggregates.

Senescence-Associated β-Gal Activity in Vitro. SA–β-gal activity was assessed by flow cytometry by using a fluorogenic substrate (C_{12}FDG; Invitrogen). After exposure to SS, HUVECs were pretreated with chloroquine diluted in medium without Phenol Red to increase the internal pH of lysosomes to 6. C_{12}FDG was then added to the medium. HUVECs were then washed and analyzed immediately. Cells not treated with C_{12}FDG were used as a negative control.

Animal Models. All mice were on a C57BL/6 background with the exception of $Ampk\alpha 1^{-/-}$ mice, which were on a mixed C57Bl6/129 Sv background as a result of embryonic lethality on C57Bl6 background.

Mice constitutively deficient in endothelial autophagy were obtained by crossing *VE-cadherin-Cre* transgenic mice provided by Oberlin et al. (48) with $Atg5^{flox/flox}$ mice provided by N. Mizushima as described by Hara et al. (49) or $Atg7^{flox/flox}$ mice provided by Komatsu et al. (50). Baseline morphological and metabolic features were observed, and endothelial apoptosis was assessed, in 8–17-wk-old mice fed a chow diet. For p53 experiments, 13–17-wk-old mice were fed a high fat diet for 5 wk (9). For assessment of endothelial senescence, 42–54 wk-old mice were fed the same high-fat diet for 16 wk (34). For investigation of autophagic flux in vivo, 8–9-wk-old C57BL/6 mice were injected i.p. with chloroquine (51), rapamycin (4 mg/kg/d for two consecutive days), or vehicle. To investigate the effect of endothelial autophagy on atherosclerosis development, mice constitutively deficient in endothelial autophagy ($Atg5^{flox/flox}$;*VE-cadherin-Cre*) were crossed with $ApoE^{-/-}$ mice purchased from Charles River Laboratory. Thirteen-week-old mice were fed a Western diet for 10 wk. AMPK$\alpha 1^{-/-}$ mice were described previously (52). $CD31^{-/-}$ mice were provided by Duncan et al. (53). All experiments were performed in accordance with the European Community guidelines for the care and use of laboratory animals (no. 07430) and were approved by the institutional ethical committee (no. 02526.02).

Senescence-Associated β-Gal Assay on Mouse Aortas. SA–β-gal staining was performed by incubating the aortas for 48 h at 37 °C in a CO_2-free incubator with a fresh staining solution containing 1 mg/mL X-gal. After staining, aortas were mounted en face on glass slides and imaged by using a bright-field AxioImager Z1 microscope (Zeiss).

Red-Oil Staining. Aortas were stained with a freshly prepared Oil Red O working solution, differentiated by using 70% ethanol, mounted en face, and then observed by using a bright-field microscope.

Murine Aortic Endothelial Cell Isolation. After exposure to type II collagenase, mouse aortic endothelial cells (MAECs) were collected from the aortas and seeded in a 0.1% gelatin-coated plate in DMEM supplemented with 20% FCS. MAECs were used for Western blot analysis after one passage.

En Face Immunofluorescence Microscopy on Mouse Aortas. Mouse aortas were fixed with paraformaldehyde and permeabilized by using Triton X-100. Tissues were then exposed to an anti-LC3, an anti-p53, or an anti-p16 antibody (*SI Appendix*, Table S2) and then to the respective secondary antibody. To assess apoptosis level, aortas were stained with the in situ cell death detection kit from Roche (red). In all experiments, endothelial cells were recognized by their morphology. Still, in most series of experiments, costaining with anti-CD31 antibody or anti-CD144 antibody was performed. In all mice, 8–10 images were obtained from regions in the aortic arch exposed to low SS and the thoracic aorta exposed to high SS.

Immunoblotting. HUVEC or MAEC lysates were mixed with reducing sample buffer for electrophoresis and subsequently transferred onto nitrocellulose for all blots except for p16, KLF-2, p-ACC, and ACC (PVDF membranes). Equal loading was checked by using Ponceau red solution. Membranes were incubated with primary antibodies (*SI Appendix*, Table S2). After secondary antibody incubation, immunodetection was performed by using an enhanced chemiluminescence kit [Immun-Star Western C kit (Bio-Rad) or

WesternBright Sirius (Advansta) for p16 blot], and bands were revealed by using the Las-4000 imaging system. After initial immunodetection, membranes were stripped of antibodies and reprobed with anti-GAPDH, anti-actin, or anti anti-tubulin antibodies (*SI Appendix*, Table S2).

Statistical Analysis. Data are expressed as mean ± SEM for in vitro experiments and as median (interquartile range) for in vivo experiments. Comparisons between different SS conditions or between control and treatment conditions were performed by using a Wilcoxon test. Comparisons between groups of mice were performed by using the Mann–Whitney *U* test. Comparison between sexes was performed by using a χ^2 test. Statistical analyses and figures were performed by using the SPSS statistical package software for Windows (version 20.0; SPSS) and GraphPad Prism 5 software, respectively. All tests were two-sided and used a significance level of 0.05.

Data Sharing. The data that support the findings of this study are available from the corresponding author on request.

ACKNOWLEDGMENTS. The authors acknowledge Lamia Ouchia and Marion Tanguy for their helpful contributions, Alain Grodet and Cyrielle Sophie for technical assistance in EM, the members of the INSERM U970 ERI facility, N. Mizushima for providing *Atg5*$^{flox/flox}$ mice, M. Komatsu for providing *Atg7*$^{flox/flox}$ mice, and T. W. Mak and G. Caliguiri for providing *CD31*$^{-/-}$ mice. This work was supported by the Institut National de la Santé et de la Recherche Médicale, Paris Descartes University; Fondation pour la Recherche Médicale Grant DPC20111122979; Agence Nationale pour la Recherche Grants ANR-14-CE12-0011, ANR-14-CE35-0022, and ANR-16-CE14-0015-01; Association Francaise pour l'Etude du foie Grant AFEF 2014; poste d'accueil INSERM (J.P.); Cardiovasculaire, Obésité, Diabète Domaine d'Interêt Majeur Ile de France (A.-C.V.); Ministère de la Recherche et de l'Enseignement Supérieur (M.K. and A.H.); and Fondation pour la Recherche Médicale Grant FDT20160435690 (to M.K.).

1. Chiu JJ, Chien S (2011) Effects of disturbed flow on vascular endothelium: Pathophysiological basis and clinical perspectives. *Physiol Rev* 91:327–387.
2. Gimbrone MA, Jr, García-Cardeña G (2013) Vascular endothelium, hemodynamics, and the pathobiology of atherosclerosis. *Cardiovasc Pathol* 22:9–15.
3. Hahn C, Schwartz MA (2009) Mechanotransduction in vascular physiology and atherogenesis. *Nat Rev Mol Cell Biol* 10:53–62.
4. Lusis AJ (2000) Atherosclerosis. *Nature* 407:233–241.
5. Bombeli T, Schwartz BR, Harlan JM (1999) Endothelial cells undergoing apoptosis become proadhesive for nonactivated platelets. *Blood* 93:3831–3838.
6. Dimmeler S, Haendeler J, Rippmann V, Nehls M, Zeiher AM (1996) Shear stress inhibits apoptosis of human endothelial cells. *FEBS Lett* 399:71–74.
7. Tricot O, et al. (2000) Relation between endothelial cell apoptosis and blood flow direction in human atherosclerotic plaques. *Circulation* 101:2450–2453.
8. Minamino T, et al. (2002) Endothelial cell senescence in human atherosclerosis: Role of telomere in endothelial dysfunction. *Circulation* 105:1541–1544.
9. Warboys CM, et al. (2014) Disturbed flow promotes endothelial senescence via a p53-dependent pathway. *Arterioscler Thromb Vasc Biol* 34:985–995.
10. Bai B, et al. (2012) Cyclin-dependent kinase 5-mediated hyperphosphorylation of sirtuin-1 contributes to the development of endothelial senescence and atherosclerosis. *Circulation* 126:729–740.
11. Davies PF, Civelek M, Fang Y, Fleming I (2013) The atherosusceptible endothelium: Endothelial phenotypes in complex haemodynamic shear stress regions in vivo. *Cardiovasc Res* 99:315–327.
12. Choi AM, Ryter SW, Levine B (2013) Autophagy in human health and disease. *N Engl J Med* 368:1845–1846.
13. Torisu K, et al. (2016) Intact endothelial autophagy is required to maintain vascular lipid homeostasis. *Aging Cell* 15:187–191.
14. Liu J, et al. (2015) Shear stress regulates endothelial cell autophagy via redox regulation and Sirt1 expression. *Cell Death Dis* 6:e1827.
15. Lien SC, et al. (2013) Mechanical regulation of cancer cell apoptosis and autophagy: Roles of bone morphogenetic protein receptor, Smad1/5, and p38 MAPK. *Biochim Biophys Acta* 1833:3124–3133.
16. Li R, et al. (2015) Disturbed flow induces autophagy, but impairs autophagic flux to perturb mitochondrial homeostasis. *Antioxid Redox Signal* 23:1207–1219.
17. Guo F, et al. (2014) Autophagy regulates vascular endothelial cell eNOS and ET-1 expression induced by laminar shear stress in an ex vivo perfused system. *Ann Biomed Eng* 42:1978–1988.
18. Ding Z, et al. (2015) Hemodynamic shear stress modulates endothelial cell autophagy: Role of LOX-1. *Int J Cardiol* 184:86–95.
19. Bharath LP, et al. (2014) Impairment of autophagy in endothelial cells prevents shear-stress-induced increases in nitric oxide bioavailability. *Can J Physiol Pharmacol* 92:605–612.
20. Yao P, Zhao H, Mo W, He P (2016) Laminar shear stress promotes vascular endothelial cell autophagy through upregulation with Rab4. *DNA Cell Biol* 35:118–123.
21. Hashem SI, et al. (2015) Brief report: Oxidative stress mediates cardiomyocyte apoptosis in a human model of Danon disease and heart failure. *Stem Cells* 33:2343–2350.
22. Klionsky DJ, et al. (2016) Guidelines for the use and interpretation of assays for monitoring autophagy (3rd edition). *Autophagy* 12:1–222, and erratum (2016) 12:443.
23. Ku DN, Giddens DP, Zarins CK, Glagov S (1985) Pulsatile flow and atherosclerosis in the human carotid bifurcation. Positive correlation between plaque location and low oscillating shear stress. *Arteriosclerosis* 5:293–302.
24. Zarins CK, et al. (1983) Carotid bifurcation atherosclerosis. Quantitative correlation of plaque localization with flow velocity profiles and wall shear stress. *Circ Res* 53:502–514.
25. Gatica D, Chiong M, Lavandero S, Klionsky DJ (2015) Molecular mechanisms of autophagy in the cardiovascular system. *Circ Res* 116:456–467.
26. Guo D, Chien S, Shyy JY (2007) Regulation of endothelial cell cycle by laminar versus oscillatory flow: Distinct modes of interactions of AMP-activated protein kinase and Akt pathways. *Circ Res* 100:564–571.
27. Zhang Y, et al. (2006) AMP-activated protein kinase is involved in endothelial NO synthase activation in response to shear stress. *Arterioscler Thromb Vasc Biol* 26:1281–1287.
28. Kröller-Schön S, et al. (2012) α1AMP-activated protein kinase mediates vascular protective effects of exercise. *Arterioscler Thromb Vasc Biol* 32:1632–1641.
29. Chien S (2007) Mechanotransduction and endothelial cell homeostasis: The wisdom of the cell. *Am J Physiol Heart Circ Physiol* 292:H1209–H1224.
30. Wang C, Baker BM, Chen CS, Schwartz MA (2013) Endothelial cell sensing of flow direction. *Arterioscler Thromb Vasc Biol* 33:2130–2136.
31. Tzima E, et al. (2005) A mechanosensory complex that mediates the endothelial cell response to fluid shear stress. *Nature* 437:426–431.
32. Egorova AD, van der Heiden K, Poelmann RE, Hierck BP (2012) Primary cilia as biomechanical sensors in regulating endothelial function. *Differentiation* 83:S56–S61.
33. Orhon I, Dupont N, Pampliega O, Cuervo AM, Codogno P (2015) Autophagy and regulation of cilia function and assembly. *Cell Death Differ* 22:389–397.
34. Wang CY, et al. (2009) Obesity increases vascular senescence and susceptibility to ischemic injury through chronic activation of Akt and mTOR. *Sci Signal* 2:ra11.
35. Gottlieb RA, Andres AM, Sin J, Taylor DP (2015) Untangling autophagy measurements: All fluxed up. *Circ Res* 116:504–514.
36. LaRocca TJ, et al. (2012) Translational evidence that impaired autophagy contributes to arterial ageing. *J Physiol* 590:3305–3316.
37. Mai S, Muster B, Bereiter-Hahn J, Jendrach M (2012) Autophagy proteins LC3B, ATG5 and ATG12 participate in quality control after mitochondrial damage and influence lifespan. *Autophagy* 8:47–62.
38. Bretón-Romero R, et al. (2014) Laminar shear stress regulates mitochondrial dynamics, bioenergetics responses and PRX3 activation in endothelial cells. *Biochim Biophys Acta* 1843:2403–2413.
39. Paneni F, Diaz Cañestro C, Libby P, Lüscher TF, Camici GG (2017) The aging cardiovascular system: Understanding it at the cellular and clinical levels. *J Am Coll Cardiol* 69:1952–1967.
40. Grootaert MO, et al. (2015) Defective autophagy in vascular smooth muscle cells accelerates senescence and promotes neointima formation and atherogenesis. *Autophagy* 11:2014–2032.
41. De Meyer GR, et al. (2015) Autophagy in vascular disease. *Circ Res* 116:468–479.
42. Razani B, et al. (2012) Autophagy links inflammasomes to atherosclerotic progression. *Cell Metab* 15:534–544.
43. Liao X, et al. (2012) Macrophage autophagy plays a protective role in advanced atherosclerosis. *Cell Metab* 15:545–553.
44. Choi G, et al. (2015) Coronary artery axial plaque stress and its relationship with lesion geometry: Application of computational fluid dynamics to coronary CT angiography. *JACC Cardiovasc Imaging* 8:1156–1166.
45. Ramkhelawon B, et al. (2009) Shear stress regulates angiotensin type 1 receptor expression in endothelial cells. *Circ Res* 105:869–875.
46. Eskelinen EL (2005) Maturation of autophagic vacuoles in mammalian cells. *Autophagy* 1:1–10.
47. Eng KE, Panas MD, Karlsson Hedestam GB, McInerney GM (2010) A novel quantitative flow cytometry-based assay for autophagy. *Autophagy* 6:634–641.
48. Oberlin E, et al. (2010) VE-cadherin expression allows identification of a new class of hematopoietic stem cells within human embryonic liver. *Blood* 116:4444–4455.
49. Hara T, et al. (2006) Suppression of basal autophagy in neural cells causes neurodegenerative disease in mice. *Nature* 441:885–889.
50. Komatsu M, et al. (2005) Impairment of starvation-induced and constitutive autophagy in Atg7-deficient mice. *J Cell Biol* 169:425–434.
51. Orhon I, et al. (2016) Primary-cilium-dependent autophagy controls epithelial cell volume in response to fluid flow. *Nat Cell Biol* 18:657–667.
52. Jørgensen SB, et al. (2004) Knockout of the alpha2 but not alpha1 5′-AMP-activated protein kinase isoform abolishes 5-aminoimidazole-4-carboxamide-1-beta-4-ribofuranosidebut not contraction-induced glucose uptake in skeletal muscle. *J Biol Chem* 279:1070–1079.
53. Duncan GS, et al. (1999) Genetic evidence for functional redundancy of platelet/endothelial cell adhesion molecule-1 (PECAM-1): CD31-deficient mice reveal PECAM-1-dependent and PECAM-1-independent functions. *J Immunol* 162:3022–3030.

Materials and methods

Endothelial immunofluorescence in human carotid arteries.

Human atherosclerotic plaques obtained from 5 patients were remnants of the surgical specimen routinely processed for pathology following *en bloc* carotid endarterectomy surgery performed after patient consent. Institutional Review Board approval was not required for the specimens at the time the work was done. The surgeon identified the upstreaming from the downstream area of the lesion using a silk threat. The clinical features of these patients are presented in SI Appendix, Table S1. The plaques were immediately scraped off in order to isolate endothelial cells. The upstream part of the plaque was defined as the area between the beginning of the plaque and the site of maximal stenosis. The downstream part was defined as the area between the site of maximal stenosis and the end of the plaque. Endothelial cells coming from the upstream (high SS) or the downstream (low SS) part of the plaque were collected separately (1,2). Plaques were included in this study when upstream and downstream parts were clearly visible and occlusion was absent. We did not include plaques with erosion or rupture because we could not determine whether the rupture occurred *in vivo* or during the surgical manipulation of the specimen. Endothelial cells were then pulled down on a slide using a cytospin centrifuge (Cytospin™ 4 Cytocentrifuge, Thermo scientific), fixed in 4% paraformaldehyde and permabilized (0.01% triton-X100). Cells were incubated with an anti-LC3 antibody (SI Appendix, Table S2) and then with secondary antibody (anti-rabbit AlexaFluor594, Life technologies). Co-staining with anti-CD31 antibody (using a secondary anti-goat AlexaFluor488 antibody, Life technologies) was performed to identify endothelial cells. Cells were then co-stained with DAPI (0.1 µg/mL, Sigma) in order to identify cell nuclei. Samples were analyzed using a Zeiss Axio Imager Z1 fluorescence microscope equipped with a Zeiss ApoTome system (Zeiss).

Human Umbilical Vein Endothelial Cell culture.

Confluent Human Umbilical Vein Endothelial cells (HUVEC; passage 2 to 4; 10 different primary cultures were used; Promocell, Heidelberg, Germany) were cultured on 0.2 %

gelatin-coated slides (Menzel Glazer; Braunschweig, Germany) in endothelial cell basal medium containing growth factors, 1 % fetal calf serum (Promocell), streptomycin (100 IU/mL), penicillin (100 IU/mL) and Amphotericin B (10 μg/L) (Gibco).

Plasmid electroporation.

DNA vector encoding the tandem mRFP-GFP-LC3 was used to transiently express the RFP-GFP tagged LC3 protein, in order to monitor the LC3 translocation and autophagosomes fusion with lysosomes. In the absence of autophagy induction, the LC3 fluorescent signals are evenly distributed; upon autophagy induction, punctate fluorescent signals (yellow LC3 dots) appear as a result of LC3 accumulation on the membrane of autophagosomes; when fusion with lysosomes occurs, the punctate signal becomes red by acidic degradation of the GFP. Cells were used at 50 to 60% confluence for cDNA transfection by use of Nucleofector (Lonza/Amaxa) according to the manufacturer's instructions. Briefly, 5×10^6 HUVECs were electroporated with 2 µg of plasmid, using the U-01 program, and then replated in endothelial cell basal medium containing 1% fetal calf serum for 6h. The medium was then changed and cells reached confluence within 48 hours. Transfection efficacy was assessed by expression of fluorescent LC3 protein.

Lentiviral transduction.

Lentiviruses expressing inducible shRNA (Sigma Aldrich) were used to silence Kinesin-like protein (KIF3A), ATG5 and CD31. HUVECs were infected in the presence of hexadimethrine bromide (at 8 µg/mL) with lentiviruses at multiplicity of infection (MOI) 2.5 for KIF3a and ATG5 or MOI 5 for CD31. Negative controls were lentiviruses expressing a non-target shRNA used at the same MOI as for the protein of interest. Transduced cells were amplified and selected using puromycine (Sigma Aldrich #P9620) at 1 µg/mL during amplification and experiments. ShRNA expression was induced by treating HUVECs for 10 days using Isopropyl β-D-1-thiogalactopyranoside (IPTG, Sigma Aldrich; #I6758) at 1 mmol/L for KIF3A, 0.1 mmol/L for CD31 and 5 days at 1 mmol/L for ATG5.

Shear stress experiment in vitro.

A unidirectional steady laminar SS was applied to confluent HUVECs using a parallel plate chamber system as described elsewhere (3). Endothelial cell medium previously filtered on a 0.1 μm membrane was perfused at different rates and for different times (1 min to 48 hours). Local SS was calculated using Poiseuille's law and was 20, 2 or 0 dynes/cm^2, corresponding to high, low SS or static conditions, respectively.

In some experiments, cells were treated with Bafilomycin A1 (Vacuolar-type H+ -ATPase inhibitor, 100 nmol/L) for 2 hours before ending the SS experiment in order to assess autophagic flux, or with rapamycin (0.5 µmol/L, Sigma) or wortmannin (5 µmol/L, Sigma) in order to modulate autophagy level. For inflammation experiments, cells were treated with TNFα (1 ng/mL) 12 hours before the end of the flow experiment. In control conditions, HUVECs were incubated with the same concentration of the solvent (DMSO). Cells were then collected for Western blot, immunofluorescent microscopy or transmission electron microscopy, as detailed below. For ELISA, the supernatant were collected after the SS experiment, centrifuged for 15 minutes at 600g in order to remove cell debris and stored at -80°C until analysis.

Immunofluorescent staining and Immunofluorescence microscopy in vitro.

After SS exposure, HUVECs were fixed with 4% PFA and permeabilized using 0.1% Triton X-100 and blocked with 5% bovine serum albumin for 1 hour. To assess autophagy flux, cells were incubated with an anti-LC3 antibody and an anti-LAMP2 antibody (SI Appendix, Table S2) and then with secondary antibody (anti-rabbit AlexaFluor594 or anti-goat AlexaFuor 488 respectively, Life technologies). Autophagic flux was also assessed using cells transfected with the tandem mRFP-GFP-LC3 plasmid and exposed to SS. Images were acquired using a Leica SP5 confocal microscope (Leica).

For assessment of the morphology and orientation of endothelial cells under shear stress, HUVECs were stained with an anti-CD144 antibody (SI Appendix, Table S2) and a secondary anti-goat AlexaFluor594 antibody (Life technologies). Samples were analyzed using a Zeiss Axio Imager Z1 fluorescence microscope equipped with a Zeiss ApoTome system (Zeiss).

For all the immunofluorescence experiments, samples were costained with DAPI (0.1 µg/mL, Sigma) in order to identify cell nuclei.

Transmission electron microscopy (TEM).

Transmission electron microscopy observations were performed at the IFR83-Jussieu-Paris core facility. Briefly, HUVECs were fixed with Karnovsky's fixative adapted for vascular tissues and cells (2% paraformaldehyde, 2.5% glutaraldehyde and 0.1 mol/L sodium phosphate buffer, Electron Microscopy Sciences, Hatfield, PA). After dehydration in ethanol, cells were embedded in Epon. Grids were analyzed with a transmission electron microscope (EM 912 OMEGA, ZEISS) equipped with a LaB6 filament at 80 kV. Images were captured with a digital camera (SS-CCD, Proscan 1kx1k) and with custom software.

For morphometric analysis, a minimum of 10 random fields per condition and per experiment were taken in a blinded manner at a magnification of 23,200x (>450 µm² per condition and per experiment). Electron microscopy findings were then assessed by 3 readers (ACV, PER and AH) unaware of SS condition. For TEM experiments, the term autophagic vesicle refers to autophagosome or autolysosome since it is often not possible to determine from TEM images whether or not an autophagosome has fused with a lysosome (4).

In vitro LC3 assessment using flow cytometry.

After exposure to SS, HUVECs were permeabilized using 0.2% saponin for 10 minutes and then washed 3 times with phosphate buffered saline (PBS). Saponin specifically extracts the nonautophagosome-associated form of LC3 (5). Then, HUVECs were fixed in 95% ethanol and incubated with an anti-LC3 antibody (SI Appendix, Table S2) and with an anti-rabbit anti-rabbit AlexaFluor488 antibody as described (5). Costaining with propidium iodide for 5 min prior to flow cytometry analysis was performed to identify live cells and exclude cell aggregates. HUVECs were analyzed using a LSRII flow cytometer (BD Biosciences), and results were expressed as mean fluorescent intensity among live cells.

Senescence-associated beta-galactosidase activity in vitro.

SA-β-galactosidase activity was assessed by flow cytometry using a fluorogenic substrate (C_{12}FDG, Invitrogen). After exposure to SS, HUVECs were pretreated with chloroquine (300 μmol/L, Sigma) diluted in endothelial cell medium without phenol red for 1 hr in order to increase the internal pH of lysosomes to 6. C_{12}FDG (33 μmol/L) was then added to the medium for 1 hr. HUVECs were then washed with PBS at 4°C, resuspended and analyzed immediately using a LSR FortessaTM flow cytometer (BD Biosciences). Light scatter parameters were used to exclude dead cells and subcellular debris. The C_{12}-fluorescein signal was acquired using the FL1 detector. Data were analyzed using FlowJo software to determine the percentage of SA-β-gal positive cells. Cells not treated with C_{12}FDG were used as a negative control.

Animal models.

All mice were on a C57BL/6 background with the exception of *Ampkα1 -/-* mice, which were on a mixed C57Bl6/129 Sv background due to embryonic letality on C57Bl6 background.

Mice constitutively deficient in endothelial autophagy were obtained by crossing *VE-cadherin-Cre* transgenic mice provided by M. Souyri (6), with *Atg5*$^{flox/flox}$ mice provided by N. Mizushima (7) or *Atg7*$^{flox/flox}$ mice were provided by M. Komatsu (8). For characterization of baseline morphological and metabolic features and assessment of endothelial apoptosis, mice were fed a chow diet and were euthanized between 8 and 17 weeks of age. For assessment of endothelial p53 expression, 13 to 17 week old mice were fed a high fat diet (D12492, 26.2% protein, 26.3% carbohydrate, 34.9% fat weight to weight, Research Diets) for 5 weeks and were euthanized (9). For assessment of endothelial senescence, 42 to 54 week old mice were fed the same high fat diet for 16 weeks and were euthanized (10).

To investigate the effect of endothelial autophagy on atherosclerosis development, mice constitutively deficient in endothelial autophagy (*Atg5*$^{flox/flox}$*;VE-cadherin-Cre*) were crossed with *ApoE*$^{-/-}$ mice purchased from the Charles Rivers laboratory. 13 week-old mice were fed a western diet (D12079B, 20% protein, 50% carbohydrate, 21% fat weight to weight, Research Diets) for 10 weeks and were then euthanized. AMPKα*1*-/- mice were described previously (11). *CD31-/-* mice were provided by T.W. Mak (12). All experiments were performed in accordance with the European Community guidelines for the care and use of laboratory animals (N°07430) and were approved by our institutional ethical committee (02526.02).

For investigation of autophagic flux *in vivo*, 8 to 9 weeks old C57BL/6 mice were injected intraperitoneally with chloroquine (60 mg/kg/day for 3 consecutive days, as described previously (13)) or rapamycin (4 mg/kg/day for 2 consecutive days) or with the corresponding vehicle.

Blood pressure measurement.

Arterial blood pressure was measured every 30 seconds at the tail of conscious mice using a CODA non-invasive blood pressure device (Kent Scientific Corporation) (mean value of 15 measurements). Blood pressure was measured for 3 consecutive days after 2 days of acclimation in the chamber.

Fasting plasma glucose and cholesterol levels.

Three days before sacrifice, mice were fasted for 6 hours. For blood glucose analysis, the distal 1 mm of the tail was excised using sterile scissors. The first blood drop was discarded; then serum glucose level was determined using OneTouch Ultra® reactive strips and OneTouch Ultra® reader (Lifescan). For plasma cholesterol analysis, mice were anesthetized with 2% isoflurane. Then, 75 μL of blood were collected from the peri-orbital venous sinus using a heparinized microhematocrit tube (Hirschmann-Laborgeräte). Blood was then centrifuged twice at 2,500 g for 15 min at room temperature to prepare platelet free plasma and stored at -80°C until analysis. Plasma cholesterol level was determined using the Cholesterol RTU™ commercial kit (BioMérieux).

Plasma preparation.

On the day of sacrifice, non-fasted mice were sedated with 2% isofluorane. Blood was collected from the inferior vena cava using a 25 gauge x 1' needle in a 1 mL syringe pre-coated with 3.8% sodium citrate. The mice were then humanely euthanized. Blood was centrifuged at 1,500 g for 15 minutes at 18°C in order to pellet cells. Then, plasma was centrifuged at 13,000 g for 5 minutes at 18°C to pellet platelets and cell debris. Platelet free plasma (PFP) was aliquoted and stored at -80°C for measurement of circulating levels of inflammatory molecules.

Senescence-associated beta-galactosidase assay on mouse aortas.

Mouse aortas were collected fresh, micro-dissected under a Nikon SMZ 745 dissecting microscope to remove extra fat and fixed for 8 min in 2% formaldehyde and 0.2% glutaraldehyde in PBS. Beta-galactosidase staining was performed by incubating the aortas for 48 hours at 37°C in a CO_2-free incubator with a fresh staining solution containing 1 mg/mL X-gal, 0.2 mol/L citric acid/sodium phosphate, 5 mmol/L potassium ferrocyanide, 5 mmol/L potassium ferricyanide, 150 mmol/L NaCl and 2 mmol/L $MgCl_2$ at pH 6.0. After staining, aortas were washed with PBS, mounted "*en face*" on glass slides and imaged using a bright field Zeiss Axio Imager Z1 (Zeiss) microscope. Images were acquired at 100 X magnification and the number of SA-β-gal positive cells/μm^2 was quantified by two independent operators (MK and JP) unaware of mice genotype.

Red-oil staining.

Mouse aortas were first injected with PBS then with PBS supplemented with 4% paraformaldehyde, dissected and kept in PBS supplemented with 4% paraformaldehyde for 2 hours. Then, aortas were stained with a freshly prepared Oil Red O working solution (40%

distilled water, 60% of a 5 g/L Oil Red O in isopropanol; Sigma) for 30 minutes under agitation. Aortas were then differentiated using 70% ethanol for 5 minutes, mounted "*en face*" on glass slides and then observed using a bright field microscope (Leica M165FC, camera 425). Plaque size was quantified using the ImageJ software.

Murine aortic endothelial cell isolation.

The mouse vasculature was rinsed by injecting *in situ* 10 mL of Dulbecco's modified Eagle's medium (DMEM) (Gibco) into the left ventricle. Aortas were then retrieved, injected with 1 mg/mL type II Collagenase (Worthington) using a BD Insyte™ Autoguard™ catheter (BD) and incubated at 37°C for 45 minutes. Mouse aortic endothelial cells (MAEC) were collected by flushing the aortas with 10 mL DMEM, and then pelleted by centrifugation at 1000 g for 7 min before being seeded in a 0.1% gelatin-coated 12 well plate in DMEM supplemented with 20 % fetal calf serum (Gibco). After 24 hours, the medium was changed to Endothelial cell growth medium MV with growth factors (Promocell) and 5% fetal calf serum. By flow cytometry, we observed that 92% and 62% of the MAECs were positive for the endothelial markers CD-31 and eNOS, respectively and 0% were positive for smooth muscle cell and fibroblast markers (α-SMC-actin and ER-TR7, respectively). MAECs were used for Western blot analysis after one passage.

En face immunofluorescence microscopy on mouse aortas.

Mouse aortas were injected *in situ* with PBS supplemented with 4% paraformaldehyde. After dissection, the tissues were permeabilized using 0.2% Triton X-100 and blocked with 5% bovine serum albumin for 20 minutes. To assess autophagy level, aortas were first incubated with an anti-LC3 antibody (SI Appendix, Table S2) and then with secondary antibody (anti-rabbit AlexaFluor594, Life technologies). To assess p53 and p16 localization, aortas were first incubated with an anti-p53 or an anti-p16 antibody (SI Appendix, Table S2) and then with secondary antibody (anti-mouse AlexaFluor594, Thermo Scientific, respectively). To assess apoptosis level, aortas were stained with the *in situ* cell death detection kit from Roche (red, Neuilly-sur-Seine, France) according to manufacturer's instructions. In all experiments, endothelial cells were easily recognized by their morphology. Still, in most series of experiment, a co-staining with anti-CD31 antibody (using a secondary anti-goat AlexaFluor488 antibody, Life technologies) or anti-CD144 antibody (Santa Cruz biotechnology sc-6458) was performed. In all mice, 8 to 10 images were obtained from regions in the aortic arch exposed to low SS and the thoracic aorta exposed to high SS. For all these immunofluorescence experiments samples were co-stained with DAPI (0.1 µg/mL, Sigma) in order to identify cell nuclei. Samples were analyzed using a Zeiss Axio Imager Z1 fluorescence microscope equipped with a Zeiss ApoTome system (Zeiss).

ELISA.

Levels of MCP-1 in surpernatant of HUVECs were assessed by an ELISA assay (R&D, human MCP-1 Duo-set DY279) following the manufacturer's instructions.

Immunoblotting.

HUVECs or MAECs were washed with cold PBS and scraped off in RIPA buffer (150 mmol/L NaCl, 50 mmol/L TrisHCl, pH 7.4, 2 mmol/L EDTA, 0.5% sodium deoxycholate, 0.2% sodium dodecyl sulfate, 2 mmol/L activated orthovanadate, complete protease inhibitor cocktail tablet (Complet mini, Roche, France) and complete phosphatase inhibitor cocktail tablet (Roche, France)). Lysates were sonicated (15 seconds, 40 watts, Vibra Cell, Bioblock), and protein content was quantified using the Lowry protein assay (Bio-Rad; Hercules, CA). Lysates were mixed with the reducing sample buffer for electrophoresis and subsequently transferred onto nitrocellulose (Bio-Rad) for all blots except for p16, KLF-2, p-ACC and ACC (PVDF membranes, Thermo Scientific). Equal loading was checked using Ponceau red solution. Membranes were incubated with primary antibodies (SI Appendix, Table S2). After secondary antibody incubation (anti-goat, anti-rabbit, anti-rat or anti-mouse, Amersham, GE Healthcare, UK 1/3000), immunodetection was performed using an enhanced chemiluminescence kit (Immun-Star Western C kit, Bio-Rad, or WesternBright™ Sirius, Advansta for p16 blot) and bands were revealed using the Las-4000 imaging system. After initial immunodetection, membranes were stripped of antibodies and re-probed with anti-GAPDH, anti-actin or anti anti-tubulin antibodies (SI Appendix, Table S2). Values reported from Western blots were obtained by band density analysis using Image Gauge software (Fujifilm, Tokyo, Japan) and expressed as the ratio protein of interest compared to GAPDH, actin or tubulin expression for whole cell extract.

Statistical analysis.

Data are expressed as mean ± SEM for *in vitro* experiments and as median (interquartile range) for *in vivo* experiments. Comparisons between different SS conditions or between control and treatment conditions were performed using a Wilcoxon test. Comparisons between groups of mice were performed using the Mann-Whitney U-test. Comparison between genders was performed using a Chi-square test. Statistical analyses and Figures were performed using the SPSS statistical package 20.0 software for Windows (SPSS Inc., Chicago, IL, United States) and GraphPad Prism 5 software, respectively. All tests were two-sided and used a significance level of 0.05.

Data sharing.

The data that support the findings of this study are available from the corresponding author on reasonable request.

References :

1. Tricot O*, et al.* (2000) Relation between endothelial cell apoptosis and blood flow direction in human atherosclerotic plaques. *Circulation* 101(21):2450-2453.

2. Choi G*, et al.* (2015) Coronary Artery Axial Plaque Stress and its Relationship With Lesion Geometry: Application of Computational Fluid Dynamics to Coronary CT Angiography. (Translated from eng) *JACC Cardiovasc Imaging* 8(10):1156-1166 (in eng).
3. Ramkhelawon B*, et al.* (2009) Shear stress regulates angiotensin type 1 receptor expression in endothelial cells. *Circ Res* 105(9):869-875.

4. Eskelinen EL (2005) Maturation of autophagic vacuoles in Mammalian cells. *Autophagy* 1(1):1-10.

5. Eng KE, Panas MD, Karlsson Hedestam GB, & McInerney GM (2010) A novel quantitative flow cytometry-based assay for autophagy. *Autophagy* 6(5):634-641.

6. Oberlin E*, et al.* (2010) VE-cadherin expression allows identification of a new class of hematopoietic stem cells within human embryonic liver. *Blood* 116(22):4444-4455.
7. Hara T*, et al.* (2006) Suppression of basal autophagy in neural cells causes neurodegenerative disease in mice. *Nature* 441(7095):885-889.
8. Komatsu M*, et al.* (2005) Impairment of starvation-induced and constitutive autophagy in Atg7-deficient mice. *J Cell Biol* 169(3):425-434
9. Warboys CM*, et al.* (2014) Disturbed flow promotes endothelial senescence via a p53-dependent pathway. (Translated from eng) *Arterioscler Thromb Vasc Biol* 34(5):985-995 (in eng).
10. Wang CY*, et al.* (2009) Obesity increases vascular senescence and susceptibility to ischemic injury through chronic activation of Akt and mTOR. *Sci Signal* 2(62):ra11.
11. Jorgensen SB*, et al.* (2004) Knockout of the alpha2 but not alpha1 5'-AMP-activated protein kinase isoform abolishes 5-aminoimidazole-4-carboxamide-1-beta-4-ribofuranosidebut not contraction-induced glucose uptake in skeletal muscle. (Translated from eng) *J Biol Chem* 279(2):1070-1079 (in eng).
12. Duncan GS*, et al.* (1999) Genetic evidence for functional redundancy of Platelet/Endothelial cell adhesion molecule-1 (PECAM-1): CD31-deficient mice reveal PECAM-1-dependent and PECAM-1-independent functions. *J Immunol* 162(5):3022-3030.
13. Orhon I*, et al.* (2016) Primary-cilium-dependent autophagy controls epithelial cell volume in response to fluid flow. (Translated from eng) *Nat Cell Biol* 18(6):657-667 (in eng).

Age (yrs)	79 (72-85)
Male gender	4 (80)
Symptomatic plaques	2 (40)
Stroke	1 (20)
Amourosis	1 (20)
Cardio-vascular risk factors	
Diabetes	2 (40)
Hypertension	3 (60)
Smoking	1 (20)
Dyslipidemia	4 (80)
Body mass index (kg/m²)	28.7 (21.9-35.3)
Treatments	
Antiplatelet therapy	5 (100)
Statins	4 (80)
Beta-blockers	2 (40)
Angiotensin-converting enzyme inhibitors or Angiotensin II receptor antagonist	3 (60)
Calcium channel blockers	1 (20)
Diuretics	2 (40)

Table S1. Patient's characteristics. Data are expressed as median (interquartile range) or frequency (%) (n = 5).

Antibody anti-	Raised in	Reference		Dilution	WB Buffer	IF buffer
4EBP1	rabbit	CST	9452	1/1000	TBST milk	-
phospho-4EBP1 (Thr37/46)	rabbit	CST	2855	1/1000	TBST BSA	-
AMPK	rabbit	CST	2795	1/1000	TBST milk	-
phospho-AMPK (Thr172)	rabbit	CST	2535	1/1000	TBST BSA	-
ATG5	rabbit	CST	8540	1/500	TBST milk	-
ATG7	rabbit	CST	2631	1/1000	TBST milk	-
BECLIN1	rabbit	CST	3495	1/1000	TBST milk	-
CD144	goat	Santa Cruz	sc-6458	1/100	-	PBS BSA
CD31	goat	Santa Cruz	sc-1506	1/200	TBST milk	PBS BSA
CD41	rat	BD Pharmingen	563317	1/20		PBS BSA
ICAM1	goat	R&D	AF796	1/1000	TBST milk	-
KLF-2	goat	Novus biological	NB-10-1051	1/500	TBST milk	
KIF3a	rabbit	Abcam	ab11259	1/2000	TBST milk	-
ULK1	rabbit	CST	4773	1/1000	TBST milk	-
phospho-ULK1 (Ser555)	rabbit	CST	5869	1/1000	TBST BSA	-
LAMP2	goat	Santa Cruz	sc-8101	1/1000	TBST milk	PBS BSA
LC3B	rabbit	CST	2775	1/1000	TBST milk	PBS BSA
p16	mouse	BD Pharmingen	51-1325GR	1/1000	TBST milk	-
p16	mouse	Abcam	Ab54210	1/1000		PBS BSA
GAPDH	mouse	Millipore	mab-374	1/20000	TBST milk	-
TUBULIN	rat	Abcam	Ab6160	1/5000	TBST milk	
ACTIN	goat	Santa Cruz	sc-1616	1/10000	TBST milk	-
p53	mouse	CST	2524	1/1000		PBS BSA
p-ACC	rabbit	CST	3661	1/1000	TBST milk	-
ACC	rabbit	CST	3662	1/1000	TBST milk	-

Table S2. List of antibodies used for western blot analyses. Abbreviations: BSA, Bovine Serum Albumin; CST, Cell Signaling Technologies; IF, Immunofluorescence; PBS, Phosphate Buffer Saline; TBST, Tris Buffer Saline 0.05%Tween; WB, Western Blot.

Duration of SS	**ATG5/GAPDH**			**ATG7/GAPDH**			**Beclin1/GAPDH**		
	HSS	**LSS**	**P value**	**HSS**	**LSS**	**P value**	**HSS**	**LSS**	**P value**
2 hrs	1.13±0.03	1.15±0.15	1.00	0.85±0.10	0.94±0.10	0.31	2.19±1.17	1.81±0.46	0.84
6 hrs	1.74±0.33	1.20±0.37	0.13	1.05±0.11	0.86±0.19	0.63	1.57±0.52	1.00±0.17	0.19
12 hrs	1.24±0.19	0.94±0.06	0.31	1.06±0.12	0.94±0.19	0.43	0.94±0.17	1.02±0.11	0.31
24 hrs	1.93±0.53	1.60±0.33	0.30	1.06±0.26	0.73±0.16	0.62	1.07±0.09	1.03±0.07	0.73

Table S3. Shear stress does not modulate ATG5, ATG7 or BECLIN1 expression in HUVECs. Western blot analysis of ATG5, ATG7, BECLIN1. Data are normalized to static condition and expressed as mean ± SEM. n= 5 to 7 per time point and per shear stress condition. There was no significant difference between HSS and LSS in any of these parameters.

	***ApoE$^{-/-}$; Atg5$^{flox/flox}$* (n=9)**	***ApoE$^{-/-}$; Atg5$^{flox/flox}$; VE-cadherin-Cre* (n=11)**	***P value***
Metabolic and morphological features			
Body weight (g)	27.4 (24.3 - 34.8)	28.2 (25.8 - 31.4)	0.76
Male gender (%)	5 (55)	5 (45)	0.44
Arterial blood pressure (mm Hg)	79 (74 - 85)	78 (71 - 83)	0.81
Cholesterol (g/L)	8.9 (7.7 - 10.1)	10.0 (7.5 - 11.3)	0.087
Fasting serum glucose (mg/dL)	84 (77 - 109)	111 (102 - 125)	**0.048**
Spleen weight / body weight (%)	0.5 (0.5 - 0.6)	0.5 (0.4 - 0.6)	0.59
Kidney weight / body weight (%)	ND	ND	-
Liver weight / body weight (%)	4.9 (4.7 - 5.2)	5.0 (4.6 - 5.6)	0.49
Heart weight / body weight (%)	0.6 (0.5 - 0.6)	0.5 (0.5 - 0.6)	0.59
Blood cell count			
WBC (x10^3/mm^3)	4.7 (4.0 – 6.4)	5.4 (3.0 – 9.4)	0.66
Lymphocytes (x10^3/mm^3)	2.9 (2.3 – 3.3)	2.6 (2.1 – 4.4)	0.73
Monocytes (x10^3/mm^3)	0.2 (0.1 - 0.3)	0.2 (0.1 - 0.2)	0.45
Granulocytes (x10^3/mm^3)	2.1 (1.1 – 2.8)	2.7 (0.9 – 3.9)	0.40
RBC (x10^3/mm^3)	6.9 (6.2 - 7.7)	7.3 (6.7 - 7.5)	0.80
Hemoglobin (g/dL)	9.8 (8.5 - 10.4)	10.1 (9.4 - 10.3)	0.66
Platelets (x10^3/mm^3)	626 (556 - 964)	656 (560 - 715)	0.88

Table S4. Metabolic features and blood cell count of 23 weeks old *ApoE$^{-/-}$; Atg5$^{flox/flox}$* vs. *ApoE$^{-/-}$; Atg5$^{flox/flox}$; VE-cadherin-cre* mice fed a Western diet for 10 weeks. Blood cell count was available for 3 mice per group. Data are expressed as median (interquartile range) or number (%) for the gender. There was no significant difference between both groups in any of these parameters except for fasting glucose (p=0.048).

Abbreviations: ND, not determined; RBC, red blood cell; WBC, white blood cell.

	Atg5$^{flox/flox}$ **(n=12)**	***Atg5$^{flox/flox}$; VE-cadherin-Cre*** **(n=10)**	***P value***
Metabolic and morphological features			
Body weight (g)	22.4 (20.1 - 27.6)	21.5 (19.9 - 25.0)	0.48
Male gender (number)	5 (42)	4 (40)	0.079
Arterial blood pressure (mm Hg)	78 (73 - 82)	78 (75 - 81)	0.74
Cholesterol (g/L)	1.1 (0.9 - 1.4)	1.4 (1.1 - 1.8)	0.93
Fasting serum glucose (mg/dL)	134 (107 - 144)	125 (108 - 162)	0.93
Spleen weight / body weight (%)	0.4 (0.3 - 0.4)	0.4 (0.3 - 0.4)	0.27
Kidney weight / body weight (%)	0.6 (0.5 - 0.6)	0.6 (0.5 - 0.6)	0.80
Liver weight / body weight (%)	4.0 (3.8 - 4.2)	4.2 (3.5 - 4.5)	0.51
Heart weight / body weight (%)	0.6 (0.5 - 0.7)	0.6 (0.6 - 0.7)	0.91
Blood cell count			
WBC (x10^3/mm^3)	4.3 (3.2 - 5.3)	3.8 (2.7 - 4.8)	0.27
Lymphocytes (x10^3/mm^3)	3.4 (2.8 - 5.0)	3.5 (2.7 - 4.4)	0.89
Monocytes (x10^3/mm^3)	0.3 (0.2 - 0.4)	0.2 (0.2 - 0.3)	0.29
Granulocytes (x10^3/mm^3)	0.2 (0.1 - 0.4)	0.2 (0.1 - 0.2)	0.30
RBC (x10^3/mm^3)	7.1 (6.9 - 7.5)	6.9 (6.5 - 7.6)	0.29
Hemoglobin (g/dL)	13.9 (12.8 - 16.8)	14.3 (12.7 - 15.4)	0.93
Platelets (x10^3/mm^3)	689 (602 - 733)	684 (572 - 787)	0.99

Table S5. Metabolic features and blood cell count of 10 weeks old *Atg5$^{flox/flox}$ vs. Atg5$^{flox/flox}$; VE-cadherin-Cre* mice fed a chow diet.

Data are expressed as median (interquartile range) or number (%) for the gender. There was no significant difference between the two groups in any of these parameters.

Abbreviations: RBC, red blood cell; WBC, white blood cell.

	Atg7$^{flox/flox}$ **(n=12)**	***Atg7$^{flox/flox}$; VE-cadherin-Cre*** **(n=10)**	***P value***
Metabolic and morphological features			
Body weight (g)	22.6 (20.2 - 24.1)	21.0 (19.6 - 21.7)	0.27
Male gender (number)	6 (50)	4 (40)	0.46
Arterial blood pressure (mm Hg)	77 (74 - 83)	81 (76 - 84)	0.49
Cholesterol (g/L)	1.5 (1.1 - 1.7)	1.3 (1.1 - 1.6)	0.51
Fasting serum glucose (mg/dL)	150 (139 - 171)	150 (124 - 156)	0.53
Spleen weight / body weight (%)	0.4 (0.3 - 0.5)	0.5 (0.5-0.7)	**0.005**
Kidney weight / body weight (%)	0.6 (0.5 - 0.6)	0.6 (0.6-0.6)	0.55
Liver weight / body weight (%)	5.0 (4.5 - 5.4)	5.1 (5.0-5.3)	0.64
Heart weight / body weight (%)	0.47 (0.45 - 0.49)	0.54 (0.53 - 0.60)	**0.001**
Blood cell count			
WBC ($x10^3/mm^3$)	3.1 (1.5 - 4.4)	3.3 (2.2 - 3.5)	0.66
Lymphocytes ($x10^3/mm^3$)	2.8 (1.1 - 3.1)	2.6 (1.8 - 2.7)	0.98
Monocytes ($x10^3/mm^3$)	0.1 (0.0 - 0.1)	0.1 (0.1 - 0.1)	0.30
Granulocytes ($x10^3/mm^3$)	0.5 (0.1 - 0.9)	0.6 (0.2 - 1.0)	0.72
RBC ($x10^3/mm^3$)	6.9 (6.2 - 7.6)	6.1 (5.8 - 6.9)	0.079
Hemoglobin (g/dL)	9.5 (9.1 - 10.6)	9.1 (8.2 - 9.7)	0.18
Platelets ($x10^3/mm^3$)	657 (456 - 697)	617 (589 - 696)	0.64

Table S6. Metabolic features and blood cell count of 10 weeks old *Atg7$^{flox/flox}$ vs. Atg7$^{flox/flox}$; VE-cadherin-Cre* mice fed a chow diet. Blood cell count was available in *Atg7$^{flox/flox}$; and in 9 Atg7$^{flox/flox}$; VE-cadherin-Cre mice.*

Data are expressed as median (interquartile range) or number (%) for the gender

Abbreviations: RBC, red blood cell; WBC, white blood cell.

	Atg5$^{flox/flox}$ **(n=7)**	***Atg5$^{flox/flox}$*; *VE-cadherin-Cre*** **(n=10)**	***P value***
Metabolic and morphological features			
Body weight (g)	47.1 (43.5 - 52.9)	44.2 (41.8 - 50.7)	0.49
Male gender (%)	7 (100)	10 (100)	-
Cholesterol (g/L)	2.3 (1.8 - 2.9)	3.0 (2.2 - 3.4)	0.19
Fasting serum glucose (mg/dL)	132 (126 - 156)	134 (129 - 144)	0.65
Liver weight / body weight (%)	6.4 (5.1 - 7.1)	4.4 (3.8 - 5.0)	**0.022**
Heart weight / body weight (%)	0.4 (0.4 - 0.5)	0.4 (0.4 - 0.5)	0.47

Table S7. Metabolic features of 64 weeks old *Atg5$^{flox/flox}$ vs. Atg5$^{flox/flox}$; VE-cadherin-Cre* mice fed a high fat diet for 16 weeks.

Data are expressed as median (interquartile range) or number (%) for the gender.

	***Atg7*$^{flox/flox}$** **(n=14)**	***Atg7*$^{flox/flox}$*;* *VE-cadherin-Cre*** **(n=10)**	***P value***
Metabolic and morphological features			
Body weight (g)	54.2 (52.4 - 59.6)	54.1 (52.5 - 56.1)	0.69
Male gender (number)	14 (100)	10 (100)	-
Cholesterol (g/L)	2.5 (1.9 - 3.0)	2.0 (1.8 - 2.5)	0.31
Fasting serum glucose (mg/dL)	191 (171 - 207)	184 (159 - 203)	0.66
Liver weight / body weight (%)	5.3 (4.5 - 6.4)	4.8 (3.7 - 6.0)	0.26
Heart weight / body weight (%)	0.3 (0.3 - 0.3)	0.4 (0.3 - 0.4)	**0.028**

Table S8. Metabolic features of 64 weeks old *Atg7*$^{flox/flox}$ *vs.* *Atg7*$^{flox/flox}$*; VE-cadherin-Cre* mice fed a high fat diet for 16 weeks. Data are expressed as median (interquartile range) or number (%) for the gender.

Figure S1

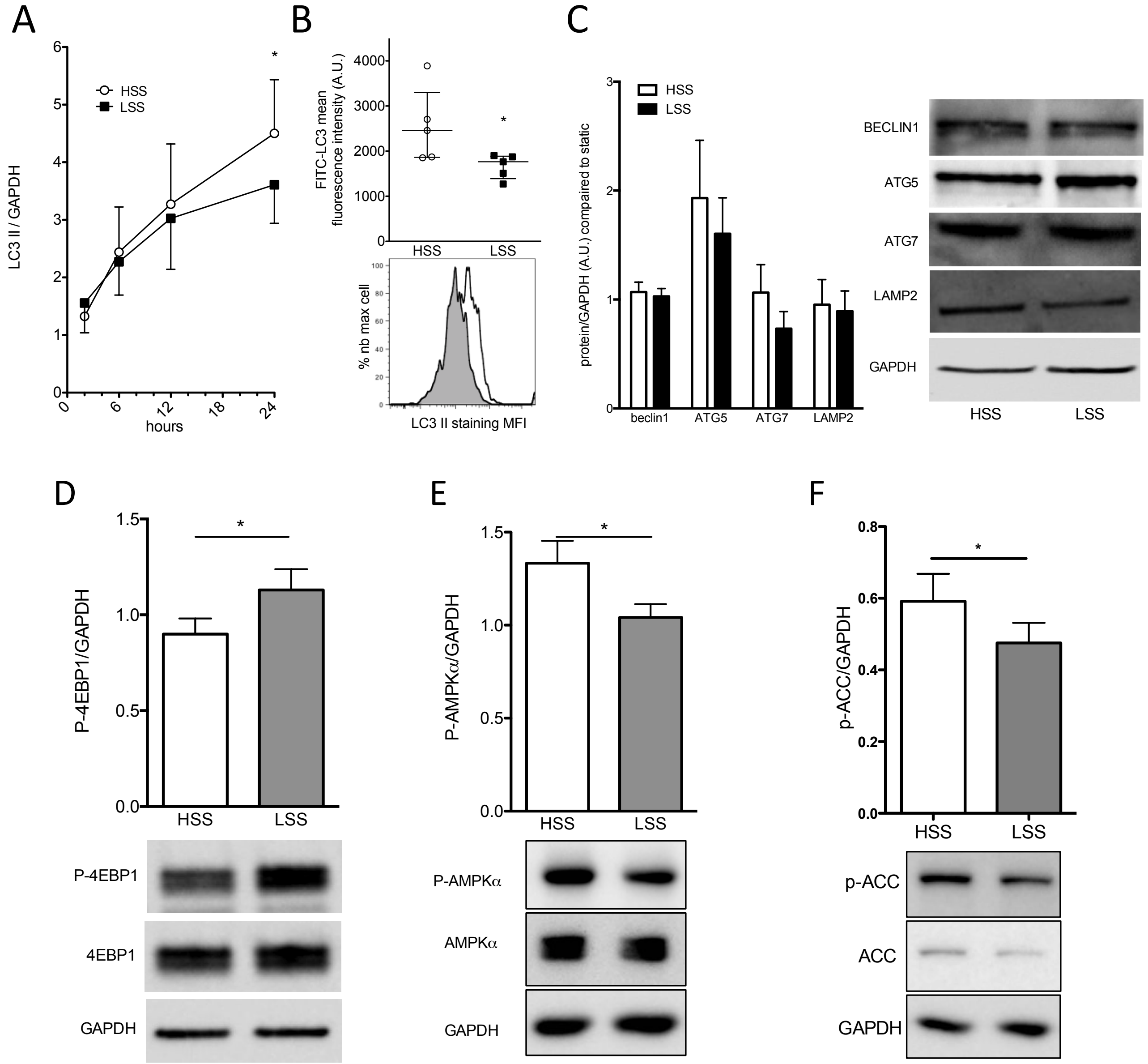

Supplementary Figure 1. Autophagy is defective in endothelial cells exposed to low shear stress. (A) Quantification of LC3 II compared to GAPDH (n ≥ 5 per time point and per condition) in HUVECs exposed to high shear stress (HSS) and low shear stress (LSS). Data are normalized to static condition and are presented as mean ± SEM. (B) Assessment of autophagy level in HUVECs exposed to HSS and LSS for 24 hrs by measuring LC3 staining using flow cytometry (n = 5). Upper panel, quantification; lower panel, representative histogram (gray represents HUVECs exposed to LSS and white HUVECs exposed to HSS). (C) Autophagy related proteins expression in HUVECs exposed for 24 hrs to HSS and LSS (n ≥ 6 per condition). (D-F) 4EBP1, AMPKα and acetyl-CoA carboxylase (ACC) phosphorylations were quantified by western blot in HUVECs exposed to high and low shear stress for 1 (4-EBP1) and 5 min (AMPKα and ACC) (n = 6 for p-4EBP1 and p-AMPKα. n = 9 for p-ACC). *, $p < 0.05$. MFI, mean fluorescent intensity. Figure related to Figures 1 and 3.

Figure S2

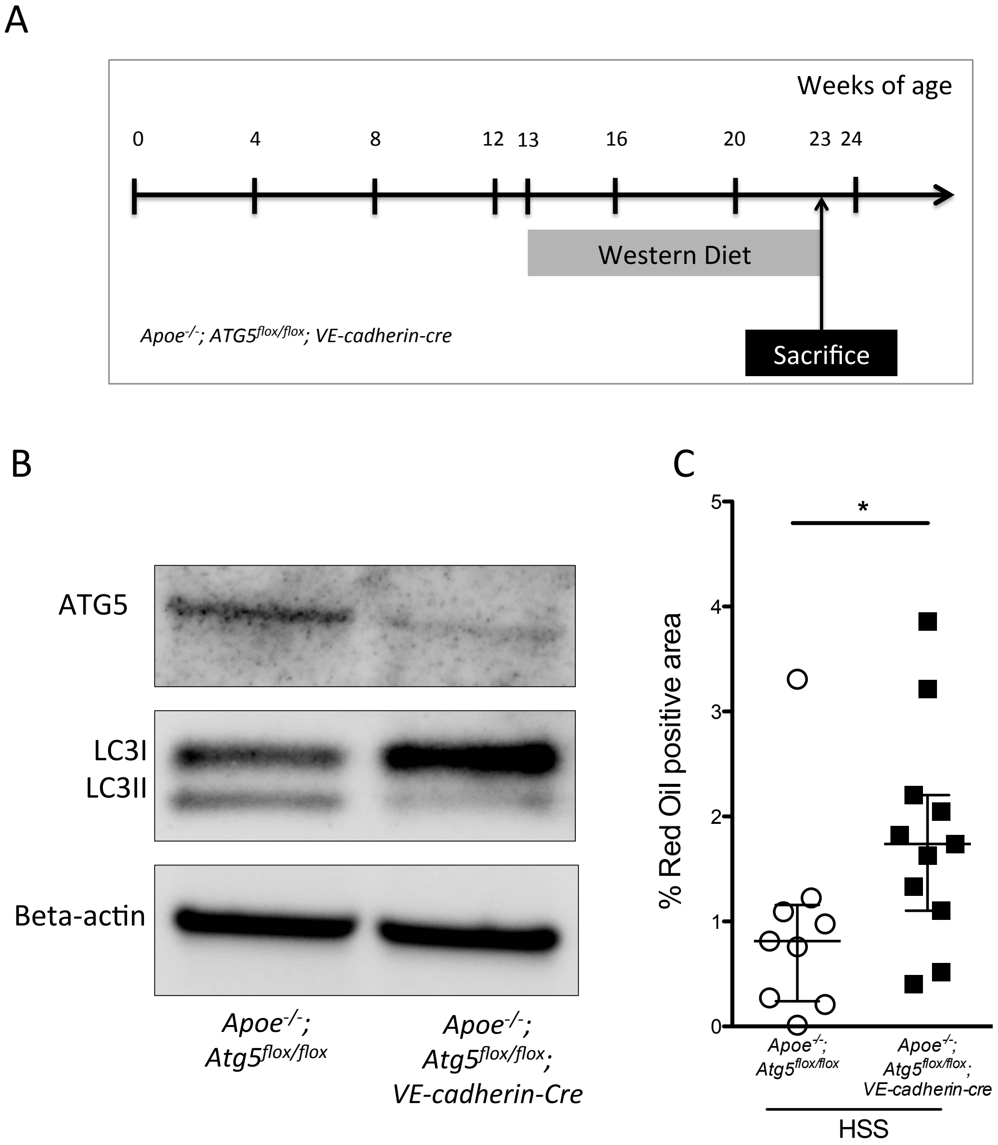

Supplementary Figure 2. *ApoE-/-; Atg5flox/flox; VE-cadherin-Cre* mice are deficient in autophagy in aortic endothelial cells and display increased plaque burden in HSS areas. (A) Protocol to investigate atherosclerosis formation in *Apoe-/-; Atg5flox/flox* and *Apoe-/-; Atg5flox/flox; VE-cadherin-Cre* mice. (B) ATG5 and LC3 levels evaluated by western blot in murine aortic endothelial cells isolated from *Apoe-/-; Atg5flox/flox* and *Apoe-/-; Atg5flox/flox; VE-cadherin-Cre* mice (representative of 2 pools of 4 mice). (C) Quantification of *"en face"* red oil staining of atherosclerotic lesions in the aorta of these mice excluding the ostia of branching points. *, $p < 0.05$. Figure related to Figure 4.

Figure S3

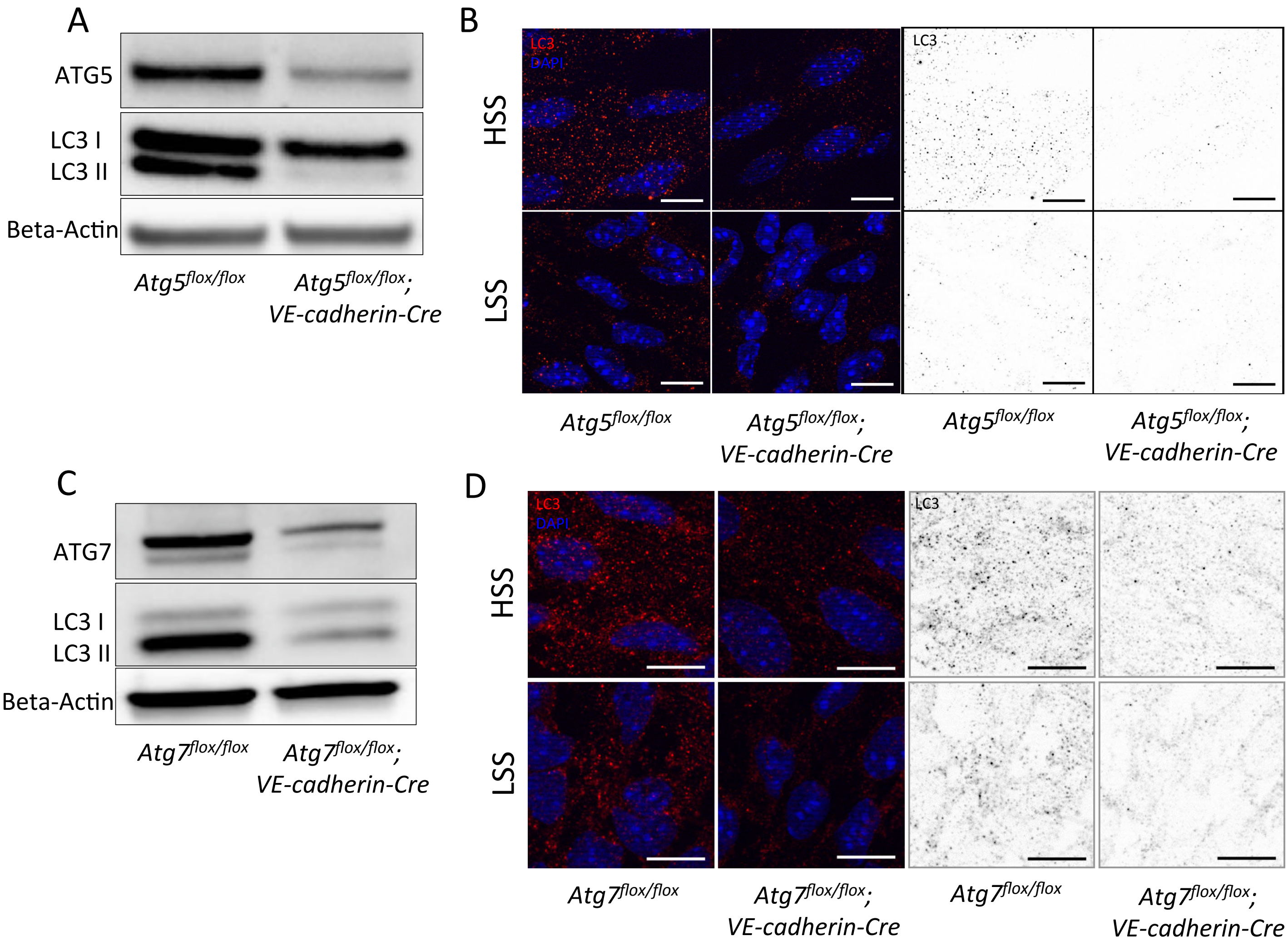
A
ATG5
LC3 I
LC3 II
Beta-Actin
Atg5flox/flox
Atg5flox/flox; VE-cadherin-Cre
B
HSS
LSS
LC3
DAPI
LC3
Atg5flox/flox
Atg5flox/flox; VE-cadherin-Cre
Atg5flox/flox
Atg5flox/flox; VE-cadherin-Cre
C
ATG7
LC3 I
LC3 II
Beta-Actin
Atg7flox/flox
Atg7flox/flox; VE-cadherin-Cre
D
HSS
LSS
LC3
DAPI
LC3
Atg7flox/flox
Atg7flox/flox; VE-cadherin-Cre
Atg7flox/flox
Atg7flox/flox; VE-cadherin-Cre

Supplementary Figure 3. *Atg5*$^{flox/flox}$*; VE-cadherin-Cre and Atg7*$^{flox/flox}$*; VE-cadherin-Cre* mice are deficient in autophagy in aortic endothelial cells. (A) ATG5 and LC3 levels evaluated by western blot in murine aortic endothelial cells isolated from *Atg5*$^{flox/flox}$ and *Atg5*$^{flox/flox}$*; VE-cadherin-Cre* mice (representative of 2 pools of 4 mice). (B) representative images of LC3 *en face* staining of the aorta of 10 week old *Atg5*$^{flox/flox}$ *vs. Atg5*$^{flox/flox}$*; VE-cadherin-Cre* mice (red, LC3; blue, DAPI; n = 5; bar scale, 10 µm; N = 5). (C) ATG7 and LC3 levels evaluated by western blot in murine aortic endothelial cells isolated from *Atg7*$^{flox/flox}$ and *Atg7*$^{flox/flox}$*;VE-cadherin-Cre* mice (representative of 2 pools of 4 mice). (D**)** Representative images of LC3 *en face* staining of the aorta of 10 week old *Atg7*$^{flox/flox}$ *vs. Atg7*$^{flox/flox}$*; VE-cadherin-Cre* mice (red, LC3; blue, DAPI; bar scale, 10 µm).-Related to Figure 5.

Figure S4

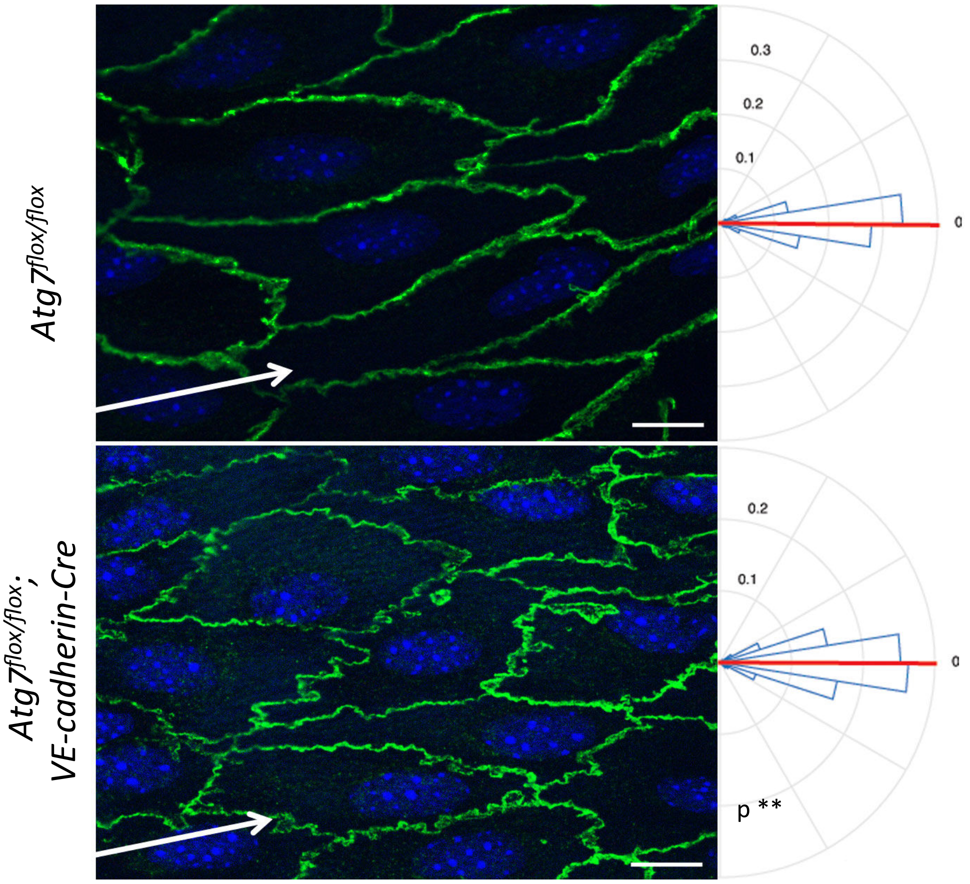
Atg7flox/flox
0.3
0.2
0.1
0
Atg7flox/flox;
VE-cadherin-Cre
0.2
0.1
0
p **

Supplementary Figure 4. Deficiency in endothelial autophagy impairs endothelial cells ability to align in the direction of flow. Quantification of cell alignment in direction of flow in the linear part of the aorta (HSS) of *Atg7*$^{flox/flox}$ or *Atg7*$^{flox/flox}$; *VE-cadherin-Cre* mice (green, CD144 staining; blue, DAPI; n = 5; bar scale 10 μm). **Kp<0.01

figure S5

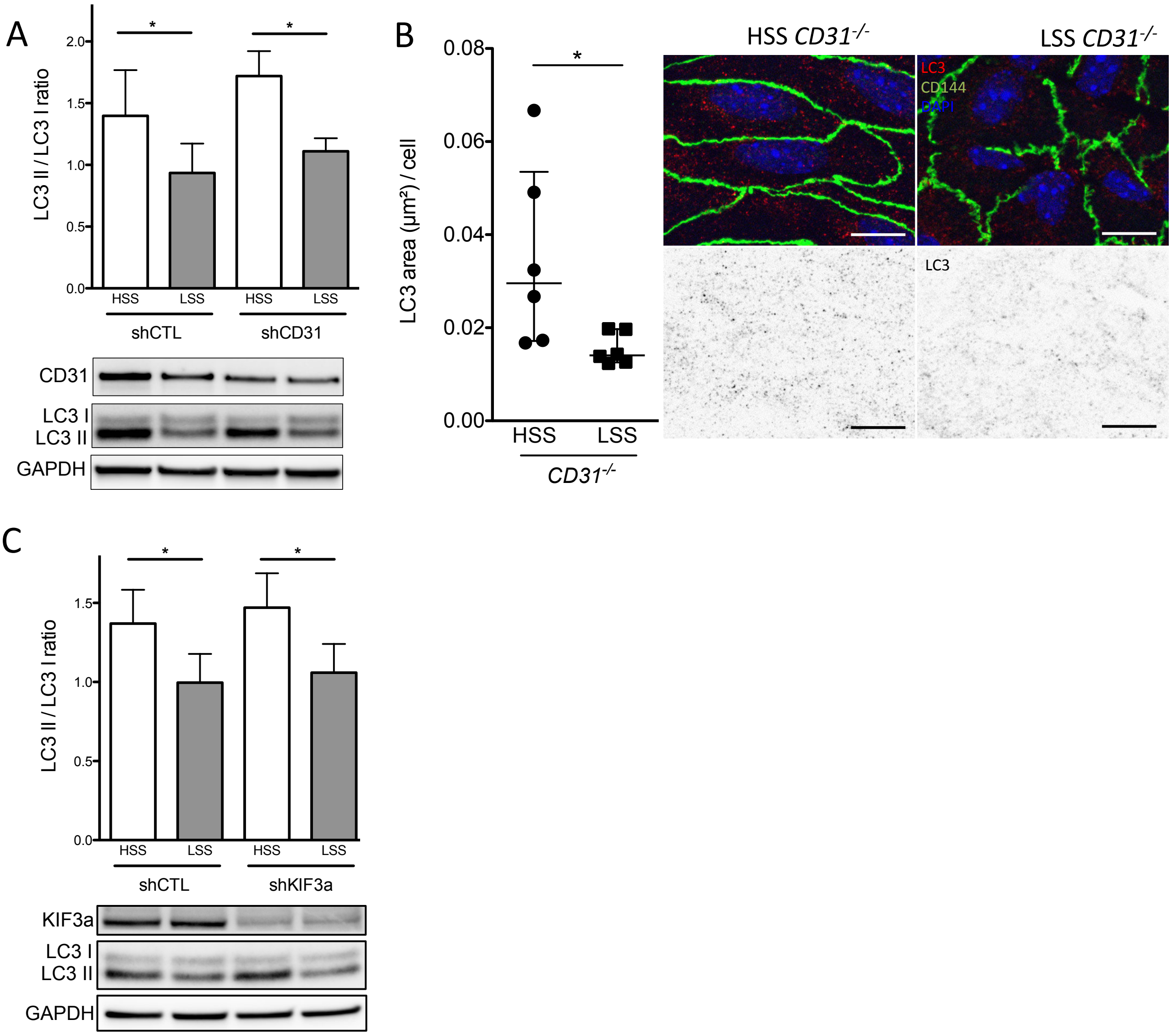

Supplementary Figure 5. The mechanosensor mediating endothelial shear stress effect on autophagy is neither CD31 nor the primary cilium. (A) Western blot analysis of CD31 and LC3 protein expression in HUVECs transduced with a lentivirus expressing CD31 or control shRNA and exposed for 24 hrs to high and low SS (n = 5; shRNA induction: 0.1 mmol/L of IPTG). Data are expressed as mean ± SEM. (B) LC3 *en face* staining of the aorta of 10 week old *CD31-/-* mice (n = 6; green, CD144; red, LC3; blue, DAPI; bar scale, 10 µm). Left, quantification of LC3 area; Data are given as median (horizontal bar) and interquartile range (error bar). Right, representative images. (C) Western blot analysis of KIF3A and LC3 protein expression in HUVECs transduced with a lentivirus expressing KIF3a or control shRNA and exposed for 24 hrs to high and low SS (n = 5, shRNA induction: 1 mmol/L of IPTG). *, $p < 0.05$. HSS, High shear stress; LSS, low shear stress.

Figure S6

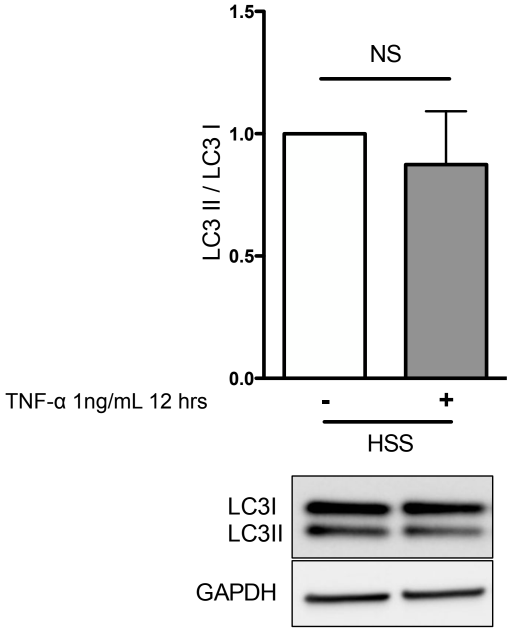

Supplementary Figure 6. TNF-α treatment does not change autophagy level in HUVECs exposed to high shear stress. Western blot analysis of LC3 protein expression in HUVECs exposed for 24 hrs to high SS with or without TNF-α treatment for 12 hrs (n = 6). NS, non significant; HSS, High shear stress.

Figure S7

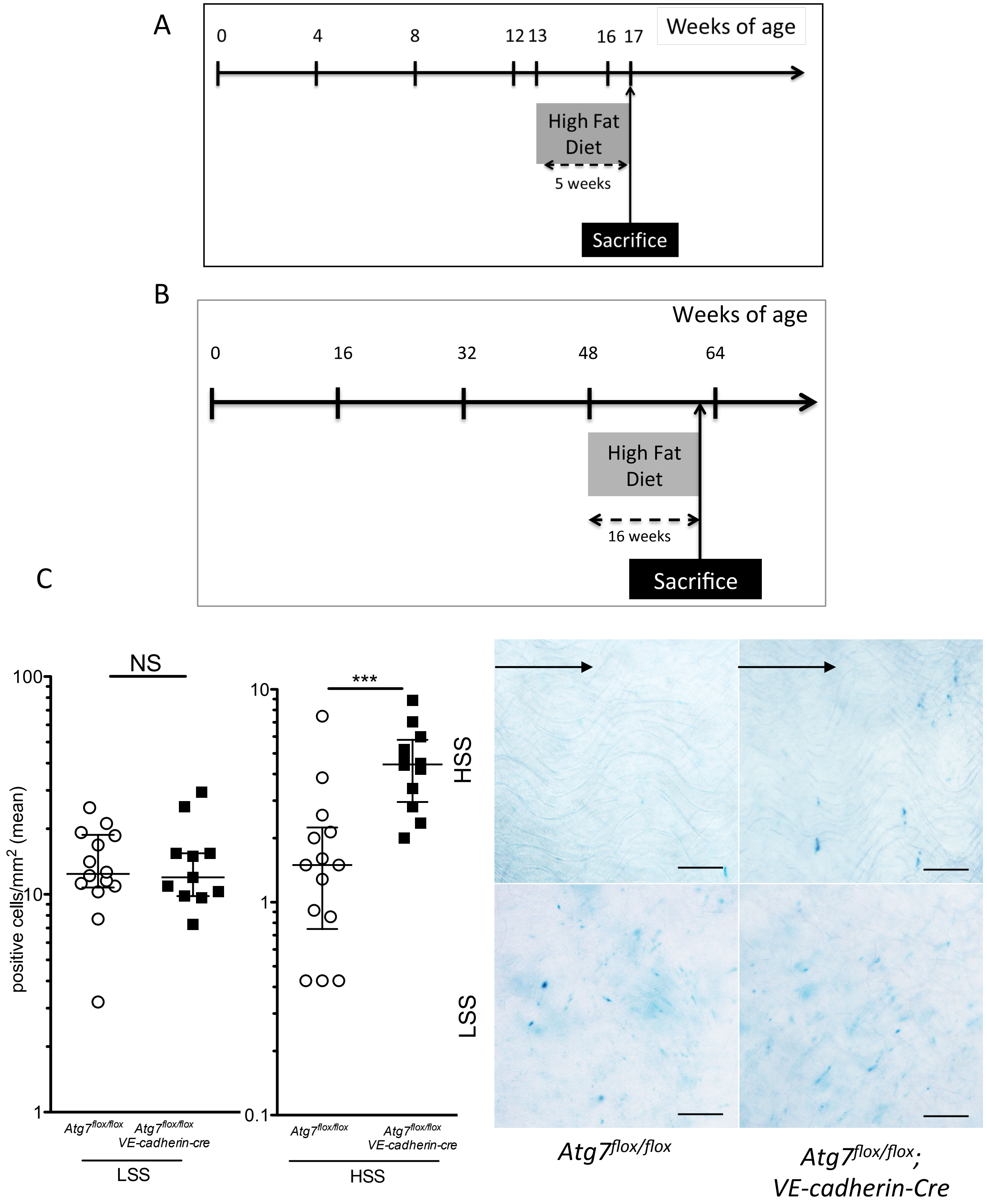

Supplementary Figure 7. Deficiency in endothelial autophagy increases senescence. (A) Protocol to investigate endothelial P53 expression. (B) Protocol to investigate *in vivo* senescence. (C) "*en face*" β-galactosidase staining of the aorta of *Atg7*$^{flox/flox}$ *vs. Atg7*$^{flox/flox}$*; VE-cadherin-Cre* mice (n=13 and n=11 respectively). Bar scale, 100 µm; black arrow represents the flow direction. The inner part of the curvature is exposed to SS and the descendant linear part is exposed to high SS. Abbreviations: HSS, High shear stress; LSS, low shear stress. ***, $p < 0.001$ (Mann Whitney test).

Endothelial autophagic flux hampers atherosclerotic lesion development

Authors: Marouane Kheloufi[a,b,c,1], Anne-Clemence Vion[a,b,1], **Adel Hammoutene**[a,b], Johanne Poisson[a,b], Juliette Lasselin[a,b], Cecile Devue[a,b], Isabelle Pic[a,b], Nicolas Dupont[b,d,e], Johanna Busse[f], Konstantin Stark[f], Julie Lafaurie-Janvore[g], Abdul I. Barakat[g], Xavier Loyer[a,b], Michele Souyri[h], Benoit Viollet[b,i,j], Pierre Julia[b,k], Alain Tedgui[a,b], Patrice Codogno[b,d,e], Chantal M. Boulanger[a,b,2,3], and Pierre-Emmanuel Rautou[a,b,c,l,2]

Affiliations: [a] INSERM, U970, Paris Cardiovascular Research Center, 75015 Paris, France; [b] Université Paris Descartes, Sorbonne Paris Cité, 75006 Paris, France; [c] Université Paris Diderot, Sorbonne Paris Cité, 75013 Paris, France ; [d] INSERM U1151, Institut Necker-Enfants Malades-INEM, 75014 Paris, France ; [e] CNRS UMR 8253, 75014 Paris, France ; [f] Medizinische Klinik I, Klinikum der Universität München, 81377 Munich, Germany; [g] Mechanics & Living Systems, Cardiovascular Cellular Engineering, Laboratoire d'Hydrodynamique, Ecole Polytechnique, UMR 7646, 91128 Palaiseau, France; [h] INSERM UMR_S1131/IHU/Université Paris Diderot, 75013 Paris, France; [i] INSERM U1016, Institut Cochin, 75014 Paris, France; [j] CNRS, UMR 8104, 75014 Paris, France; [k] Service de Chirurgie Cardiaque et Vasculaire, Hôpital Européen Georges Pompidou, AP-HP, 75015 Paris, France; [l] Département Hospitalo-Universitaire Unity, Pôle des Maladies de l'Appareil Digestif, Service d'Hépatologie, Centre de Référence des Maladies Vasculaires du Foie, Hôpital Beaujon, Assistance Publique-Hopitaux de Paris, 92110 Clichy, France

Puncta published in Autophagy. 2018;14(1):173-175

AUTOPHAGY, 2018
VOL. 14, NO. 1, 173–175
https://doi.org/10.1080/15548627.2017.1395114

AUTOPHAGIC PUNCTA

Endothelial autophagic flux hampers atherosclerotic lesion development

Marouane Kheloufi[a,b,c†], Anne-Clemence Vion[a,b†], Adel Hammoutene[a,b], Johanne Poisson[a,b], Juliette Lasselin[a,b], Cecile Devue[a,b], Isabelle Pic[a,b], Nicolas Dupont[b,d,e], Johanna Busse[f], Konstantin Stark[f], Julie Lafaurie-Janvore[g], Abdul I. Barakat[g], Xavier Loyer[a,b], Michele Souyri[h], Benoit Viollet[b,i,j], Pierre Julia[a,b,k], Alain Tedgui[a,b], Patrice Codogno[b,d,e], Chantal M. Boulanger[a,b†] and Pierre-Emmanuel Rautou[a,b,l†]

[a]INSERM, U970, Paris Cardiovascular Research Center - PARCC; [b]Université Paris Descartes, Sorbonne Paris Cité, Paris, France; [c]Université Paris Diderot, Sorbonne Paris Cité, France; [d]INSERM U1151, Institut Necker-Enfants Malades-INEM, Paris, France; [e]CNRS UMR8253, Paris, France; [f]Medizinische Klinik I, Klinikum der Universität München, Munich, Germany; [g]LadHyX - CNRS - Ecole Polytechnique UMR 7646; Mechanics & Living Systems; Cardiovascular Cellular Engineering; Palaiseau, France; [h]INSERM UMR_S 1131/IUH/Université Paris Diderot, Paris; [i]INSERM U1016, Institut Cochin, Paris, France; [j]CNRS UMR8104, Paris, France; [k]Service De Chirurgie Cardiaque Et Vasculaire - Hôpital Européen Georges Pompidou, AP-HP, Paris, France; [l]DHU Unity, Pôle des Maladies de L'appareil Digestif, Service d'Hépatologie, Centre de Référence des Maladies Vasculaires Du Foie, Hôpital Beaujon, AP-HP, Clichy, France

ABSTRACT

Blood flowing in arteries generates shear forces at the surface of the vascular endothelium that control its anti-atherogenic properties. However, due to the architecture of the vascular tree, these shear forces are heterogeneous and atherosclerotic plaques develop preferentially in areas where shear is low or disturbed. Here we review our recent study showing that elevated shear forces stimulate endothelial autophagic flux and that inactivating the endothelial macroautophagy/autophagy pathway promotes a proinflammatory, prosenescent and proapoptotic cell phenotype despite the presence of atheroprotective shear forces. Specific deficiency in endothelial autophagy in a murine model of atherosclerosis stimulates the development of atherosclerotic lesions exclusively in areas of the vasculature that are normally resistant to atherosclerosis. Our findings demonstrate that adequate endothelial autophagic flux limits atherosclerotic plaque formation by preventing endothelial apoptosis, senescence and inflammation.

ARTICLE HISTORY
Received 2 October 2017
Revised 13 October 2017
Accepted 17 October 2017

KEYWORDS
atherosclerotic plaques; autophagic flux; endothelial cells; inflammation; senescence; shear stress

Cardiovascular diseases are the leading cause of death in western countries. Most of these events are due to complications of atherosclerosis. Although risk factors for atherosclerosis are systemic, atherosclerotic plaques develop in specific areas where blood flow is disturbed and shear stress (SS) is low, such as arterial bifurcations and at the inner part of curvatures. Conversely, areas exposed to undisturbed blood flow, generating high laminar SS on the vascular endothelium, remain lesion-free. Endothelial cells exposed to low SS express a prosenescent and proinflammatory phenotype, thereby favoring atherosclerotic plaque development, but intracellular mechanisms linking these events remain elusive. Autophagy being generally a prosurvival and antisenescence mechanism, we tested the hypothesis that SS-induced autophagy could be the missing link between low SS and atherosclerosis development.

We first observed an impressive effect of SS on endothelial autophagy. High SS increases the number of endothelial autophagosomes and LC3 puncta in murine and human arteries. In addition, the LC3-II:LC3-I ratio in cultured endothelial cells exposed to high SS is 5-fold higher than in cells in static conditions and even higher than in those exposed to starvation. These findings extended the results of previous studies showing that SS increases endothelial autophagy in vitro. Using a RFP-GFP-LC3 construct, we demonstrated in vitro that autophagic flux is active under high SS but blocked under low SS conditions; these findings were confirmed in vivo in mice treated with chloroquine. We then investigated the master negative and positive regulators of autophagy, namely the MTOR and AMPK pathways. We observed that low endothelial SS is associated with increased MTOR activity and decreased AMPK activity, when compared to high SS conditions. The involvement of these pathways in the regulation of endothelial autophagy level by shear stress was further confirmed in vivo.

We then evaluated the role of high SS-induced autophagy on atherosclerotic plaque development, and demonstrated that hypercholesterolemic mice bearing an endothelial specific deletion of *Atg5* (*apoe*$^{-/-}$; *atg5*$^{flox/flox}$; *Cdh5/VE-cadherin-Cre*), develop larger atherosclerotic lesions only in normally atheroprotected areas exposed to high SS, when compared to littermate controls. These results are in line with a previous report of larger plaque size in mice deficient in ATG7 in endothelial cells, although the effect of SS was not investigated in that study.

CONTACT Chantal M. Boulanger Chantal.boulanger@inserm.fr Paris Cardiovascular Research Center, INSERM-UMR970, 56 rue Leblanc, 75737 Paris cedex 15, France.

Punctum to: Vion AC, Kheloufi M, Hammoutene A, Poisson J, Lasselin J, Devue C, Pic I, Dupont N, Busse J, Stark K, Lafaurie-Janvore J, Barakat AI, Loyer X, Souyri M, Viollet B, Julia P, Tedgui A, Codogno P, Boulanger CM, Rautou PE. *Autophagy is required for endothelial cell alignment and atheroprotection under physiological blood flow*. PNAS 2017 Sept 25.

† These authors contributed equally to this work.

© 2018 Taylor & Francis

This increase in plaque burden in areas normally resistant to atherosclerosis suggests a role for defective endothelial autophagy in the impairment of flow-dependent atheroprotective mechanisms. A hallmark of atheroresistant areas is endothelial cell alignment in the direction of flow. In mice lacking either endothelial ATG5 or ATG7, we observed that endothelial cells fail to align with the direction of flow in areas of high SS. Similar findings are observed in cultured cells where ATG5 expression had been silenced using shRNA, or in cells treated with wortmannin. Conversely, activation of endothelial autophagy using rapamycin in cells exposed to low SS increases cell alignment with flow direction.

Endothelial proinflammatory activation is a critical step in initiation and progression of atherosclerosis. We observed that cultured endothelial cells deficient in autophagy display an enhanced inflammatory response when stimulated with TNF/TNFα in the presence of high SS. Endothelial cells lacking ATG5 express significantly less antiinflammatory KLF2, more proinflammatory ICAM1, and release more CCL2/MCP-1 than control cells, therefore establishing that activation of endothelial autophagy by high SS is required for curbing the response to proinflammatory stimuli.

Atheroprone low SS is associated with a prosenescent and proapoptotic endothelial phenotype. We observed a greater number of TUNEL- and TRP53/p53-positive nuclei in mice deficient in endothelial ATG5, attesting to increased endothelial apoptosis in areas of high SS, when compared to littermate control mice. Endothelial senescence in cells exposed to high SS in vivo and in vitro was characterized by lower senescence associated-GLB1/β-galactosidase activity and decreased nuclear CDKN2A/p16 expression when compared to cells exposed to low SS. Interestingly, pharmacological and genetic strategies compromising the autophagic process increase endothelial senescence under high SS both in cultured cells and in mice. Conversely, pharmacological activation of autophagy using rapamycin in cultured endothelial cells exposed to low SS decreases senescence.

Altogether, our data demonstrate that defective autophagy in low SS areas is responsible for the preferential plaque formation in these areas, whereas its activation by high SS protects against atherosclerosis by preventing endothelial inflammation, senescence and apoptosis, and promoting endothelial alignment in the direction of flow.

Our findings, together with those from the literature, enhance our understanding of the role of autophagy in atherosclerosis (Fig. 1). Indeed, deficiency in autophagy specifically in macrophages increases apoptosis, oxidative stress, accumulation of cholesterol crystals, and inflammasome activation in lesional macrophages, thereby promoting plaque necrosis, and worsening efferocytosis. Defective autophagy in vascular smooth muscle cells also promotes diet-induced atherogenesis

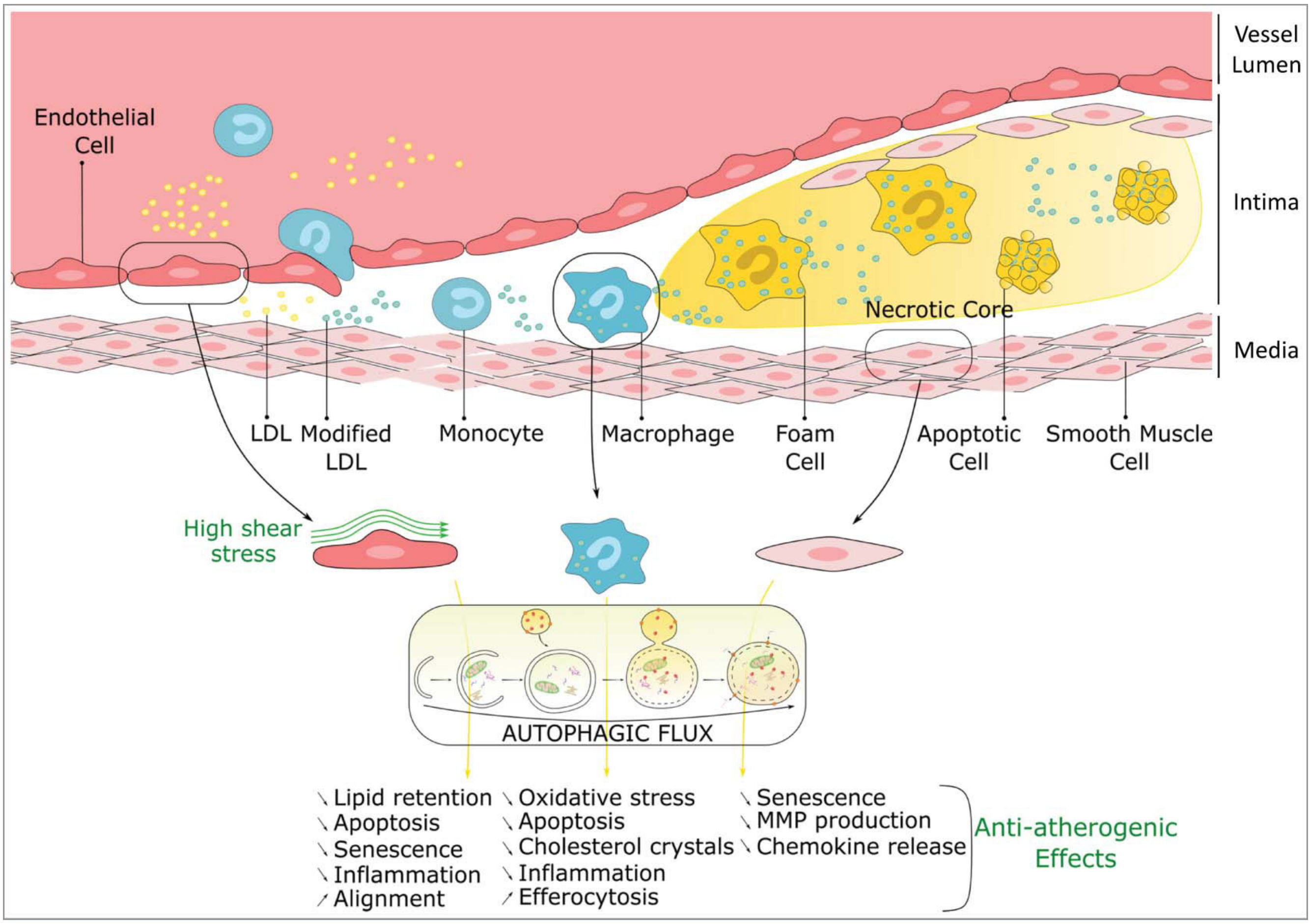
Vessel Lumen
Intima
Media
Endothelial Cell
Necrotic Core
LDL
Modified LDL
Monocyte
Macrophage
Foam Cell
Apoptotic Cell
Smooth Muscle Cell
High shear stress
AUTOPHAGIC FLUX
↘ Lipid retention
↘ Apoptosis
↘ Senescence
↘ Inflammation
↗ Alignment
↘ Oxidative stress
↘ Apoptosis
↘ Cholesterol crystals
↘ Inflammation
↗ Efferocytosis
↘ Senescence
↘ MMP production
↘ Chemokine release
Anti-atherogenic Effects

Figure 1. Atheroprotective role of autophagy in endothelial, macrophage and smooth muscle cells. LDL, low-density lipoprotein; MMP, matrix metalloproteinase.

by accelerating senescence and increasing metalloproteinase production and chemokine release.

Altogether, these data indicate that stimulation of autophagic flux constitutes an attractive therapeutic strategy for preventing atherosclerosis development.

Disclosure of potential conflicts of interest

No potential conflict of interest was reported by the authors.

Funding

This work was supported by INSERM, Paris Descartes University, the « *Fondation pour la Recherche Médicale* » (DPC20111122979), the « *Agence Nationale pour la Recherche* » (ANR-14-CE12-0011, ANR-14-CE35-0022, ANR-16-CE14-0015-01) and by AFEF (2014), J.P by the '*poste d'accueil INSERM*', and A-C.V. by *CODDIM Ile de France*, M.K and A.H. by the '*Ministère de la Recherche et de l'Enseignement Supérieur*', and M.K. by the « *Fondation pour la Recherche Médicale* » (FDT20160435690).

3. Endothelial JAK2^{V617F} does not enhance liver lesions in mice with Budd-Chiari syndrome

Endothelial JAK2^{V617F} does not enhance liver lesions in mice with Budd-Chiari syndrome

Athors: Johanne Poisson[1,2] Moira B. Hilscher[3] Marion Tanguy[1,2] **Adel Hammoutene**[1,2] Chantal M. Boulanger[1,2] Jean-Luc Villeval[4,5] Douglas A. Simonetto[3] Dominique Valla[6,7] Vijay H. Shah[3] Pierre-Emmanuel Rautou[1,2,6,7]

Affiliations:

[1] INSERM, UMR-970, Paris Cardiovascular Research Center – PARCC, Paris, France

[2] Université Paris Descartes, Sorbonne Paris Cité, Paris, France

[3] Gastroenterology Research Unit, Division of Gastroenterology and Hepatology, Mayo Clinic, Rochester, MN, USA [4]INSERM, Institut Gustave Roussy, INSERM U1170, Villejuif, France

[5] University Paris XI, Villejuif, France

[6] Service d'hépatologie, DHU Unity Hôpital Beaujon, APHP, Clichy, France [7]Université Denis Diderot-Paris 7, Sorbonne Paris Cité, 75018 Paris, France

Letter to the editor published in J Hepatol. 2018 May;68(5):1086-1087

JOURNAL
OF HEPATOLOGY

Endothelial *JAK2*^{V617F} does not enhance liver lesions in mice with Budd-Chiari syndrome

To the Editor:

Budd-Chiari syndrome is defined as hepatic venous outflow obstruction in the absence of congestive or restrictive heart disease. Myeloproliferative neoplasms are the leading cause of Budd-Chiari syndrome, diagnosed in 25–50% of such patients.[1,2] In most patients with Budd-Chiari syndrome and myeloproliferative neoplasms, Janus kinase 2 gene (*JAK2*) V617F mutation is found in myeloid cells. *JAK2*^{V617F} has also been detected in liver endothelial cells of patients with Budd-Chiari syndrome, attributed to a common cell of origin for myeloid and endothelial cells, called hemangioblast.[3–5] In Budd-Chiari syndrome, *JAK2*^{V617F} is associated with poorer prognostic features at presentation and earlier need for hepatic decompression procedures.[1] This observation leads to the hypothesis that *JAK2*^{V617F} enhances liver injury and fibrosis induced by hepatic venous outflow obstruction, thus worsening Budd-Chiari syndrome.

In order to test this hypothesis, we applied a recently described surgical model of Budd-Chiari syndrome to mice expressing *JAK2*^{V617F}.[6] *JAK2*^{V617F} expression in myeloid cells promotes major vasodilation and hemostasis impairment, making surgery extremely challenging in these animals.[7] Accordingly, we analyzed the endothelial component using mice expressing *JAK2*^{V617F} specifically in endothelial cells. We generated these transgenic mice by crossing conditional *Jak2*^{V617F} knock-in mice with inducible *Cadherin5*$^{Cre\text{-}ERT2}$ mice. Recombination was induced in *Jak2*^{V617F} *knock-in – Cadherin5*$^{Cre\text{-}ERT2}$ (hereafter referred to as *JAK*^{V617F}) mice by tamoxifen injection (1 mg/day/mice intraperitoneously for five consecutive days, two consecutive weeks) at the age of five weeks. Littermate controls (hereafter referred to as *JAK2*^{WT}) received the same treatment. Partial inferior vena cava ligation (pIVCL), or sham surgeries were performed at the age of 12 weeks and mice were sacrificed six weeks postoperatively (Fig. 1).[6] Based on previous experiments using this surgical model, we included 8 to 10 mice per group.[6] All experiments were performed in accordance with the European Community guidelines for the care and use of laboratory animals (N°07,430) and were approved by our institutional ethical committee (17-053).

As expected, *JAK2*^{WT} mice undergoing pIVCL had higher portal pressure, liver expression of profibrogenic genes and liver

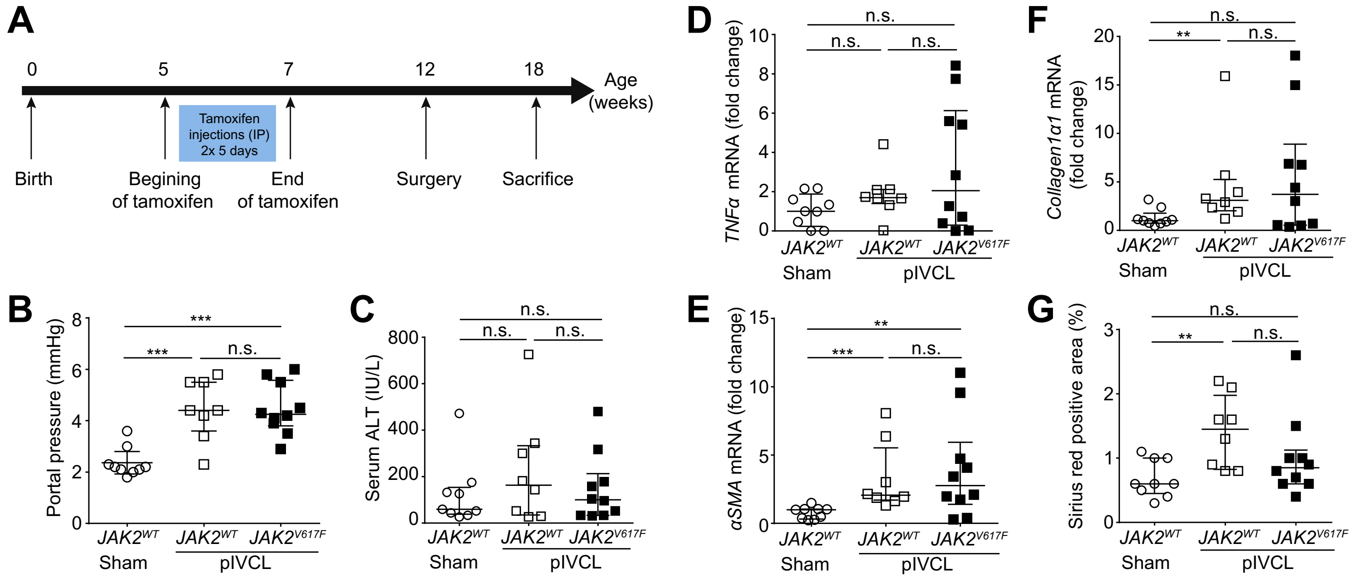

Fig. 1. Endothelial *JAK2*^{V617F} does not enhance liver injury in mice after partial inferior vena cava ligation. Partial inferior vena cava ligation was performed in 12-week aged male and female *Jak2*^{V617F} knock-in - *Cadherin5*$^{Cre\text{-}ERT2}$ (*JAK*^{V617F}) mice and in littermate controls (*JAK2*^{WT}). Sham surgery was also performed. All mice were on a C57BL/6 background. (A) Mice were sacrificed 6 weeks postoperatively. (B) Portal pressure, (C) serum ALT level, (D) liver *TNFα*, (E) *αSMA* and (F) *collagen1α1* gene expressions were determined (supplementary CTAT Table) and (G) liver fibrosis was quantified (Sirius red positive areas). Data are given as median (horizontal bar) and interquartile range (error bar). Comparisons between groups of mice were performed using the Mann–Whitney U test. $^{*}p$ <0.05; $^{**}p$ <0.01; and $^{***}p$ <0.001. ALT, alanine aminotransferase; *JAK2*, Janus kinase 2; pIVCL, partial inferior vena cava ligation; n.s., no significant difference.

Keywords: Myeloproliferative neoplasm; Liver fibrosis; Portal hypertension; Hepatic venous outflow obstruction; Splanchnic thrombosis.

fibrosis than sham mice, while showing no change in serum aminotransferases or in liver expression of proinflammatory genes (Fig. 1).[6] However, as shown (Fig. 1), the expression of *JAK*^{V617F} in liver endothelial cells did not affect any of these parameters.

In conclusion, we found no evidence in an animal model that endothelial *JAK2*^{V617F} can explain the more severe presentation of patients with Budd-Chiari syndrome and *JAK2*^{V617F}. The explanation for increased severity of these patients should therefore be sought mostly in myeloid *JAK2*^{V617F}. Thus, future therapeutic strategies to improve the management of patients with Budd-Chiari syndrome and myeloproliferative neoplasms might focus on myeloid cells rather than on endothelial cells. Beside the cytoreductive agent hydroxyurea, treatments for myeloproliferative neoplasms now also include the JAK2/1 inhibitor ruxolitinib. One phase II trial recently reported that ruxolitinib is safe in patients with splanchnic vein thrombosis.[8] Whether ruxolitinib is useful in this setting to improve patient outcomes should be evaluated in larger studies.

Financial support

This work was supported by the Agence Nationale pour la Recherche (ANR-14-CE12-0011 and ANR-14-CE35-0022) and J.P by the "poste d'accueil INSERM".

Conflict of interest

The authors declare no conflicts of interest that pertain to this work.

Please refer to the accompanying ICMJE disclosure forms for further details.

Authors' contributions

J.P. and M.B.H contributed equally to the work. M.B.H. and D.A.S. performed mouse surgeries. J.P., A.H. and M.T. analyzed liver samples. J-L.V. generated *Jak2*^{V617F} *knock-in* mice. J.P. and P-E. R. wrote the manuscript. C.M.B, D.V. and V.H.S discussed and analyzed the results. All authors critically revised the manuscript.

Acknowledgements

We thank the members of the INSERM UMR-970 animal facility (ERI), Fatoumata Camara for superb technical assistance, and the Hôpital Bichat biochemistry core facility. We also thank R. Adams for having provided *Cadherin5*$^{Cre\text{-}ERT2}$ mice.

Supplementary data

Supplementary data associated with this article can be found, in the online version, at https://doi.org/10.1016/j.jhep.2018.01.010.

References

Author names in bold designate shared co-first authorship

[1] Kiladjian J-J, Cervantes F, Leebeek FW, Marzac C, Cassinat B, Chevret S, et al. The impact of JAK2 and MPL mutations on diagnosis and prognosis of splanchnic vein thrombosis: a report on 241 cases. Blood 2008;111:4922–4929.
[2] European Association for the Study of the Liver. EASL clinical practice guidelines: vascular diseases of the liver. J Hepatol 2016;64:179–202.
[3] Sozer S, Fiel MI, Schiano T, Xu M, Mascarenhas J, Hoffman R. The presence of JAK2V617F mutation in the liver endothelial cells of patients with Budd-Chiari syndrome. Blood 2009;113:5246–5249.
[4] Rosti V, Villani L, Riboni R, Poletto V, Bonetti E, Tozzi L, et al. Spleen endothelial cells from patients with myelofibrosis harbor the JAK2V617F mutation. Blood 2013;121:360–368.
[5] **Teofili L**, **Martini M**, Iachininoto MG, Capodimonti S, Nuzzolo ER, Torti L, et al. Endothelial progenitor cells are clonal and exhibit the JAK2(V617F) mutation in a subset of thrombotic patients with Ph-negative myeloproliferative neoplasms. Blood 2011;117:2700–2707.
[6] Simonetto DA, Yang H, Yin M, de Assuncao TM, Kwon JH, Hilscher M, et al. Chronic passive venous congestion drives hepatic fibrogenesis via sinusoidal thrombosis and mechanical forces. Hepatology 2015;61:648–659.
[7] Lamrani L, Lacout C, Ollivier V, Denis CV, Gardiner E, Ho Tin Noe B, et al. Hemostatic disorders in a JAK2V617F-driven mouse model of myeloproliferative neoplasm. Blood 2014;124:1136–1145.
[8] Pieri L, Paoli C, Arena U, Marra F, Mori F, Zucchini M, et al. Safety and efficacy of ruxolitinib in splanchnic vein thrombosis associated with myeloproliferative neoplasms. Am J Hematol 2017;92:187–195.

Johanne Poisson[1,2,†]
Moira B. Hilscher[3,†]
Marion Tanguy[1,2]
Adel Hammoutene[1,2]
Chantal M. Boulanger[1,2]
Jean-Luc Villeval[4,5]
Douglas A. Simonetto[3]
Dominique Valla[6,7]
Vijay H. Shah[3]
Pierre-Emmanuel Rautou[1,2,6,7,*]
[1] *INSERM, UMR-970, Paris Cardiovascular Research Center – PARCC, Paris, France*
[2] *Université Paris Descartes, Sorbonne Paris Cité, Paris, France*
[3] *Gastroenterology Research Unit, Division of Gastroenterology and Hepatology, Mayo Clinic, Rochester, MN, USA*
[4] *INSERM, Institut Gustave Roussy, INSERM U1170, Villejuif, France*
[5] *University Paris XI, Villejuif, France*
[6] *Service d'hépatologie, DHU Unity Hôpital Beaujon, APHP, Clichy, France*
[7] *Université Denis Diderot-Paris 7, Sorbonne Paris Cité, 75018 Paris, France*
*Corresponding author. Address: Service d'Hépatologie, Hôpital Beaujon, 100 boulevard du Général Leclerc, 92110 Clichy, France.
Tel.: +33 1 40 87 52 83; fax: +33 1 40 87 54 87.
E-mail address: pierre-emmanuel.rautou@inserm.fr

[†] J.P. and M.B.H. contributed equally to this study.

Primary cilia sensitize endothelial cells to BMP and prevent excessive vascular regression

Authors: Anne-Clémence Vion[1,2,3], Silvanus Alt[1], Alexandra Klaus-Bergmann[1,3], Anna Szymborska[1,3], Tuyu Zheng[1], Tijana Perovic[1], **Adel Hammoutene**[4,5], Marta Bastos Oliveira[1], Eireen Bartels-Klein[1,3], Irene Hollfinger[1], Pierre-Emmanuel Rautou[4,5,6], Miguel O. Bernabeu[7,8], and Holger Gerhardt[1,2,3,9,10,11]

Affiliations: [1] Max Delbrück Center for Molecular Medicine, Berlin, Germany; [2] Vascular Biology Laboratory, London Research Institute – Cancer Research UK, Lincoln's Inn Fields Laboratories, London, England, UK; [3] German Center for Cardiovascular Research, Berlin, Germany; [4] Institut National de la Santé et de la Recherche Medicale, U970, Paris Cardiovascular Research Center, Paris, France; [5] Université Paris Descartes, Sorbonne Paris Cité, Paris, France; [6] Departement Hospitalo-Universitaire Unity, Pôle des Maladies de l'Appareil Digestif, Service d'Hépatologie, Centre de Référence des Maladies Vasculaires du Foie, Hôpital Beaujon, Assistance Publique - Hopitaux de Paris, Clichy, France; [7] Centre for Medical Informatics, Usher Institute, University of Edinburgh, Edinburgh, Scotland, UK; [8] Centre for Computational Science, Department of Chemistry, University College London, London, England, UK; [9] Vascular Patterning Laboratory, VIB Center for Cancer Biology, Leuven, Belgium; [10] Vascular Patterning Laboratory, Department of Oncology, KU Leuven, Leuven, Belgium; [11] Berlin Institute of Health, Berlin, Germany.

Original article published in J Cell Biol. 2018 May 7;217(5):1651-1665

Published Online: 2 March, 2018 | Supp Info: http://doi.org/10.1083/jcb.201706151
Downloaded from jcb.rupress.org on October 11, 2018

JCB Journal of Cell Biology

REPORT

Primary cilia sensitize endothelial cells to BMP and prevent excessive vascular regression

Anne-Clémence Vion[1,2,3], Silvanus Alt[1], Alexandra Klaus-Bergmann[1,3], Anna Szymborska[1,3], Tuyu Zheng[1], Tijana Perovic[1], Adel Hammoutene[4,5], Marta Bastos Oliveira[1], Eireen Bartels-Klein[1,3], Irene Hollfinger[1], Pierre-Emmanuel Rautou[4,5,6], Miguel O. Bernabeu[7,8], and Holger Gerhardt[1,2,3,9,10,11]

Blood flow shapes vascular networks by orchestrating endothelial cell behavior and function. How endothelial cells read and interpret flow-derived signals is poorly understood. Here, we show that endothelial cells in the developing mouse retina form and use luminal primary cilia to stabilize vessel connections selectively in parts of the remodeling vascular plexus experiencing low and intermediate shear stress. Inducible genetic deletion of the essential cilia component intraflagellar transport protein 88 (IFT88) in endothelial cells caused premature and random vessel regression without affecting proliferation, cell cycle progression, or apoptosis. IFT88 mutant cells lacking primary cilia displayed reduced polarization against blood flow, selectively at low and intermediate flow levels, and have a stronger migratory behavior. Molecularly, we identify that primary cilia endow endothelial cells with strongly enhanced sensitivity to bone morphogenic protein 9 (BMP9), selectively under low flow. We propose that BMP9 signaling cooperates with the primary cilia at low flow to keep immature vessels open before high shear stress–mediated remodeling.

Introduction

Efficient oxygen and nutrient supply through the formation of a hierarchically branched network of blood vessels is essential for vertebrate development. A primary vascular plexus initially expands by sprouting angiogenesis (Isogai et al., 2003; Potente et al., 2011) followed by vascular remodeling to adapt vessel organization, shape, and size; in its course, superfluous and inefficient connections are pruned away by active regression (Franco et al., 2015). Mice with genetic inactivation of factors involved in vascular remodeling die during midgestation (Potente et al., 2011), demonstrating the critical importance of remodeling. Nevertheless, the maintenance of redundant collateral vessels, despite being poorly perfused in normal physiology, is critical for recovery after injury; in this context, superfluous connections become active, increase in size, and substitute damaged vessels (Liu et al., 2014). Thus, excessive remodeling and the removal of all nonperfused vessels carry long-term risk, whereas too little remodeling impedes vascular function.

Cells need to respond appropriately to mechanical cues to ensure healthy tissue development and homeostasis. Endothelial cells (ECs) in particular are under constant mechanical strains exerted by blood flow. Interestingly, ECs are able to sense small variations in the direction, magnitude, and regularity of blood flow–induced shear stress (Wang et al., 2013; Givens and Tzima, 2016) and respond to such changes by influencing vasculature remodeling (Culver and Dickinson, 2010; Baeyens et al., 2016a). Adaptation of ECs to flow is critical for the development and maintenance of a well-functioning cardiovascular system; for example, in adult mice flow-sensing through VEGFR3 controls vessel caliber (Baeyens et al., 2015). However, how ECs sense and transduce mechanical signals during vascular remodeling to achieve a balanced network of blood vessels is still poorly understood (Dolan et al., 2013). Vascular regression has been shown to rely on axial polarization of ECs against the direction of blood flow and their consequent migration from poorly perfused vessels into well-perfused neighboring segments, thus removing superfluous connections and reinforcing vessels that experience higher shear stress (Franco et al., 2015, 2016).

---

[1]Max Delbrück Center for Molecular Medicine, Berlin, Germany; [2]Vascular Biology Laboratory, London Research Institute – Cancer Research UK, Lincoln's Inn Fields Laboratories, London, England, UK; [3]German Center for Cardiovascular Research, Berlin, Germany; [4]Institut National de la Santé et de la Recherche Medicale, U970, Paris Cardiovascular Research Center, Paris, France; [5]Université Paris Descartes, Sorbonne Paris Cité, Paris, France; [6]Departement Hospitalo-Universitaire Unity, Pôle des Maladies de l'Appareil Digestif, Service d'Hépatologie, Centre de Référence des Maladies Vasculaires du Foie, Hôpital Beaujon, Assistance Publique - Hopitaux de Paris, Clichy, France; [7]Centre for Medical Informatics, Usher Institute, University of Edinburgh, Edinburgh, Scotland, UK; [8]Centre for Computational Science, Department of Chemistry, University College London, London, England, UK; [9]Vascular Patterning Laboratory, VIB Center for Cancer Biology, Leuven, Belgium; [10]Vascular Patterning Laboratory, Department of Oncology, KU Leuven, Leuven, Belgium; [11]Berlin Institute of Health, Berlin, Germany.

Correspondence to Holger Gerhardt: holger.gerhardt@mdc-berlin.de; Anne-Clemence Vion: anne-clemence.vion@mdc-berlin.de.

© 2018 Vion et al. This article is distributed under the terms of an Attribution–Noncommercial–Share Alike–No Mirror Sites license for the first six months after the publication date (see http://www.rupress.org/terms/). After six months it is available under a Creative Commons License (Attribution–Noncommercial–Share Alike 4.0 International license, as described at https://creativecommons.org/licenses/by-nc-sa/4.0/).

Check for updates

https://doi.org/10.1083/jcb.201706151

Many structures and receptors have been identified as flow sensors in ECs (Traub and Berk, 1998; Baeyens et al., 2016a). Among them, the primary cilium has been shown to bend in response to blood flow and to be required for flow sensing, thus controlling endothelial function in both normal and pathological conditions (Goetz et al., 2014; Dinsmore and Reiter, 2016). The primary cilium extends from the membrane of the cell and is stabilized by a microtubule scaffold known as the axoneme. The ciliary axoneme is surrounded by the ciliary membrane, a specialized compartment in which many receptors, ion channels, and transporter proteins are embedded, where they recruit second messengers and effectors (Satir et al., 2010). Several intraflagellar transport proteins, including intraflagellar transport protein 88 (IFT88), specific kinesin motors like KIF3a, and other structural components like ARL13b, are essential for formation and maintenance of primary cilia (Nonaka et al., 1998; Taulman et al., 2001; Hori et al., 2008). Their selective deletion has been useful to investigate the role of primary cilia in many cells. However, some cilia independent functions can also be found for IFT88 and KIF3a (Delaval et al., 2011; Boehlke et al., 2013, 2015; Borovina and Ciruna, 2013). In blood vessels, the endothelial primary cilium extends into the lumen of the vessels. Activation of the primary cilium by flow triggers calcium signaling and nitric oxide production in vitro (Nauli et al., 2008). In adult mice, loss of endothelial primary cilia aggravates atherosclerosis caused by reduced nitric oxide synthase activity (Dinsmore and Reiter, 2016). In zebrafish embryos, the primary cilium acts as a mechanical sensor for ECs exposed to low shear stress (LSS; Goetz et al., 2014) and contributes to blood–brain barrier integrity (Kallakuri et al., 2015). Finally, the maintenance of cilia has been described to be dependent on flow (Iomini et al., 2004). During valve formation, for example, extreme high shear stress (HSS) levels disrupt cilia, leading to mesenchymal transition through activation of TGFβ/ALK5 signaling (Ten Dijke et al., 2012). Interestingly, in other cell types, the primary cilium has been shown to transmit signals coming from the Notch, TGFβ, and Wnt pathways (Goetz and Anderson, 2010; Gerhardt et al., 2016; Pedersen et al., 2016) by allowing the clustering of kinases and their targets. Additionally, hair cells forming the cochlea require a primary cilium to specifically position their basal body on one side of the nucleus, and therefore polarize (Jones et al., 2008).

ECs are highly responsive to bone morphogenetic proteins (BMPs) and TGFβ, which share common effectors and engage in signaling cross talk (Guo and Wang, 2009). Recent studies reveal that the BMP pathway is important for flow-induced responses through SMAD1/5/8 activity (Zhou et al., 2012; Laux et al., 2013; Baeyens et al., 2016b). SMAD1/5 activation downstream of BMP receptors can be induced by flow in the absence of ligand suggesting a direct effect of mechanical forces on the BMP receptors (Zhou et al., 2012). In zebrafish, the BMP receptor ALK1, responsible for SMAD1/5/8 phosphorylation, has been shown to trigger a flow-sensitive BMP10 response (Laux et al., 2013) contributing to EC migration against the blood flow (Rochon et al., 2016). Latest studies identified that BMP9/10–induced signaling upon HSS stimulation is dependent on the coreceptor Endoglin (Baeyens et al., 2016b).

Here, we demonstrate that IFT88 and most likely the endothelial primary cilium are essential for appropriate vascular patterning by protecting nascent blood vessels exposed to LSS from premature regression. Mechanistically, we show that ECs with primary cilia show strongly enhanced BMP9–Smad1/5/8 signaling selectively when exposed to LSS.

Results

Presence of endothelial primary cilia inversely correlates with shear stress levels during vascular remodeling

To assess the distribution of primary cilia in the developing vasculature of the mouse retina, we used immunofluorescence staining for ARL13b. We identified cilia localizing within vascular staining and close to endothelial nuclei (Fig. 1 A) distributed across all parts of the vascular plexus (Fig. 1, B and C), except in tip cells at the sprouting front. Quantification in arteries, veins, and plexus at different developmental stages showed that the number of ECs with primary cilia decreased in arteries as the vasculature developed (Fig. 1, B and C). In vitro, in confluent monolayers of human umbilical vein endothelial cells (HUVECs), ~15% of cells showed an apical primary cilium under static conditions. This percentage decreased with increasing shear stress levels, dropping to 5% under HSS (Fig. 1 D). To investigate potential population dynamics of ECs with cilia, we studied a zebrafish line expressing a membrane reporter for ECs and GFP-tagged ARL13b (Tg(kdr-l:ras–Cherrys916; β-actin::arl13b-eGfp)). Although most of the luminal cilia in ECs were stable over the acquisition time (Video 1, 6 h), we identified several appearing (Fig. 1, E and F; and Video 2) or retracting cilia (Fig. 1, E and F; and Video 3). Using adenoviral expression of GFP-tagged ARL13b in HUVECs, we confirmed that only a fraction of ECs (10%) harbored a primary cilium (Fig. S1, A and B). Time-lapse imaging revealed that most of the ciliated cells remained so over the 5-h observation time (Video 4; and Fig. S1, B and C) although, as in zebrafish, some cilia retracted and others appeared de novo (Fig. S1, B and C).

Primary cilia prevent vascular regression by maintaining collective polarization of ECs

To assess the function of endothelial primary cilia in the retinal vasculature, we performed genetic deletion of *Ift88* specifically in ECs. To do so, we bred mice expressing a tamoxifen-inducible Cre recombinase under the control of the endothelial-specific promoter of *Pdgfb* (*Pdgfb-iCre-ERT2-Egfp*; Claxton et al., 2008) with mice expressing floxed alleles of *Ift88* (Haycraft et al., 2007). *Ift88*$^{fl/fl}$; *Pdgfb-iCre-ERT2-Egfp*$^{+/wt}$ offspring were then injected with tamoxifen at postnatal day 1 (P1) and P3 to induce recombination of the floxed alleles (referred to as IFT88 iEC-KO). Western blot analyses on lung ECs, quantitative PCR on retinal ECs, and immunofluorescence staining of retinas confirmed deletion of IFT88 and the loss of primary cilia, respectively (Fig. S1, D–F).

At P6, IFT88 iEC-KO mice showed decreased radial expansion of the retinal vasculature (Fig. 2 A), decreased vascular density (Fig. 2 B), and fewer sprouting cells at the front of the plexus (Fig. 2 C) compared with littermate controls. This phenotype was transient as retinas from P15 mice recovered from the decrease in radial expansion and vascular density (Fig. S1 G).

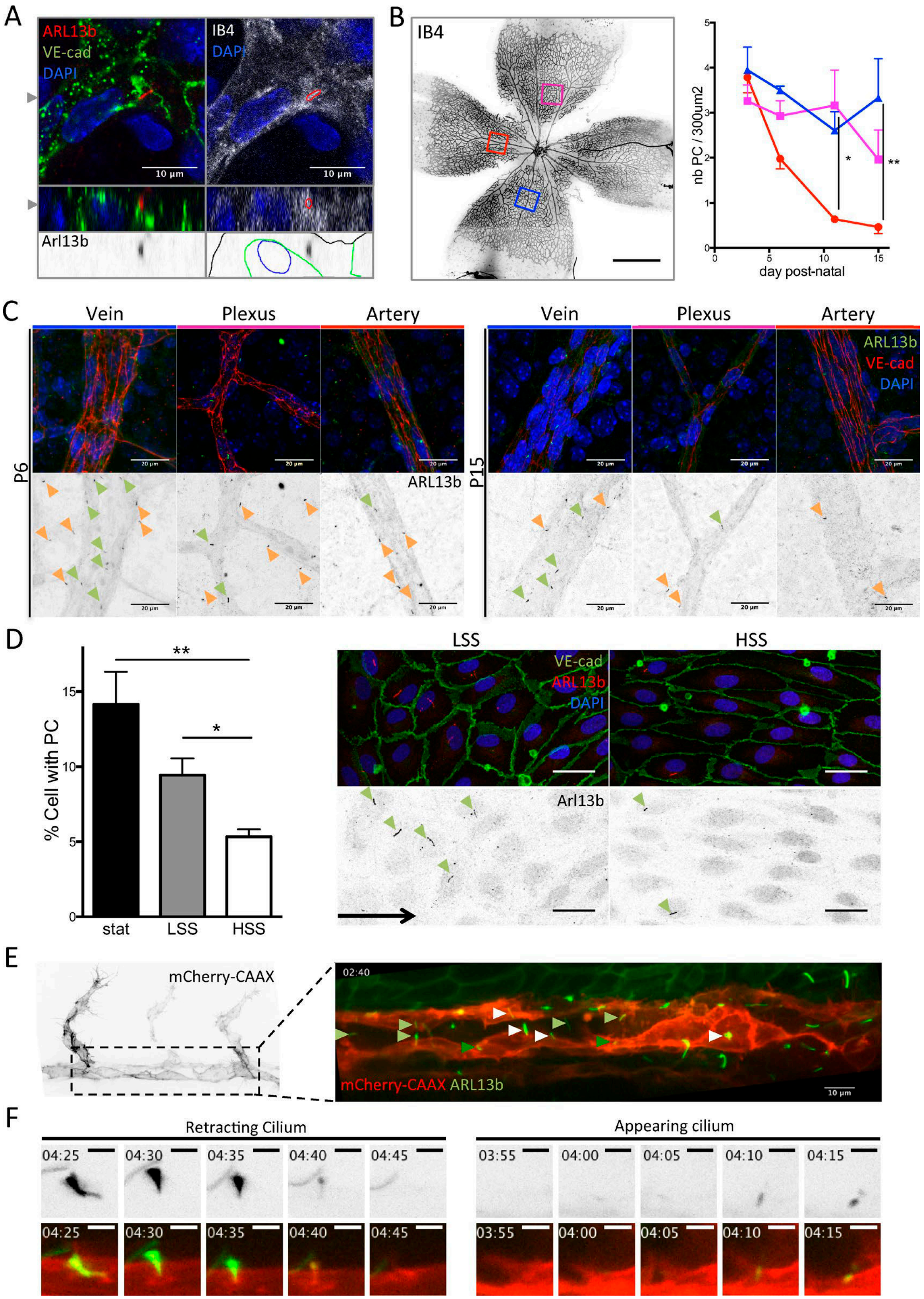
A
ARL13b
VE-cad
DAPI
10 µm
IB4
DAPI
10 µm
Arl13b
B
IB4
nb PC / 300um2
0
1
2
3
4
5
0
5
10
15
day post-natal
*
**
C
Vein
Plexus
Artery
Vein
Plexus
Artery
ARL13b
VE-cad
DAPI
P6
P15
ARL13b
20 µm
D
% Cell with PC
0
5
10
15
**
*
stat
LSS
HSS
LSS
HSS
VE-cad
ARL13b
DAPI
Arl13b
E
mCherry-CAAX
02:40
mCherry-CAAX ARL13b
10 µm
F
Retracting Cilium
04:25
04:30
04:35
04:40
04:45
Appearing cilium
03:55
04:00
04:05
04:10
04:15

Figure 1. **Primary cilia are present in ECs, and their presence correlates with shear stress levels. (A)** Primary cilia belonging to ECs were found in the retinal vasculature. Top images present one z-stack (depth 0.26 µm) showing the cilium within the vasculature and overlapping with Isolectin staining (red outline on the right upper image highlights the cilium localization). Bottom images present the corresponding z-projection showing the cilium embedded in the endothelial layer (black outline, Isolectin B4; blue outline, DAPI; green outline, VE-cadherin). The gray arrowheads indicate the cut-planes corresponding to the z-stack visualization. **(B)** Retinas from mouse pups were collected at P3, P6, P11, and P15 and stained for VE-cadherin (EC junctions), ARL13b (primary cilia), and DAPI (nuclei). The number of primary cilia present in the different areas of the vasculature was quantified over time and maturation of the vessels in different animals (red, artery; magenta, plexus; blue, vein; *n* = 3 for each time point; median ± interquartile range (IQ); two-way ANOVA. Data distribution was assumed to be normal but this was not formally tested). Bar, 700 µm. **(C)** Representative images are shown for each region. Green arrowheads, endothelial

IFT88 is implicated in spindle orientation in HeLa and epithelial cells (Delaval et al., 2011; Taulet et al., 2017) and is required for orienting cell divisions during gastrulation (Borovina and Ciruna, 2013). Using flow cytometry and propidium iodide staining, we investigated whether ECs lacking IFT88 exhibit cell cycle–related defects or increased apoptosis, two possible causes for reduced vascular density. We found no changes in the proportion of ECs undergoing apoptosis in retinas of iEC-IFT88 mice compared with controls (Fig. S2 A). We confirmed these results by staining retinas for cleaved caspase-3 (Fig. S2 B). The percentage of polyploid ECs and of ECs in G2-M was not increased, suggesting that IFT88 expression levels do not interfere with the final steps of cell division (Fig. S2 A). In contrast, the proportion of ECs in G0-G1 was increased, whereas ECs in S phase were decreased in IFT88 iEC-KO mice compared with controls. However, we found that the proportion of ECs incorporating 5-ethynyl-2´-deoxyuridine (EdU) was increased in IFT88 iEC-KO retinas (Fig. S2 D), suggesting that these cells may remain in S phase for a longer period of time. Nevertheless, the number of ECs forming the retinal vasculature in the remodeling area at P6 was not different between IFT88 iEC-KO and control mice (Fig. S2 C), arguing against a role of proliferation or cell number in regulating vascular density.

As previously described, the ultimate density of the retinal vasculature is regulated by vascular regression (Franco et al., 2015). In retinas, lumen loss (visualized by intercellular adhesion molecule 2 [ICAM2] staining) and the presence of empty collagen sleeves are indicators of vascular regression. We observed that IFT88 iEC-KO retinas showed significantly more collapsed lumens (Fig. 3 A) and more empty collagen sleeves than controls (Fig. 3 B), suggesting that the decrease in vascular density observed in IFT88 iEC-KO mice is caused by increased regression of preexisting vessels. Interestingly, by analyzing the distribution of empty sleeves throughout the retina between vein and artery (Fig. 3 C), we found that vessels in IFT88 iEC-KO retinas preferentially regressed close to veins, whereas vessels in control retinas preferentially regressed close to arteries (Fig. 3 D).

Previous work identified that vascular regression is regulated by blood flow (Chen et al., 2012; Udan et al., 2013). Above a critical threshold, flow induces axial polarization and migration of ECs against the flow direction. In vessel segments exposed to low or discontinuous flow, ECs migrate away from each other into adjacent vessels experiencing higher flow, leading to the regression of the low-flow segment (Franco et al., 2015). To understand the influence of the loss of endothelial primary cilia on vessel stability and regression, we evaluated the flow pattern and polarity profiles in IFT88 iEC-KO retinas, combining in silico simulation of blood flow patterns (Bernabeu et al., 2014, 2017 *Preprint*) and in vivo polarity data (assessed by Golgi–nucleus axis direction; Fig. S2 E, white arrows). The overall flow simulation pattern was similar between control and IFT88 iEC-KO retinas (Fig. S2 F). By correlating local shear stress values obtained from these simulations with axial polarity of the ECs in the same retinas, we found that ECs in IFT88 iEC-KO retinas showed similar polarity profiles as those in control retinas, both in regions of LSS and HSS (Fig. 3 E). However, in areas of intermediate shear stress, polarization against the flow was significantly reduced in ECs of IFT88 iEC-KO retinas compared with controls (Fig. 3 E). Interestingly, this range of shear stress prevailed precisely in the areas of increased regression in IFT88 iEC-KO retinas (Fig. 3 F). We further manually quantified the number of vessel segments displaying two or more ECs oriented in opposite directions (referred to as divergent polarity; Fig. 3 G). Localization of these events was shifted significantly toward veins in IFT88 iEC-KO retinas (Fig. 3 H). Together, the loss of flow-induced polarity and increased regression preferentially in LSS areas (i.e., close to veins) suggest that IFT88, very likely by supporting cilia formation, contributes to flow sensing and vessel maintenance in poorly perfused segments.

Primary cilium augments BMP9 responses in ECs and decreases their migration speed

In search for the cellular and molecular mechanisms under control of the primary cilium in ECs, we silenced IFT88 in HUVECs using siRNAs (Fig. S3 A), reducing the number of primary cilia by 75% (Fig. S3 B). As the basal body of the primary cilium has been shown in different cell types to be required for the activation of several signaling pathways (Goetz and Anderson, 2010; Gerhardt et al., 2016; Pedersen et al., 2016) as well as the inhibition of the BMP7 pathway (Fuentealba et al., 2007), we asked whether IFT88 silencing in ECs affected these pathways under LSS using quantitative PCR for downstream targets. First, we observed that the BMP pathway (*SMAD6*) was highly up-regulated by LSS (Fig. 4 A). TGFβ (*SERPIN1*) and Notch (*HES1*) pathways were also up-regulated, but to lesser extent than BMP. As in other cell types, *PTCH1* expression, a reference gene for activation of the SHH pathway, was significantly decreased (Fig. 4 A). Although Notch, TGFβ, and Wnt (*AXIN2*) signaling appeared unchanged (Fig. 4 A), BMP signaling was significantly decreased in IFT88-deficient ECs compared with controls (Fig. 4 A). Further, we investigated whether IFT88-deficient cells were still responsive to BMP9 stimulation. Both *ID1* and *SMAD6* expression were up-regulated by BMP9 stimulation (25 pg/ml) in control cells (8- and 20-fold, respectively) but were reduced

---

primary cilia; orange arrowheads, primary cilia from surrounding cells. Bars, 20 µm. **(D)** Monolayers of HUVECs were subjected to different shear stress conditions for 24 h ($n = 8$; mean ± SEM; two-sided Wilcoxon test) and then stained for VE-cadherin, ARL13b (primary cilia), and DAPI. The percentage of cells with a PC within the monolayers was quantified. Representative images are shown for static (stat) and HSS conditions. Green arrowheads, endothelial primary cilia; black arrow, flow direction. Bars, 20 µm. **(E)** A 24- to 30-hpf zebrafish embryo of double transgenic line Tg(kdr-l:ras–Cherrys916; β-actin::arl13b-eGfp) was used to identify the dynamics of endothelial cilia over time. First image shows the EC labeling (referred to as mCherry-CAAX). Second image shows the luminal cilia (white arrowhead, disappearing cilia; light green arrowhead, stable cilia; dark green arrowhead, appearing cilia). Movie of the cilia dynamics is provided in Video 1. Bar, 10 µm. **(F)** Stills extracted from Videos 2 and 3 showing the retraction of the cilium (“retracting cilium”) or its formation (“appearing cilium"). Bars, 3 µm. *, $P < 0.05$; **, $P < 0.01$. PC, primary cilium.

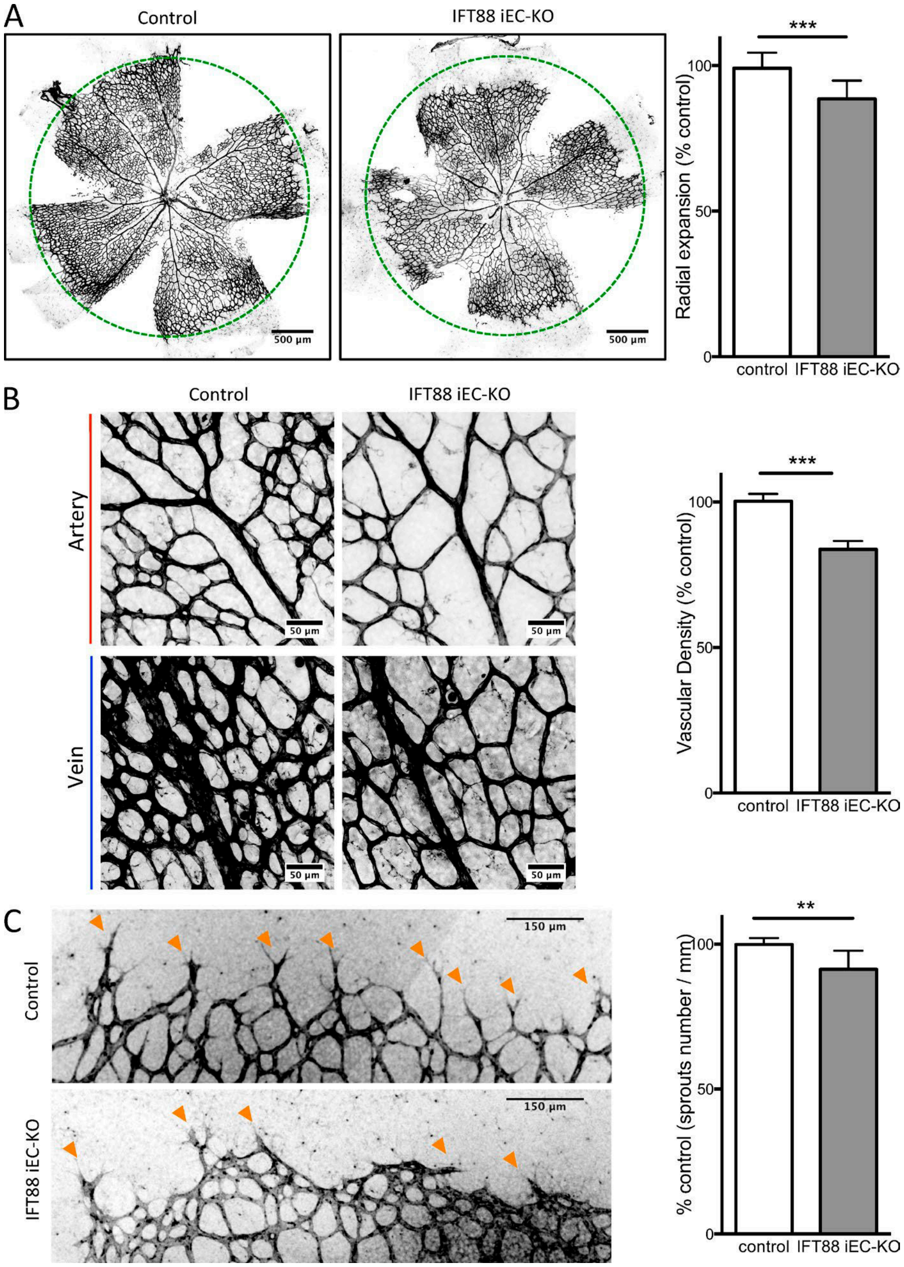

Figure 2. **IFT88 iEC-KO mice show defects in vascular expansion and density.** *Ift88*$^{fl/fl}$;*Pdgfb-iCre-ERT2-Egfp*$^{+/wt}$ (IFT88 iEC-KO) and littermate mice (control) were injected with tamoxifen at P1 and P3 and eyes collected at P6. **(A)** Representative images of retinal wholemounts stained with Isolectin B4 (IB4, black; green circles represent the radial expansion in control mice) and quantification of the radial expansion of the vascular plexus in IFT88 iEC-KO mice and littermate controls (WT, *n* = 9; KO, *n* = 12; median ± IQ; two-sided Wilcoxon test). **(B)** Representative images (black, IB4) and quantification of vascular density of the plexus in IFT88 iEC-KO mice and littermate controls (expressed as vascularized area normalized to control situation; WT, *n* = 5; KO, *n* = 9; median ± IQ; two-sided Wilcoxon test). **(C)** Representative images (black, IB4) and quantification of the number of sprouting cells (orange arrowheads) in IFT88 iEC-KO mice and littermate controls (WT, *n* = 6; KO, *n* = 5; median ± IQ; two-sided Wilcoxon test). **, P < 0.01; ***, P < 0.001.

by 50% after IFT88 silencing (Fig. S3 C). To understand if this was related to a specific range of shear stress, we evaluated the response of ECs to BMP9 under different shear stress conditions (Fig. 4, B and C; and Fig. S3, D–F). A recent study demonstrated that HUVECs exposed to shear stress show increased sensitivity to BMP9 (Baeyens et al., 2016b). Indeed, when repeating the very same dose–response study using semiquantitative Western blot analysis of phospho-SMAD1/5/8 (p-SMAD1/5/8) levels, we confirmed the dramatic increase in the sensitivity of ECs to BMP9 stimulation when exposed to shear stress compared with static conditions. Surprisingly, however, this effect was much more pronounced at LSS values (not tested in Baeyens et al., 2016b). We identified a half-maximal effective concentration (EC50) of BMP9 of 1.26 pg/ml for ECs under LSS compared with 9.27 pg/ml for ECs under HSS and 38.44 pg/ml for the static condition (Fig. 4, B and C; and Fig. S3, D–F). Intriguingly, IFT88-deficient cells completely lost this differential response to LSS and HSS, displaying very similar sensitivities to BMP9 with values comparable to control cells under HSS ($EC50_{\text{low shear IFT88}}$ = 10.61 pg/ml; $EC50_{\text{high shear IFT88}}$ = 7.89 pg/ml; Fig. 4, B and C; and Fig. S3, D–F). These results demonstrate that IFT88, likely by supporting formation of the primary cilium, equips ECs with a sharp sensitivity to BMP9, selectively at LSS levels. Surprisingly, although further increases in BMP9 levels eventually caused signal saturation, only control cells exposed to LSS desensitized at the highest concentrations of BMP9, as indicated by a drop in p-SMAD1/5/8 levels (Fig. 4, B and C; and Fig. S3, E and F). Together, this suggests that ECs capable of forming a primary cilium are highly sensitive to BMP9 with a unique dose–response curve at LSS values.

The activation of downstream target genes by p-SMAD1/5/8 requires their translocation to the nucleus. We therefore analyzed nuclear translocation of p-SMAD1/5/8 by immunostaining at

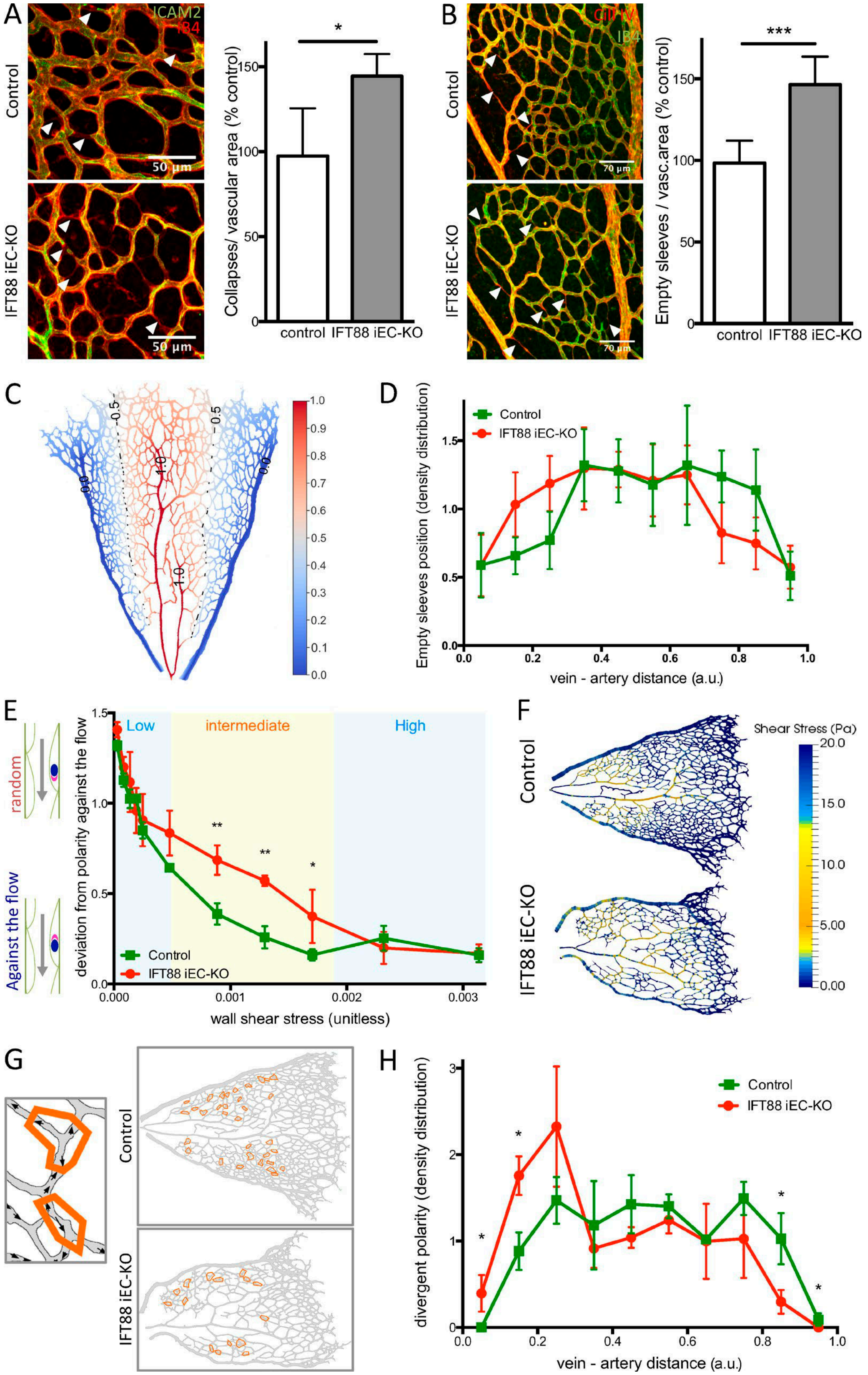

Figure 3. **IFT88 iEC-KO mice show increased random vascular regression and loss of flow-induced polarity. (A)** Retinas from P6 IFT88 iEC-KO and littermate control mice were stained for ICAM2 (green) and with Isolectin B4 (red). Arrowheads show collapsed vessels. The number of collapsed lumens per vascular area was quantified in both groups (*n* = 8; median ± IQ; two-sided Wilcoxon test; *, $P < 0.05$). Bars, 50 µm. **(B)** Retinas from P6 IFT88 iEC-KO and littermate control mice were stained for Collagen IV (red) and with Isolectin B4 (green). Arrowheads show collagen empty sleeves. The number of empty sleeves

different levels of shear stress. Stimulation with 10 pg/ml BMP9 strongly triggered translocation of p-SMAD1/5/8 to the nucleus in control cells in all shear stress conditions and at a higher rate at LSS and HSS levels (5.8- and 4.5-fold, respectively; Fig. 4 D) compared with static conditions (1.7-fold; not depicted). Interestingly, the pronounced translocation of p-SMAD1/5/8 after BMP9 stimulation under LSS was abolished upon silencing of IFT88. In contrast, IFT88-deficient ECs exposed to HSS remained responsive to BMP9 stimulation, but at lower levels than control cells (3.6-fold increase instead of 4.5-fold; Fig. 4 D). Because IFT88 has been shown to have cilium-independent roles (Delaval et al., 2011; Boehlke et al., 2015; Taulet et al., 2017), we evaluated the effect of KIF3a silencing, another key protein in cilium maintenance, on BMP signaling. First, we confirmed by qPCR that ECs expressing shRNA targeting KIF3a was effective (Fig. S3 G). This silencing led to a decrease in SHH activity (*PTCH1* and *GLI1*), as expected from the loss of the primary cilium (Fig. S3 G). Similar to the IFT88 silencing experiment, both *ID1* and *SMAD6* gene expression were up-regulated by 25 pg/ml BMP9 stimulation in control ECs (four- and fivefold, respectively) but were reduced by 40% after KIF3a silencing (Fig. S3 H). Additionally, LSS-induced translocation of p-SMAD1/5/8 into the nucleus was abolished in KIF3a-deficient ECs, whereas HSS-induced translocation was maintained (Fig. 4 E). These results suggest that in ECs, the ability to form primary cilia is critical for both SMAD1/5/8 phosphorylation and nuclear translocation under LSS, but not under HSS.

Furthermore, staining for p-SMAD1/5/8 in the retina confirmed this observation; in the remodeling area p-SMAD1/5/8 was decreased in endothelial nuclei in the IFT88 iEC-KO mice compared with controls (Fig. 4 F). Expression of *Smad6* and *Serpin1* was also reduced in ECs extracted from IFT88 iEC-KO retinas (Fig. 4 G) but the expression levels of receptors for BMP9 or TGFβ (*Alk1* and *Alk5*) and the coreceptor Endoglin (*Eng*) were unchanged (Fig. 4 G). Interestingly, in vitro, ALK1 appears enriched around the cilium in ciliated ECs (Fig. 5 A); this specific localization close to the Golgi was reduced in nonciliated ECs (Fig. 5 A). We also identified prominent phosphorylation of SMAD1/5/8 at the basal body and along the cilium (Fig. 5 B) as well as SMAD4 localization along the cilium (Fig. 5 C) upon LSS stimulation in vitro.

BMP9/10 signaling through ALK1 has been proposed as a regulator of vascular remodeling by stimulating cell migration against the flow and promoting EC quiescence in zebrafish (Laux et al., 2013; Rochon et al., 2016). Given previous studies that directional migration is a key factor during vascular regression (Franco et al., 2015), we asked whether migration was affected by IFT88 loss. Interestingly, Both IFT88-deficient and KIF3a-deficient ECs migrated significantly faster than control cells to close a scratch wound in vitro (Fig. 5, D and E). Trapping BMP9 in the medium using the ALK1-Fc receptor-body equally accelerated wound closure of control cells but had no additional effect on KIF3a-deficient ECs or IFT88-deficient ECs (Fig. 5, D and E). These data highly suggest that BMP9 signaling is responsible for the decreased migration in ECs capable of forming a primary cilium. Finally, IFT88-deficient ECs, KIF3a-deficient ECs, and ALK1-Fc receptor body–treated ECs harbored significantly more ECs with a long and continuous lamellipodium along the free edge of the wound (Fig. 5, E and F). Such lamellipodia correlate with higher speed of migration in other cell types (Lee et al., 1993) and point toward changes in cytoskeletal organization during migration as a potential downstream target of BMP signaling through IFT88 and KIF3a and hence likely through the primary cilium.

Discussion

Our present results identify that ECs display primary cilia in a temporal and spatial pattern that correlates with particular hemodynamic settings during vascular remodeling in the mouse retina. Similar to earlier observations in the developing zebrafish embryo (Goetz et al., 2014), we find primary cilia most frequently in ECs exposed to LSS and moderate shear stress, whereas most cells exposed to HSS do not show a cilium. This corroborates several studies demonstrating that HSS disrupts endothelial primary cilia (Iomini et al., 2004; Egorova et al., 2011; Ten Dijke et al., 2012). We show that even at lower shear values, cilia dynamically form and disappear, suggesting that ECs may experience differential or recurring phases of cilia expression during vascular development. Dinsmore and Reiter (2016) reported that genetic constitutive deletion of IFT88 in ECs has no effect on the vasculature of the retina in newborns but causes the formation of large atherosclerotic lesions in turbulent/LSS areas of the aorta. In our present work, we find that inducible genetic deletion of primary cilia in ECs during postnatal retina development causes premature and widespread vessel regression.

Morphological telltale signs of apical shear forces experienced by ECs are their elongated morphology and the polarized positioning of their Golgi and centrosome ahead of the nucleus, against the direction of flow (Vyalov et al., 1996). Accumulating evidence indicates that this axial polarity coincides with directional cell migration against the flow (Ostrowski et al., 2014; Franco et al., 2015; Rochon et al., 2016). Combined simulation of hemodynamics (Bernabeu et al., 2014) and analysis of axial

---

was quantified in both groups (WT, *n* = 9; KO, *n* = 7; median ± IQ; two-sided Wilcoxon test; ***, P < 0.001). Bars, 70 µm. **(C)** Representation of the method determining the distance value for elements placed between a vein and an artery (0 = touching the vein, 1 = touching the artery). **(D)** The distribution of empty sleeves was quantified in IFT88 iEC-KO mice and littermate controls (WT, *n* = 9; KO, *n* = 7; mean + SEM; one-sided Mann–Whitney *U* test). **(E)** Flow-induced polarity profile depending on shear stress value in the retina of the IFT88 iEC-KO mice compared with littermate controls (*n* = 3; mean + SEM; 0 = perfect polarity against the flow direction; 1.6 = random polarity; one-sided Mann–Whitney *U* test; *, P < 0.10; **, P < 0.05). **(F)** Visualization of simulated shear profiles in P6 IFT88 iEC-KO and littermate control retinas. The color-coding is adjusted to highlight the intermediate shear range where ECs in the KO show reduced polarity (shown in yellow, representative images of six animals). **(G)** Schematics showing examples of divergent polarity events in the remodelling plexus. Arrows, polarity vectors; orange contours, regions of divergent polarity. **(H)** The density distribution of divergent polarity events was determined for both IFT88 iEC-KO mice and littermate controls (*n* = 3; mean + SEM; one-sided Mann–Whitney *U* test; *, P < 0.10; **, P < 0.05). a.u., arbitrary unit.

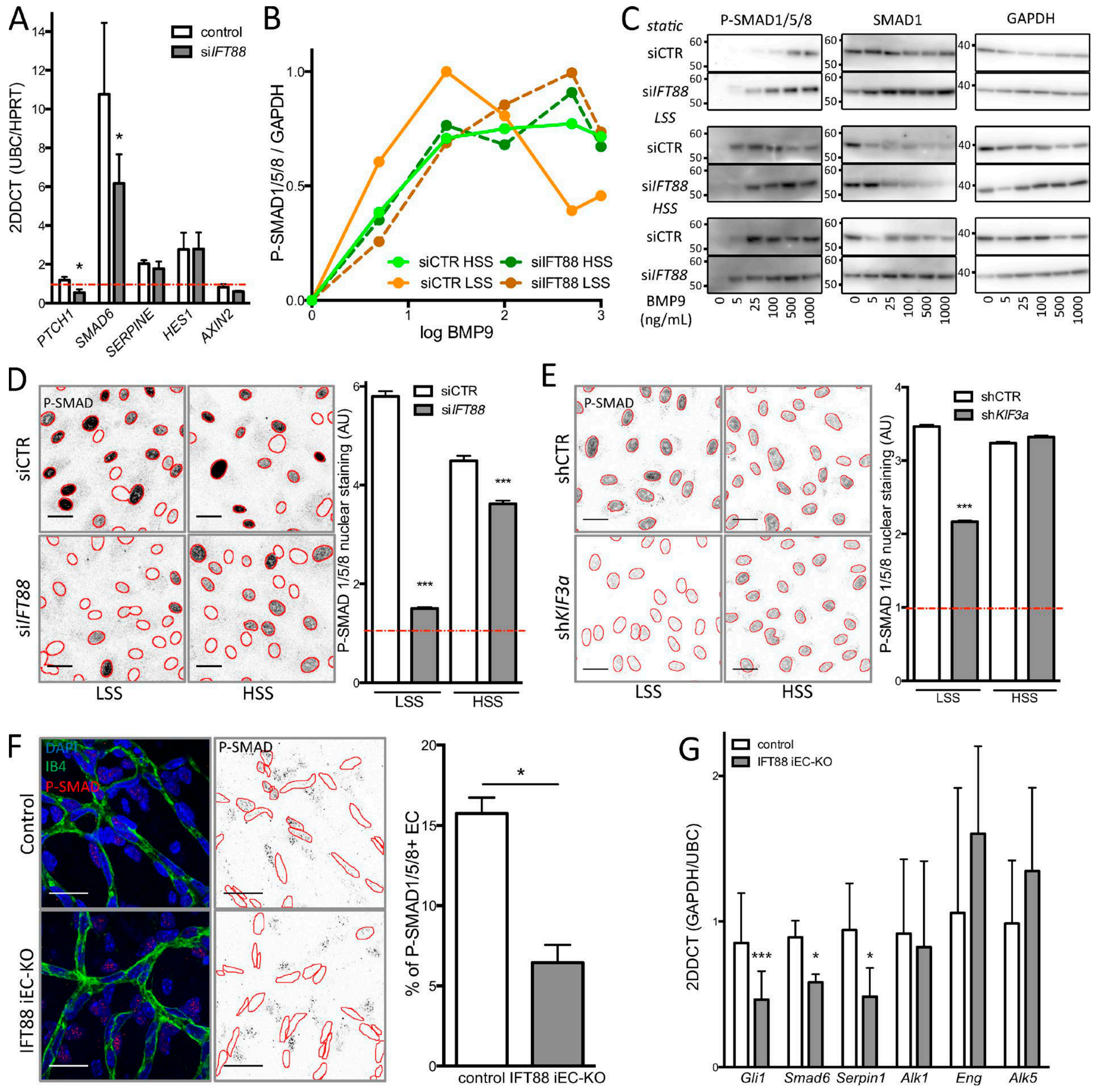

Figure 4. **Loss of the primary cilium leads to increased migration and blocks the differential response to BMP9 under flow. (A)** quantitative PCR was used to assess levels of SHH (*PTCH1*), BMP (*SMAD6*), TGFβ (*SERPINE*), Notch (*HES1*), and Wnt (*AXIN2*) signaling in ECs transfected with siIFT88 or siCTR under LSS conditions (n = 5; all conditions were normalized to 1 for siCTR under the static condition [red line, n = 4]; mean± SEM; two-sided Wilcoxon test; *, $P < 0.05$). **(B)** Dose–response curves were generated for p-SMAD1/5/8 levels after BMP9 stimulation based on Western blot analysis (n = 3; mean: LSS = 2 dyn/cm^2; HSS = 20 dyn/cm^2). **(C)** Representative images of the Western blots used for the dose–response analysis. Molecular masses are indicated on the images based on prestained protein standard. **(D)** Representative images (red outline based on DAPI segmentation) and quantification of p-SMAD1/5/8 nuclear staining (PFA fixation) in ECs transfected with siCTR or siIFT88 and treated with 10 pg/ml BMP9 (the red line represents nontreated cell level of staining; n = 3; between 1,900 and 3,300 cells per condition; mean± SEM [of cell individual values]; two-sided Mann–Whitney U test; ***, $P < 0.001$). Bars, 30 µm. **(E)** Representative images and quantification of p-SMAD1/5/8 nuclear staining (PFA fixation) in ECs transfected with shCTR or shKIF3a and treated with 10 pg/ml BMP9 (the red line represents nontreated cell level of staining; n = 3; between 1,900 and 3,300 cells per condition; mean± SEM [of cell individual values]; two-sided Mann–Whitney U test; ***, $P < 0.001$). Bars, 30 µm. **(F)** Representative images of immunofluorescent staining of p-SMAD1/5/8 in the retina of IFT88 iEC-KO mice or littermate control and quantification of the nuclear signal in ECs. Positive staining in surrounding cells is still visible in the IFT88 iEC-KO retina (control, n = 5; IFT88 iEC-KO, n = 7, blue: DAPI; red: p-SMAD1/5/8; green: Isolectin; mean± SEM; two-sided Wilcoxon test; *, $P < 0.05$). Bars, 20 µm. **(G)** qPCR analysis was performed on ECs extracted from IFT88 iEC-KO (gray) and littermate retinas (white; n = 7; mean± SEM; two-sided Wilcoxon test; *, $P < 0.05$; ***, $P < 0.001$).

endothelial polarity has recently proven to be a powerful tool to dissect the behavior of ECs during vessel regression (Franco et al., 2015, 2016). Our polarity analysis in vivo revealed a profound reduction of axial polarity in IFT88-deficient ECs precisely in the vascular plexus region that experiences intermediate shear values and high levels of regression. Vessels experiencing the highest shear stress, specifically arteries, showed the most robust polarization against flow. This effect appears to

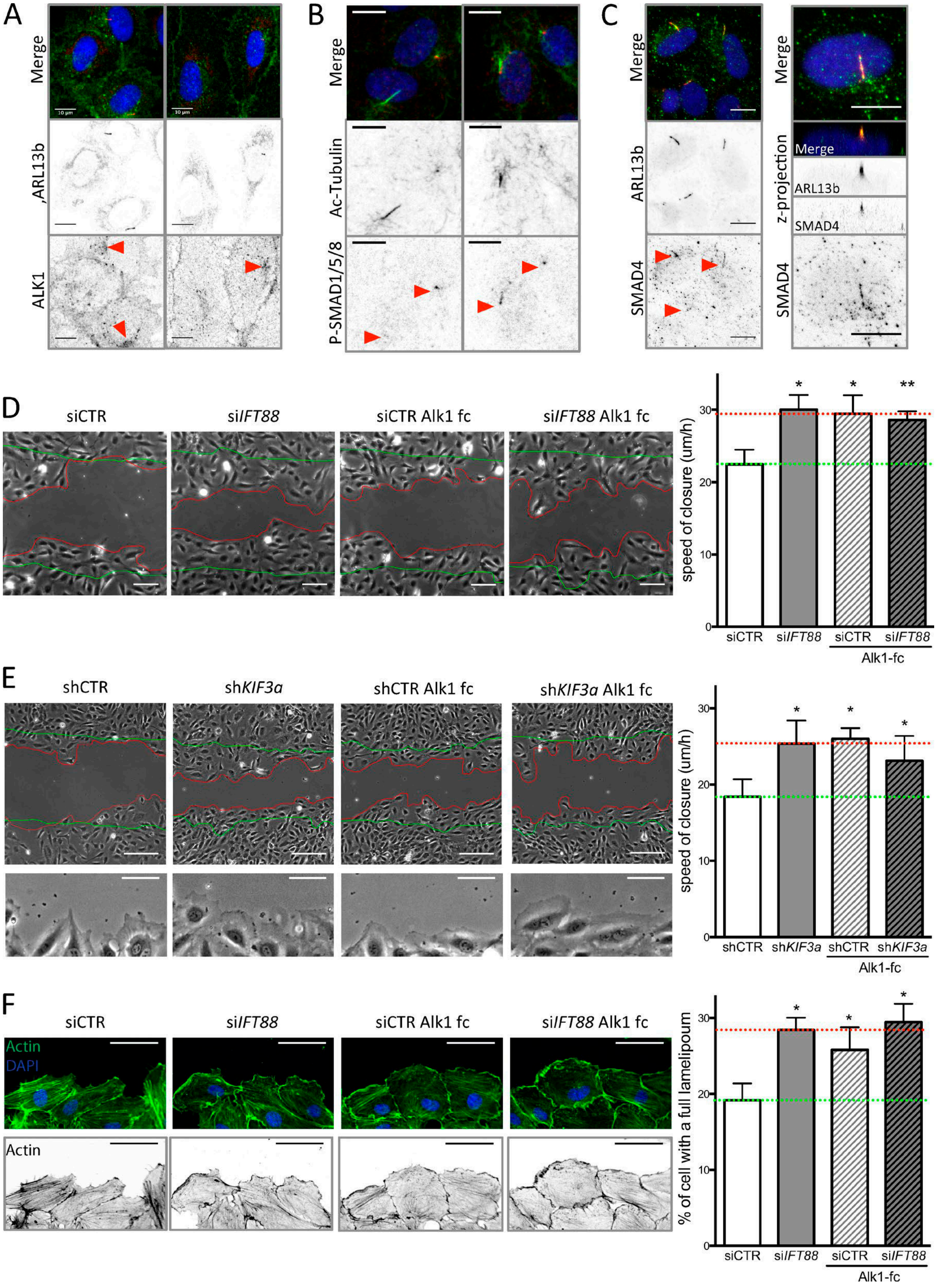
A
Merge
ARL13b
ALK1
10 μm
10 μm
B
Merge
Ac-Tubulin
P-SMAD1/5/8
C
Merge
ARL13b
SMAD4
Merge
z-projection
Merge
ARL13b
SMAD4
SMAD4
D
siCTR
si*IFT88*
siCTR Alk1 fc
si*IFT88* Alk1 fc
speed of closure (um/h)
0
10
20
30
*
*
**
siCTR
si*IFT88*
siCTR
si*IFT88*
Alk1-fc
E
shCTR
sh*KIF3a*
shCTR Alk1 fc
sh*KIF3a* Alk1 fc
speed of closure (um/h)
0
10
20
30
*
*
*
shCTR
sh*KIF3a*
shCTR
sh*KIF3a*
Alk1-fc
F
siCTR
si*IFT88*
siCTR Alk1 fc
si*IFT88* Alk1 fc
Actin
DAPI
Actin
% of cell with a full lamelipoum
0
10
20
30
*
*
*
siCTR
si*IFT88*
siCTR
si*IFT88*
Alk1-fc

Figure 5. **Loss of BMP9 signaling through the cilium increases EC migration. (A)** HUVECs were stained for ARL13b (primary cilium; red), ALK1 (green), and DAPI (blue; methanol fixation, $n = 2$) under static conditions. Bars, 10 µm. **(B)** HUVECs were stained for acetylated tubulin (primary cilium; green), P-SMAD1/5/8 (red), and DAPI (blue; methanol fixation, $n = 2$) under LSS conditions. Bars, 10 µm. **(C)** HUVECs were stained for ARL13b (primary cilium; red), SMAD4 (green), and DAPI (blue; methanol fixation, $n = 2$) under LSS conditions. Bars, 10 µm. **(D)** A wound-closure assay was performed on ECs transfected with siCTR and si*IFT88*, treated or not with a BMP9 trap, an ALK1-Fc receptorbody (25 ng/ml, for the duration of the wound experiment). Representative images were taken 9 h after the wound was made (green lines, wound at $t = 0$; red lines, wound at $t = 9$ h) and the speed of closure was quantified ($n = 5$; mean ± SEM; two-sided

be independent of the primary cilium, as it is not expressed at these locations. Also, IFT88 mutants showed no change in axial polarity in ECs in areas exposed to HSS and displayed normal arterial morphologies.

Why then do some vessels lacking IFT88 show altered polarity and premature regression? The BMP–ALK1–SMAD pathway recently emerged as an important player in both endothelial flow responses and vessel stability. The complete loss of BMP9/10–ALK1 signaling reduces cellular quiescence in nascent vascular networks, resulting in dramatic hypersprouting (Larrivée et al., 2012), and triggers the formation of arteriovenous shunts (Laux et al., 2013; Baeyens et al., 2016b). In zebrafish embryos, ALK1 deficiency has been shown to drive shunt formation by impairing polarization and movement of ECs against flow (Rochon et al., 2016). Loss of the coreceptor Endoglin, a flow-sensitive enhancer of ALK1–BMP signaling (Baeyens et al., 2016b), also triggers arteriovenous shunts, but it does not mimic the excessive sprouting seen in ALK1 mutants (Jin et al., 2017). Interestingly, Endoglin profoundly increases EC SMAD1/5/8 phosphorylation through BMP9-mediated Alk1 activation, particularly under HSS (Baeyens et al., 2016b), and promotes EC migration against the flow (Jin et al., 2017). Our present work reinforces the idea that BMP9–ALK1–SMAD1/5/8 signaling is intimately connected with endothelial flow responses and polarized migration, but it suggests the existence of a tunable range of shear and BMP sensitivity involving distinct molecular mechanisms. Whereas Endoglin operates at high shear, we find that the cilium components IFT88 and KIF3a, and likely the cilium itself, confer a particular sensitivity to BMP9 at low shear levels. Given that arteriovenous shunts form in high-flow regions, the differential involvement of Endoglin and the cilium at high and low flow, respectively, may also explain why IFT88 deficiency does not cause shunt formation. Mechanistically, how SMAD signaling promotes endothelial polarity against flow remains unclear. Nevertheless, our data identify, for the first time in ECs, the presence of phosphorylated SMAD1/5/8 and SMAD4 along the primary cilium, a mechanosensitive structure that is linked to the polarized microtubular organization of the cell and its Golgi position. In human mesenchymal stem cells, phosphorylated SMAD2/3 was detected at the basal body of primary cilia, promoting signaling after TGFβ stimulation (Labour et al., 2016). In *Xenopus laevis* embryos, SMAD1 is recruited to the base of the cilium for degradation and signal termination (Fuentealba et al., 2007). In contrast, given that ALK1-Fc treatment mimics IFT88 or KIF3a depletion, our data point toward an activating process in ECs.

Interestingly, in IFT88-deficient ECs, p-SMAD1/5/8 levels were identical between ECs exposed to LSS and HSS, whereas nuclear localization was decreased only in LSS. This suggests that the primary cilium, or IFT88, may also contribute to transport of p-SMAD1/5/8 to the nucleus. The microtubule motors Kinesin and Dynein actively transport SMADs to the activating receptor kinases at the membrane and to the nucleus, respectively, (Chen and Xu, 2011), and are also important for cilium-dependent mechanisms (Verhey et al., 2011). Our data showing identical effects of losing either of two unrelated essential components of the primary cilium, and of inhibiting BMP signaling on cell migration in vitro, together with the localization of BMP–ALK1–SMAD signals at the primary cilium, favor the idea that it is the primary cilium that mediates flow-dependent sensitization to BMP, thereby affecting cell rearrangements. Conceptually, our discovery of the primary cilium sensitizing ECs to the activity of BMP–ALK1–SMAD signaling at low shear levels, together with the earlier findings of Endoglin performing a similar function at high shear levels, suggest that critical endothelial responses to the changing hemodynamic conditions across the remodeling network are fine-tuned through the integration of mechanosensing and receptor kinases to ensure proper vascular patterning and flow distribution. How well and in which direction ECs polarize and migrate as flow response appear to take center stage in this morphogenic process. Future work will need to address how the primary cilium sensitizes ECs to BMP and what downstream effectors of BMP signaling are critical for cell polarization and stabilization of vessels during remodeling.

Materials and methods

Mice and treatments

The following mouse strains were used: C57/BL6J, *Ift88*^{fl} (Haycraft et al., 2007), *Pdgfb-iCre-ERT2-Egfp* (Claxton et al., 2008), and *R26mTmG* (Muzumdar et al., 2007). Mice were maintained at the Max Delbrück Center for Molecular Medicine under standard husbandry conditions. Tamoxifen (Sigma-Aldrich) was injected i.p. (20 µg/g animal) at P1 and P3. Eyes were then collected at P4, P6, or P15 onwards. For C57/BL6J mice, eyes were collected at P3, P6, P11, and P15. For EC proliferation assessment in the retina, mouse pups were injected i.p. 2 h before collection of eyes with 20 µl/g EdU solution (0.5 mg/ml; C10340; Invitrogen). Animal procedures were performed in accordance with the animal license IC113 G 0117/15. The investigators were blinded to allocation during experiments.

Fish maintenance and stocks

Zebrafish (*Danio rerio*) were raised and staged as previously described (Kimmel et al., 1995). We used the double transgenic line Tg(kdr-l:ras–Cherrys916; β-actin::arl13b-eGfp) by crossing two previously described fish lines (Borovina et al., 2010; Phng et

---

Wilcoxon test; *, P < 0.05; **, P < 0.01). Bars, 100 µm. **(E)** A wound-closure assay was performed on ECs transfected with shCTR and sh*KIF3a*, treated or not with ALK1-Fc (25 ng/ml, for the duration of the wound experiment). Representative images were taken 9 h after the wound was made (green lines, wound at t = 0; red lines, wound at t = 9 h) and the speed of closure was quantified (n = 7; mean ± SEM; two-sided Wilcoxon test; *, P < 0.05; **, P < 0.01). Bars, 150 µm. Bottom images of the panel highlight lamellipodia formation in sh*KIF3a*, ALK1-fc, and sh*KIF3a*+ALK1-fc condition compared with control. Bars, 60 µm. **(F)** Representative images of actin staining (phalloidin–Alexa Fluor 594; green, top panel; black, bottom panel) of the ECs leading the wound closure and quantification of the number of cell with an undisrupted front lamellipodium (observed after 6 h of wound; n = 3; two-sided paired t test. Data distribution was assumed to be normal, but this was not formally tested. *, P < 0.05. Bars, 60 µm.

al., 2013). The β-actin::arl13b-eGfp line was a gift from B. Ciruna (University of Toronto, Toronto, Ontario, Canada).

Dynabead-mediated isolation of lung ECs from neonatal mice

Lungs of P6 mouse pups were removed, minced using a scalpel and digested with 2.2 µg/ml Dispase in HBSS with calcium/magnesium for 60 min at 37°C. Digested tissues were homogenized using a P1000 pipette and filtrated through a 40-µm cell strainer. After centrifugation, the cell suspension was incubated for 30 min at room temperature with 100 µl magnetic Dynabeads (Invitrogen) that had been conjugated overnight with anti–mouse CD144 antibody in PBS/EDTA 0.5 mM and 0.5% BSA. Cells attached to the beads were collected using an MPC magnet (Invitrogen) and washed three times with PBS/EDTA 2 mM and 0.5% BSA. Collected cells were then plated on 0.5% gelatin-coated wells and treated with 1 µM tamoxifen (every 2 d) to induce deletion once they reached confluency at P1.

Dynabead-mediated isolation of retinal ECs from neonatal mice

Eyes of P6 mouse pups were removed, dissected in DMEM, and digested with 1 mg/ml Collagenase-A for 10 min at 37°C. Digested tissues were filtrated through a 40-µm cell strainer. The cell suspension was incubated for 20 min at 4°C with 10 µl magnetic Dynabeads (Invitrogen) per retina that had been conjugated overnight with anti–mouse CD31 antibody in 0.5 mM PBS/EDTA and 0.1% BSA. Cells coated with beads were collected using an MPC magnet (Invitrogen) and washed three times with 0.5 mM PBS/EDTA and 0.1% BSA. Cells not coated with beads were collected as a negative control. Collected cells were then processed for RNA extraction.

Cell culture and microfluidic chamber experiments

HUVECs (passage 2 to 6; PromoCell) were routinely cultured in EBM-Bulletkit (Promocell). For siRNA experiments, HUVECs were transfected with ON-TARGET smart pool control nontargeting siRNAs (D-001210-02-20; Dharmacon) and siRNAs against human IFT88 (L-012281-01-0005, siRNA 1: 5′-GAGAAUUAUAUGAUCGUGA-3′; siRNA 2: 5′-AGGCAAAUGGAACGUGAAA-3′, siRNA 3: 5′-AGGAAGUGCUAGCGGUGAU-3′; siRNA 4: 5′-AGUAAAGGUGAACGACUAA-3′; Dharmacon). HUVECs were transfected with 25 nM siRNA using Dharmafect 1 transfection reagent. In brief, siRNA and Dharmafect1 were diluted in Optimen medium in separated vials for 5 min and then carefully mixed. After 20 min, the mix was added to the cells. For static experiments, cells were used between 24 and 48 h after transfection. For flow experiments, cells were cultured on 0.2% gelatin-coated slides (Menzel Glazer), and unidirectional laminar shear stress was applied 36 h after transfection using peristaltic pumps (Gilson) connected to a glass reservoir (ELLIPSE) and the chamber containing the slide. Local shear stress was calculated using Poiseuille's law and averaged to 2 (LSS) or 20 dyn/cm^2 (HSS). Cells were exposed to shear stress for 45 min using EBM media (Promocell) and costimulated with 0, 5, 25, 100, 500, and 1,000 pg/ml BMP9 (3209-BP-010; R&D) under the different flow conditions for the dose–response experiment (Fig. 4 C and Fig. S3, D–F), with 10 pg/ml for staining (Fig. 4, D and E). For quantitative PCR under static conditions, ECs were stimulated with 25 pg/ml BMP9 for 2 h. For wound assays, ECs were treated with 25 ng/ml Alk1-fc (R&D) or vehicle for the duration of the wound.

Adenoviral transduction

pENTR-Arl13b2 was a gift from T. Caspary (Emory University, Atlanta, GA; plasmid 40871; Addgene). The cDNA of mEGFP was inserted upstream of the Arl13b2 cDNA using the NEB Builder HiFi DNA Assembly system (New England Biolabs). Arl13b-mEGFP cDNA was then cloned into pAd/CMV/V5-DEST vector from the ViraPower Adenoviral Expression system (ThermoFisher Scientific). Replication-incompetent viral particles were produced in 293A cells following the manufacturer's instructions.

Lentiviral transduction

Lentivirus expressing inducible shRNA (Sigma-Aldrich) was used to silence Kinesin-like protein (KIF3A, shRNA sequence: 5′-CCGGCGTCAGTCTTTGATGAAACTACTCGAGTAGTTTCATCAAAGACTGACGTTTTTG-3′). HUVECs were infected in the presence of hexadimethrine bromide (at 8 µg/ml) with lentivirus at MOI 2.5. Negative controls were lentivirus expressing a nontarget shRNA used at the same MOI as for the protein of interest. Transduced cells were amplified and selected using puromycin (P9620; Sigma-Aldrich) at 1 µg/ml during amplification. Puromycin treatment was stopped during experiments. shRNA expression was induced by treating HUVECs for 5 d using IPTG (I6758; Sigma-Aldrich) at 1 mmol/liter.

Western blotting

HUVECs were washed with cold PBS and scraped off in M-PER (Mammalian Protein Extraction Reagent; Thermoscientific) completed protease and phosphatase inhibitors (Roche). Lysates were centrifuged and protein supernatant was quantified using the Lowry protein assay (Bio-Rad). Lysates were mixed with reducing sample buffer for electrophoresis and subsequently transferred onto polyvinylidene fluoride membranes. Equal loading was checked using Ponceau red solution. Membranes were incubated with primary antibodies (see below). After incubation with secondary antibodies (1:3,000; GE Healthcare), immunodetection was performed using an enhanced chemiluminescence kit (SuperSignal West Dura; Pierce), and bands were revealed using the Las-4000 imaging system. After initial immunodetection, membranes were stripped of antibodies and reprobed with anti–GAPDH antibody. Values reported from Western blots were obtained by band density analysis using Image Gauge software (Fujifilm) and expressed as the ratio of the protein of interest to GAPDH. The following antibodies were used: GAPDH (ref MAB374, goat; 1:10,000; Millipore), IFT88 (ref 13967-1-AP, rabbit; 1:500; Proteintech), p-SMAD1/5/8 (ref 13820, rabbit; 1:500; CST), SMAD1 (ref 385400, rabbit; 1:500; CST).

Immunofluorescence staining

Eyes were collected and fixed with 4% PFA in PBS for 1 h at 4°C, and retinas were then dissected in PBS. Blocking/permeabilization was performed using Claudio's blocking buffer (CBB; Franco et al., 2013), consisting of 1% FBS (Gibco), 3% BSA (Sigma-Aldrich), 0.5% Triton X-100 (Sigma-Aldrich), 0.01% sodium deoxycholate

(Sigma-Aldrich), and 0.02% sodium azide (Sigma-Aldrich) in PBS at pH 7.4 for 1–2 h with rocking at 4°C. Primary antibodies were incubated at the desired concentration in 1:1 CBB/PBS with rocking at 4°C overnight and secondary antibodies were incubated at the desired concentration in 1:1 CBB/PBS for 2 h at room temperature. DAPI (Sigma-Aldrich) was used for nuclear labeling. Retinas were mounted on slides using Vectashield mounting medium (H-1000; Vector Labs).

HUVECs were fixed using 100% cold methanol for 10 min (for cilium staining) or PFA 4% for 10 min (for all other stainings) and washed three times in PBS. Cells were then stained for 2 h with primary antibodies in 1:1 CBB/PBS followed by incubation for 1 h with secondary antibodies in 1:1 CBB/PBS (see list below). DAPI (Sigma-Aldrich) was used for nuclear labeling. Cells were mounted in Mowviol.

The following antibodies were used in vivo: ARL13b (ref 17711-1-AP, rabbit; 1:500; Proteintech), cleaved caspase (ref 9661, rabbit; 1:200; CST), collagen IV (ref ab6586, rabbit; 1:200; Abcam), ERG (ref ab92513, rabbit; 1:1,000; Abcam), GOLPH4 (ref ab28049, rabbit; 1:500; Abcam), ICAM2 (ref 553326, rat; 1:200; BD Biosciences), p-SMAD1/5/8 (rabbit; 1:200; CST; ref 13820), vascular endothelial (VE)–cadherin (ref 555289; rat; 1/100; BD Biosciences), Isolectin 488 (ref I21411, 1:400; Invitrogen), and Isolectin 568 (ref I21412, 1:400; Invitrogen). The following antibodies were used in vitro: acetylated tubulin (ref T6793, rabbit; 1:500; Sigma-Aldrich), ALK1 (ref AF370, goat; 1:500; RandD), detyrosinated tubulin (ref AB3201, rabbit; 1:500; Millipore), p-SMAD1/5/8 (ref 13820, rabbit; 1:500; CST), SMAD4 (ref sc-7966, rabbit; 1:500; Santa Cruz;), p-SMAD1/5/8 (ref 13820, rabbit; 1:500; CST), VE-cadherin (ref sc-6458, goat; 1:100; Santa Cruz), and Phalloidin 568 (ref A12380, 1:100; Invitrogen).

Microscope image acquisition

Retina imaging

Images of retinas were taken using a LSM 780 inverted microscope (Zeiss) equipped with a Plan-Apochromat 20×/0.8 NA Ph2 objective or with a Plan-Apochromat 63×/1.4 NA DIC objective or using a LSM 700 upright microscope (Zeiss) equipped with a Plan-Apochromat 20×/0.8 NA Ph2 objective. Both microscopes were equipped with a photon multiplier tube detector. Images were taken at room temperature using Zen 2.3 software (Zeiss).

In vitro imaging

Images from fluorescently labeled HUVECs were acquired using a LSM 700 upright microscope equipped with a Plan-Apochromat 20×/0.8 NA Ph2 objective. Images were taken at room temperature using Zen 2.3 software.

Bright-field images were taken using a Leica DMIL LED microscope equipped with a 10×/0.22 NA Ph1 objective and a CCD camera (DFC3000 G). Images were acquired at room temperature while the cells were still in their culture medium using LAS X software (Leica).

Live-cell imaging

HUVEC cells were plated in ibidi slides 0.6 and infected with the Arl13b2-mEGP virus. 48 h later, cells were stained with 1 µM siR-DNA nuclear dye (Spirochrome) and incubated for an additional hour. Cells were subsequently imaged using an LSM 780 inverted microscope (Zeiss) equipped with Plan-Apochromat 20×/0.8 NA Ph2 objective and the Definite Focus system. Time series of single planes were acquired at five randomly selected positions with 5 min resolution, 0.42 × 0.42 µm pixel, and an open pinhole. Images were taken at 37°C, 5% CO_2 using Zen 2.3 software. Images were analyzed in Fiji (Schindelin et al., 2012).

Zebrafish live imaging

Zebrafish embryos (24–30 hpf) were dechorionated, anaesthetized with 0.16 mg/ml Tricaine methanesulfonate (Sigma-Aldrich), mounted in 0.8% low-melting-point agarose (Life Technologies), and immersed in E3 buffer with 1× Tricaine for image acquisition. Live imaging was performed on a Yokogawa CSU-W1 upright 3i spinning-disc confocal microscope using a Zeiss Plan-Apochromat 63×/1.0 NA water-dipping objective and a CMOS C11440-22cu camera (Hamamatsu Photonics). Images were acquired using SlideBook 6 at a constant temperature of 28°C.

Image analysis

In vivo, the primary cilia belonging to ECs were identified as finger-like structures close to endothelial nuclei and localized inside the vessel (luminal side of Isolectin- or VE-cadherin–stained ECs). Veins and arteries of the retinal vasculature were identified based on their distinct morphological characteristics, with arteries showing dichotomous branching and a capillary free zone and veins appearing wider and mostly unbranched, surrounded by dense plexus. For quantifying the endothelial cilium in the iEC-IFT88 retinas, primary cilia were quantified only in veins, where their density was the highest in the control retinas. The few residual endothelial primary cilium appeared distributed along the vein. Lumen collapses were identified as ICAM2-negative/Isolectin-positive vessel segments; empty sleeves were identified as Collagen IV–positive/Isolectin-negative vessel segments. EdU-positive ECs were identified as cells positive for both ERG and EdU. EC density was assessed in the remodeling plexus and quantified as number of ECs per field of view. In vitro, the primary cilium was identified as a finger-like structure protruding above the cell and either close to the nucleus or on top of the Golgi apparatus. Translocation of p-SMAD to the nucleus was quantified using Cellprofiler (Broad Institute). In brief, nuclei were segmented based on the DAPI staining, and the nuclear signal measured. For all animal experiments, experimenters were unaware of the genotypes of the animals while acquiring images. For zebrafish experiments, images were analyzed using Fiji software. Z-stacks and time-lapse sequences were first flattened by maximum intensity projection. XY drift was corrected using the MultiStackReg plugin (B. Busse, National Institute of Child Health and Human Development, Bethesda, MD). Fluorescence bleaching was corrected by histogram matching.

Arteriovenous coordinate system

To characterize the position of events and structures within a mouse retina, we introduced a vein–artery coordinate system, which characterizes the relative position in the mouse retina with respect to the closest distance to arteries and veins. To obtain this coordinate system, the position of the midlines of the 2D projections of veins and arteries were identified manually in images of quarters of the retinas. For each point in the image, the closest distance to any vein and artery are given by d_v and d_a, respectively, and the corresponding arteriovenous distance is thus defined by

$$d_v/d_v + d_a.$$

It is 0 on veins and 1 on arteries and scales linearly between veins and arteries. The positions of empty collagen sleeves (Fig. 3, E and F) and divergent regions (Fig. 4, E and F) were analyzed within this coordinate system.

Mouse retina rheology model

Analysis of the axial polarity of ECs was performed by measuring the angle formed by the nucleus–Golgi axis and the flow direction using a mouse retina rheology model (Bernabeu et al., 2014). In brief, retinal vascular plexuses were stained for ICAM2 and imaged following the previously mentioned protocol. The resulting images were postprocessed in ImageJ to isolate the luminal region of interest, which was further processed with MATLAB (MathWorks) to extract the image skeleton and compute vessel radii along the network. Based on the computed image skeleton and radii, a 3D triangulation of the plexus luminal surface was generated with VMTK (Orobix srl). The computational fluid dynamics software package HemeLB (Bernabeu et al., 2014) was used to compute high-resolution estimates of pressure, velocity, and shear stress across the domain. Shear stress values obtained from simulation are impacted by the choice of inlet/outlet boundary conditions on the simulated hemodynamics. Ideally, one would use experimental measurements of flow rate and/or pressure to close the system. We could not obtain these data experimentally and relied on the data surveyed in Bernabeu et al. (2014) obtained from adult animals. Therefore, shear stress values in Fig. 4 C are theoretical values bound to our specific settings. Flow visualization was generated with Paraview (Kitware), and postprocessing of the results was performed with custom-made MATLAB scripts.

Flow-induced polarity analysis

To analyze the coupling between the polarization of cells (given by the Golgi–nucleus orientation) and the local direction and velocity of blood flow (obtained by the polnet analysis), we averaged the angles between flow and cell orientation after the binning with the local blood velocity. A deviation of 0 corresponds to the case where the Golgi–nucleus vector is opposite to the blood flow, whereas a deviation of π corresponds to the vectors being in the same direction as the blood flow. Thus, if all cells at a given flow velocity were perfectly polarized against the flow, the mean deviation would be 0; if they were all polarized with the flow, the mean deviation would be π; and if they were randomly polarized, one would expect to find the mean deviation to be π/2.

Cell cycle analysis of ECs from retinas

Eyes of P6 *Ift88*$^{fl/fl}$*;Pdgfb-iCre-ERT2-Egfp*$^{Tg/wt}$*;R26-mTmG*$^{Tg/Tg}$ or *Pdgfb-iCre-ERT2-Egfp*$^{Tg/wt}$*;R26-mTmG*$^{Tg/Tg}$ mouse pups were collected, dissected in DMEM, and digested with 1 mg/ml Collagenase-A for 10 min at 37°C. Digested tissues were filtrated through a 40-µm cell strainer, centrifuged and fixed with cold 100% methanol. Cells were stored in 90% methanol at −80°C before being further processed. Cells were then centrifuged to remove methanol and resuspended in PI/RNase staining solution (Cell Signaling) for 30 min before analysis by flow cytometry (LSRII; BD). In brief, ECs were identified as GFP positive, cell doublets were excluded, and the cell cycle was analyzed in the phycoerythrin channel. Acquisition was done using DIVA software and analysis using Flow-Jo software.

Wound-closure assay

Previously transfected cells were passed into wound-healing assay culture insert (ibidi) 24 h after transfection. After 24 h of culture in the device, the insert was removed to make a wound of ∼450 µm. Images were taken at three different locations along the wound at every hour for 9 h. The distance between both sides of the wound was measured to calculate the speed of closure over the 9 h. For staining experiments, cells were fixed 6 h after removing the insert.

RNA extraction and real-time quantitative RT-PCR

RNA was extracted and purified using the Qiagen RNeasy kit following the manufacturer's instructions for the experiment under static conditions or using Trizol and the Direct-zol RNA kit (zymo research) for experiments under flow. After measuring concentration and purity, RNA was kept at −80°C before use. RT-PCR was performed with 0.5 µg RNA using QIAGEN products and protocols; quantitative PCR was performed using Taqman products and protocols. A set of three housekeeping genes was selected for both human and mouse samples. Normalization was done using the 2deltaCT method.

The following human Taqman probes were used: *ID1 (*Hs03676575), *SMAD6* (Hs00178579), *SERPIN1* (Hs01126606), *IFT88* (Hs00167926), *PTCH1* (Hs00121117), *GLI1*(Hs00171790), *KIF3a* (Hs00199901), *AXIN2* (Hs00610344), *HES1* (Hs00172878), *UBC* (Hs01060665), and *HPRT* (Hs02800695). The following mouse Taqman probes were used: *Ift88* (Mm01313467), *Smad6* (Mm00484738), *Serpin1* (Mm00435858), *Gli1* (Mm00494654), *Cdh5* (Mm00486938), *Gapd* (Mm00484668), *Ubc* (Mm01201237), and *Hprt* (Mm03024075).

Statistical analysis

Statistical analysis was performed using GraphPad Prism software. For in vivo experiments, two-sided Mann–Whitney *t* tests (unpaired, nonparametric) or two-way ANOVAs (data distribution was assumed to be normal, but this was not formally tested) were used. For in vitro experiments, two-sided Wilcoxon *t* tests (paired, nonparametric) were used, except for p-SMAD translocation, where a two-sided Mann–Whitney *t* test was used, and for the lamellipodia quantification, were a two-sided paired *t* test was used (data distribution was assumed to be normal, but this was not formally tested). Details of the statistical test used or each experiment can be found in the figure legends. The investigators were blinded to genotype during experiments and quantification.

Online supplemental material

Fig. S1 shows the dynamic formation and retraction of cilia in ECs in vitro. Additionally, it provides evidence for efficient silencing of IFT88 in vivo both at the RNA and protein level, as well as for the loss of endothelial cilia. IFT88 iEC-KO retina displayed a normal vasculature at P15, suggesting recovery from the earlier developmental defect. Fig. S2 shows the results of flow cytometry, cleaved caspase-3, and EdU stainings of retinas, together demonstrating that cell cycle or apoptosis changes are unlikely the drivers of altered vascular density in cilia mutants. It also provides a visual explanation of the in silico flow modeling and the corresponding polarity analysis. Fig. S3 provides evidence for IFT88 and KIF3a silencing efficiency in vitro, additional graphic presentation for the dose–response curves of ECs to BMP9 stimulation, and a table of EC50 values. Quantitative PCR results show that silencing KIF3a also affects the BMP response of ECs. Video 1 shows that endothelial cilia are luminal and dynamic in the zebrafish embryo. Video 2: shows endothelial cilium formation in a zebrafish embryo. Video 3 shows endothelial cilium retraction in a zebrafish embryo. Video 4 shows endothelial cilia dynamics in vitro.

Acknowledgments

We thank Dr. Veronique Gebala and Dr. Andre Rosa for helpful comments on the manuscript. We also thank Francois Billeaud for realization of the cartoon of the summary schematic.

This work was supported by the Britain Israel Research and Academic Exchange Partnership (A.-C. Vion and H. Gerhardt), the German Centre for Cardiovascular Research, the German Ministry of Education and Research (A.-C. Vion and A. Klaus-Bergmann), and European Research Council consolidator grant 311719 Reshape (H. Gerhardt). A. Szymborska was supported by European Molecular Biology Organization long-term fellowship ALTF 2014-1625. P.-E. Rautou was funded by the Agence Nationale pour la Recherche (grants ANR-14-CE12-0011, ANR-14-CE35-0022, and ANR-16-CE14-0015-01). M.O. Bernabeu was supported by the UK Engineering and Physical Sciences Research Council under the project "UK Consortium on Mesoscale Engineering Sciences" (grant EP/L00030X/1). This work used the ARCHER UK National Supercomputing Service (http://www.archer.ac.uk).

The authors declare no competing financial interests.

Author contributions: A.-C. Vion designed the study, performed experiments, analyzed the results, and wrote the manuscript. T. Zheng, T. Perovic, and A. Klaus-Bergmann performed experiments and analyzed the results. A. Hamouten, A. Szymborska, E. Bartels-Klein, and I. Hollfinger performed experiments. S. Alt performed quantitative analysis, analyzed results, and reviewed the manuscript. P.-E. Rautou provided reagents and reviewed the manuscript; M.O. Bernabeu performed experiments and reviewed the manuscript; H. Gerhardt designed the study and wrote the manuscript.

Submitted: 27 June 2017
Revised: 1 July 2017
Accepted: 30 January 2018

References

Baeyens, N., S. Nicoli, B.G. Coon, T.D. Ross, K. Van den Dries, J. Han, H.M. Lauridsen, C.O. Mejean, A. Eichmann, J.L. Thomas, et al. 2015. Vascular remodeling is governed by a VEGFR3-dependent fluid shear stress set point. *eLife.* 4: e04645. https://doi.org/10.7554/eLife.04645

Baeyens, N., C. Bandyopadhyay, B.G. Coon, S. Yun, and M.A. Schwartz. 2016a. Endothelial fluid shear stress sensing in vascular health and disease. *J. Clin. Invest.* 126:821–828. https://doi.org/10.1172/JCI83083

Baeyens, N., B. Larrivée, R. Ola, B. Hayward-Piatkowskyi, A. Dubrac, B. Huang, T.D. Ross, B.G. Coon, E. Min, M. Tsarfati, et al. 2016b. Defective fluid shear stress mechanotransduction mediates hereditary hemorrhagic telangiectasia. *J. Cell Biol.* 214:807–816. https://doi.org/10.1083/jcb.201603106

Bernabeu, M.O., M.L. Jones, J.H. Nielsen, T. Krüger, R.W. Nash, D. Groen, S. Schmieschek, J. Hetherington, H. Gerhardt, C.A. Franco, and P.V. Coveney. 2014. Computer simulations reveal complex distribution of haemodynamic forces in a mouse retina model of angiogenesis. *J. R. Soc. Interface.* 11:11. https://doi.org/10.1098/rsif.2014.0543

Bernabeu, M.O., Jones, M.L., Nash, R.W., Pezzarossa, A., Coveney, P.V., Gerhardt, H., and Franco, C.A. PolNet Analysis: a software tool for the quantification of network-level endothelial cell polarity and blood flow during vascular remodelling. bioRxiv. doi: https://doi.org/https://doi.org/10.1101/237602 (Preprint posted December 22, 2017)

Boehlke, C., F. Kotsis, B. Buchholz, C. Powelske, K.U. Eckardt, G. Walz, R. Nitschke, and E.W. Kuehn. 2013. Kif3a guides microtubular dynamics, migration and lumen formation of MDCK cells. *PLoS One.* 8:e62165. https://doi.org/10.1371/journal.pone.0062165

Boehlke, C., H. Janusch, C. Hamann, C. Powelske, M. Mergen, H. Herbst, F. Kotsis, R. Nitschke, and E.W. Kuehn. 2015. A Cilia Independent Role of Ift88/Polaris during Cell Migration. *PLoS One.* 10:e0140378. https://doi.org/10.1371/journal.pone.0140378

Borovina, A., and B. Ciruna. 2013. IFT88 plays a cilia- and PCP-independent role in controlling oriented cell divisions during vertebrate embryonic development. *Cell Rep.* 5:37–43. https://doi.org/10.1016/j.celrep.2013.08.043

Borovina, A., S. Superina, D. Voskas, and B. Ciruna. 2010. Vangl2 directs the posterior tilting and asymmetric localization of motile primary cilia. *Nat. Cell Biol.* 12:407–412. https://doi.org/10.1038/ncb2042

Chen, X., and L. Xu. 2011. Mechanism and regulation of nucleocytoplasmic trafficking of smad. *Cell Biosci.* 1:40. https://doi.org/10.1186/2045-3701-1-40

Chen, Q., L. Jiang, C. Li, D. Hu, J.W. Bu, D. Cai, and J.L. Du. 2012. Haemodynamics-driven developmental pruning of brain vasculature in zebrafish. *PLoS Biol.* 10:e1001374. https://doi.org/10.1371/journal.pbio.1001374

Claxton, S., V. Kostourou, S. Jadeja, P. Chambon, K. Hodivala-Dilke, and M. Fruttiger. 2008. Efficient, inducible Cre-recombinase activation in vascular endothelium. *Genesis.* 46:74–80. https://doi.org/10.1002/dvg.20367

Culver, J.C., and M.E. Dickinson. 2010. The effects of hemodynamic force on embryonic development. *Microcirculation.* 17:164–178. https://doi.org/10.1111/j.1549-8719.2010.00025.x

Delaval, B., A. Bright, N.D. Lawson, and S. Doxsey. 2011. The cilia protein IFT88 is required for spindle orientation in mitosis. *Nat. Cell Biol.* 13:461–468. https://doi.org/10.1038/ncb2202

Dinsmore, C., and J.F. Reiter. 2016. Endothelial primary cilia inhibit atherosclerosis. *EMBO Rep.* 17:156–166. https://doi.org/10.15252/embr.201541019

Dolan, J.M., J. Kolega, and H. Meng. 2013. High wall shear stress and spatial gradients in vascular pathology: a review. *Ann. Biomed. Eng.* 41:1411–1427. https://doi.org/10.1007/s10439-012-0695-0

Egorova, A.D., P.P. Khedoe, M.J. Goumans, B.K. Yoder, S.M. Nauli, P. ten Dijke, R.E. Poelmann, and B.P. Hierck. 2011. Lack of primary cilia primes shear-induced endothelial-to-mesenchymal transition. *Circ. Res.* 108:1093–1101. https://doi.org/10.1161/CIRCRESAHA.110.231860

Franco, C.A., J. Blanc, A. Parlakian, R. Blanco, I.M. Aspalter, N. Kazakova, N. Diguet, E. Mylonas, J. Gao-Li, A. Vaahtokari, et al. 2013. SRF selectively controls tip cell invasive behavior in angiogenesis. *Development.* 140:2321–2333. https://doi.org/10.1242/dev.091074

Franco, C.A., M.L. Jones, M.O. Bernabeu, I. Geudens, T. Mathivet, A. Rosa, F.M. Lopes, A.P. Lima, A. Ragab, R.T. Collins, et al. 2015. Dynamic endothelial cell rearrangements drive developmental vessel regression. *PLoS Biol.* 13:e1002125. https://doi.org/10.1371/journal.pbio.1002125

Franco, C.A., M.L. Jones, M.O. Bernabeu, A.C. Vion, P. Barbacena, J. Fan, T. Mathivet, C.G. Fonseca, A. Ragab, T.P. Yamaguchi, et al. 2016. Non-canonical Wnt signalling modulates the endothelial shear stress flow sensor in vascular remodelling. *eLife*. 5:e07727. https://doi.org/10.7554/eLife.07727

Fuentealba, L.C., E. Eivers, A. Ikeda, C. Hurtado, H. Kuroda, E.M. Pera, and E.M. De Robertis. 2007. Integrating patterning signals: Wnt/GSK3 regulates the duration of the BMP/Smad1 signal. *Cell*. 131:980–993. https://doi.org/10.1016/j.cell.2007.09.027

Gerhardt, C., T. Leu, J.M. Lier, and U. Rüther. 2016. The cilia-regulated proteasome and its role in the development of ciliopathies and cancer. *Cilia*. 5:14. https://doi.org/10.1186/s13630-016-0035-3

Givens, C., and E. Tzima. 2016. Endothelial Mechanosignaling: Does One Sensor Fit All? *Antioxid. Redox Signal.* 25:373–388. https://doi.org/10.1089/ars.2015.6493

Goetz, S.C., and K.V. Anderson. 2010. The primary cilium: a signalling centre during vertebrate development. *Nat. Rev. Genet.* 11:331–344. https://doi.org/10.1038/nrg2774

Goetz, J.G., E. Steed, R.R. Ferreira, S. Roth, C. Ramspacher, F. Boselli, G. Charvin, M. Liebling, C. Wyart, Y. Schwab, and J. Vermot. 2014. Endothelial cilia mediate low flow sensing during zebrafish vascular development. *Cell Rep.* 6:799–808. https://doi.org/10.1016/j.celrep.2014.01.032

Guo, X., and X.F. Wang. 2009. Signaling cross-talk between TGF-beta/BMP and other pathways. *Cell Res.* 19:71–88. https://doi.org/10.1038/cr.2008.302

Haycraft, C.J., Q. Zhang, B. Song, W.S. Jackson, P.J. Detloff, R. Serra, and B.K. Yoder. 2007. Intraflagellar transport is essential for endochondral bone formation. *Development*. 134:307–316. https://doi.org/10.1242/dev.02732

Hori, Y., T. Kobayashi, Y. Kikko, K. Kontani, and T. Katada. 2008. Domain architecture of the atypical Arf-family GTPase Arl13b involved in cilia formation. *Biochem. Biophys. Res. Commun.* 373:119–124. https://doi.org/10.1016/j.bbrc.2008.06.001

Iomini, C., K. Tejada, W. Mo, H. Vaananen, and G. Piperno. 2004. Primary cilia of human endothelial cells disassemble under laminar shear stress. *J. Cell Biol.* 164:811–817. https://doi.org/10.1083/jcb.200312133

Isogai, S., N.D. Lawson, S. Torrealday, M. Horiguchi, and B.M. Weinstein. 2003. Angiogenic network formation in the developing vertebrate trunk. *Development*. 130:5281–5290. https://doi.org/10.1242/dev.00733

Jin, Y., L. Muhl, M. Burmakin, Y. Wang, A.C. Duchez, C. Betsholtz, H.M. Arthur, and L. Jakobsson. 2017. Endoglin prevents vascular malformation by regulating flow-induced cell migration and specification through VEGFR2 signalling. *Nat. Cell Biol.* 19:639–652. https://doi.org/10.1038/ncb3534

Jones, C., V.C. Roper, I. Foucher, D. Qian, B. Banizs, C. Petit, B.K. Yoder, and P. Chen. 2008. Ciliary proteins link basal body polarization to planar cell polarity regulation. *Nat. Genet.* 40:69–77. https://doi.org/10.1038/ng.2007.54

Kallakuri, S., J.A. Yu, J. Li, Y. Li, B.M. Weinstein, S. Nicoli, and Z. Sun. 2015. Endothelial cilia are essential for developmental vascular integrity in zebrafish. *J. Am. Soc. Nephrol.* 26:864–875. https://doi.org/10.1681/ASN.2013121314

Kimmel, C.B., W.W. Ballard, S.R. Kimmel, B. Ullmann, and T.F. Schilling. 1995. Stages of embryonic development of the zebrafish. *Dev. Dyn.* 203:253–310. https://doi.org/10.1002/aja.1002030302

Labour, M.N., M. Riffault, S.T. Christensen, and D.A. Hoey. 2016. TGFβ1 - induced recruitment of human bone mesenchymal stem cells is mediated by the primary cilium in a SMAD3-dependent manner. *Sci. Rep.* 6:35542. https://doi.org/10.1038/srep35542

Larrivée, B., C. Prahst, E. Gordon, R. del Toro, T. Mathivet, A. Duarte, M. Simons, and A. Eichmann. 2012. ALK1 signaling inhibits angiogenesis by cooperating with the Notch pathway. *Dev. Cell*. 22:489–500. https://doi.org/10.1016/j.devcel.2012.02.005

Laux, D.W., S. Young, J.P. Donovan, C.J. Mansfield, P.D. Upton, and B.L. Roman. 2013. Circulating Bmp10 acts through endothelial Alk1 to mediate flow-dependent arterial quiescence. *Development*. 140:3403–3412. https://doi.org/10.1242/dev.095307

Lee, J., A. Ishihara, and K. Jacobson. 1993. The fish epidermal keratocyte as a model system for the study of cell locomotion. *Symp. Soc. Exp. Biol.* 47:73–89.

Liu, J., Y. Wang, Y. Akamatsu, C.C. Lee, R.A. Stetler, M.T. Lawton, and G.Y. Yang. 2014. Vascular remodeling after ischemic stroke: mechanisms and therapeutic potentials. *Prog. Neurobiol.* 115:138–156. https://doi.org/10.1016/j.pneurobio.2013.11.004

Muzumdar, M.D., B. Tasic, K. Miyamichi, L. Li, and L. Luo. 2007. A global double-fluorescent Cre reporter mouse. *Genesis*. 45:593–605. https://doi.org/10.1002/dvg.20335

Nauli, S.M., Y. Kawanabe, J.J. Kaminski, W.J. Pearce, D.E. Ingber, and J. Zhou. 2008. Endothelial cilia are fluid shear sensors that regulate calcium signaling and nitric oxide production through polycystin-1. *Circulation*. 117:1161–1171. https://doi.org/10.1161/CIRCULATIONAHA.107.710111

Nonaka, S., Y. Tanaka, Y. Okada, S. Takeda, A. Harada, Y. Kanai, M. Kido, and N. Hirokawa. 1998. Randomization of left-right asymmetry due to loss of nodal cilia generating leftward flow of extraembryonic fluid in mice lacking KIF3B motor protein. *Cell*. 95:829–837. https://doi.org/10.1016/S0092-8674(00)81705-5

Ostrowski, M.A., N.F. Huang, T.W. Walker, T. Verwijlen, C. Poplawski, A.S. Khoo, J.P. Cooke, G.G. Fuller, and A.R. Dunn. 2014. Microvascular endothelial cells migrate upstream and align against the shear stress field created by impinging flow. *Biophys. J.* 106:366–374. https://doi.org/10.1016/j.bpj.2013.11.4502

Pedersen, L.B., J.B. Mogensen, and S.T. Christensen. 2016. Endocytic Control of Cellular Signaling at the Primary Cilium. *Trends Biochem. Sci.* 41:784–797. https://doi.org/10.1016/j.tibs.2016.06.002

Phng, L.K., F. Stanchi, and H. Gerhardt. 2013. Filopodia are dispensable for endothelial tip cell guidance. *Development*. 140:4031–4040. https://doi.org/10.1242/dev.097352

Potente, M., H. Gerhardt, and P. Carmeliet. 2011. Basic and therapeutic aspects of angiogenesis. *Cell*. 146:873–887. https://doi.org/10.1016/j.cell.2011.08.039

Rochon, E.R., P.G. Menon, and B.L. Roman. 2016. Alk1 controls arterial endothelial cell migration in lumenized vessels. *Development*. 143:2593–2602. https://doi.org/10.1242/dev.135392

Satir, P., L.B. Pedersen, and S.T. Christensen. 2010. The primary cilium at a glance. *J. Cell Sci.* 123:499–503. https://doi.org/10.1242/jcs.050377

Schindelin, J., I. Arganda-Carreras, E. Frise, V. Kaynig, M. Longair, T. Pietzsch, S. Preibisch, C. Rueden, S. Saalfeld, B. Schmid, et al. 2012. Fiji: an open-source platform for biological-image analysis. *Nat. Methods*. 9:676–682. https://doi.org/10.1038/nmeth.2019

Taulet, N., B. Vitre, C. Anguille, A. Douanier, M. Rocancourt, M. Taschner, E. Lorentzen, A. Echard, and B. Delaval. 2017. IFT proteins spatially control the geometry of cleavage furrow ingression and lumen positioning. *Nat. Commun.* 8:1928. https://doi.org/10.1038/s41467-017-01479-3

Taulman, P.D., C.J. Haycraft, D.F. Balkovetz, and B.K. Yoder. 2001. Polaris, a protein involved in left-right axis patterning, localizes to basal bodies and cilia. *Mol. Biol. Cell*. 12:589–599. https://doi.org/10.1091/mbc.12.3.589

Ten Dijke, P., A.D. Egorova, M.J. Goumans, R.E. Poelmann, and B.P. Hierck. 2012. TGF-β signaling in endothelial-to-mesenchymal transition: the role of shear stress and primary cilia. *Sci. Signal.* 5:pt2. https://doi.org/10.1126/scisignal.2002722

Traub, O., and B.C. Berk. 1998. Laminar shear stress: mechanisms by which endothelial cells transduce an atheroprotective force. *Arterioscler. Thromb. Vasc. Biol.* 18:677–685. https://doi.org/10.1161/01.ATV.18.5.677

Udan, R.S., T.J. Vadakkan, and M.E. Dickinson. 2013. Dynamic responses of endothelial cells to changes in blood flow during vascular remodeling of the mouse yolk sac. *Development*. 140:4041–4050. https://doi.org/10.1242/dev.096255

Verhey, K.J., J. Dishinger, and H.L. Kee. 2011. Kinesin motors and primary cilia. *Biochem. Soc. Trans.* 39:1120–1125. https://doi.org/10.1042/BST0391120

Vyalov, S., B.L. Langille, and A.I. Gotlieb. 1996. Decreased blood flow rate disrupts endothelial repair in vivo. *Am. J. Pathol.* 149:2107–2118.

Wang, C., B.M. Baker, C.S. Chen, and M.A. Schwartz. 2013. Endothelial cell sensing of flow direction. *Arterioscler. Thromb. Vasc. Biol.* 33:2130–2136. https://doi.org/10.1161/ATVBAHA.113.301826

Zhou, J., P.L. Lee, C.S. Tsai, C.I. Lee, T.L. Yang, H.S. Chuang, W.W. Lin, T.E. Lin, S.H. Lim, S.Y. Wei, et al. 2012. Force-specific activation of Smad1/5 regulates vascular endothelial cell cycle progression in response to disturbed flow. *Proc. Natl. Acad. Sci. USA*. 109:7770–7775. https://doi.org/10.1073/pnas.1205476109

5. Paradoxical suppression of atherosclerosis in the absence of microRNA-146a

Paradoxical Suppression of Atherosclerosis in the Absence of microRNA-146a

Athors: Henry S. Cheng[1,2,3], Rickvinder Besla[1,2,3], Angela Li[1,2,3], Zhiqi Chen[1,2,3], Eric A. Shikatani[1,2,3], Maliheh Nazari-Jahantigh[4], **Adel Hammoutene**[5], My-Anh Nguyen[6], Michele Geoffrion[6], Lei Cai[7], Nadiya Khyzha[1,2,3], Tong Li[7], Sonya A. MacParland[1,2], Mansoor Husain[1,2,3], Myron I. Cybulsky[1,2,3], Chantal M. Boulanger[5], Ryan E. Temel[7], Andreas Schober[4], Katey J. Rayner[6], Clinton S. Robbins[1,2,3], Jason E. Fish[1,2,3]

Affiliations:

1-Toronto General Hospital Research Institute, University Health Network, Ontario, Canada

2-Department of Laboratory Medicine and Pathobiology, University of Toronto, Ontario, Canada

3-Heart and Stroke Richard Lewar Centre of Excellence in Cardiovascular Research, Toronto, Ontario, Canada

4-Institute for Cardiovascular Prevention, Ludwig-Maximilians-University Munich, Germany (M.N.-J., A.S.);

5-INSERM, Unit 970, Paris Cardiovascular Research Center—PARCC, France

6-University of Ottawa Heart Institute, Ontario, Canada

7-Pharmacology and Nutritional Sciences, University of Kentucky, Lexington

Original article published in Circ Res. 2017 Aug 4;121(4):354-367

OPEN

Paradoxical Suppression of Atherosclerosis in the Absence of microRNA-146a

Henry S. Cheng, Rickvinder Besla, Angela Li, Zhiqi Chen, Eric A. Shikatani,
Maliheh Nazari-Jahantigh, Adel Hammoutène, My-Anh Nguyen, Michele Geoffrion, Lei Cai,
Nadiya Khyzha, Tong Li, Sonya A. MacParland, Mansoor Husain, Myron I. Cybulsky,
Chantal M. Boulanger, Ryan E. Temel, Andreas Schober, Katey J. Rayner, Clinton S. Robbins,
Jason E. Fish

Rationale: **Inflammation is a key contributor to atherosclerosis. MicroRNA-146a (miR-146a) has been identified as a critical brake on proinflammatory nuclear factor κ light chain enhancer of activated B cells signaling in several cell types, including endothelial cells and bone marrow (BM)–derived cells. Importantly, miR-146a expression is elevated in human atherosclerotic plaques, and polymorphisms in the *miR-146a* precursor have been associated with risk of coronary artery disease.**

Objective: **To define the role of endogenous miR-146a during atherogenesis.**

Methods and Results: **Paradoxically, *Ldlr*$^{-/-}$ (low-density lipoprotein receptor null) mice deficient in *miR-146a* develop less atherosclerosis, despite having highly elevated levels of circulating proinflammatory cytokines. In contrast, cytokine levels are normalized in *Ldlr*$^{-/-}$*;miR-146a*$^{-/-}$ mice receiving wild-type BM transplantation, and these mice have enhanced endothelial cell activation and elevated atherosclerotic plaque burden compared with *Ldlr*$^{-/-}$ mice receiving wild-type BM, demonstrating the atheroprotective role of miR-146a in the endothelium. We find that deficiency of *miR-146a* in BM-derived cells precipitates defects in hematopoietic stem cell function, contributing to extramedullary hematopoiesis, splenomegaly, BM failure, and decreased levels of circulating proatherogenic cells in mice fed an atherogenic diet. These hematopoietic phenotypes seem to be driven by unrestrained inflammatory signaling that leads to the expansion and eventual exhaustion of hematopoietic cells, and this occurs in the face of lower levels of circulating low-density lipoprotein cholesterol in mice lacking *miR-146a* in BM-derived cells. Furthermore, we identify sortilin-1 (*Sort1*), a known regulator of circulating low-density lipoprotein levels in humans, as a novel target of miR-146a.**

Conclusions: **Our study reveals that miR-146a regulates cholesterol metabolism and tempers chronic inflammatory responses to atherogenic diet by restraining proinflammatory signaling in endothelial cells and BM-derived cells. (*Circ Res*. 2017;121:354-367. DOI: 10.1161/CIRCRESAHA.116.310529.)**

Key Words: atherosclerosis ■ endothelial cells ■ hematopoiesis ■ inflammation ■ microRNAs

Downloaded from http://ahajournals.org by on October 11, 2018

Atherosclerosis is a chronic inflammatory vascular disease characterized by the narrowing of blood vessels caused by the growth of lipid-rich plaques.[1] The initiation of atherogenesis relies on the recruitment of circulating leukocytes by activated endothelial cells (ECs) to regions of deposited oxidized low-density lipoprotein (LDL).[2] Activated ECs and leukocytes use the nuclear factor κ light chain enhancer of activated B cells (NF-κB) signaling pathway to propagate inflammatory gene expression, including induction of adhesion molecules, chemoattractants, and cytokines to drive inflammation in the vessel wall.[3,4] NF-κB signaling is tightly controlled, and this includes regulation by a network of microRNAs, which titrate the expression of signaling components post-transcriptionally.[5] In particular, microRNA-146a (miR-146a) has been well characterized

---

Original received December 21, 2016; revision received June 19, 2017; accepted June 21, 2017. In May 2017, the average time from submission to first decision for all original research papers submitted to *Circulation Research* was 12.28 days.

From the Toronto General Hospital Research Institute, University Health Network, Ontario, Canada (H.S.C, R.B., A.L., Z.C., E.A.S., N.K., S.A.M., M.H., M.I.C., C.S.R., J.E.F.); Department of Laboratory Medicine and Pathobiology, University of Toronto, Ontario, Canada (H.S.C, R.B., A.L., Z.C., E.A.S., N.K., S.A.M., M.H., M.I.C., C.S.R., J.E.F.); Heart and Stroke Richard Lewar Centre of Excellence in Cardiovascular Research, Toronto, Ontario, Canada (H.S.C, R.B., A.L., Z.C., E.A.S., N.K., M.H., M.I.C., C.S.R., J.E.F.); Institute for Cardiovascular Prevention, Ludwig-Maximilians-University Munich, Germany (M.N.-J., A.S.); INSERM, Unit 970, Paris Cardiovascular Research Center—PARCC, France (A.H., C.M.B.); University of Ottawa Heart Institute, Ontario, Canada (M.-A.N., M.G., K.J.R.); and Pharmacology and Nutritional Sciences, University of Kentucky, Lexington (L.C., T.L., R.E.T.).

The online-only Data Supplement is available with this article at http://circres.ahajournals.org/lookup/suppl/doi:10.1161/CIRCRESAHA.116.310529/-/DC1.

Correspondence to Jason E. Fish, PhD, Toronto General Hospital Research Institute, University Health Network, Toronto Medical Discovery Tower, MaRS Bldg, 101 College St, 3-308, Toronto, ON M5G 1L7, Canada. E-mail jason.fish@utoronto.ca

© 2017 The Authors. *Circulation Research* is published on behalf of the American Heart Association, Inc., by Wolters Kluwer Health, Inc. This is an open access article under the terms of the Creative Commons Attribution Non-Commercial-NoDerivs License, which permits use, distribution, and reproduction in any medium, provided that the original work is properly cited, the use is noncommercial, and no modifications or adaptations are made.

Novelty and Significance

What Is Known?

- MicroRNA-146a (miR-146a) suppresses inflammatory responses in endothelial cells and bone marrow (BM)–derived cells by targeting adaptor proteins in the nuclear factor κ light chain enhancer of activated B cells signaling pathway.
- Increased levels of miR-146a have been detected in human atherosclerotic plaques, and polymorphisms in the miR-146a precursor are associated with risk of coronary artery disease.
- Injection of exogenous miR-146a reduces atherogenesis in mouse models.

What New Information Does This Article Contribute?

- Deletion of *miR-146a* in BM-derived cells enhances the production of proinflammatory cytokines, but paradoxically reduces circulating proatherogenic leukocytes, ultimately resulting in decreased atherosclerosis.
- miR-146a in BM-derived cells protects against high cholesterol diet–induced hematopoietic progenitor cell exhaustion in the BM and prevents extramedullary hematopoiesis and splenomegaly.
- Circulating very-low-density lipoprotein levels are progressively decreased in mice lacking *miR-146a* in the BM, and this is accompanied by enhanced inflammation in the liver and dysregulation of a newly identified miR-146a target gene, *sortilin 1* (*Sort1*).

Elevation of miR-146a expression in atherosclerotic plaques in humans and polymorphisms in the miR-146a precursor that are associated with coronary artery disease are suggestive of a role for this microRNA in atherogenesis. Although numerous studies have placed miR-146a among the echelon of anti-inflammatory microRNAs, the role of endogenous *miR-146a* in atherosclerosis remains unknown. Surprisingly, despite the ability of this microRNA to restrain cytokine production in BM-derived cells, loss of this microRNA resulted in reduced atherosclerosis. This was accompanied by hematopoietic stem cell exhaustion and a corresponding reduction in levels of circulating proatherogenic cells. Enhanced inflammatory signaling occurred even though circulating levels of very-low-density lipoprotein cholesterol were diminished in these mice. Within the vasculature, miR-146a restrained endothelial activation, and loss of *miR-146a* in the vasculature enhanced atherosclerosis. This study reveals a critical function for a single microRNA in the control of the intensity of inflammatory responses to hypercholesterolemia and highlights the detrimental effects of unrestrained inflammatory signaling in multiple organs: BM (hematopoietic stem cell exhaustion), spleen (extramedullary hematopoiesis and splenomegaly), liver (cholesterol homeostasis defects), and the vasculature (enhanced endothelial cell activation and monocyte recruitment). Importantly, these findings provide a further impetus to therapeutically augment miR-146a expression/function in atherosclerosis.

Nonstandard Abbreviations and Acronyms

BM	bone marrow
BMT	bone marrow transplant
DKO	double knockout
EC	endothelial cell
HCD	high cholesterol diet
HSC	hematopoietic stem cell
HuR	human antigen R
ICAM-1	intercellular adhesion molecule-1
IL	interleukin
IRAK1	interleukin receptor–associated kinase 1
KO	knockout
LDL	low-density lipoprotein
LDLR	low-density lipoprotein receptor
LPS	lipopolysaccharide
miR-146a	microRNA-146a
NCD	normal chow diet
NF-κB	nuclear factor κ light chain enhancer of activated B cells
SELE	E-selectin
sICAM-1	soluble intercellular adhesion molecule-1
SORT1	sortilin-1
TNF-α	tumor necrosis factor-α
TRAF6	TNF receptor–associated factor 6
VCAM-1	vascular cell adhesion molecule-1
VLDL	very-low-density lipoprotein
WT	wild type

in both ECs and leukocytes as a negative regulator of NF-κB activity through its ability to target upstream adaptor proteins, including TRAF6 (TNF receptor–associated factor 6) and IRAK1 (interleukin receptor–associated kinase 1).[6,7]

In This Issue, see p 311

Characterization of *miR-146a*–deficient mice has revealed defects in multiple aspects of immune cell biology.[8,9] Older (>1 year) *miR-146a*$^{-/-}$ mice develop multiorgan inflammation, bone marrow (BM) failure, splenomegaly, and lymphoadenopathy.[9,10] When challenged by proinflammatory stimuli (eg, lipopolysaccharide [LPS] or IL-1β [interleukin-1β]), these mice have exacerbated NF-κB–dependent inflammatory responses and demonstrate expansion of proinflammatory Ly6C^{hi} monocytes.[6,10,11] Interestingly, the hyperactivation of NF-κB caused by low-grade inflammation during normal aging or through repeated LPS challenge drives the proliferation and eventual exhaustion of hematopoietic and progenitor stem cells in these mice, resulting in eventual loss of circulating leukocytes and lymphocytes.[10]

The NF-κB pathway is activated in ECs, macrophages, and smooth muscle cells within human atherosclerotic lesions.[12] However, defining the role of NF-κB signaling in atherogenesis has been complicated, as ablation of NF-κB activity in ECs reduces atherogenesis,[3] whereas inhibition within macrophages enhances atherogenesis.[13] Of interest, recent studies have shown that injection of miR-146a mimic into atheroprone mice reduces atherogenesis, and it has been suggested that this is because of suppression of macrophage NF-κB signaling.[14] The role of endogenous miR-146a in atherogenesis remains undefined. Here, we show that genetic ablation of *miR-146a* in BM-derived cells reduces atherogenesis and that this is paradoxically accompanied by enhanced circulating levels of proinflammatory cytokines despite reduced levels of circulating LDL cholesterol. Lack of *miR-146a* in BM-derived cells leads to monocytosis

Downloaded from http://ahajournals.org by on October 11, 2018

in response to high cholesterol diet (HCD), followed by BM exhaustion, depleting circulating levels of proatherogenic cells. Conversely, deletion of *miR-146a* in the vasculature promotes atherogenesis by increasing endothelial activation. Thus, unrestrained inflammatory signaling in *miR-146a*–deficient tissues has diverse consequences during atherogenesis, and our studies emphasize the importance of tight control of inflammatory pathways in the setting of hypercholesterolemia.

Methods

A complete description of Methods is included in the Online Data Supplement.

Results

miR-146a Expression Is Increased in ECs and Intimal Cells During Murine Atherogenesis

Ldlr$^{-/-}$ (low-density lipoprotein receptor null) mice were placed on a HCD for 18 weeks to visualize the expression of miR-146a in atherosclerotic plaque (Figure 1A). In situ polymerase chain reaction on aortic root cross-sections revealed that miR-146a was expressed in intimal cells, including Mac-2$^+$ macrophages, and was robustly expressed in CD31$^+$ ECs. The in situ signal was specific for miR-146a, as staining was not detected in *miR-146a*$^{-/-}$ mice (Figure 1A). Expression of miR-146a in the aortic root seemed to progressively increase in the intima during the progression of atherosclerosis (Online Figure I). The absence of signal in the media implies that contractile smooth muscle cells in the aortic root do not express miR-146a at sufficient levels to be detected by this technique. In addition, using quantitative reverse transcriptase-polymerase chain reaction at an early stage of atherogenesis (ie, *Ldlr*$^{-/-}$ mice, 4-week HCD), we found a significant elevation of miR-146a expression in the lesser curvature of the aortic arch, a region of the aorta where atherosclerotic plaque forms, compared with regions that are protected from atherosclerosis, namely the greater curvature of the aortic arch and the descending thoracic aorta (Figure 1B and 1C). However, miR-146a expression was at appreciable levels in all regions examined (not shown), which may reflect the known expression of miR-146a in the vascular endothelium.[6]

Global Deletion of miR-146a Activates Proinflammatory Pathways Yet Suppresses Atherogenesis and Is Accompanied by Reduced Circulating LDL Cholesterol Levels in Mice on HCD

To elucidate the role of miR-146a during atherogenesis, we generated global double knockout (DKO; *miR-146a*$^{-/-}$; *Ldlr*$^{-/-}$) mice by crossing *miR-146a*$^{-/-}$ mice with *Ldlr*$^{-/-}$ mice. Two time points (12 and 18 weeks of HCD) were assessed to determine the effect of miR-146a on the progression of atherosclerotic phenotypes (Figure 2A). Analyses of male and female mice were grouped together as we found no significant differences between sexes for the parameters measured, except

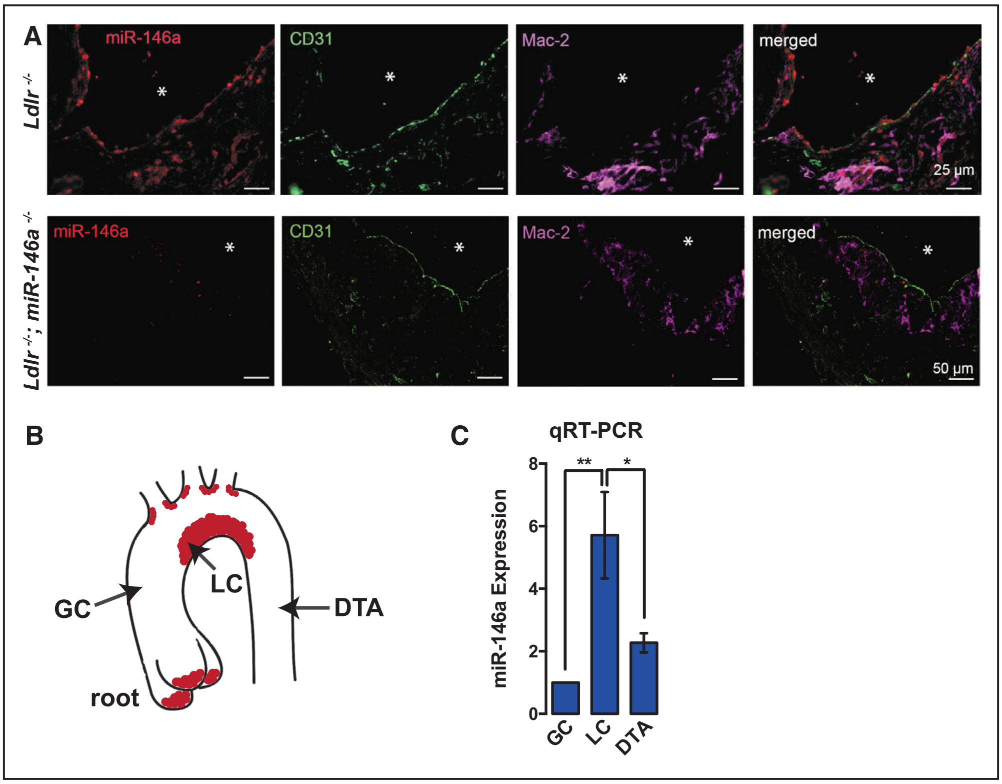

Figure 1. MicroRNA-146a (miR-146a) is expressed in murine atherosclerotic plaques. A, Cross-sections of *Ldlr*$^{-/-}$ or *Ldlr*$^{-/-}$;*miR-146a*$^{-/-}$ mouse aortic roots after 18 wk of high cholesterol diet (HCD). Expression of miR-146a, assessed by in situ polymerase chain reaction (red) overlaps with Mac-2–positive macrophages (purple) and CD31-positive endothelial cells (ECs; green) in the intima, and signal is absent in *miR-146a*$^{-/-}$ mice. miR-146a expression during the progression of atherosclerosis is shown in Online Figure I. **B**, Schematic of the aorta, indicating the aortic root (examined in **A**), the greater curvature (GC, atheroprotective) and lesser curvature (LC, atherosusceptible) of the aortic arch and the descending thoracic aorta (DTA, atheroprotective). **C**, Expression of miR-146a (normalized to U6 levels) in the specified regions of the aorta in *Ldlr*$^{-/-}$ mice after 4 wk of HCD (n=5). Ldlr indicates low-density lipoprotein receptor.

Downloaded from http://ahajournals.org by on October 11, 2018

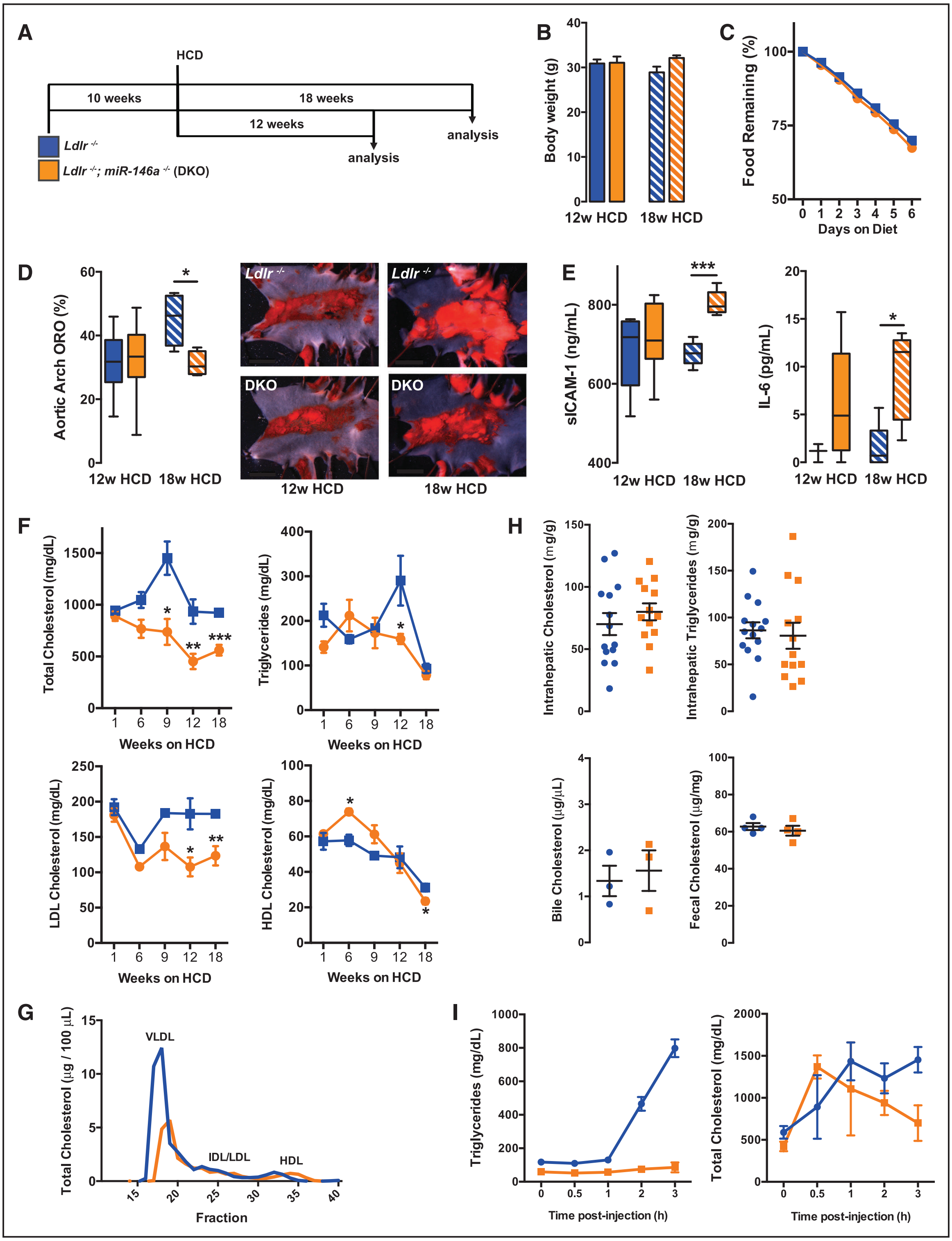

Figure 2. Reduced atherosclerosis in mice with global deletion of microRNA-146a (miR-146a). A, Schematic of high cholesterol diet (HCD) regimen for *Ldlr*$^{-/-}$ and *Ldlr*$^{-/-}$;*miR-146a*$^{-/-}$ (double knockout [DKO]) mice. **B**, Weights of male mice after 12- or 18-wk HCD (n=3–5). Weights of female mice were also unchanged between genotypes (not shown). **C**, Food consumption in mice (n=4 mice per cage). T_0 is 18 wk of HCD. **D**, Percentage of Oil Red-O (ORO) regions quantified from aortic arches of *Ldlr*$^{-/-}$ and DKO mice after HCD for 12 or 18 wk. Representative images are shown to the right. The descending side of the aorta is to the right. Aortic root and descending thoracic aorta analyses are shown in Online Figure II. n=18 to 22 for 12-wk time point and n=4 for 18-wk time point. **E**, Circulating levels of proinflammatory markers, IL-6 (interleukin-6) and soluble intercellular adhesion molecule-1 (sICAM-1) in wild-type and DKO mice (n=5–8). **F**, Time course of plasma cholesterol measurements (n=3–5; 1 group of mice were used for weeks 1, 6, and 9, and a separate group was used for weeks 12 and 18). Mice were fasted overnight before sample collection. **G**, FPLC (fast protein liquid chromatography) trace of cholesterol content in lipoprotein fractions in plasma after 18 wk of HCD (pooled analysis of 5 samples). **H**, Intrahepatic cholesterol and triglyceride levels in mice after 12-wk HCD (n=13–14). Eighteen-week HCD is shown in Online Figure IID. Bile cholesterol (n=3) and fecal cholesterol (n=4) in mice after 18-wk HCD. **I**, Assessment of very-low-density lipoprotein (VLDL) secretion by measurement of triglycerides and cholesterol in plasma after injection of Poloxamer 407 (12-wk HCD; n=4, 2). Ldlr indicates low-density lipoprotein receptor.

Downloaded from http://ahajournals.org by on October 11, 2018

for body weight (not shown). At the 12-week time point, no differences in body weight (Figure 2B) or aortic arch plaque burden (Figure 2D) were observed between *Ldlr*$^{-/-}$ and DKO mice. However, the circulating inflammatory marker, IL-6, was elevated in the majority of DKOs at this stage, although the difference did not reach statistical significance (Figure 2E). By 18 weeks, despite no differences in body weight (Figure 2B) or food intake (Figure 2C), DKO mice surprisingly had less lipid plaque in the aortic arch (Figure 2D). This decrease in atherosclerosis occurred despite signs of elevated systemic inflammatory signaling, including enhanced circulating levels of soluble intercellular adhesion molecule-1 (sICAM-1) and IL-6 (Figure 2E). Atherosclerotic plaque formation was unaltered in the descending thoracic aorta of DKO mice: this region is typically protected from atherosclerosis (Online Figure IIA). Plaque burden in the aortic root was also comparable between groups (Online Figure IIB and IIC).

Unexpectedly, DKO mice displayed progressive lipid metabolism defects, resulting in lower circulating total cholesterol and LDL cholesterol. High-density lipoprotein levels and triglyceride levels were modestly affected (Figure 2F). Assessment of lipoprotein profiles by fast protein liquid chromatography (FPLC) revealed a striking decrease in cholesterol content in very-low-density lipoprotein (VLDL) fractions (Figure 2G). Measurement of total cholesterol and triglyceride levels in the liver revealed no significant differences at 12 weeks (Figure 2H) or 18 weeks of HCD (Online Figure IID). Likewise, cholesterol levels in bile and feces were unchanged at 12 weeks of HCD (Figure 2H). Assessment of VLDL secretion from the liver suggested a decrease in cholesterol and triglyceride secretion in DKO mice (Figure 2I). Taken together, these data demonstrate that lack of *miR-146a* decreases circulating VLDL/LDL cholesterol yet paradoxically enhances inflammatory signaling in mice on a proatherogenic diet.

Deletion of miR-146a in BM-Derived Cells Enhances Inflammatory Signaling, Yet Paradoxically Suppresses Atherogenesis and Alters Cholesterol Metabolism

Next, we performed BM transplantation (BMT) experiments to elucidate the role of miR-146a in BM-derived cells during atherogenesis. *Ldlr*$^{-/-}$ mice were lethally irradiated and reconstituted with either *miR-146a*$^{+/+}$ (wild-type [WT]) or *miR-146a*$^{-/-}$ (knockout [KO]) BM (Figure 3A). Reconstitution of hematopoiesis after transplantation of WT or KO BM cells seemed to be normal, as circulating levels of leukocytes and lymphocytes were similar 8 weeks after BMT, before the administration of HCD (Online Figure IIIA). Body weight was similar between the 2 groups after 12 weeks of HCD (Figure 3B), as was food intake (Figure 3C). Although lipid plaque burden was not significantly altered at early stages (ie, 4-week HCD), mice receiving KO BM developed less lipid plaque in the aorta after 12 weeks of HCD (Figure 3D; Online Figure IIIB), and markers of macrophage content in the aortic arch were reduced (Online Figure IIIC). Plaque burden in the descending thoracic aorta (Online Figure IIIB) and aortic root (Online Figure IIID) appeared to be unchanged. The decrease in plaque burden in the aortic arch was paradoxically accompanied by signs of systemic inflammatory signaling, with higher levels of circulating sICAM-1, IL-6, and TNF-α (tumor necrosis factor-α) detected in the plasma of mice receiving KO BM after 12 weeks of HCD (Figure 3E), with a trend toward elevated IL-6 levels being observed after 4 weeks of HCD (Figure 3E). These findings suggest that loss of miR-146a expression in BM-derived cells surprisingly results in reduced atherosclerosis, despite the ability of miR-146a to restrain inflammatory signaling. The similarity in phenotypes observed in DKO mice and mice receiving KO BM suggests that loss of miR-146a function in BM-derived cells is the predominant contributor to the observed phenotypes.

Interestingly, we found a progressive decrease in total cholesterol, LDL, triglycerides, and high-density lipoprotein levels in the plasma of mice receiving KO BM (Figure 3F). FPLC revealed a marked reduction in cholesterol content in VLDL fractions (Figure 3G). However, levels of total and free cholesterol and triglycerides in the liver were not significantly different (Figure 3H), neither were cholesterol esters (not shown), and fecal cholesterol levels were also unchanged (Figure 3H). To determine potential mechanisms for the altered lipid metabolism, we assessed gene expression in livers of *Ldlr*$^{-/-}$ and DKO mice (18-week HCD), and *Ldlr*$^{-/-}$ mice receiving WT or KO BM (12-week HCD). We observed an elevation of a macrophage marker (*F4/80*), as well as several proinflammatory cytokines, such as *IL-1*β and *IL-6*, and an increase in *IL-10*, in DKO livers and in the livers of *Ldlr*$^{-/-}$ mice receiving KO BM, compared with their respective controls (Figure 3I). Importantly, dysregulation of IL-6 and IL-10 has previously been implicated in altered lipid metabolism.[15–17] Indeed, we found that exposing primary hepatocytes to IL-6 decreased triglyceride secretion (Figure 3J). Acute phase response genes were elevated in DKO livers, but not in recipients of KO BM (not shown). We also assessed the expression of a panel of 84 lipid signaling and cholesterol metabolism genes by quantitative reverse transcriptase-polymerase chain reaction arrays. A small number of genes were significantly dysregulated in either experimental group (9 genes in DKOs compared with *Ldlr*$^{-/-}$ mice, and 19 genes in KO BMT recipients compared with WT BMT recipients; Online Figure IV; Online Table I). However, the only genes that were significantly decreased in both models were *ApoB* (apolipoprotein B; 1.25-fold decrease in DKOs versus *Ldlr*$^{-/-}$ and 1.61-fold decrease in KO BMT versus WT BMT recipients) and *Cnbp* (CCHC-type zinc finger nucleic acid binding protein; 1.43-fold decrease in DKOs versus *Ldlr*$^{-/-}$ and 1.69-fold decrease in KO BMT versus WT BMT recipients), but these changes were modest. Although not on the quantitative reverse transcriptase-polymerase chain reaction array, we also assessed the expression of sortilin-1 (*Sort1)* because it is a known regulator of circulating LDL levels that was identified by genome-wide association studies in humans,[18] and it has been shown to promote IL-6 signaling and secretion in macrophages in mouse models.[19] Interestingly, *Sort1* is also predicted to be an miR-146a target gene (Figure 3K). We found that *Sort1* expression in the liver was elevated in both models (2.21-fold increase in DKOs versus *Ldlr*$^{-/-}$ and 1.68-fold increase in KO BMT versus WT BMT recipients; Figure 3I). Furthermore, we confirmed that *Sort1* is a bone fide miR-146a target gene by luciferase assay (Figure 3K). Thus, loss of miR-146a from BM-derived cells perturbs

Downloaded from http://ahajournals.org by on October 11, 2018

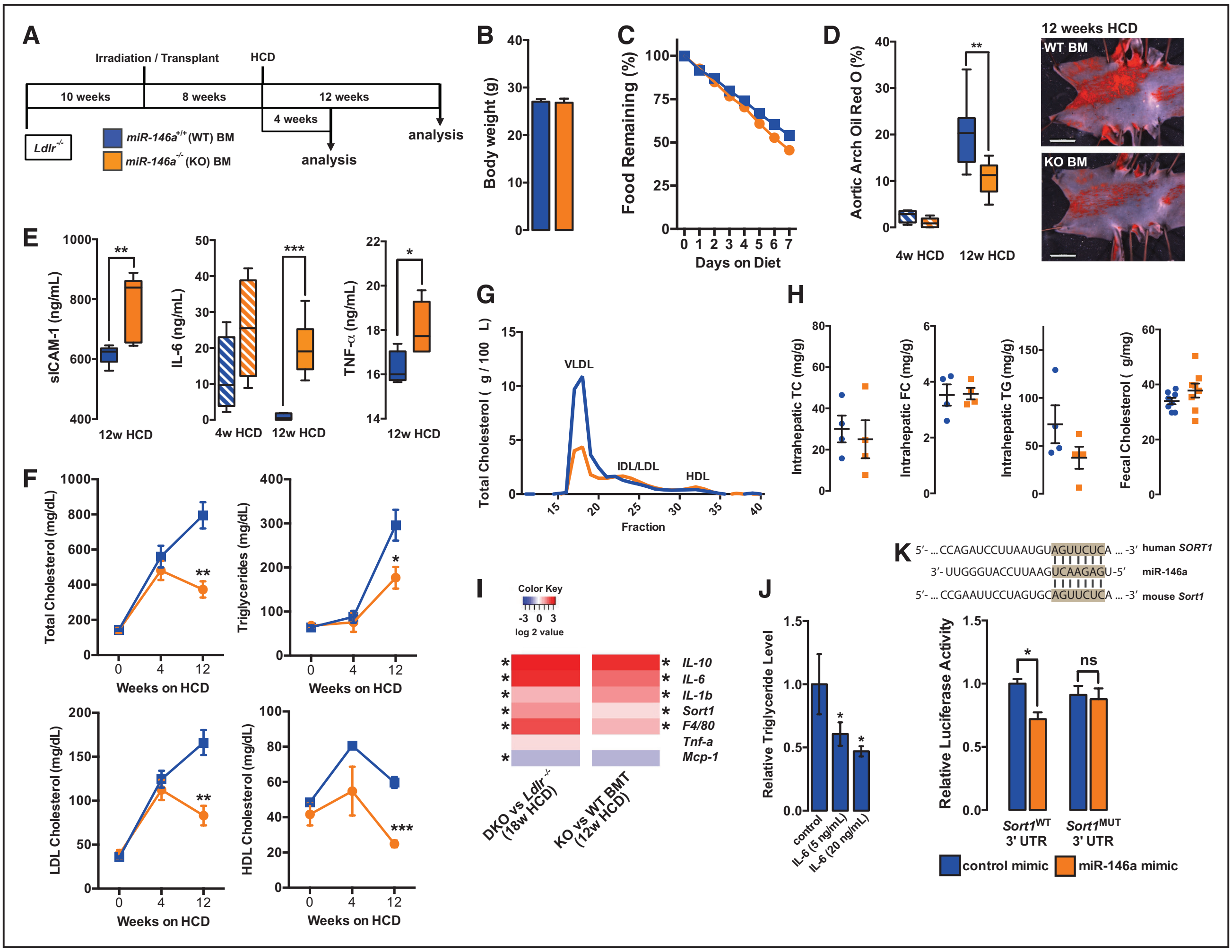

Figure 3. MicroRNA-146a (miR-146a) in bone marrow (BM)–derived cells contributes to atherogenesis. A, *Ldlr*$^{-/-}$ mice lethally irradiated and given BM transplantation (BMT) from wild-type (WT BM) or *miR-146a*$^{-/-}$ (knockout [KO] BM) donors followed by high cholesterol diet (HCD) for 4 or 12 wk. **B**, Body weights of female mice after 12-wk HCD (n=5–7). Weights of male mice were also unchanged (not shown). **C**, Food consumption in mice (n=4 mice per cage). T_0 is 12 wk of HCD. **D**, Percentage of Oil Red-O (ORO) regions per aortic arch measured by en face imaging after 4- or 12-wk HCD (n=9–11). Representative images of plaque burden in aortas of *Ldlr*$^{-/-}$ mice with WT BM (**top**) and KO BM (**bottom**) after 12-wk HCD are shown to the right. Aortic root and descending thoracic aorta analyses are shown in Online Figure IIIB and IIID. **E**, Circulating proinflammatory markers, soluble intercellular adhesion molecule-1 (sICAM-1), IL-6 (interleukin-6), and TNF-α (tumor necrosis factor-α), measured by ELISA of plasma samples (n=4–7). **F**, Time course of plasma cholesterol measurement in *Ldlr*$^{-/-}$ mice receiving WT or KO BM (n=4–7; 1 group of mice was used for weeks 0 and 4, and a separate group was used for week 12). **G**, FPLC (fast protein liquid chromatography) trace of cholesterol content of lipoprotein fractions from plasma after 12 wk of HCD (pooled analysis of 4 samples). **H**, Intrahepatic total cholesterol (TC), free cholesterol (FC), and triglycerides (TG) after 12-wk HCD (n=4). Fecal cholesterol levels after 12 wk of HCD (n=8). **I**, Expression of inflammatory genes, *Sort1,* and a macrophage marker (*F4/80*) from liver tissues. Shown is a heat map of quantitative reverse transcriptase-polymerase chain reaction data (n=4–8). Values are relative to the controls for each group, as indicated. *Significant difference in expression. **J**, TG measurements in the media of cultured primary mouse hepatocytes treated with recombinant mouse IL-6 for 6 h (n=4). **K**, The predicted miR-146a binding in the human and mouse *SORT1* 3′ UTR (untranslated region; above) and luciferase analyses in bovine aortic endothelial cells (BAECs; n=5). HDL indicates high-density lipoprotein; and Ldlr, low-density lipoprotein receptor.

cholesterol metabolism, potentially through dysregulated NF-κB–dependent inflammatory pathways in the liver, including macrophage accumulation and IL-6 secretion, and perhaps through regulation of *Sort1*. Of note, despite the lower levels of VLDL/LDL cholesterol, *miR-146a*$^{-/-}$ mice display an exaggerated inflammatory response to HCD.

Diet- and Age-Dependent Hematopoiesis Defects in miR-146a$^{-/-}$ Mice

Strikingly, the spleens of DKO mice fed HCD for 18 weeks (6–7 months of age) were ≈2.5× larger than *Ldlr*$^{-/-}$ mice on the same atherogenic diet (Figure 4A). At earlier stages (ie, 12 weeks of HCD; 5–6 months of age) spleen weight was not significantly changed (Figure 4A). Of note, aged *miR-146a*$^{-/-}$ mice (>8 months of age) have previously been shown to spontaneously develop splenomegaly, which is accompanied by BM hematopoiesis defects.[10] Because we observed a splenomegaly phenotype in young mice on HCD, this suggests that atherogenic diet may accelerate the development of splenomegaly. Similar to global KOs, mice receiving KO BMT and fed HCD developed larger spleens and had pale femurs, suggestive of BM dysfunction (Figure 4B and 4C). We previously

Downloaded from http://ahajournals.org by on October 11, 2018

Downloaded from http://ahajournals.org by on October 11, 2018

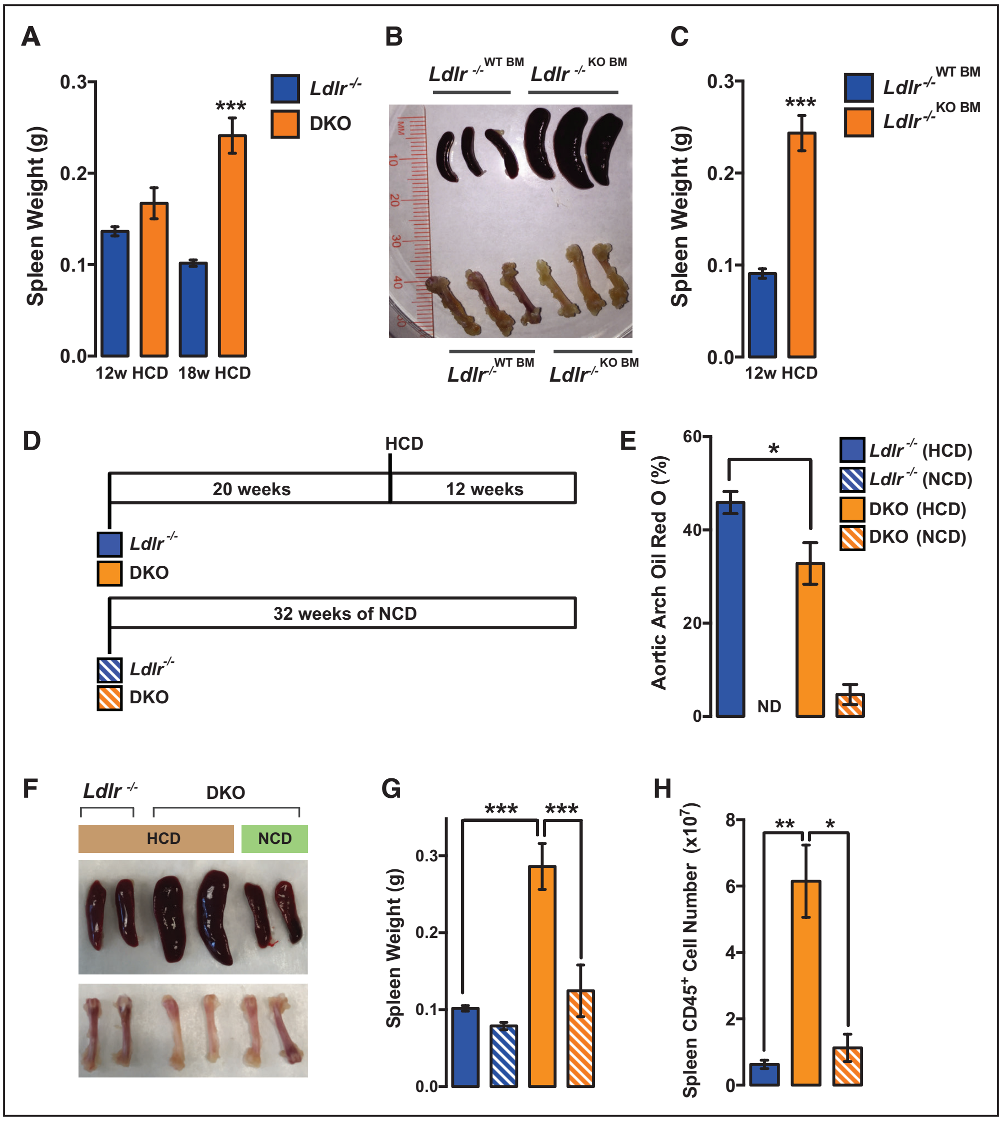

Figure 4. Diet- and age-dependent splenomegaly in double knockout (DKO) mice. A, Spleen weight in *Ldlr*$^{-/-}$ or DKO mice after 12 or 18 wk of high cholesterol diet (HCD; n=12–16 for 12-wk HCD; n=5 for 18-wk HCD). **B**, Representative images of spleens and femurs in wild-type (WT) and KO bone marrow transplant (BMT) mice on HCD for 12 wk. **C**, Quantification of spleen weight in WT and KO BMT mice on HCD for 12 wk (n=5–7). **D**, Mice were placed on HCD or normal chow diet (NCD) at 20 wk of age for 12 wk. **E**, Percentage of Oil Red-O (ORO) region per aortic arch measured en face (n=3–4). *Ldlr*$^{-/-}$ mice on NCD were from a separate experiment and are included for comparison purposes (n=5). **F**, Representative images of spleens and femurs. **G**, Quantification of spleen weights (n=3–4). *Ldlr*$^{-/-}$ mice on NCD were from a separate experiment and are included for comparison purposes (n=5). **H**, Quantification of total CD45$^+$ cells in spleens by fluorescence-activated cell sorting (FACS) analysis (n=3–4). Ldlr indicates low-density lipoprotein receptor.

showed that prolonged hypercholesterolemia results in the outsourcing of hematopoiesis from the BM to the spleen.[20] It seems that this phenotype may be accelerated and exaggerated in *miR-146a*$^{-/-}$ mice, even in the face of lower circulating VLDL/LDL cholesterol levels.

To further investigate the effects of aging on splenomegaly and atherogenesis, DKO mice were fed a 12-week HCD regime starting at 20 weeks of age (rather than the typical 10 weeks of age; Figure 4D). In contrast to younger DKO mice, which had unaltered plaque burden in the aorta after 12 weeks of HCD (Figure 2D), older mice had reduced atherosclerosis in the aortic arch after the same duration of diet (Figure 4E). No differences in plaque formation were observed in the descending thoracic aorta (not shown). This reduction in aortic arch atherosclerosis was accompanied by splenomegaly (Figure 4F and 4G). Importantly, the splenomegaly phenotype at this age was dependent on exposure to HCD, as this was not observed in DKO mice on a regular chow diet (Figure 4F and 4G). The pale femur phenotype in older DKO mice also seemed to be dependent on exposure to HCD (Figure 4F). The increased spleen size in older DKO mice on HCD corresponded with an increase in splenic CD45$^+$ leukocytes (Figure 4H). Intriguingly, these findings highlight a potential relationship between the reduced atherogenesis observed in DKO mice on HCD and development of splenomegaly and pale femurs, suggesting that defective hematopoiesis may contribute to the phenotype. Although previous studies have linked splenomegaly with reduced circulating cholesterol,[21] the contribution of splenomegaly to reduced LDL cholesterol in *miR-146a*$^{-/-}$ mice remains unclear. Although leukocyte content in the spleen at 12 weeks of HCD was not significantly different in DKOs (Online Figure VA) and spleens were not significantly larger (Figure 4A)—despite reduced levels of plasma cholesterol at this stage (Figure 2F)—mice receiving *miR-146a*$^{-/-}$ BMT had greatly enlarged spleens at 12 weeks of HCD (Figure 4C), which coincided with reduced circulating LDL (Figure 3F). Furthermore, oxidized LDL uptake and cholesterol efflux were similar in WT and *miR-146a*$^{-/-}$ macrophages (Online Figure VB and VC), suggesting that *miR-146a*–deficient macrophages seem not to be more avid at sequestering cholesterol. However, expansion of macrophages in the liver and spleen may contribute to the sequestering of cholesterol from circulation. The contribution of splenomegaly to cholesterol lowering in *miR-146a*$^{-/-}$ mice will require further exploration.

Loss of miR-146a Leads to Reduced BM Hematopoiesis While Promoting Extramedullary Hematopoiesis in the Spleen in Mice Fed a HCD

The enlarged spleens in DKO mice on 18 weeks of HCD contained more CD45$^+$ leukocytes and lymphocytes (Figure 5A;

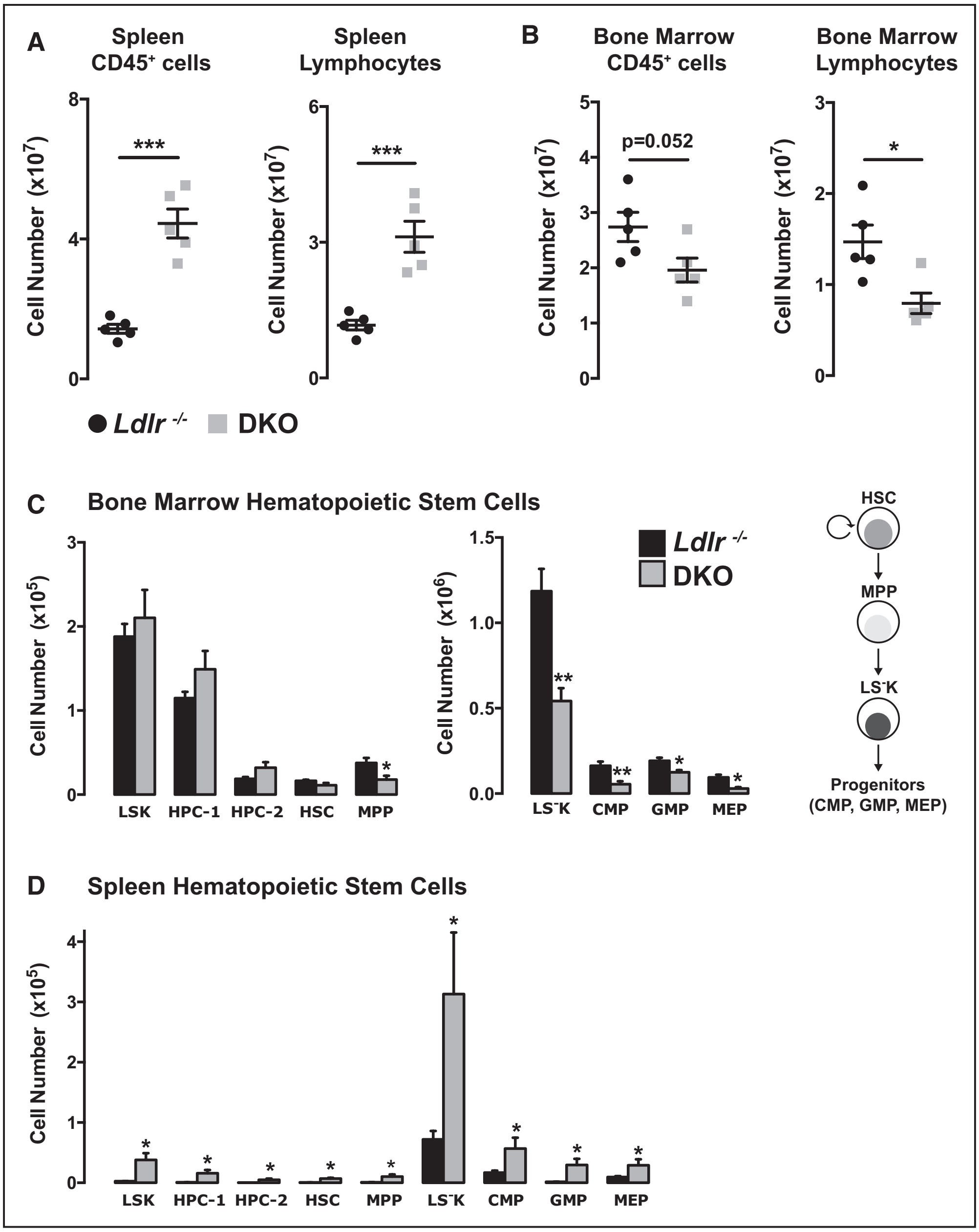

Figure 5. Global loss of microRNA-146a (miR-146a) inhibits bone marrow (BM) hematopoiesis and promotes extramedullary hematopoiesis in the spleen. Increase of splenic (**A**) and decrease in BM (**B**) CD45$^+$ leukocytes and Ly6G$^-$/CD115$^-$ lymphocytes in DKO mice on diet for 18 wk, determined by fluorescence-activated cell sorting (FACS) analysis (n=5). **C**, Decrease of multipotent progenitor cells (MPPs) and downstream progenitor cells (eg, Sca-1 [stem cells antigen-1]–negative progenitor [LS$^-$K], megakaryocyte–erythroid progenitor [MEP], common myeloid progenitor [CMP], and granulocyte–macrophage progenitor [GMP]) in BM of double knockout (DKO) mice after 18 wk of high cholesterol diet (HCD; n=5). **D**, Increase of splenic hematopoietic and multipotent stem cells in DKO mice after 18 wk of HCD (n=5; Online Figure VII). HPC indicates hematopoietic progenitors cell; HSC, hematopoietic stem cell; Ldlr, low-density lipoprotein receptor; and LSK, lineage$^-$ Sca-1$^+$ Kit$^+$.

Downloaded from http://ahajournals.org by on October 11, 2018

Online Figure VI for flow cytometry gating strategies). This was in contrast to the depletion of these cells from the BM of DKO mice (Figure 5B). Previous studies have observed defects in BM hematopoietic stem cell (HSC) longevity in aged (>8 months) *miR-146a*$^{-/-}$ mice, or in younger mice after repeated challenge with LPS.[10] Assessing the spectrum of hematopoietic cells in the BM revealed normal levels of hematopoietic progenitors cells 1 and 2 and HSCs, but levels of multipotent progenitor cells were significantly decreased in DKOs (Figure 5C; Online Figure VIIA). The consequences of decreased multipotent progenitor cell levels were further evident in the decreased numbers of downstream progenitor cells (eg, Sca-1 [stem cells antigen-1]–negative progenitors, common myeloid progenitors, granulocyte–macrophage progenitors, megakaryocyte–erythroid progenitors; Figure 5C). Taken together, these data are suggestive of an HSC functional defect in the BM. Interestingly, despite this defect in HSC function in the BM, HSCs and downstream progenitor cells appeared in the spleens of DKO mice on HCD for 18 weeks but not in *Ldlr*$^{-/-}$ mice (Figure 5D), demonstrating that loss of *miR-146a* accelerates extramedullary hematopoiesis. The dysregulation of hematopoiesis in the spleen and BM was accompanied by modest effects on circulating leukocytes, such as neutrophils and B cells, although anti-inflammatory Ly6C^{lo} monocytes were significantly increased (Online Figure VIIB).

miR-146a in BM-Derived Cells Regulates BM and Extramedullary Hematopoiesis and Levels of Circulating Leukocytes and Lymphocytes

Similar to the nontransplanted DKO mice on 18-week HCD, mice receiving KO BM accumulated more CD45^{+} leukocytes and lymphocytes in their spleens; however, this occurred after just 12-week HCD (Figure 6A). The BM in these mice was depleted of these cells by 12-week HCD (Figure 6B). This was accompanied by elevated NF-κB signaling in the BM of KO mice, as well as enhanced expression of TRAF6, an miR-146a target gene (Figure 6C). Progenitors downstream of HSCs, namely multipotent progenitor cells, Sca-1–negative progenitors, common myeloid progenitors, granulocyte–macrophage progenitors and megakaryocyte–erythroid progenitors, were diminished in the BM (Figure 6D), whereas extramedullary hematopoiesis was evident in mice receiving KO BM (Figure 6E). Correspondingly, mice receiving KO BM had decreased levels of circulating atherogenic leukocytes, including neutrophils, B cells, and Ly6C^{hi} monocytes, but levels of atheroprotective Ly6C^{lo} monocytes were increased after 12 weeks of HCD (Figure 6F). Assessing circulating levels of leukocytes and lymphocytes at earlier stages (ie, 4 weeks of HCD) revealed monocytosis in mice receiving KO BM (Figure 6F), suggesting that the reduction of hematopoiesis at later stages of atherosclerosis is preceded by enhanced hematopoiesis at earlier stages, similar to previous studies that revealed HSC exhaustion in KO mice in the context of repeated LPS stimulation.[10]

We next assessed the functionality of WT (CD45.1) and KO (CD45.2) BM-derived cells in a competitive 1:1 BMT. After reconstitution of the BM compartment of lethally irradiated *Ldlr*$^{-/-}$ mice for 8 weeks, mice were placed on either normal chow diet (NCD) or HCD diet. Assessing circulating levels of leukocytes in mice fed an NCD revealed that KO BM cells preferentially contributed to neutrophil and Ly6C^{hi} monocyte populations compared with WT BM cells (Figure 7A). A short duration on HCD (4 weeks) expanded the leukocyte populations examined, and KO cells were predominant compared with WT cells (Figure 7A). This was especially the case for neutrophils and Ly6C^{hi} monocytes. However, in mice that received HCD for 12 or 32 weeks, the abundance of KO BM-derived cells was decreased. WT BM-derived cells were less affected (Figure 7A). This suggests that long-term HCD impairs the ability of KO BM-derived cells to contribute to circulating leukocyte populations. Assessing the abundance of WT versus KO leukocytes in the aorta at advanced stages of atherosclerosis revealed that neutrophils, macrophages, and monocytes (Ly6C^{hi} and Ly6C^{lo}) seemed to be primarily WT BM derived, whereas B- and T-cell populations had similar contributions from WT and KO cells (Figure 7B). This was in contrast to the aorta in mice fed an NCD, where the majority of the cells seemed to be derived from KO cells (Figure 7B). Consistent with the reduced abundance of KO BM-derived cells in the circulation and atherosclerotic plaques in mice fed HCD, hematopoietic cells in the BM seemed to be primarily of WT origin under conditions of HCD feeding (Figure 7C). However, the opposite was observed in mice fed an NCD (Figure 7C).

miR-146a in the Vasculature Restrains EC Activation and Atherosclerosis

Deletion of *miR-146a* has a major effect on BM-derived cell function, promoting systemic inflammatory signaling, extramedullary hematopoiesis, BM failure, and lipid dysregulation. To further distinguish the role of miR-146a in BM-derived cells versus the rest of the body, we transplanted lethally irradiated *Ldlr*$^{-/-}$ and DKO mice with *miR-146a*$^{+/+}$ (WT) BM (Figure 8A). Transplanted mice were placed on HCD for 12 weeks. Interestingly, we found no differences in circulating IL-6, sICAM-1, or TNF-α levels (Figure 8B) or circulating cholesterol or lipoproteins (Figure 8C). This suggests that the dysregulation of inflammation and circulating lipoprotein levels are dependent on deletion of *miR-146a* from BM-derived cells, rather than in other cell types, such as hepatocytes. In addition, no changes were observed in spleen size (Figure 8D). Levels of leukocytes in the spleen and in the circulation were also normalized, and only a modest decrease in leukocyte levels in the BM was seen (Figure 8E). Interestingly, NF-κB–dependent cytokines known to accelerate HSC proliferation (ie, IL-6, TNF-α, and IL-10)[10,22,23] were highly expressed in the BM of *Ldlr*$^{-/-}$ mice reconstituted with KO BM, but this was not observed in DKO mice reconstituted with WT BM (Figure 8F). Finally, with the normalization of these parameters after transplantation of WT BM in DKO mice, lipid plaque burden in the aorta was elevated compared with *Ldlr*$^{-/-}$ mice receiving WT BMT (Figure 8G).

To determine whether miR-146a in the vasculature affects EC activation in the aorta, we stimulated WT or KO mice with the proinflammatory cytokine, IL-1β. We found that miR-146a target genes (eg, HuR [human antigen R] and TRAF6) were elevated in the aortic arch of KO mice, and that levels of *VCAM-1* (vascular cell adhesion molecule-1), E-Selectin (*SELE*), and *ICAM-1* (intercellular adhesion molecule-1) were induced to a greater extent in KO compared with WT mice (Online Figure VIIIA and

Downloaded from http://ahajournals.org by on October 11, 2018

Downloaded from http://ahajournals.org by on October 11, 2018

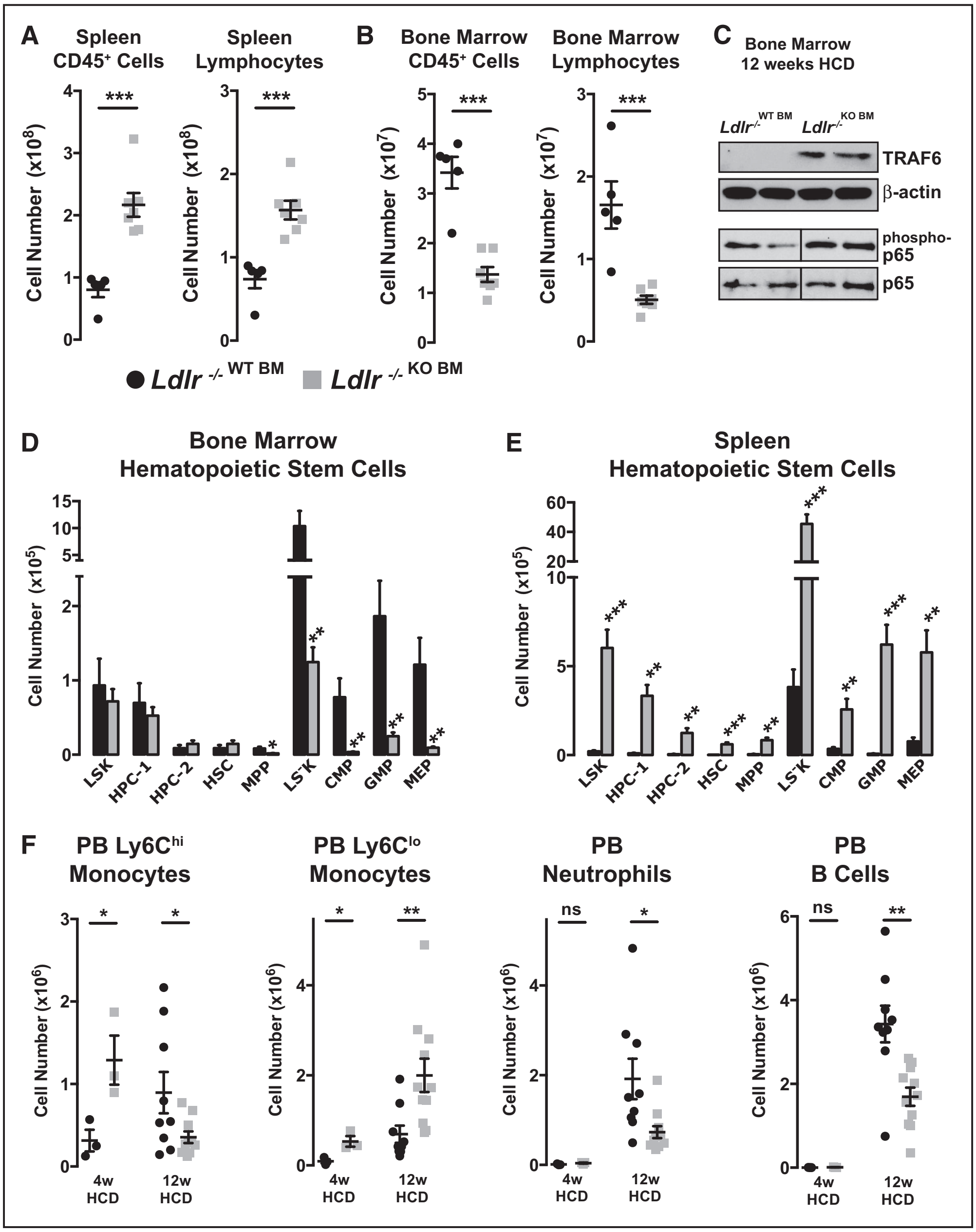

Figure 6. MicroRNA-146a (miR-146a) in bone marrow (BM)–derived cells regulates BM and extramedullary hematopoiesis and levels of circulating leukocytes and lymphocytes. Lethally irradiated *Ldlr*$^{-/-}$ mice (mix of males and females) were reconstituted with BM from wild-type (WT BM) or miR-146a$^{-/-}$ (knockout [KO] BM) donors, followed by high cholesterol diet (HCD) for 12 wk. Increase of splenic (**A**) and a decrease of BM (**B**) leukocytes and lymphocytes, as assessed by fluorescence-activated cell sorting (FACS) analysis (n=5–7). **C**, Western blot of TRAF6 (TNF receptor–associated factor 6) and phospho-p65 (normalized to β-actin and total p65, respectively), in mice receiving WT or KO BM after 12 wk of HCD. Phospho-p65/p65 blots from WT/KO animals are from the same membrane with identical imaging parameters. **D**, Decrease of a subset of multipotent stem cells, but no changes to the long-term HSCs in the BM of mice receiving KO BM transplants (BMT; n=5–7). **E**, Increase of splenic hematopoietic and multipotent stem cells in mice receiving KO BM (n=5–7). **F**, Early monocytosis (4-wk HCD), followed by a decrease in peripheral blood (PB) proatherogenic cells (neutrophils, B Cells, and Ly6C^{hi} monocytes), and an increase of antiatherogenic Ly6C^{lo} monocytes after 12 wk of HCD (n=3 for 4-wk HCD; n=9–11 for 12-wk HCD). CMP indicates common myeloid progenitor; GMP, granulocyte–macrophage progenitor; HPC, hematopoietic progenitors cell; HSC, hematopoietic stem cell; Ldlr, low-density lipoprotein receptor; LS⁻K, Sca-1 (stem cells antigen-1)–negative progenitor; MEP, megakaryocyte–erythroid progenitor; and MPP, multipotent progenitor cell.

VIIIB). In the setting of atherosclerosis, we found that expression of adhesion and chemokine genes seemed to be elevated in intimal cells of the aorta from DKO mice receiving WT BM compared with *Ldlr*$^{-/-}$ mice receiving WT BM (Online Figure VIIIC). These observations are consistent with our previous study that demonstrated that miR-146a restrains EC activation.[6]

Discussion

miR-146a has been identified as a vital brake in inflammatory signaling pathways,[6,8,10,24] and levels are elevated in human atherosclerotic plaques.[25] Recent studies have also uncovered a single-nucleotide polymorphism in the *miR-146a* gene that influences miR-146a expression and

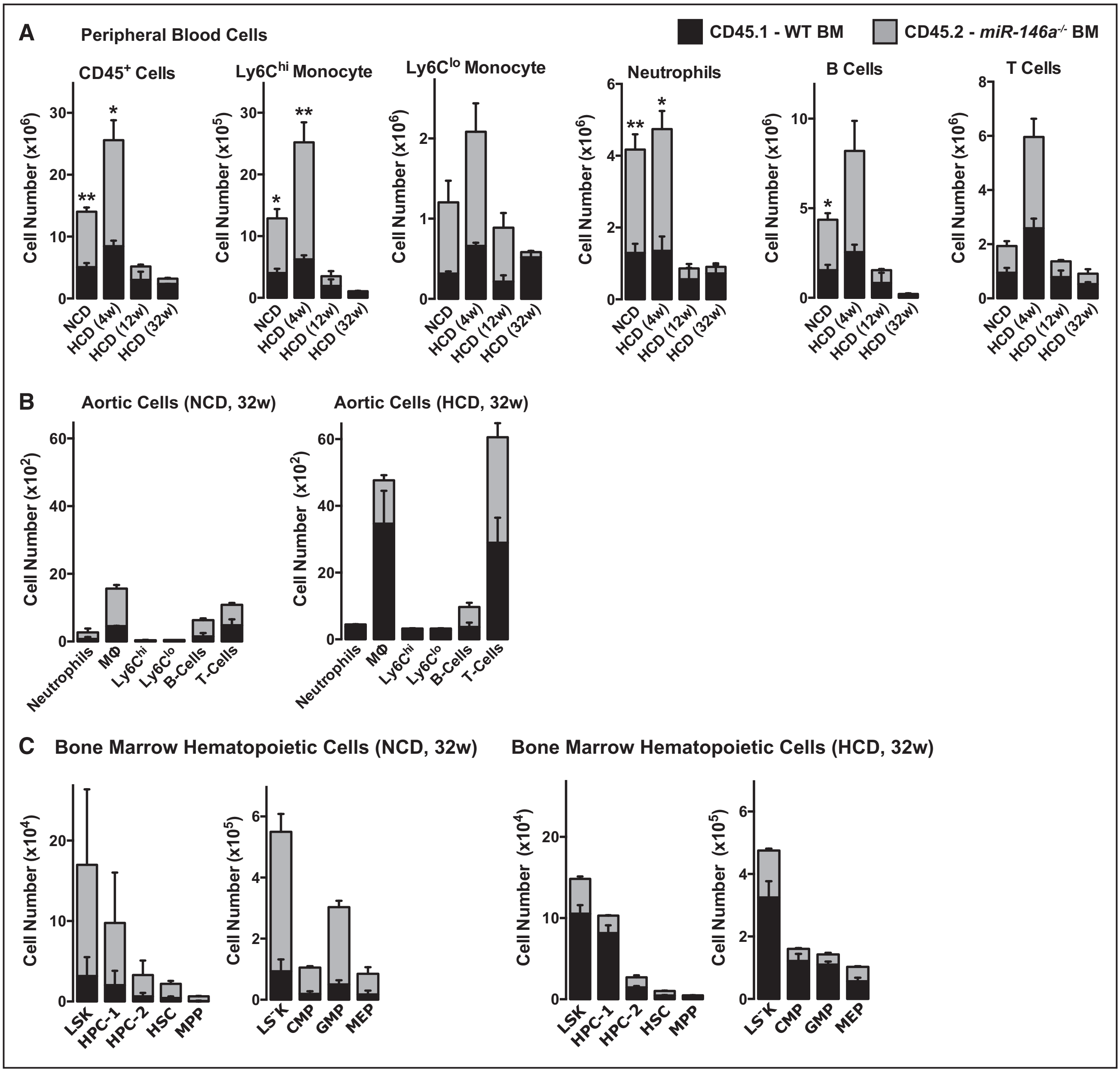

Figure 7. MicroRNA-146a (miR-146a)–deficient cells seem to be outcompeted by wild-type (WT) cells in the bone marrow (BM), circulation, and in atherosclerotic plaques in high cholesterol diet (HCD)–treated animals, but not in normal chow diet (NCD)–treated animals. Competitive BM transplantation (BMT) was performed into *Ldlr*$^{-/-}$ recipients. A 1:1 mix of BM from WT (CD45.1) and knockout (KO; CD45.2) was used. **A**, Peripheral blood was analyzed by fluorescence-activated cell sorting (FACS) after NCD or HCD for 4, 12, or 32 wk (n=8, 5, 4, 2, respectively). Comparison was made between WT and KO within each time point. **B**, Cells in the aorta (**B**) and the BM (**C**) were analyzed by FACS in animals receiving NCD or HCD for 32 wk (n=2 per group). CMP indicates common myeloid progenitor; GMP, granulocyte–macrophage progenitor; HPC, hematopoietic progenitors cell; HSC, hematopoietic stem cell; Ldlr, low-density lipoprotein receptor; LS$^-$K, Sca-1 (stem cells antigen-1)–negative progenitor; MEP, megakaryocyte–erythroid progenitor; and MPP, multipotent progenitor cell.

susceptibility to coronary artery disease.[26–29] However, no studies have directly assessed the function of endogenous miR-146a during atherogenesis. Here, we report that deletion of *miR-146a* within BM-derived cells surprisingly reduces atherosclerotic plaque formation, whereas deletion of *miR-146a* in the vasculature enhances endothelial activation and atherogenesis. These diverse phenotypes arise from a common defect in distinct cellular compartments, namely unrestrained NF-κB–dependent inflammatory signaling.

To our surprise, ablation of *miR-146a* from BM-derived cells reduced atherosclerosis, while paradoxically elevating indices of systemic inflammatory signaling (ie, proinflammatory cytokines and sICAM-1; an overview of *miR-146a*–deficient phenotypes is given in Online Figure IX). This increase in circulating cytokines would typically be accompanied by abundant inflammatory immune cells in circulation. However, we observed a decrease in proatherogenic cells, including Ly6C^{hi} monocytes, T cells and neutrophils, and an increase in atheroprotective Ly6C^{lo} monocytes. This implies that

Downloaded from http://ahajournals.org by on October 11, 2018

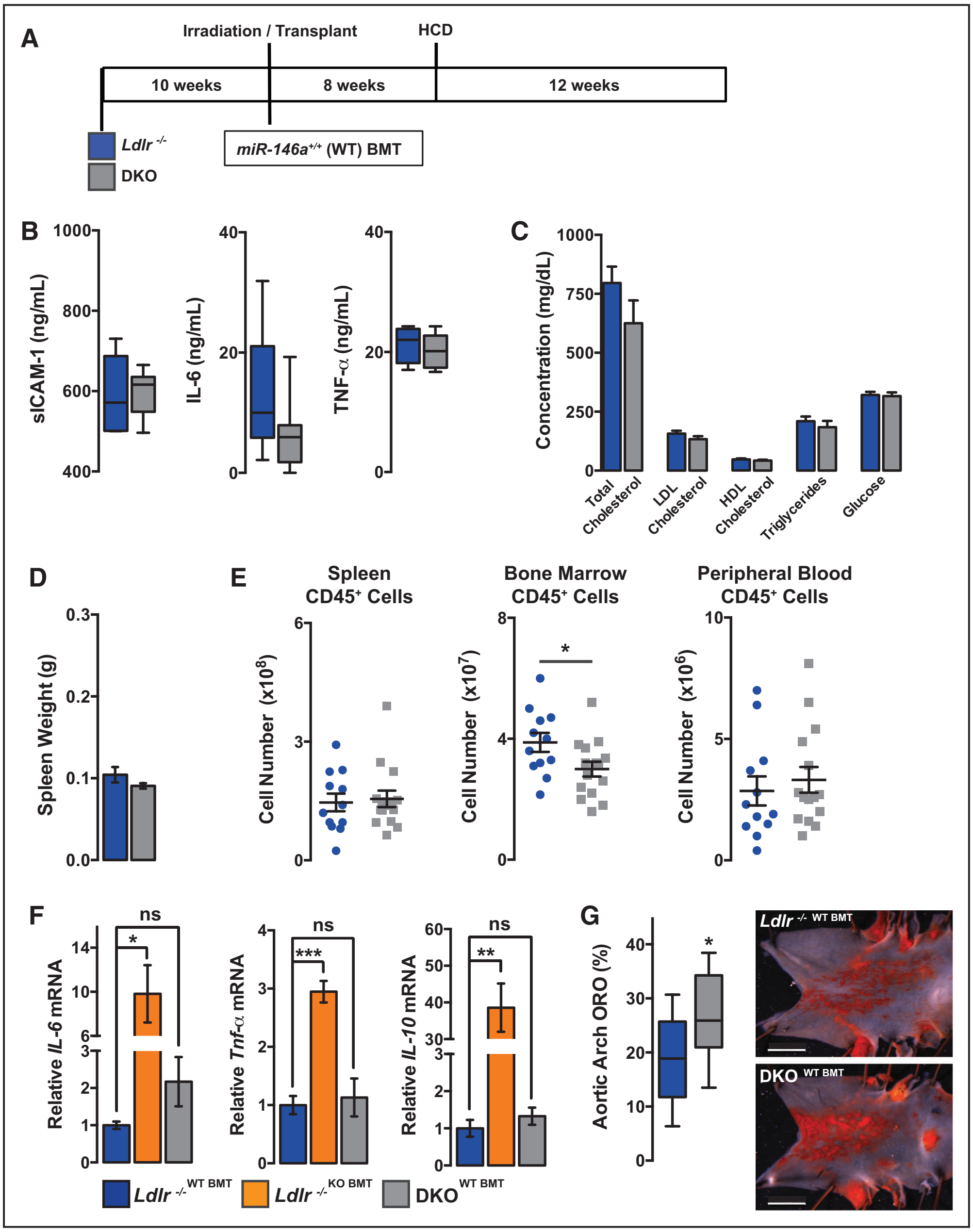

Figure 8. MicroRNA-146a (miR-146a) in the vasculature restrains endothelial cell (EC) activation and atherosclerosis. A, Schematic of lethally irradiated *Ldlr*$^{-/-}$ or double knockout (DKO) mice given bone marrow transplantation (BMT) from wild-type (WT BM) donors followed by high cholesterol diet (HCD) for 12 wk. **B**, Circulating proinflammatory markers, soluble intercellular adhesion molecule-1 (sICAM-1), IL-6 (interleukin-6), and TNF-α (tumor necrosis factor-α), measured by ELISA (n=5–8). **C**, Circulating cholesterol, high-density lipoprotein (HDL), triglycerides (TG), low-density lipoprotein (LDL) and glucose levels after 12 wk of HCD (n=5). **D**, Quantification of spleen weight after 12 wk of HCD (n=12–15). **E**, Fluorescence-activated cell sorting (FACS) analysis of myeloid cells from spleen, BM, and peripheral blood (n=12–15). **F**, Gene expression in BM cells from BM transplanted animals (n=3–7). **G**, Percentage of Oil Red-O (ORO) region per aortic arch measured by en face staining (n=11–14). Representative images are shown to the right. Data on EC activation in the aorta are given in Online Figure VIII.

miR-146a–deficient leukocytes present in circulation are likely to be especially proinflammatory, demonstrating that miR-146a is important in quelling their activation. The paucity of circulating immune cells is the consequence of defective BM hematopoiesis, which likely arises because of hematopoietic cell exhaustion. Hypercholesterolemia stimulates hematopoiesis in the BM and spleen to produce proinflammatory cells, such as Ly6C^{hi} monocytes that contribute to plaque growth.[20,30–33] We find evidence of precocious monocytosis at early stages of atherogenesis in mice that received *miR-146a*$^{-/-}$ BM. In addition, transplanted *miR-146a*–deficient cells outcompete transplanted WT cells in the BM and in circulation during early atherogenesis. However, prolonged exposure to hypercholesterolemia seems to lead to a defect in the contribution of *miR-146a*$^{-/-}$ cells to hematopoietic cell populations in the BM, circulation, and in atherosclerotic plaques, implying that the activation of BM hematopoiesis by HCD cannot be sustained in the absence of *miR-146a*. Consequently, these mice initiate

Downloaded from http://ahajournals.org by on October 11, 2018

extramedullary hematopoiesis in the spleen. Although spleen-derived Ly6C^{hi} monocytes can contribute to atherogenesis,[20] the circulating cells generated in the spleen of mice receiving *miR-146a*–deficient BM seem to be insufficient to compensate for the reduction in leukocyte output from the BM.

Defects in hematopoiesis have previously been observed in aged *miR-146a*$^{-/-}$ mice.[10] In this case, older mice (>8 months of age) developed a progressive loss of hematopoietic stem and progenitor cells as a result of increased NF-κB–dependent IL-6 production in the BM. Enhanced IL-6 production in *miR-146a*$^{-/-}$ mice promoted hematopoietic cell proliferation leading to eventual exhaustion. This phenotype could be accelerated by repeated challenge with LPS, which drives IL-6 production.[10] Similarly, in our model of atherosclerosis, we observed an increase in TRAF6 expression, NF-κB activity, and *IL-6* expression (an NF-κB–regulated cytokine) in the BM, as well as IL-6 protein levels in circulation. Because hypercholesterolemia drives stress-induced hematopoiesis[33–35] and premature HSC aging and senescence,[36] it is likely that increased cycling of hematopoietic cells leads to stem cell exhaustion in the absence of *miR-146a*.

A notable phenotype observed in both the global and BM-restricted *miR-146a* loss-of-function models is the reduction in VLDL/LDL cholesterol in circulation. Defects in cholesterol homeostasis in *miR-146a* global KOs could be rescued by transplantation of WT BM, demonstrating that miR-146a in BM-derived cells, rather than hepatocytes, regulates lipid metabolism. It is important to note that the defects that we observe in *miR-146a*$^{-/-}$ mice (ie, enhanced levels of circulating cytokines, monocytosis, outsourcing of hematopoiesis to extramedulary sites, splenomegaly, and eventual BM failure) are known to be driven by hypercholesterolemia.[20,32,33] That we observe these phenotypes even in the face of lower VLDL/LDL cholesterol suggests that it is not lower cholesterol per se that is solely responsible for the decrease in atherosclerosis in these mice, although it likely contributes. *miR-146a*$^{-/-}$ mice are especially sensitive to the inflammatory effects of hypercholesterolemia (even though VLDL/LDL cholesterol levels are decreased), and the hematopoietic phenotypes that we observe are not apparent in mice fed an NCD. The reduced atherosclerosis seems to be at least partly attributable to an unchecked chronic inflammatory response to hypercholesterolemia that drives BM hematopoiesis defects and a decrease in circulating proatherogenic inflammatory cells. The role of miR-146a in monocyte recruitment and macrophage biology in the plaque has not been explored here, but should be assessed in future studies.

We demonstrate that a lack of *miR-146a* seems to impair VLDL secretion from the liver. This is accompanied by macrophage accumulation, inflammatory gene expression (including IL-6), and an increase in *Sort1* expression in the liver; each of which may contribute to the phenotype. Although *miR-146a*–deficient BM-derived macrophages have unaltered oxidized LDL uptake and cholesterol efflux, the expansion of macrophages in the liver or spleen may influence circulating cholesterol levels through cholesterol sequestration. Altered VLDL secretion also occurs in response to proinflammatory cytokines such as IL-6,[37–39] and we confirm that exposure to IL-6 reduces triglyceride secretion from cultured primary mouse hepatocytes. Finally, we identify *Sort1* as a novel miR-146a target gene. SORT1 has been shown to play an important, though controversial role in VLDL secretion.[40] Genome-wide association studies in humans identified *SORT1* as a causative gene in the regulation of circulating LDL levels and risk of atherosclerotic disease.[18] Overexpression of SORT1 in the liver of mice enhances VLDL destruction in the liver and inhibits secretion.[18] SORT1 can also bind extracellular LDL and direct its catabolism.[41] However, other studies have found that deletion of *Sort1* in mice can also result in reduced LDL levels,[19,42] suggesting that the contribution of SORT1 to cholesterol metabolism remains to be fully resolved. Finally, additional studies found that lack of SORT1 in macrophages can inhibit secretion and signaling of cytokines, such as IL-6,[19] whereas overexpression can enhance LDL uptake.[43] This is of interest considering that *Sort1* is likely dysregulated in BM-derived cells in our *miR-146a* loss-of-function models. Further studies will be required to delineate the contribution of miR-146a–dependent *Sort1* regulation within BM-derived cells to the VLDL/LDL phenotype. Furthermore, additional miR-146a target genes in BM-derived cells may contribute.

Our study emphasizes the important role that miR-146a plays in controlling the output of inflammatory signaling pathways in ECs and hematopoietic cells in the setting of an atherogenic diet and further confirms the critical role of hypercholesterolemia in hematopoietic cell stress. Our findings are intriguing in light of polymorphisms in *miR-146a* in human patients that alters susceptibility to coronary artery disease. Furthermore, our studies suggest that elevating the expression of miR-146a in BM-derived cells or ECs is likely to suppress human atherogenesis by restraining NF-κB signaling, which is in agreement with recent studies in mouse models.[14,44]

Sources of Funding

This research was supported by a group grant to J.E. Fish, A. Schober, and C.M. Boulanger (Canadian Institutes of Health Research [CIHR] MTA-118968), an operating grant from the Heart & Stroke Foundation of Canada (NA-7282), a bridge grant from CIHR (OCN-126570), a seed grant from the CIHR-funded Canadian Vascular Network and a Leaders Opportunity Fund/Canada Foundation for Innovation equipment grant (to J.E. Fish, No. 26422). J.E. Fish was supported by an Early Researcher Award from the Ontario Ministry of Research and Innovation and a Canada Research Chair from CIHR. H.S. Cheng received funding from the Heart & Stroke Richard Lewar Centre of Excellence in Cardiovascular Research, the Ontario Graduate Studentship program, and the Canadian Vascular Network.

Disclosures

None.

References

1. Hansson GK. Inflammation, atherosclerosis, and coronary artery disease. *N Engl J Med*. 2005;352:1685–1695. doi: 10.1056/NEJMra043430.
2. Weber C, Noels H. Atherosclerosis: current pathogenesis and therapeutic options. *Nat Med*. 2011;17:1410–1422. doi: 10.1038/nm.2538.
3. Gareus R, Kotsaki E, Xanthoulea S, van der Made I, Gijbels MJ, Kardakaris R, Polykratis A, Kollias G, de Winther MP, Pasparakis M. Endothelial cell-specific NF-kappaB inhibition protects mice from atherosclerosis. *Cell Metab*. 2008;8:372–383. doi: 10.1016/j.cmet.2008.08.016.
4. Kempe S, Kestler H, Lasar A, Wirth T. NF-kappaB controls the global proinflammatory response in endothelial cells: evidence for the regulation of a pro-atherogenic program. *Nucleic Acids Res*. 2005;33:5308–5319. doi: 10.1093/nar/gki836.

Downloaded from http://ahajournals.org by on October 11, 2018

5. Cheng HS, Njock MS, Khyzha N, Dang LT, Fish JE. Noncoding RNAs regulate NF-κB signaling to modulate blood vessel inflammation. *Front Genet*. 2014;5:422. doi: 10.3389/fgene.2014.00422.
6. Cheng HS, Sivachandran N, Lau A, Boudreau E, Zhao JL, Baltimore D, Delgado-Olguin P, Cybulsky MI, Fish JE. MicroRNA-146 represses endothelial activation by inhibiting pro-inflammatory pathways. *EMBO Mol Med*. 2013;5:1017–1034. doi: 10.1002/emmm.201202318.
7. Taganov KD, Boldin MP, Chang KJ, Baltimore D. NF-kappaB-dependent induction of microRNA miR-146, an inhibitor targeted to signaling proteins of innate immune responses. *Proc Natl Acad Sci USA*. 2006;103:12481–12486. doi: 10.1073/pnas.0605298103.
8. Zhao JL, Rao DS, Boldin MP, Taganov KD, O'Connell RM, Baltimore D. NF-kappaB dysregulation in microRNA-146a-deficient mice drives the development of myeloid malignancies. *Proc Natl Acad Sci USA*. 2011;108:9184–9189. doi: 10.1073/pnas.1105398108.
9. Boldin MP, Taganov KD, Rao DS, Yang L, Zhao JL, Kalwani M, Garcia-Flores Y, Luong M, Devrekanli A, Xu J, Sun G, Tay J, Linsley PS, Baltimore D. miR-146a is a significant brake on autoimmunity, myeloproliferation, and cancer in mice. *J Exp Med*. 2011;208:1189–1201. doi: 10.1084/jem.20101823.
10. Zhao JL, Rao DS, O'Connell RM, Garcia-Flores Y, Baltimore D. MicroRNA-146a acts as a guardian of the quality and longevity of hematopoietic stem cells in mice. *Elife*. 2013;2:e00537. doi: 10.7554/eLife.00537.
11. Etzrodt M, Cortez-Retamozo V, Newton A, et al. Regulation of monocyte functional heterogeneity by miR-146a and Relb. *Cell Rep*. 2012;1:317–324. doi: 10.1016/j.celrep.2012.02.009.
12. Brand K, Page S, Rogler G, Bartsch A, Brandl R, Knuechel R, Page M, Kaltschmidt C, Baeuerle PA, Neumeier D. Activated transcription factor nuclear factor-kappa B is present in the atherosclerotic lesion. *J Clin Invest*. 1996;97:1715–1722. doi: 10.1172/JCI118598.
13. Kanters E, Pasparakis M, Gijbels MJ, Vergouwe MN, Partouns-Hendriks I, Fijneman RJ, Clausen BE, Förster I, Kockx MM, Rajewsky K, Kraal G, Hofker MH, de Winther MP. Inhibition of NF-kappaB activation in macrophages increases atherosclerosis in LDL receptor-deficient mice. *J Clin Invest*. 2003;112:1176–1185. doi: 10.1172/JCI18580.
14. Li K, Ching D, Luk FS, Raffai RL. Apolipoprotein E enhances microRNA-146a in monocytes and macrophages to suppress nuclear factor-κB-driven inflammation and atherosclerosis. *Circ Res*. 2015;117:e1–e11. doi: 10.1161/CIRCRESAHA.117.305844.
15. Von Der Thüsen JH, Kuiper J, Fekkes ML, De Vos P, Van Berkel TJ, Biessen EA. Attenuation of atherogenesis by systemic and local adenovirus-mediated gene transfer of interleukin-10 in LDLr-/- mice. *FASEB J*. 2001;15:2730–2732. doi: 10.1096/fj.01-0483fje.
16. Hashizume M, Yoshida H, Koike N, Suzuki M, Mihara M. Overproduced interleukin 6 decreases blood lipid levels via upregulation of very-low-density lipoprotein receptor. *Ann Rheum Dis*. 2010;69:741–746. doi: 10.1136/ard.2008.104844.
17. Lehtimäki T, Ojala P, Rontu R, Goebeler S, Karhunen PJ, Jylhä M, Mattila K, Metso S, Jokela H, Nikkilä M, Wuolijoki E, Hervonen A, Hurme M. Interleukin-6 modulates plasma cholesterol and C-reactive protein concentrations in nonagenarians. *J Am Geriatr Soc*. 2005;53:1552–1558. doi: 10.1111/j.1532-5415.2005.53484.x.
18. Musunuru K, Strong A, Frank-Kamenetsky M, et al. From noncoding variant to phenotype via SORT1 at the 1p13 cholesterol locus. *Nature*. 2010;466:714–719. doi: 10.1038/nature09266.
19. Mortensen MB, Kjolby M, Gunnersen S, Larsen JV, Palmfeldt J, Falk E, Nykjaer A, Bentzon JF. Targeting sortilin in immune cells reduces proinflammatory cytokines and atherosclerosis. *J Clin Invest*. 2014;124:5317–5322. doi: 10.1172/JCI76002.
20. Robbins CS, Chudnovskiy A, Rauch PJ, et al. Extramedullary hematopoiesis generates Ly-6C(high) monocytes that infiltrate atherosclerotic lesions. *Circulation*. 2012;125:364–374. doi: 10.1161/CIRCULATIONAHA.111.061986.
21. Aviram M, Brook JG, Tatarsky I, Levy Y, Carter A. Increased low-density lipoprotein levels after splenectomy: a role for the spleen in cholesterol metabolism in myeloproliferative disorders. *Am J Med Sci*. 1986;291:25–28.
22. Rezzoug F, Huang Y, Tanner MK, Wysoczynski M, Schanie CL, Chilton PM, Ratajczak MZ, Fugier-Vivier IJ, Ildstad ST. TNF-alpha is critical to facilitate hemopoietic stem cell engraftment and function. *J Immunol*. 2008;180:49–57.
23. Baldridge MT, King KY, Goodell MA. Inflammatory signals regulate hematopoietic stem cells. *Trends Immunol*. 2011;32:57–65. doi: 10.1016/j.it.2010.12.003.
24. Yang L, Boldin MP, Yu Y, Liu CS, Ea CK, Ramakrishnan P, Taganov KD, Zhao JL, Baltimore D. miR-146a controls the resolution of T cell responses in mice. *J Exp Med*. 2012;209:1655–1670. doi: 10.1084/jem.20112218.
25. Raitoharju E, Lyytikäinen LP, Levula M, Oksala N, Mennander A, Tarkka M, Klopp N, Illig T, Kähönen M, Karhunen PJ, Laaksonen R, Lehtimäki T. miR-21, miR-210, miR-34a, and miR-146a/b are up-regulated in human atherosclerotic plaques in the Tampere Vascular Study. *Atherosclerosis*. 2011;219:211–217. doi: 10.1016/j.atherosclerosis.2011.07.020.
26. Bao MH, Xiao Y, Zhang QS, Luo HQ, Luo J, Zhao J, Li GY, Zeng J, Li JM. Meta-analysis of miR-146a polymorphisms association with coronary artery diseases and ischemic stroke. *Int J Mol Sci*. 2015;16:14305–14317. doi: 10.3390/ijms160714305.
27. He Y, Yang J, Kong D, Lin J, Xu C, Ren H, Ouyang P, Ding Y, Wang K. Association of miR-146a rs2910164 polymorphism with cardio-cerebrovascular diseases: a systematic review and meta-analysis. *Gene*. 2015;565:171–179. doi: 10.1016/j.gene.2015.04.020.
28. Ramkaran P, Khan S, Phulukdaree A, Moodley D, Chuturgoon AA. miR-146a polymorphism influences levels of miR-146a, IRAK-1, and TRAF-6 in young patients with coronary artery disease. *Cell Biochem Biophys*. 2014;68:259–266. doi: 10.1007/s12013-013-9704-7.
29. Xiong XD, Cho M, Cai XP, Cheng J, Jing X, Cen JM, Liu X, Yang XL, Suh Y. A common variant in pre-miR-146 is associated with coronary artery disease risk and its mature miRNA expression. *Mutat Res*. 2014;761:15–20. doi: 10.1016/j.mrfmmm.2014.01.001.
30. Ma X, Feng Y. Hypercholesterolemia tunes hematopoietic stem/progenitor cells for inflammation and atherosclerosis. *Int J Mol Sci*. 2016;17:E1162.
31. Murphy AJ, Tall AR. Disordered haematopoiesis and athero-thrombosis. *Eur Heart J*. 2016;37:1113–1121. doi: 10.1093/eurheartj/ehv718.
32. Feng Y, Schouteden S, Geenens R, Van Duppen V, Herijgers P, Holvoet P, Van Veldhoven PP, Verfaillie CM. Hematopoietic stem/progenitor cell proliferation and differentiation is differentially regulated by high-density and low-density lipoproteins in mice. *PLoS One*. 2012;7:e47286. doi: 10.1371/journal.pone.0047286.
33. Soehnlein O, Swirski FK. Hypercholesterolemia links hematopoiesis with atherosclerosis. *Trends Endocrinol Metab*. 2013;24:129–136. doi: 10.1016/j.tem.2012.10.008.
34. Ye YX, Calcagno C, Binderup T, et al. Imaging macrophage and hematopoietic progenitor proliferation in atherosclerosis. *Circ Res*. 2015;117:835–845. doi: 10.1161/CIRCRESAHA.115.307024.
35. Westerterp M, Gourion-Arsiquaud S, Murphy AJ, Shih A, Cremers S, Levine RL, Tall AR, Yvan-Charvet L. Regulation of hematopoietic stem and progenitor cell mobilization by cholesterol efflux pathways. *Cell Stem Cell*. 2012;11:195–206. doi: 10.1016/j.stem.2012.04.024.
36. Tie G, Messina KE, Yan J, Messina JA, Messina LM. Hypercholesterolemia induces oxidant stress that accelerates the ageing of hematopoietic stem cells. *J Am Heart Assoc*. 2014;3:e000241. doi: 10.1161/JAHA.113.000241.
37. Park EJ, Lee JH, Yu GY, He G, Ali SR, Holzer RG, Osterreicher CH, Takahashi H, Karin M. Dietary and genetic obesity promote liver inflammation and tumorigenesis by enhancing IL-6 and TNF expression. *Cell*. 2010;140:197–208. doi: 10.1016/j.cell.2009.12.052.
38. Glund S, Krook A. Role of interleukin-6 signalling in glucose and lipid metabolism. *Acta Physiol*. 2008;192:37–48. doi: 10.1111/j.1748-1716.2007.01779.x.
39. Murthy S, Mathur S, Bishop WP, Field EJ. Inhibition of apolipoprotein B secretion by IL-6 is mediated by EGF or an EGF-like molecule in CaCo-2 cells. *J Lipid Res*. 1997;38:206–216.
40. Westerterp M, Tall AR. SORTILIN: many headed hydra. *Circ Res*. 2015;116:764–766. doi: 10.1161/CIRCRESAHA.115.306036.
41. Strong A, Ding Q, Edmondson AC, et al. Hepatic sortilin regulates both apolipoprotein B secretion and LDL catabolism. *J Clin Invest*. 2012;122:2807–2816. doi: 10.1172/JCI63563.
42. Kjolby M, Andersen OM, Breiderhoff T, Fjorback AW, Pedersen KM, Madsen P, Jansen P, Heeren J, Willnow TE, Nykjaer A. Sort1, encoded by the cardiovascular risk locus 1p13.3, is a regulator of hepatic lipoprotein export. *Cell Metab*. 2010;12:213–223. doi: 10.1016/j.cmet.2010.08.006.
43. Patel KM, Strong A, Tohyama J, Jin X, Morales CR, Billheimer J, Millar J, Kruth H, Rader DJ. Macrophage sortilin promotes LDL uptake, foam cell formation, and atherosclerosis. *Circ Res*. 2015;116:789–796. doi: 10.1161/CIRCRESAHA.116.305811.
44. Ma S, Tian XY, Zhang Y, Mu C, Shen H, Bismuth J, Pownall HJ, Huang Y, Wong WT. E-selectin-targeting delivery of microRNAs by microparticles ameliorates endothelial inflammation and atherosclerosis. *Sci Rep*. 2016;6:22910. doi: 10.1038/srep22910.

Downloaded from http://ahajournals.org by on October 11, 2018

B. Curriculum vitae

Adel Hammoutene

02/11/1991
adel.hammoutene@inserm.fr ; amsadel@hotmail.com

Education

2015-now	PhD in liver pathophysiology and vascular biology. Paris Descartes University. Supervisor Pr. Pierre-Emmanuel Rautou (defending in December 2018)
2016	Diploma of animal experimentation. Level 1. Paris Descartes University
2014-2015	Master 2 of science. Cellular biology, physiology and pathophysiology, speciatily « epithelia ». Paris Descartes University
2013-2014	Master 2 of science. Cellular biology, physiology and pathophysiology, speciatily « vascular biology and hemostasis ». Paris Descartes University
2012-2013	Master 1 of science. Cellular biology, physiology and pathophysiology. Paris Descartes University
2011-2012	Bachelor in cellular biology. Aix-Marseille University.

Work experience

2015-now	Paris Cardiovascular Center (PARCC), Inserm U970. Paris. France PhD Thesis: Role of autophagy in liver sinusoidal endothelial cells in nonalcoholic steatohepatitis (NASH)
2015	Paris Cardiovascular Center (PARCC). Inserm U970 and Institute Necker Enfants Malades (INEM), Inserm U1151. Paris. France Traineeship: Role of endothelial primary cilium in the shear stress sensing and autophagy regulation
2014	Paris Cardiovascular Center (PARCC). Inserm U970. Paris. France Traineeship: Role of endothelial autophagy in nonalcoholic steatohepatitis (NASH)
2013	Paris Cardiovascular Center (PARCC). Inserm U970. Paris. France Traineeship: Role of endothelial autophagy in nonalcoholic atherosclerosis

Bursaries and Prices

2015-2018	PhD fellowship « Doctoral grant from the French education and research ministry, Paris Descartes University »
2018	Young investigator bursary from the AFEF (French society for the study of the liver) to attend the annual congress in october 2018, Lyon, France.
2018	Young investigator bursary from the EASL (European Association for the Study of the Liver) to attend the international liver congress (ILC 2018) in April 2018, Paris, France.
2017	Young investigator bursary from the NSFA (New French society of atherosclerosis) to attend the annual congress in June 2017, Biarritz, France.
2016	Young investigator bursary from the CFATG (French society of autophagy) to attend the annual congress in October 2016, Bordeaux, France.
2015	Best poster award at the annual PARCC meeting.

Scientific communications

- October 2018: Oral communication at the annual congress of the French society for the study of the liver, Lyon, France.
- September 2018: Invited speaker at Beaujon Hôspital: Role of endothelial cells in nonalcoholic steatohepatitis, Clichy, France.
- April 2018: Oral communication at the International Liver Congress 2018 (ILC2018, EASL), Paris, France.
- November 2017: Poster at the 7th congress of the French society of autophagy (CFATG7), Paris, France.
- June 2017: Oral communication at the 13th congress of the French society of atherosclerosis (NSFA), Biarritz, France.
- May 2017: Oral communication at the annual PARCC meeting.
- October 2016: Poster at the 6th congress of the French society of autophagy (CFATG6), Bordeaux France.
- May 2015: Poster at the annual PARCC meeting. best poster award*

List of publications

- Vion AC, Alt S, Klaus-Bergmann A, Szymborska A, Zheng T, Perovic T, Hammoutene A, Bastos Oliveira M, Bartels-Klein E, Hollfinger I, Rautou PE, Bernabeu M, Gerhardt H. Primary Cilia Sensitize Endothelial Cells to BMP and Prevent Excessive Vascular Regression. J Cell Biol. 2018 Mar 2. pii: jcb.201706151

- Poisson J, Hilscher MB, Tanguy M, Hammoutene A, Boulanger CM, Villeval JL, Simonetto DA, Valla D, Shah VH, Rautou PE. Endothelial JAK2^{V617F} does not enhance liver lesions in mice with Budd-Chiari syndrome. J Hepatol. 2018 Jan 31. pii: S0168-8278(18)30022-9

- Kheloufi M*, Vion AC*, Hammoutene A, Poisson J, Lasselin J, Devue C, Pic I, Dupont N, Busse J, Stark K, Lafaurie-Janvore J, Barakat AI, Loyer X, Souyri M, Viollet B, Julia P, Tedgui A, Codogno P, Boulanger CM, Rautou PE. Endothelial autophagic flux hampers atherosclerotic lesion development. Autophagy. 2017 Nov 20:1-6.

- Vion AC*, Kheloufi M*, Hammoutene A, Poisson J, Lasselin J, Devue C, Pic I, Dupont N, Busse J, Starke K, Lafaurie-Janvore J, Barakatf AI, Loyer X, Souyri M, Viollet B, Julia P, Tedgui A, Codogno P, Boulanger CM*, Rautou PE*. Autophagy is required for endothelial cell alignment and atheroprotection under physiological blood flow. Proc Natl Acad Sci U S A. 2017 Oct 10;114(41):E8675-E8684

- Cheng HS, Besla R, Li A, Chen Z, Shikatani EA, Nazari-Jahantigh M, Hammoutene A, Nguyen MA, Geoffrion M, Cai L, Khyzha N, Li T, MacParland SA, Husain M, Cybulsky MI, Boulanger CM, Temel RE, Schober A, Rayner KJ, Robbins CS, Fish JE. Paradoxical Suppression of Atherosclerosis in the Absence of microRNA-146a. Circ Res. 2017 Aug 4;121(4):354-367

Other activities

- Representative of PhD students on the PARCC laboratory board

- Member of the animal wellbeing and care committee of the PARCC

Résumé

La stéatohépatite non alcoolique (NASH) est définie par une accumulation excessive de lipides dans le foie (stéatose), une atteinte hépatocytaire et une inflammation hépatique avec ou sans fibrose. La NASH peut évoluer vers la cirrhose et le carcinome hépatocellulaire. De récentes études ont montré que des altérations endothéliales précèdent l’atteinte fibreuse et inflammatoire de la NASH et favorisent le développement de la maladie.
L’autophagie est un processus cellulaire par lequel du matériel cytoplasmique dysfonctionnel rejoint les lysosomes pour y être dégradé. L’autophagie a été étudiée dans les différents types cellulaires du foie, mais le rôle de l’autophagie dans les cellules endothéliales sinusoïdales du foie (LSECs) n’a à ce jour jamais été évalué dans le contexte des maladies chroniques du foie incluant la NASH. Le but de mon projet de thèse a été d’évaluer le rôle de l’autophagie dans les LSECs dans la NASH.

Dans cette étude, j’ai démontré en utilisant des biopsies hépatiques humaines qu’un défaut d’autophagie dans les LSECs se produit spécifiquement dans la NASH. *In vitro*, j’ai démontré que la combinaison de médiateurs inflammatoires tels que le TNFα et l’IL6 inhibait l’autophagie dans les LSECs *via* l’inhibition de l’activité AMPKα. Le défaut d’autophagie dans les LSECs induisait une surexpression de marqueurs d’inflammation endothéliale (*Mcp1*, *Rantes* et VCAM1), de transition endothélio-mésenchymateuse (*α-SMA*, *Tgf-β1* et *Collagène1a2*) et induisait l’apoptose des LSECs. *In vivo*, les souris déficientes en autophagie endothéliale soumises à un régime alimentaire riche en matières grasses présentaient une surface hépatique irrégulière, une augmentation de l’inflammation hépatique (surexpression hépatique de *Mcp1*, *Rantes* et VCAM1) et plus de fibrose hépatique (surexpression hépatique de α-SMA, *Tgf-β1* et *Collagène1a2* et plus de déposition de collagène). Les souris déficientes en autophagie endothéliale traitées par du tétrachlorure de carbone avaient également une fibrose hépatique augmentée (surexpression hépatique de *α-SMA*, *Tgf-β1* et *Collagène1a2* et plus de déposition de collagène).

En conclusion, cette étude démontre qu’un défaut d’autophagie se produit dans les LSECs de patients atteints de NASH. Ce défaut peut être attribué aux médiateurs inflammatoires présents dans le sang portal de ces patients. Le défaut d’autophagie dans les LSECs induit des altérations endothéliales (inflammation endothéliale, transition endothélio- mésenchymateuse et apoptose) et contribue fortement à l’établissement de l’inflammation et de la fibrose hépatique aux stades précoces et avancées des maladies chroniques du foie. Le défaut d’autophagie dans les LSECs pourrait en partie expliquer comment les patients atteints de NASH évoluent vers la NASH. Cette première observation du rôle protecteur de l'autophagie endothéliale complète les connaissances sur l'autophagie dans les maladies chroniques du foie. Cibler l'autophagie dans les LSECs constitue une stratégie thérapeutique intéressante pour le traitement de la NASH.